# Characterisation of Purine Nucleotide Metabolism in an Acute Promyelocytic Leukaemia (APL) cell line using Mathematical Models

Janine Delia Symonds

A thesis submitted in partial fulfilment of the requirements for the degree of:

Doctor of Philosophy
of
University College London
2023

Supervisors:

Prof. Geraint Thomas and Dr. Kevin Bryson

I, Janine Delia Symonds, hereby confirm that the work presented in this thesis is my own. Where information has been derived from other sources, I confirm that this has been indicated in the thesis.

## Abstract

Acute promyelocytic leukaemia (APL) is usually treated using All-trans Retinoic acid (ATRA), but this has potentially life-threatening side effects; prompting the search for novel treatments. Interference with purine metabolism, through inhibition of the enzyme inosine monophosphate dehydrogenase (IMPDH) causes differentiation of HL60 cells, an APL cell line; however, the exact mechanism of action is unknown. Purine metabolism is complex with many internal regulatory mechanisms, thus determining expected outcomes within this system is difficult. The aim of this study was to provide insights into purine metabolism in HL60 cells and investigate the effects of IMPDH inhibition on this system, using a dual approach of mathematical modelling and experimentation.

Through refinement and expansion of an existing framework, an HL60 cell specific mathematical model of purine metabolism was established that allows examination of key metabolites. This model is robust with a stable steady state. IMPDH inhibition was simulated and metabolite concentrations were determined.

Experimental data was obtained from IMPDH inhibitor treated HL60 cells. Comparison of this data to model output showed low concordance; however this is partly due to the literature data used to refine the model, which this new data also failed to match. Nevertheless, with further refinement the model will be a useful tool in furthering our understanding of purine metabolism in HL60 cells and specifically the effects of IMPDH inhibition. Furthermore, the model could be used to identify other potential novel targets within the purine metabolic network which could be used as new APL therapies.

Additionally, this study provides previously uncharacterised data of purine levels in HL60 cells treated with either an IMPDH inhibitor or ATRA alongside guanosine. Furthermore, data showed a synergistic effect on HL60 cell differentiation when ATRA was used alongside an IMPDH inhibitor, raising the possibility of using both drugs together clinically to treat APL.

## Impact Statement

Acute myeloid leukaemia (AML) is the most common form of myeloid leukaemia and in the UK each year it accounts for approximately 2 % of cancer deaths. There are different forms of the disease, such as Acute promyelocytic leukaemia (APL), and various cells lines exist which are used to study the disease *in vitro*. HL60 cells, an APL cell line, have been shown to have altered metabolism and differentiate in the presence of inosine monophosphate dehydrogenase (IMPDH) inhibitors. IMPDH is a crucial enzyme in the purine metabolic network, however the exact mechanism by which IMPDH inhibition brings about HL60 cell differentiation is unknown.

Purine metabolism is a very complicated system with many internal feedback mechanisms and as such it is especially difficult to make predictions regarding the outcomes when the system is perturbed. Therefore, the main part of this work was to create a mathematical model of the purine metabolic network specific to HL60 cells. The resultant model is a useful tool which serves to elucidate some of the details of purine metabolism and the effects IMPDH inhibitors have on the system; ultimately garnering new insights into this area of research.

Furthermore, the model could be used and adapted by others to investigate purine metabolism in their own systems of interest. Indeed, this thesis provides a detailed record of how to tailor the model to a specific cell type and as such the procedures detailed within could be followed to create a model specific for any cell or tissue type of interest. Thus, the model has the potential to be used in the study of purine metabolism in a variety of other contexts outside of APL, such as diseases affecting purine metabolism among others. Furthermore, model predictions could be used to better understand how current or future therapies for any disease that target enzymes within this network will potentially affect purine metabolites, furthering our understanding of these drugs' pharmacodynamics.

The experimental data obtained in this study increases the available existing data on

purine nucleotide levels in cells differentiated with either All-trans Retinoic acid (ATRA) or the IMPDH inhibitors Mycophenolic acid or Mizoribine. Furthermore, the data obtained from cells treated with differentiating agents in the presence of guanosine is previously uncharacterised and as such adds to the knowledge available on this topic.

Lastly, the observation of a synergistic effect on HL60 cell differentiation when lower doses of ATRA are used in combination with an IMPDH inhibitor may translate to potential clinical applications. This synergy raises the possibility of treating patients with APL with the two drugs together in the hope that the lower doses of both may ameliorate some of the potential side effects seen with these drugs.

In conclusion, given the renewed interest in the altered metabolic landscape of leukaemic cells and the advances in metabolomics technology, it is hoped that the results presented here will prove to be a useful resource to aid in this new direction of research.

## Acknowledgements

Firstly, I would like to thank my supervisors Geraint Thomas and Kevin Bryson for their support and help throughout the years. Their knowledge and expertise enabled me to navigate the interesting, but sometimes daunting, sphere of interdisciplinary work knowing that their guidance was always available.

In addition, I am grateful for the friendship and help received from the various lab and wider group members who have come and gone over the years, namely Chris Barnes, Nathan Blake, Alex Fedorec, Riana Gaifulina, Miriam Leon, Aaran Lewis, Tanel Ozdemir and Mae Woods, with special thanks going to Jack Rutter for being my companion whilst navigating the idiosyncrasies of a very old HPLC machine and to Lewis Tanner who always had advice and encouragement when it was most needed and who helped conduct experiments during the Covid-19 pandemic; for which I am very grateful. Furthermore, I will always be thankful to Florence Stanley and Lourdes Sriraja, whose constant support and help throughout their time in the lab was much needed and even after they moved to pastures new they have remained close friends whose support has been invaluable.

My thanks also to Stuart Harrison, Silvana Pinna and Sean Jordan for all their help with the HPLC experiments.

I would also like to thank Eberhard Voit, whose lab I was fortunate enough to visit for three months. It was a privilege to work with Eberhard and members of his group, whose skills and expertise in mathematical modelling enabled me to advance the theoretical side of the project significantly; therefore, special thanks go to Zhen Qi and Luis Fonseca. Moreover, I am grateful to the Bogue Fellowship committee for granting me the funding to undertake this opportunity.

My thanks also go to the EPSRC and the CoMPLEX doctoral training programme for funding my studies. In addition, I am grateful to the support staff both in CoMPLEX and my host department CDB for ensuring the smooth running of administrative matters, of special note is the super-efficient Gemma Ludbrook. Moreover, I would especially like to thank Michael Hanley and Nicky Virdee for ensuring it was aways possible for the lab to be well stocked with consumables and clean equipment; but for their hard work behind the scenes, experiments would have halted.

Lastly, the biggest thank you goes to my family: my parents, brother, sister, partner and cats, to whom I will always be indebted for their unwavering support, encouragement and love during the many long years.

In loving memory of my Dad, who sadly isn't here to see me finish and submit but, who always thought computer coding was amazing!

# Contents

Al	ostra	$\operatorname{ct}$	3
In	ıpact	Statement	4
A	cknov	vledgements	6
Li	st of	Figures	10
Li	st of	Tables	12
Al	Gene Enzy	viations eral ymes ne metabolites	14 14 14 15
-1			10
1	1.1 1.2 1.3 1.4 1.5 1.6	Leukaemia	16 18 19 22 25 27 29 31 33 33
	1.8	Rationale and aims	36
2	Mat 2.1 2.2 2.3	Chematical Introduction  Ordinary differential equations (ODE)  Reaction kinetics  2.2.1 Mass action  2.2.2 Michaelis-Menten equation  Biochemical Systems Theory (BST)  2.3.1 BST formulation for a single variable system  2.3.2 BST formulation for a multivariable system  2.3.3 Generalised Mass Action (GMA)	38 39 39 40 41 43 47 48
	2.4	2.3.3.1 GMA example system	52 54
9	Ma		ξŪ
3	3.1	del Adaptation         Model refinement	<b>59</b> 59
	3.2	3.1.1 RNAseq analysis for ATRA treated HL60 cells	59 64

		3.2.1	Amendment of existing reactions	65
		3.2.2	New interconversion reactions	65
		3.2.3	ATP synthesis and degradation	68
		3.2.4	Rate constant calculations	71
	3.3	Model	version 2	74
		3.3.1	ATP synthesis and degradation revisited	74
	3.4	Final r	nodel - version 3	76
		3.4.1	Model tweaking towards the Curto et al. (1998b) model steady stat	e 78
		3.4.2	Flux value adjustments	79
		3.4.3	Better scaling	81
	3.5	Exami	nation of the model	88
		3.5.1	Sensitivity analysis	89
		3.5.2	Model simulation tests	91
	3.6	Issues	with the model	96
		3.6.1	Grid search parameter simulations	98
		3.6.2	Combined large-scale parameter simulations	100
1	Fun	onimor	atal Mathoda and Deculta	103
4	4.1		als and methods	103
	4.1	4.1.1	Purine standards	103
		4.1.1 $4.1.2$		103
		4.1.2	Differentiating agents	103
		4.1.3	HPLC procedure	104 $105$
		4.1.4 $4.1.5$	Call culture	100
		4.1.5 $4.1.6$	Cell culture	100
			Phosphoribosylpyrophosphate synthetase (PRPPS) assay	100
		4.1.7	Flow cytometry analysis of HL60 cell differentiation	107
		110	3 3 3 3 3 3 3 3 3 3 3 3 3 3 3 3 3 3 3 3	
		4.1.8	HL60 cell reactive oxygen species detection experiments	108
		4.1.9	HL60 cell purine extraction	109
		4.1.10 4.1.11	v i	109 110
	4.2	Results	Statistical analysis	110
	4.2	4.2.1	S	110
		4.2.1 $4.2.2$		111
		4.2.2	Flow cytometry analysis of HL60 cell differentiation	
		4.2.3	HL60 cell reactive oxygen species detection experiments	116
		4.2.3 $4.2.4$	HPLC analysis of HL60 cell purine levels	118 120
		4.2.4	THE C analysis of filloo cen purine levels	120
5	Disc	cussion	and Conclusions	127
	5.1	Data i	nterpretation and model comparison	127
		5.1.1	Model scaling	127
		5.1.2	Cellular changes upon IMPDH inhibition	127
			5.1.2.1 Phenotypic markers	127
			5.1.2.2 Functional assay	128
			5.1.2.3 Purine levels	128
		5.1.3	Effects of combining ATRA and IMPDH inhibitors	131

5.2	Model evaluation	132
5.3	Future work	132
5.4	Conclusions	134
Bibliog	raphy	136
Appen		<b>152</b>
App	endix A	152
App	endix B	153
App	endix C	155
App	endix D	165
App	endix E	168
App	endix F	179
App	endix G	181
App	endix H	185
$\operatorname{Cod}$	e Appendix	190

# List of Figures

1.1 1.2 1.3 1.4 1.5	Retinoic acid signalling in myeloid cell development	23 26 27 28 28
2.1	Schematic for GMA formulation example	52
3.11 3.12	Comparison of mRNA expression levels between HL60 cells treated with ATRA and untreated cells	63 66 66 67 67 73 76 77 78 79 85 91
3.14	Model network with parameter search results	101
4.1 4.2 4.3 4.4 4.5 4.6 4.7 4.8	Time course of HL60 cell differentiation	112 113 114 115 116 117 118 119 121 123
	Percentage change in purine concentrations after incubation with guanosin	
4.12	Percentage change in purine concentrations after combination treatment	126
A.1 E.1	Network schematic from the Curto <i>et al.</i> (1998b) model	152 169

Parameter sensitivities for fluxes 2	170
Parameter sensitivities for fluxes 3	171
Parameter sensitivities for fluxes 4	172
Parameter sensitivities for fluxes 5	173
Parameter sensitivities for metabolites 1	174
Parameter sensitivities for metabolites 2	175
Parameter sensitivities for metabolites 3	176
Logarithmic gains for metabolites and fluxes	177
HPLC calibration curves for Ado, AMP, ADP, ATP, HX and IMP	182
HPLC calibration curves for Guo, GMP, GDP, GTP and XMP	183
Chromatograms for PRPPS assay time course	185
Change in AMP concentration over PRPPS assay time course	186
Example flow cytometry gating strategy	187
Effect of ATRA plus MZ	188
HPLC chromatograms from HL60 cell differentiation experiments	189
	Parameter sensitivities for fluxes 3 Parameter sensitivities for fluxes 4 Parameter sensitivities for fluxes 5 Parameter sensitivities for metabolites 1 Parameter sensitivities for metabolites 2 Parameter sensitivities for metabolites 3 Logarithmic gains for metabolites and fluxes HPLC calibration curves for Ado, AMP, ADP, ATP, HX and IMP HPLC calibration curves for Guo, GMP, GDP, GTP and XMP Chromatograms for PRPPS assay time course Change in AMP concentration over PRPPS assay time course Example flow cytometry gating strategy Effect of ATRA plus MZ

# List of Tables

1.1 1.2	French-American-British AML classification	20 21
2.1 2.2	Metabolites from the Curto $et\ al.\ (1998b)$ model of human purine metabolism Reactions from the Curto $et\ al.\ (1998b)$ model of human purine metabolism	
3.1	Relevant Reads Per Million values from the Raz $\operatorname{et}$ al. (2011) RNAseq data	
3.2	set	61
	guanylate metabolites	64
3.3	List of hand curated adenylate & adenosine and guanylate interconversion reaction enzymes	68
3.4	Kinetic data for each of the adenylate & adenosine and guanylate inter-	
3.5	conversion reactions	70
	reactions	75
3.6	Guanylate and adenylate & adenosine steady state simultaneous equation systems	80
3.7	Kinetic order values for the final model	82
3.8	Initial flux values for the final model	83
3.9	Rate constants for the final model	84
3.10	ODE equations for the final model	86
3.11	-	93
	PRPPS superactivity and HGPRT deficiency simulation results	95
	Literature data for MPA treated HL60 cells	97
3.14	Metabolite concentration ranges for parameter grid search	99
4.1	HPLC gradient methods and specifications	104
B.1	HL60 cell samples used in RNAseq data analysis	153
B.2	List of purine enzyme abbreviations with corresponding gene names	153
C.1	Kinetic order values for existing reactions for model versions $1$ and $2$	160
C.2	Kinetic order values for the new interconversion reactions for model versions 1 and 2	161
C.3		161
C.4		162
C.5		163
C.6		164
D.1		165
D.2		166
D.3		167
D.4		167
D.5	, ,	167
E.1	Model eigenvalues	168

E.2	Consistency of $X_4$ and $X_8$ metabolites in the Curto <i>et al.</i> (1998b) model	178
F.1	Parameter grid search results	179
F.2	Parameter grid search large-scale simulation results	180
G.1	Metabolite concentration ranges used for HPLC calibration curves	181
G.2	HPLC calibration equations	184

## Abbreviations

#### General

AML Acute myeloid leukaemia

APL Acute promyelocytic leukaemia

ATRA All-trans Retinoic acid

BST Biochemical Systems Theory
EC number Enzyme Commission number
GEO Gene Expression Omnibus
GMA Generalised Mass Action

HPLC High performance liquid chromatography

HSC Haematopoietic stem cell

KEGG Kyoto Encyclopaedia of Genes and Genomes

MPA Mycophenolic acid

MZ Mizoribine

NAD<sup>+</sup> Nicotinamide adenine dinucleotide (oxidised) NADH Nicotinamide adenine dinucleotide (reduced)

ODE Ordinary differential equation

RA Retinoic acid

RAR Retinoic acid receptor ROS Reactive oxygen species RXR Retinoid X receptor

SBML Systems Biology Markup Language

WHO World Health Organisation

#### **Enzymes**

HGPRT Hypoxanthine-guanine phosphoribosyltransferase

IMPDH Inosine monophosphate dehydrogenase

PRPPS Phosphoribosylpyrophosphate synthetase

#### Purine metabolites

Ade Adenine Ado Adenosine

ADP Adenosine diphosphate
AMP Adenosine monophosphate
ATP Adenosine triphosphate

dAdo Deoxyadenosine

dADP Deoxyadenosine diphosphate
dAMP Deoxyadenosine monophosphate
dATP Deoxyadenosine triphosphate
dGDP Deoxyguanosine diphosphate
dGMP Deoxyguanosine monophosphate

Deoxyguanosine triphosphate

dGuo Deoxyguanosine dIno Deoxyinosine

dGTP

DNA Deoxyribonucleic acid
GDP Guanosine diphosphate
GMP Guanosine monophosphate
GTP Guanosine triphosphate

Gua Guanine
Guo Guanosine
HX Hypoxanthine

IMP Inosine monophosphate

Ino Inosine Pi Phosphate

PRPP Phosphoribosylpyrophosphate

R5P Ribose-5-phosphate RNA Ribonucleic acid

SAM S-adenosyl-L-methionine

S-AMP Adenylosuccinate

UA Uric acid Xa Xanthine

XMP Xanthosine monophosphate

# Chapter 1: Introduction

Humans have many regulatory mechanisms and systems that help the body to maintain equilibrium. If an infection occurs within the body, then specialised cells, tissues and organs collectively known as the immune system are activated to fight the infection and ultimately return the body to a steady state. The immune system can be subdivided into the innate and adaptive parts, which share a degree of overlap and synergy (Janeway and Medzhitov, 2002; Chaplin, 2010; Turvey and Broide, 2010; Yatim and Lakkis, 2015). The innate immune system is capable of generating a rapid immune response which can occur within minutes but has no lasting immunological memory (Janeway and Medzhitov, 2002; Chaplin, 2010; Turvey and Broide, 2010). In contrast, the adaptive immune response is generally slower to initiate but yields a response that is more specific and targeted against the pathogen encountered (Bonilla and Oettgen, 2010; Chaplin, 2010; Yatim and Lakkis, 2015). It also allows for the development of varying degrees of immunological memory which facilitates a quicker and more efficient response should the same pathogen be encountered in the future (Janeway and Medzhitov, 2002; Bonilla and Oettgen, 2010; Chaplin, 2010; Yatim and Lakkis, 2015). Another important function of the immune system is to monitor for abnormal or uncontrolled growth of cells, both of which can result in the development of cancer. The immune system also maintains a state of non-responsiveness to normal self components which is termed self-tolerance, but in some instances this can be disrupted resulting in the development of autoimmune disease (Janeway and Medzhitov, 2002; Chaplin, 2010).

Organs that have a role in the immune system include the spleen, bone marrow and lymph nodes, while specialised immune tissues exist within many other organs, such as the lungs (Janeway and Medzhitov, 2002; Turvey and Broide, 2010; Yatim and Lakkis, 2015). The cells of the immune system can circulate between these tissues and organs via the blood and lymphatic vessels. In addition, some immune cells are present within

peripheral tissues, whilst others are recruited to these tissues when pathogens are detected (Chaplin, 2010; Turvey and Broide, 2010; Marshall *et al.*, 2018).

The cells of the immune system can be classified as either myeloid or lymphoid but ultimately they are all derived from self-renewing haematopoietic stem cells (HSC) in the bone marrow (Chaplin, 2010). Through the process of haematopoietic differentiation, HSC give rise to both myeloid and lymphoid progenitors which generate all the cells in the myeloid and lymphoid lineages, respectively. The lymphoid lineage contains cells such as B cells, T cells and natural killer cells, whilst the myeloid progenitor gives rise to monocytes and macrophages, granulocytes, dendritic cells, erythrocytes and platelets (Chaplin, 2010). With the exception of erythrocytes and platelets, all cells formed from HSC are collectively know as leukocytes. Each type of leukocyte has specific roles within the immune system; for example B cells can produce antibodies which can neutralise pathogenic particles, whilst macrophages can ingest and destroy foreign material, in a process known as phagocytosis (Gordon, 2008; Marshall et al., 2018).

Granulocytic cells, part of the innate immune system, are so called as they contain cytoplasmic granules, the specific staining of these granules along with nuclear conformation further divides granulocytes into three subclasses: basophils, eosinophils and neutrophils (Marshall et al., 2018). The cytoplasmic granules in basophils stain with the basic dye methylene blue and they have lobed nuclei, whilst the acidic dye eosin red stains the granulocytic cytoplasm of eosinophils, which have bilobed nuclei (Stone et al., 2010). Lastly, neutrophils have granules that are stained with both acidic and basic dyes and their nuclei are multilobed. Neutrophilic maturation occurs in the bone marrow and involves the sequential progression through different immature cell types until the cell terminally differentiates into a mature neutrophil (Häger et al., 2010; Rosales, 2018). During the maturation process, granules containing different constituents are synthesised at different stages; first to appear are the primary or myeloperoxidase containing granules, followed by the secondary granules which are rich in lactoferrin, an iron-binding protein, and lastly the tertiary granules containing matrix metalloproteinases (Sheshachalam et al.,

2014; Rosales, 2018). Mature neutrophils then enter into the blood, where they are the most abundant type of leukocyte (Häger *et al.*, 2010; Rosales, 2018). However, they live for only a few days before undergoing programmed cell death and being replaced (Beutler, 2004; von Vietinghoff and Ley, 2008; Rosales, 2018).

When an infection or injury occurs the circulating neutrophils are recruited into tissues, where they perform phagocytic functions (Chaplin, 2010; Rosales, 2018). After neutrophils ingest microorganisms they kill them using one of two methods (Chaplin, 2010). Firstly, through the use of hydrolytic enzymes, contained within their cytoplasmic granules, which digest the microorganism and secondly using highly toxic reactive oxygen species (ROS) that are generated by the metabolic process respiratory burst, which occurs during phagocytosis (Beutler, 2004; Chaplin, 2010). Only terminally differentiated neutrophils are capable of phagocytosis and thus respiratory burst. This fact is utilised experimentally to determine if precursor myeloid cells have undergone full differentiation, as only terminally differentiated myeloid cells of the innate immune system can be induced to produce ROS (Goldsby et al., 2002).

Problems involving haematopoietic differentiation or the control of programmed cell death in leukocytes can lead to cancer (Hospital *et al.*, 2017). Generally, if the aberrant cells are associated with the lymph nodes or other lymphatic sites then the cancer is know as lymphoma, otherwise it is termed leukaemia (Tebbi, 2021).

#### 1.1 Leukaemia

Leukaemia is the result of dysregulation of differentiation and/or uncontrolled proliferation of precursor leukocytes from the bone marrow (Hospital et al., 2017). These immature cells, also termed blast cells, are highly proliferative and can directly result in the plethora of symptoms associated with leukaemia. When these cells are released into the blood they are unable to function in the same way as mature leukocytes, therefore leading to increased susceptibility to infection (De Kouchkovsky and Abdul-Hay, 2016; Newell and Cook, 2021). Other symptoms of leukaemia include: bleeding, bruising, fa-

tigue, weight loss and swollen lymph nodes (Shephard *et al.*, 2016). Several of these symptoms are caused by other improperly functioning blood cells, such as platelets and erythrocytes, whose proper generation and maturation has been disrupted by the large volume of leukaemic cells in the bone marrow (Döhner *et al.*, 2015; Thomas and Majeti, 2017; Newell and Cook, 2021).

Leukaemia can be classified as either chronic or acute. In the former, the disease progresses slowly often over years and symptoms are slow to develop as the aberrant leukocytes usually retain some function. However in the latter, the disease progresses very quickly with rapid onset of symptoms (CRUK, 2019).

Around 9,900 new cases of leukaemia are diagnosed every year in the UK, approximately 3 % of all cancers diagnosed annually. It is the twelfth most common form of cancer in the UK with incidence increasing with age; most cases are reported in individuals aged 80 - 85 and around 40 % of all new cases are in those aged 70 or over (CRUK, 2022). Leukaemia accounts for around 3 % of all cancer related deaths annually in the UK, with approximately 4,700 deaths each year; about 60 % of these are in patients aged 75 years and over.

There are four main types of leukaemia: Chronic lymphocytic leukaemia (CLL), Acute lymphocytic leukaemia (ALL), Chronic myeloid leukaemia (CML) and Acute myeloid leukaemia (AML) (Shephard *et al.*, 2016). The first two types involve lymphoid cells, whilst the latter two involve cells in the myeloid lineage. Myeloid leukaemia accounts for around 4,100 leukaemia diagnoses each year, with approximately 3,000 of those being the AML form (BloodCancerUK, 2019; CRUK, 2022). AML also accounts for around 2 % of all cancer deaths each year in the UK (CRUK, 2022).

### 1.2 Acute Myeloid Leukaemia (AML)

Acute myeloid leukaemia (AML) is a cancer of the precursors of granulocytes, where affected cells continually proliferate and never differentiate into the terminal granulocytic state (Hospital *et al.*, 2017). There are different mutations that give rise to the various

types of AML and research strongly suggests that these mutations can arise in either the HSC or subsequent progenitor cells of the myeloid lineage (Bonnet, 2005). As well as the differences in mutations present, leukaemic cells in AML can also exhibit differing cytological features and thus AML can be classified in different ways. Traditionally the French-American-British (FAB) classification system was used, which categorises the disease into seven subtypes based upon morphological characteristics, as outlined in Table 1.1 (Bennett et al., 1976). However with advances in genetic sequencing, the main system now adopted categorises AML based on patients' genetic markers and appears to be used more as a tool for prognostic guidance and treatment selection. This system, defined by the World Health Organisation (WHO), is detailed in Table 1.2 (Arber et al., 2016). Within this system, types 1 and 4 are further subdivided based upon specific mutation or cytology present (Arber et al., 2016).

Туре	Description
M0	Undifferentiated acute myeloblastic leukaemia
M1	Acute myeloblastic leukaemia with minimal maturation
M2	Acute myeloblastic leukaemia with maturation
M3	Acute promyelocytic leukaemia (APL)
M4	Acute myelomonocytic leukaemia
M4 eos	Acute myelomonocytic leukaemia with eosinophilia
M5	Acute monocytic leukaemia
M6	Acute erythroid leukaemia
M7	Acute megakaryoblastic leukaemia

**Table 1.1:** French-American-British AML classification.

Recently, extensive investigations have been conducted into the metabolic landscape in cancer, including in AML. Although these build on much earlier work, which showed that cancer cells switch to a heavy reliance on aerobic glycolysis for their increased energy requirements compared to healthy cells, termed the Warburg effect (Warburg et al., 1927; Warburg, 1956), the recent advances in metabolomics and our increased understanding of metabolic control through gene expression, has led to renewed interest and exploration

Туре	Description
1	AML with recurrent genetic abnormalities
2	AML with myelodysplasia-related changes
3	Therapy-related myeloid neoplasms
4	AML, not otherwise specified
5	Myeloid sarcoma
6	Myeloid proliferations related to Down syndrome

Table 1.2: World Health Organisation's AML classification.

in this area of research in AML. As well as the switch in ATP production method, AML leukaemic cells also exhibit other metabolic changes, such as increased lipid and amino acid metabolism (Dembitz and Gallipoli, 2021; Mesbahi et al., 2022). Indeed, these observations are being further investigated in both the exploration of novel drug therapies and in the analysis of patient response and/or resistance to current treatment options (Stuani et al., 2019; Grønningsæter et al., 2020; Dembitz and Gallipoli, 2021; Kim et al., 2021; Lo Presti et al., 2021). In the former, new drugs have been licensed for use in the treatment of AML (Stuani et al., 2019; Dembitz and Gallipoli, 2021). Whilst in the latter, the observed correlation between certain altered metabolic states and poor prognostic outcome has raised the possibility of incorporating additional drugs, which specifically target this dysregulated metabolism, into current therapeutic regimes (Rashkovan and Ferrando, 2019; Grønningsæter et al., 2020; Dembitz and Gallipoli, 2021; Kim et al., 2021; Lo Presti et al., 2021).

Whilst this area of research is gaining momentum, it may be some time before the full benefits will be seen in the clinic. As such, standard chemotherapeutic protocols using cytotoxic drugs are currently used in the treatment of most forms of AML. However, more specific, targeted therapies are used for certain types of the disease, especially in one particular form of the disease called Acute promyelocytic leukaemia (Roboz, 2012).

#### 1.3 Acute Promyelocytic Leukaemia (APL)

Acute promeylocytic leukaemia (APL) was first identified as a distinct form of AML in the 1950s and was associated with an extremely poor prognosis and a rapidly progressive disease course (Hillestad, 1957; Thomas, 2019). Patients exhibit a propensity for severe bleeding, blood clots, increased susceptibility to infection, fatigue and weight loss (Hillestad, 1957; BloodCancerUK, 2019). APL is rare and accounts for around 10 % of all AML cases (Zelent et al., 2001). It is listed as subtype M3 in the FAB based system of classification whilst it is encompassed by type 1 'AML with recurrent genetic abnormalities' in the WHO system under the specific subdivision: APL with PML-RARA (Bennett et al., 1976; Arber et al., 2016). As such it is a specific form of AML with a well characterised genetic mutation. The mutation typically involves the translocation of chromosome 17q12; specifically within the Retinoic acid receptor  $\alpha$  (RARA) gene (Kondo and Sasaki, 1979; Mitelman, 1983b; de Thé et al., 1990; Alcalay et al., 1991). RARA encodes for the well characterised nuclear receptor and transcription factor RARa (Petkovich et al., 1987). RARα is a member of the Retinoic acid receptor family, which bind to DNA as heterodimers with members of another nuclear receptor family: Retinoid X receptors (RXR) (Yu et al., 1991; Leid et al., 1992; Kastner et al., 1995). The RARα-RXR complex binds DNA and, in the absence of ligand, recruits transcriptional co-repressors which suppress transcriptional activity of the target genes. However, upon binding of Retinoic acid (RA) derived ligands, conformational changes within the proteins occur which result in the dissociation of the co-repressors and recruitment of transcriptional coactivators, thus facilitating transcription (Dilworth and Chambon, 2001). Downstream targets of Retinoic acid signalling include p21<sup>CIP1/WAF1</sup>, which is an inhibitor of cyclin dependent kinases resulting in cell cycle arrest, and the transcription factors PU.1 and C/EBPa, which are crucial for myeloid development (Harper et al., 1993; Lawson and Berliner, 1999; Tasseff et al., 2017). PU.1 and C/EBP $\alpha$  are essential for the acquisition of phenotypic characteristics of mature myeloid cells as they induce the expression of

proteins such as p47-phox, which is critical for the respiratory burst process, and CD11b (Jackson *et al.*, 1995; Lawson and Berliner, 1999; Tasseff *et al.*, 2017). The key features of RAR $\alpha$  function in myeloid development are shown in Figure 1.1.

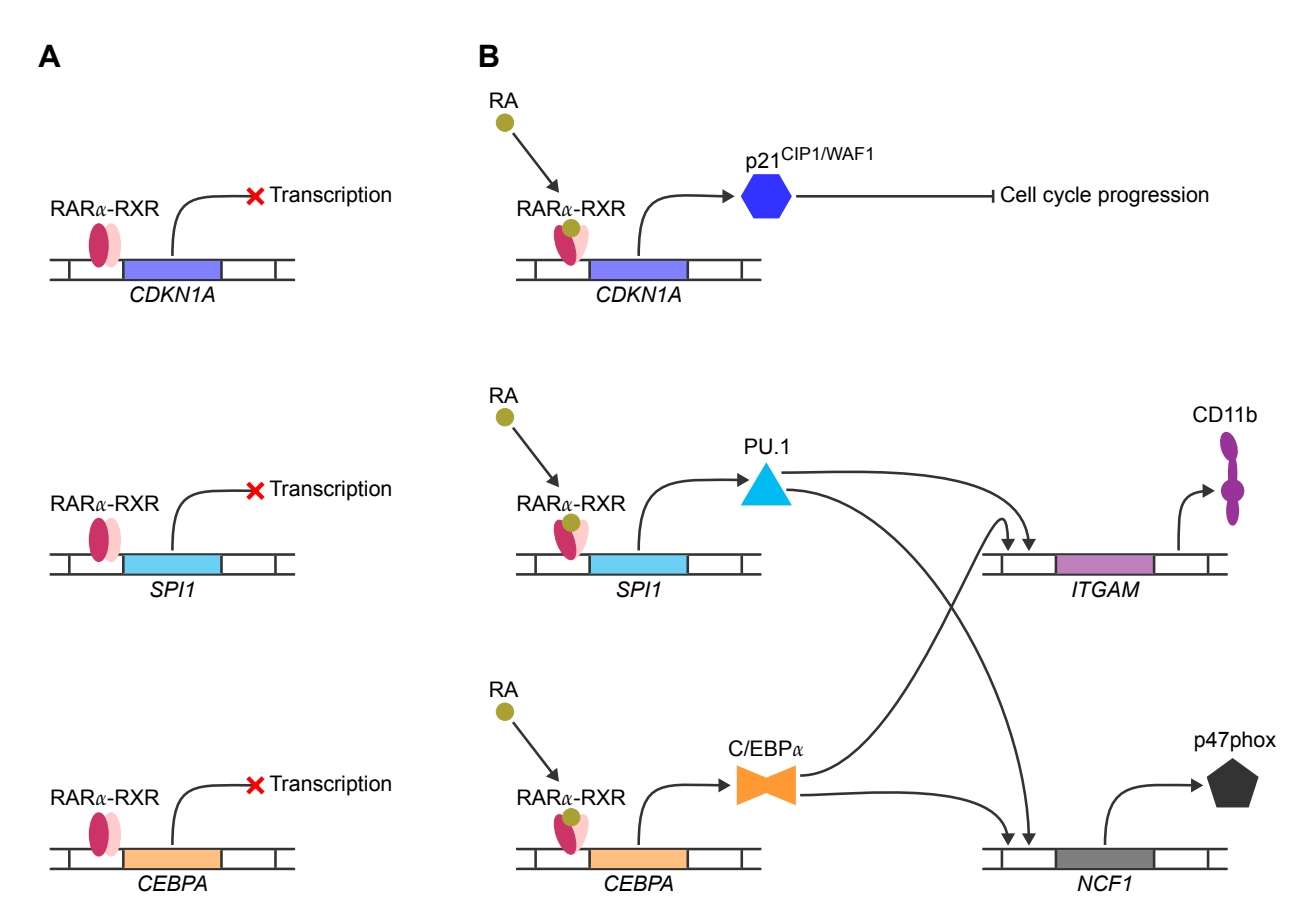


**Figure 1.1:** Retinoic acid signalling in myeloid cell development. Retinoic acid receptor  $\alpha$  (RAR $\alpha$ ) binds DNA in conjunction with Retinoid X receptor (RXR). In the absence of Retinoic acid (RA) derived ligands, the RAR $\alpha$ -RXR complex binds co-repressor proteins which suppress transcription of RA responsive genes (A). The addition of RA results in conformational changes, the dissociation of co-repressors and the recruitment of co-activators, resulting in the transcription of RA responsive genes such as *CDKN1A*, *SPI1*, and *CEBPA*; which encode p21<sup>CIP1/WAF1</sup>, PU.1, and C/EBP $\alpha$ , respectively; this leads to the cessation of proliferation and subsequent differentiation into mature myeloid cells (B).

In the majority of cases, the other chromosome involved in the translocation is chromosome 15; specifically at a locus within 15q22, the gene at this site being termed myl or more recently PML, for promyelocytic leukaemia (Kondo and Sasaki, 1979, 1982; Mitelman, 1983a,b; Borrow  $et\ al.$ , 1990; de Thé  $et\ al.$ , 1990). This translocation results in a

fusion gene between PML and RARA which is transcribed and translated to yield an aberrant fusion protein, PML-RAR $\alpha$  (de Thé et al., 1990; Kakizuka et al., 1991). In addition, alternative splice variants of PML-RARA are generated which encode aberrant PML proteins lacking the C-terminal regions (Pandolfi et al., 1992). The translocation also results in the reciprocal RARA-PML fusion gene in most patients (Alcalay et al., 1992). The relative importance of these different aberrant proteins is unclear but mice genetically modified to express the PML-RAR $\alpha$  fusion protein in cells of the myeloid lineage develop leukaemia suggesting that this is an important component of leukaemogenesis in APL patients (Grisolano et al., 1997; He et al., 1998; Westervelt et al., 2003).

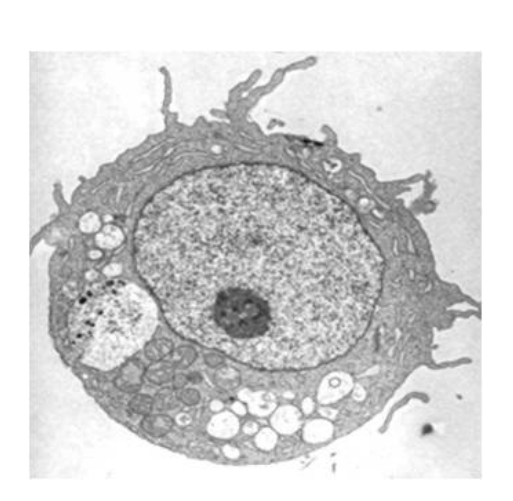
The PML-RAR $\alpha$  protein is still able to form heterodimers with RXR but can also homodimerise; both of these types of dimers are able to bind DNA and modulate transcription of RAR target genes (de Thé et al., 1991; Kakizuka et al., 1991; Kastner et al., 1992; Perez et al., 1993). PML-RAR $\alpha$  suppresses endogenous RAR transcriptional activity, implying that the fusion protein acts as a transcriptional repressor at physiological levels of RA (Kakizuka et al., 1991). However, addition of exogenous high dose RA is able to induce RAR transcriptional activity, suggesting that PML-RAR $\alpha$  can still function as an activating transcription factor (de Thé et al., 1991; Kakizuka et al., 1991).

More recently alternative translocation partners for chromosome 17 have been identified in patients with an APL-like phenotype, however these only account for a tiny fraction of cases (Liquori et al., 2020). It has been shown that some of these variants respond to the standard treatment for APL, whilst others do not and it would appear that these new variants are not covered by the WHO classification of APL (Arber et al., 2016; Liquori et al., 2020). Indeed, the WHO updated their definition of APL in 2016 to remove the previous reference to 't(15:17)q(22,12)' as some patients do not have this classical chromosomal translocation but, via complex chromosomal rearrangements or other mechanisms, still have the PML-RAR $\alpha$  fusion protein (Arber et al., 2016). Thus, this new definition of 'APL with PML-RAR $\alpha$ ' highlights the importance of the PML-RAR $\alpha$  fusion protein in determining prognosis and treatment protocols.

The most common treatment given for APL is All-trans Retinoic acid (ATRA), which is an activating ligand for RAR proteins (Petkovich et al., 1987). The addition of ATRA results in removal of the transcriptional block produced by the PML-RAR $\alpha$  fusion protein thereby facilitating differentiation (Kakizuka et al., 1991; He et al., 1998). ATRA treatment can be given in conjunction with chemotherapy but more recently it has been used alongside arsenic trioxide (ATO) which appears to act on the PML portion of the fusion protein (Zhu et al., 2001). These more tailored therapies have revolutionised APL treatment and significantly improved prognosis. This form of AML is now considered to be the most curable, with 80-100 % of patients cured when given a combination therapy comprising either ATRA + ATO or ATRA + chemotherapy (Thomas, 2019). Although ATRA is used clinically to treat APL, 2-48 % of patients develop a life-threatening condition known as differentiation syndrome which is believed to be caused by an inflammatory response induced by the differentiating leukaemic cells (Lo-Coco et al., 2008; Stahl and Tallman, 2019; Thomas, 2019). In addition, resistance to ATRA can develop and some of the alternative chromosomal variants are insensitive to this treatment (Gallagher, 2002; Liquori et al., 2020). Taken together, these observations signal the need for the identification of other drugs that could be used in conjunction with ATRA or as an alternative therapy for the treatment of APL.

#### 1.3.1 The HL60 cell line

Several human cell lines have been isolated from patients with different forms of AML (Sak and Everaus, 2016) which are used to study the disease *in vitro*, one such example is the HL60 cell line (Collins *et al.*, 1977; Gallagher *et al.*, 1979). These cells were isolated from a patient who was diagnosed with APL, thus according to the FAB system, available at the time, she was classified as having subtype M3 (Collins *et al.*, 1977; Gallagher *et al.*, 1979). Cytologically, HL60 cells have large rounded nuclei and numerous myeloperoxidase positive cytoplasmic granules (see Figure 1.2, left panel); features usually seen in progranulocytes (Gallagher *et al.*, 1979).



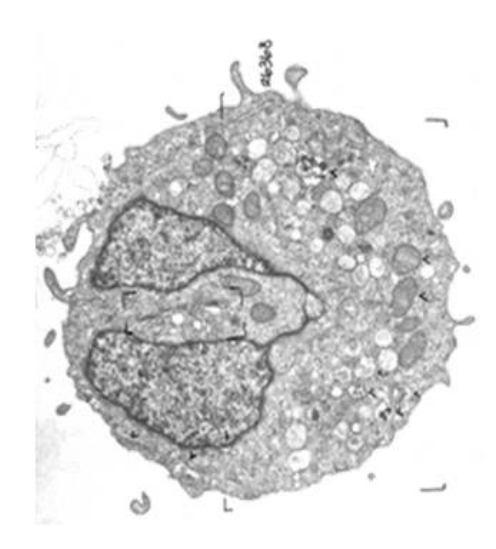


**Figure 1.2:** HL60 cells before and after differentiation. Cells were treated with ATRA (right panel) or left untreated (left panel) and visualised using a transmission electron microscope. Photomicrographs courtesy of G. Thomas.

However, more recently the M3 classification has been questioned as HL60 cells lack some of the other typical characteristics of this subgroup; namely, other morphological features and crucially the t(15:17) chromosomal translocation (Gallagher et al., 1979; Dalton et al., 1988). It has therefore been proposed that HL60 cells did in fact originate from a cancer of the M2 subtype (Dalton et al., 1988) and is thus an AML cell line. Indeed, under the WHO's classification these cells would not be classified as APL as they lack the PML-RARA fusion gene. Nevertheless, the HL60 cell line is similar to APL in one very important respect: it responds to the usual treatment for APL, ATRA (Breitman et al., 1980). So, regardless of their exact origin, HL60 cells can be induced to differentiate in vitro through the addition of ATRA into cells resembling terminally differentiated neutrophils, which show morphological and phenotypic characteristics of this cell type (see Figure 1.2, right panel). Hence for the purpose of this thesis, HL60 cells will be regarded as an APL cell line and used as a model for the examination of the differentiating effects of ATRA and other potential drugs on APL.

It has been shown that ATRA driven differentiation in HL60 cells brought about a decrease in activity of a key enzyme in purine metabolism: inosine monophosphate dehydrogenase (IMPDH) (Knight *et al.*, 1987). Furthermore, other drugs have been

shown to induce HL60 cell differentiation; one such class being IMPDH inhibitors (Lucas et al., 1983a,b; Sokoloski et al., 1986; Inai et al., 2000). These findings suggest a possible link between HL60 cell differentiation and the purine metabolic network that could be exploited in the development of new targeted therapies for AML.

#### 1.4 Purines and their metabolism

Purines are vital cellular components found in all cells. As well as providing the building blocks for nucleic acids, purines are involved in myriad processes and functions including cell signalling, protein modification, as well as energy exchange. The two purine bases, adenine and guanine, are heterocyclic compounds composed of both a six and a five carbon ring but with different side groups, see Figure 1.3. The addition of a ribose group in position 9 creates the nucleosides adenosine and guanosine. These ribose groups can be phosphorylated up to three times generating the nucleotides adenosine/guanosine mono/di/tri-phosphate.

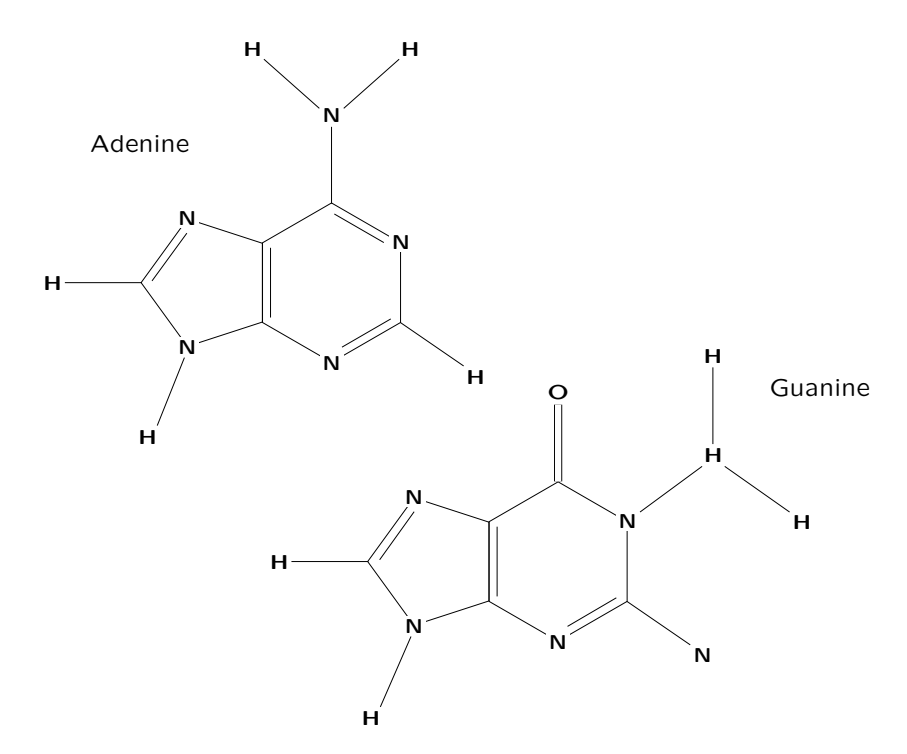


**Figure 1.3:** Chemical structures of adenine and guanine.

The purine metabolic network involves both the creation of all the nucleotides and their degradation along with the production and removal of ribonucleic acid (RNA) and deoxyribonucleic acid (DNA) and the generation of uric acid (UA) which is ultimately excreted from the body as urea in urine. The network consists of two pathways for the generation of nucleotides: the *de novo* and salvage pathways (see Figures 1.4 and 1.5, respectively). In the former, nucleotides are formed from small metabolites such as ribose-5-phosphate (R5P) and phosphoribosylpyrophosphate (PRPP) through a series of 10 reactions, the product of which is inosine monophosphate (IMP) which is then converted to either AMP or GMP; both via a two step process. Whereas in the latter, the free bases, adenine and guanine are salvaged to directly form AMP and GMP, respectively.

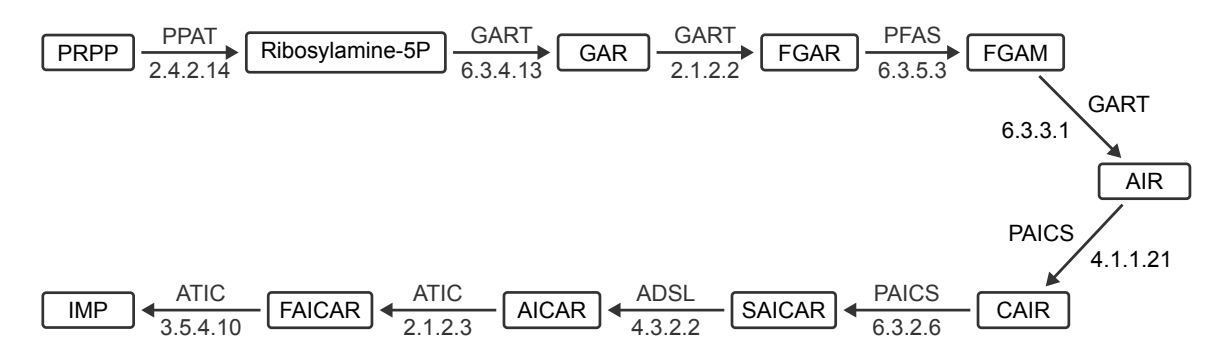


**Figure 1.4:** The *de novo* pathway of purine metabolism. Schematic based on the network from KEGG Kanehisa and Goto (2000). Abbreviated metabolite names (boxes), enzyme gene symbols and Enzyme Commission numbers are shown.



**Figure 1.5:** The adenine and guanine salvage pathways of purine metabolism. Schematic based on the network from KEGG Kanehisa and Goto (2000). Abbreviated metabolite names (boxes), enzyme gene symbols and Enzyme Commission numbers are shown.

There are many inherited diseases that affect individual enzymes within the network and cause dysregulation of purine metabolism. These illnesses range in severity from mild to life-threatening and involve numerous systems and organs of the body, including the immune system, brain and liver. The wide spectrum of symptoms include: muscle weakness, myalgia, deafness, gout, immunodeficiency, liver and kidney problems, mental & psychomotor retardation, seizures and premature death (Balasubramaniam et al., 2014).

The crucial nature of purines, and thus their metabolism, coupled with the multitude of diseases that can occur due to their metabolic dysregulation, has meant that purines and their metabolism have been extensively studied (Hartman and Buchanan, 1959; Murray, 1971; Balasubramaniam et al., 2014). Indeed, several mathematical models covering specific aspects of purine metabolism have been developed to further aid our understanding of this complex system (Frank Starmer et al., 1975; Franco and Canela, 1984; Heinmets, 1989; Bartel and Holzhütter, 1990; Curto et al., 1998b). Of particular note are the models created by Curto et al. (1997, 1998a,b), which are whole body representations of the purine metabolic network in humans, that have been used to study certain diseases of purine metabolism in silico (Curto et al., 1998a).

#### 1.5 Inosine monophosphate dehydrogenase (IMPDH)

As mentioned earlier, the final product of the 10 step *de novo* pathway is IMP, which is then converted into either AMP or GMP. For GMP synthesis, the next reaction converts IMP to xanthosine monophosphate (XMP) and is catalysed by the enzyme inosine monophosphate dehydrogenase (IMPDH). As this reaction is the rate limiting step in committed guanylate *de novo* synthesis, IMPDH is a crucial enzyme within the purine metabolic network. The reaction catalysed by IMPDH is as follows:

$$IMP + NAD^{+} + H_{2}O \xrightarrow{IMPDH} XMP + NADH + H^{+}$$

The enzyme kinetics for this reaction follow an ordered Bi-Bi mechanism; with the substrate IMP binding first followed by NAD<sup>+</sup> and the products dissociating in the order NADH followed by XMP (Carr *et al.*, 1993). GMP inhibits the reaction in a competitive way with respect to IMP binding and XMP also exhibits product inhibition, again competing with the substrate IMP (Holmes *et al.*, 1974). Other purines also inhibit but with

much less effect; thus in the mathematical models created by Curto *et al.* (1998b) only GMP inhibition was included in the reaction dynamics for IMPDH (Holmes *et al.*, 1974; Curto *et al.*, 1998b).

The enzyme IMPDH appears to be present in most organisms, with the exception of a couple of protozoan species (Hedstrom, 2009). Crystal structures of IMPDH revealed a tetrameric structure, with each of the four monomers having, in most species, two domains. The larger of the two domains is the catalytic component, comprising of an  $(\beta/\alpha)_8$  barrel, whilst the smaller regulatory domain is termed a Bateman domain and contains two CBS sequence motifs, so called as they are similar to that found in the cystathionine beta synthase enzyme (Goldstein *et al.*, 2003; Hedstrom, 2009).

It has been shown that two isoforms of IMPDH exist in humans: type I and type II (Natsumeda et al., 1990). The two isoforms are highly homologous, having 84 % protein sequence identity (Natsumeda et al., 1990). Importantly, the kinetic parameters for the metabolites involved in the reaction catalysed by IMPDH (namely, the substrates IMP & NAD and the inhibitors XMP & GMP) are similar for both isoforms (Carr et al., 1993).

Although kinetically similar, the expression patterns for the two isoforms differ. Type I appears to be constitutively expressed, whereas type II expression is more variable (Natsumeda et al., 1990; Konno et al., 1991). It has been shown that type II is upregulated in many tumour cells and leukaemic cells compared to normal control tissue, with samples from patients with AML having one of the highest levels of the leukaemic cells tested (Konno et al., 1991; Nagai et al., 1991, 1992). It therefore appears that type II is up-regulated in proliferating cells and moreover, it has been shown that levels of IMPDH type II expression decrease upon differentiation of leukaemic cells, leaving type I as the predominant isoform in differentiated cells (Nagai et al., 1992). Furthermore, this up-regulation of IMPDH type II also holds for certain leukaemia cell lines including HL60 cells (Konno et al., 1991). Finally, the up-regulation of type II correlated with increased activity of IMPDH in leukaemic cells, implying that the enhanced expression of type II is responsible for the increased IMPDH activity (Nagai et al., 1991).

#### 1.6 IMPDH inhibitors

Due to its importance within the purine metabolic network and the strong correlation between cellular proliferation and IMPDH activity, therapeutic targeting of IMPDH has been extensively investigated (Jackson et al., 1975; Shu and Nair, 2008; Cuny et al., 2017). It has been shown that interference with this enzyme impairs proliferation of various cell types, including lymphocytes as well as leukaemia cell lines such as HL60 cells (Lucas et al., 1983a; Eugui et al., 1991). Highly proliferative cells, such as lymphocytes and cancer cells, have a higher requirement for guanylates which cannot be adequately met through the salvage pathway alone and thus they have a higher dependence on de novo synthesis of purines (Allison and Eugui, 2000; Hedstrom, 2009). As such, relative reliance on de novo versus salvage generation of nucleotides determines the extent to which cells and tissues are susceptible to IMPDH inhibitors (Hedstrom, 2009).

Various drugs have been isolated or synthesised that inhibit the catalytic function of IMPDH; most are nucleoside analogues and several are used clinically in the treatment of various diseases (Hedstrom, 2009; Cholewiński *et al.*, 2015; Cuny *et al.*, 2017).

Tiazofurin, synthesised in 1977, has antiviral and anticancer properties against solid cancers as well as leukaemias and was classified as an orphan drug in the USA for the treatment of Chronic myelogenous leukemia, although severe potential side-effects limits its use (Srivastava et al., 1977; O'Dwyer et al., 1984; Tricot et al., 1989; Hedstrom, 2009).

Ribavirin, another synthetic IMPDH inhibitor, shows even greater antiviral properties than Tiazofurin (especially against DNA and RNA viruses) and for many years was the main treatment for chronic Hepatitis C infection in combination with interferon  $\alpha$ . However, due to the side-effects of this regimen and the development of more specific Hepatitis C therapies its usage has become more limited (Sidwell *et al.*, 1972; Schalm *et al.*, 1997; Mathur *et al.*, 2018).

Mizoribine (MZ), first isolated from *Eupenicillium brefeldianum*, is licenced for use in Japan as a treatment for certain autoimmune diseases such as rheumatoid arthritis

and as an immunosuppressive agent for organ transplant rejection therapy, due to its targeted suppression of *de novo* purine synthesis; the predominant production method in lymphocytes (Goldstein *et al.*, 2003; Ishikawa *et al.*, 2003; Pankiewicz and Goldstein, 2003; Shu and Nair, 2008).

Mycophenolic acid (MPA), originally isolated from a type of *Penicillium* over 100 years ago, (Bentley, 2000) is also used clinically to prevent transplant rejection (Hedstrom, 2009; Cholewiński *et al.*, 2015). Kinetic data for MPA suggests that IMPDH type II is around four-fold more sensitive to this inhibitor than IMPDH type I (Carr *et al.*, 1993). This opened up the possibility of using MPA in the treatment of certain cancers, especially leukaemia, as these drugs would be more targeted towards neoplastic cells due to their increased expression of IMPDH type II and it would be hoped that, due to their more limited effect on healthy cells, side effects would be more limited. Furthermore, studies showed that MPA resulted in differentiation of leukaemia cell lines, including HL60 cells (Lucas *et al.*, 1983a; Inai *et al.*, 2000). However, metabolism of MPA *in vivo* involves glucuronidation to Mycophenolic acid glucuronide, an inactive form of the drug which is unable to penetrate cell membranes (Sweeney *et al.*, 1972; Bullingham *et al.*, 1998). This has therapeutic importance as certain tumour cells have higher glucuronidation abilities or lower  $\beta$ -glucuronidase activities thus affecting the drugs efficacy in these settings (Sweeney *et al.*, 1971; Hedstrom, 2009).

Recently a novel modified IMPDH inhibitor, called FF-10501-01, was developed that inhibited proliferation and induced apoptosis in AML patient samples *in vitro* and also resulted in partial remission in a phase 1/2a clinical trial (Yang *et al.*, 2017; Garcia-Manero *et al.*, 2020). However, as with other IMPDH inhibitor therapies, undesirable side-effects were reported which ended the trial (Garcia-Manero *et al.*, 2020).

Therefore, despite a plethora of potential clinical uses of IMPDH inhibitors as antiviral and anticancer therapies, their use has been limited due to the unfavourable side-effects of some and/or the *in vivo* inactivation of others which has led to concerted efforts to develop modified IMPDH inhibitors that are free from these undesirable properties (Pankiewicz

#### 1.6.1 Mechanism of action of IMPDH inhibitors

The mechanism by which IMPDH inhibitors result in cellular differentiation is still not fully understood, however it is believed that the resultant reduction in guanylate levels upon inhibition is important (Lucas et al., 1983a; Sokoloski et al., 1986). This is supported by evidence that shows that the addition of an exogenous source of guanosine at the time of IMPDH inhibitor treatment, prevents the differentiating capabilities of IMPDH inhibitors in leukaemia cell lines (Sokoloski et al., 1986; Inai et al., 1997). This effect appears to be due to the recycling of guanosine through the salvage pathway to form GMP, thus rescuing cellular guanylate levels. Indeed, cells genetically deficient in the HGPRT salvage enzyme still differentiate upon treatment with both IMPDH inhibitors and guanosine (Sokoloski et al., 1986), supporting the theory that guanylate levels are key in determining cell fate upon IMPDH inhibition.

In *Drosophila melanogaster*, IMPDH has been found to also act as a transcription factor, repressing expression of genes required for proliferation (Kozhevnikova *et al.*, 2012). In human studies, IMPDH has been found to localise to the nucleus, with nuclear localisation increased upon treatment with IMPDH inhibitors (Juda *et al.*, 2014). Thus it is possible that IMPDH may also act as a transcription factor in humans, but this has not yet been investigated experimentally. In *Drosophila melanogaster*, MPA treatment did not affect the transcriptional repressor activity of IMPDH, suggesting that transcriptional activity is unlikely to explain the effects of IMPDH inhibition on cellular differentiation (Kozhevnikova *et al.*, 2012). Furthermore, the ability of guanosine supplementation to counteract IMPDH inhibitors, strongly suggests that the mechanism underlying IMPDH inhibitor driven differentiation is related to purine nucleotide levels.

#### 1.6.2 Differentiation of HL60 cells by IMPDH inhibitors

Whilst it has been shown that IMPDH inhibitors cause HL60 cells to cease proliferation and differentiate into granulocytes, precisely how these drugs achieve these effects is un-

known (Lucas et al., 1983a; Sokoloski et al., 1986). In addition to IMPDH inhibitors, various other agents can induce differentiation in HL60 cells in vitro, some of these act on the purine metabolic network whilst others have distinct modes of action. The folate metabolism inhibitor 5,10-dideazatetrahydrofolic acid (DDATHF) inhibits glycinamide ribonucleotide transformylase (a reaction in the de novo purine synthesis pathway) (Sokoloski et al., 1989), whilst deazaguanosine is another IMPDH inhibitor and 6-mercaptopurine inhibits both IMPDH and PRPP amidotransferase; the first step in the de novo pathway (Chiang et al., 1984; Elgemeie, 2005). Although other HL60 cell differentiating agents, such as ATRA; dimethyl sulphoxide (DMSO); and 3-deaza-(+/-)-aristeromycin, work on cellular processes distinct from purine metabolism, they still cause a decrease in GTP levels (Lucas et al., 1983a; Chiang et al., 1984; Aarbakke et al., 1986; Pilz et al., 1997). Thus cellular levels of guanylates appear to be an important common factor in HL60 maturation, regardless of differentiating agent and/or mechanism.

Furthermore, studies have been conducted that examined the effect of the IMPDH inhibitors MPA and MZ on certain nucleotide levels. It has been shown that MPA affects the levels of GTP, ATP to a lesser extent, and possibly GDP, whereas MZ affects levels of GTP (Lucas et al., 1983a; Sokoloski et al., 1986; Inai et al., 1997). Taken together with the aforementioned differentiation experiments involving the addition of exogenous guanosine and those involving the HGPRT deficient HL60 cell line, these results imply that it is the decrease in intracellular guanylate levels that results in maturation of HL60 cells upon treatment with IMPDH inhibitors. However, the range of purines examined is somewhat limited and thus it still remains unclear if it is the exact level of GTP or its concentration relative to other metabolites (e.g. the GTP:GDP ratio) that causes HL60 cells to differentiate after treatment with IMPDH inhibitors. Therefore, a more comprehensive examination of purine concentrations in HL60 cells treated with either MPA or MZ, seemed like a prudent next step to further increase our understanding of IMPDH inhibitor driven differentiation in this APL cell line.

# 1.7 Principles of High performance liquid chromatography (HPLC)

One method for monitoring the levels of purines in cells is High performance liquid chromatography (HPLC). This uses the principles of liquid chromatography, which involves both a mobile (liquid) and stationary phase (McMaster, 2007a). A mixture of molecules is dissolved in the liquid phase and they are separated based on their relative mobility as they pass through the stationary phase (McMaster, 2007a). Conventionally, the stationary phase consists of particles contained within a column. However as noted by Martin and Synge (Martin and Synge, 1941), better column efficiency can be achieved by using smaller beads, with a higher pressure. This is the inherent principle of HPLC, which operates at higher pressures in order for the mobile phase to pass through the stationary phase that is comprised of very small uniform particles (Nesterenko and Palamareva, 2019). This allows for the separation of more species in a faster time compared to standard column chromatography (McMaster, 2007a; Meyer, 2010).

After an analyte is eluted from the stationary phase it passes through a detector which records the signal from that metabolite. These signals, or peaks, provide both qualitative and quantitative information, and collectively the peaks from all analytes generate a chromatogram for the sample (Meyer, 2010).

One of the most amenable types of HPLC is Reversed-phase liquid chromatography (RP-HPLC) in which the mobile phase is polar, whilst the stationary phase is a non-polar bonded silica. The mobile phase consists of a polar organic solvent in an aqueous buffer, whilst the most commonly used stationary phase is an 18-carbon silane (Meyer, 2010; Soliven et al., 2013). A gradient method is usually used with this form of HPLC, such that the concentration of organic solvent is increased over time, thus decreasing the polarity of the mobile phase (Meyer, 2010). The analytes bind to the octadecylsilane coated surface of the stationary phase and as the polarity of the mobile phase decreases the metabolites detach from the stationary phase and are eluted (McMaster, 2007a; Meyer,

2010).

An amendment to RP-HPLC that is particularly useful when acids, bases and neutral analytes are all present in a sample, is the addition of an ion-pair reagent (Meyer, 2010). This type of compound has one hydrophobic end which binds to the non-polar stationary phase, whilst the other end of the molecule is charged and sticks outwards from the stationary phase into the mobile phase where it can interact with the metabolites (García-Alvarez-Coque et al., 2015). The exact mechanism of analyte retention in ion-pair RP-HPLC is unclear (McMaster, 2007b), but metabolites elute depending upon the strength of their interaction with the ion-pair reagent.

Ion-pair RP-HPLC is the technique most often used for the study of mixtures of nucleotides as they are very hydrophilic, charged molecules (Werner et al., 1989; Huang et al., 2003). The ion-pair reagent binds to the phosphate group, with more reagent binding the greater the number of phosphates present, thus nucleotides elute in order of increasing phosphate number. The ion-pair reagent most often used for nucleotide separation is Tetrabutylammonium hydrogen sulphate (TBAHS), with compound elution achieved via a gradient method with increasing methanol concentration. Compounds are detected using a UV detector; with wavelength set at 254 nm, the wavelength at which the heterocyclic bases of purines characteristically absorb light.

#### 1.8 Rationale and aims

Theoretically, other compounds that induce the differentiation of HL60 cells, or other AML cell lines, could also be efficacious in AML treatment. IMPDH inhibitors are one such drug that has been shown to induce HL60 cell differentiation (Lucas et al., 1983a,b; Sokoloski et al., 1986). Experimentation that provides a more accurate picture of cellular purine levels upon IMPDH inhibitor driven differentiation is a valuable step in furthering our understanding of how these drugs cause HL60 cell maturation. However, purine metabolism is a complex system involving numerous feedback mechanisms and thus experimentally obtained data of nucleotide and nucleoside levels may be difficult to

interpret within this metabolic context. I therefore decided to use a mathematical model of purine metabolism in conjunction with these experimentally derived data of purine levels to facilitate a greater understanding of this differentiation process.

# Chapter 2: Mathematical Introduction

Mathematics has been used in the study of biology for centuries and the development of specific tools and methodologies has helped facilitate a better understanding of these complex processes and systems. However, when adopting a mathematical modelling approach to a biological problem it is initially worth spending time to consider the main purpose of, and expected outcome from, the model, so that it is a worthwhile endeavour. Model choice should be carefully considered, as many different modelling frameworks exist, e.g. stochastic or deterministic; continuous or discrete, etc., each aspect of which will be able to better capture certain behaviours within a biological system and their combined use will produce a specific model output. Once a suitable model type has been chosen, an assessment of the underlying biological system should be undertaken to determine which parts are of most interest and should thus be included in the model explicitly, if possible. The use of assumptions and simplification forms the next important step in model creation, as any mathematical representation of a biological system will be unable to account for the myriad complex dynamics and behaviours inherent to the biology. This is a balancing act, where assumptions and simplifications are chosen so that the model can be as realistic as possible, whilst still being able to produce useful outputs. This is because, a model that is very realistic but so complicated that its output cannot be interpreted in terms of the biology is as unhelpful as a model that is so simplistic that its output provides no further insight into the underlying biology. Thus, correct model choice and construction is an important part of the model building process to ensure that the framework adopted can provide a realistic representation of the system and that the output produced is useful and can be interpreted within the context of the biology being modelled.

A common feature of many mathematical descriptions of biology is ordinary differential equations, which provide an appropriate representation for a very diverse range of biological phenomena. In addition, these mathematical systems have the advantage that there exist many analytical tools and computer programs that can be used in their analysis.

# 2.1 Ordinary differential equations (ODE)

Differential equations are used to describe how one variable changes relative to another, for example dX/dY = F(X,Y) which denotes the change in variable X relative to variable Y and is determined by a function involving both X and Y. Their use is ubiquitous throughout science, where they are used to describe many physical and biological processes e.g. motion, fluid mechanics and disease modelling.

If Y is replaced by time, t, then dX/dt, also written as  $\dot{X}$ , allows for the examination of variable X over time. A set of such equations, e.g.  $\dot{X}_i = F(X_1, X_2, ..., X_n, t)$ ; i = 1, 2, ..., n, can be established, where the rate of change of each variable is determined by its interaction with all other variables. Moreover, taken together this set allows the collective behaviour of the whole system of variables to be described over time. If, for example,  $X_i$  represent population sizes or metabolic concentrations (which are quantities that are often most usefully studied over time) then it is clear to see how differential equations offer us a framework for the mathematical examination of multivariable biological systems, such as metabolic networks, and their evolution over time.

## 2.2 Reaction kinetics

The mathematical study of enzyme-catalysed reactions dates back to the early twentieth century when it was realised that our understanding of these systems was being limited by the amount of information that could be obtained through experimentation alone (Henri, 1903; Michaelis and Menten, 1913; Johnson and Goody, 2011). Therefore, quantitative models of these systems were posited as a useful tool for furthering our understanding of this area. These mathematical representations would allow for certain kinetic quantities to be estimated that would otherwise be difficult or impossible to obtain. Initial work in

this area built upon the theories and methodologies used in the field of chemistry and in particular the The Law of Mass Action.

#### 2.2.1 Mass action

The theory of mass action was introduced by Waage and Gulberg in 1864 via their work on the formation of esters from acids and alcohols (Waage and Gulberg, 1986). Contrary to prevailing theories at the time, which proposed that molecular affinities were the driving force for the progression of reactions, Waage and Gulberg theorised that the rate of reaction also depends upon the concentrations of the substances involved (Waage and Gulberg, 1986; Voit et al., 2015), thus giving rise to the following law:

The Law of Mass Action. The rate of change of the concentration of a product is proportional to the product of the concentrations of the substrates that produce it.

So, for example, given a simple reaction that involves two substrates, A and B, that combine to produce one product, C, i.e.:

$$A + B \rightarrow C$$

then the rate of change in the concentration of product, C, is defined as:

$$\frac{d[C]}{dt} = k[A][B]$$

where [Y] = denotes the concentration of species Y k = is the rate constant

The Law of Mass Action can also be mathematically derived from thermodynamic principles, whereby the progress of the reaction is considered in terms of the probability of the two metabolites colliding and having the necessary energy required to participate in the reaction (Koudriavtsev et al., 2001; Savageau, 2009; Voit et al., 2015). The Law of Mass Action is applicable to both (enzyme) catalysed and uncatalysed reactions and for

simple systems or parts of systems a mass action representation can be sufficient. However for more complicated systems, such as enzyme-driven reactions, more tailored alternatives have been derived. These alternatives were created so that the specific reactants and more complex kinetic interactions inherent to enzyme-catalysed reactions, such as the enzyme species itself and reaction modifiers, could be modelled more explicitly, in an attempt to better capture the underlying dynamics of these systems. A well known and very commonplace example being the Michaelis-Menten equation.

### 2.2.2 Michaelis-Menten equation

The seminal work of Michaelis and Menten in 1913 (Michaelis and Menten, 1913; Johnson and Goody, 2011) built on the earlier work of Henri in 1903 (Henri, 1903) and together with the work of Briggs and Haldane in 1925 (Briggs and Haldane, 1925) led to the derivation of one of the most widely used equations in biochemical reaction kinetics; the Michaelis-Menten equation. Taking the simplest version of an enzyme-catalysed reaction; whereby a substrate, S, is converted to a product, P, by enzyme, E, and using the principle that an intermediate complex, known as the enzyme-substrate complex, ES, is formed during this reaction; gives rise to the following reaction scheme:

$$S + E \xrightarrow[k_{-1}]{k_1} ES \xrightarrow{k_2} E + P$$

where  $k_i = \text{rate constant for reaction } i; i = 1, 2$ 

The formation of product P is considered to be irreversible, whilst the formation of ES is defined as reversible; thus  $k_{-1}$  is the rate constant for the backwards part of reaction 1 and  $k_1$  is the rate constant for the forward part of this reaction. Using the The Law of Mass Action, equations for the rate of change of each species in the above reaction can be defined as follows:

$$\frac{d[S]}{dt} = -k_1[E][S] + k_{-1}[ES]$$
 (2.1a)

$$\frac{d[E]}{dt} = -k_1[E][S] + (k_{-1} + k_2)[ES]$$
 (2.1b)

$$\frac{d[ES]}{dt} = k_1[E][S] - (k_{-1} + k_2)[ES]$$
 (2.1c)

$$\frac{d[P]}{dt} = k_2[ES] = v \tag{2.1d}$$

where [Y] = denotes the concentration of species Y v = the rate of reaction

Several assumptions are then made, as follows:

#### **Assumptions:**

- 1. The free-ligand approximation, which requires the substrate concentration to far exceed that of the enzyme and leads to
- 2. The quasi-steady state assumption, that states that the concentration of ES is constant, i.e. d[ES]/dt = 0
- 3. The enzyme remains unchanged by the reaction, so total enzyme  $E_0 = E + ES$ Substituting Assumption 2 into Equation 2.1c leads to:

$$[ES] = \frac{k_1[E][S]}{(k_{-1} + k_2)} \tag{2.2}$$

Using Assumption 3 with Equation 2.2 gives:

$$[ES] = \frac{k_1[E_0][S]}{k_1[S] + (k_{-1} + k_2)}$$
 (2.3)

After substituting Equation 2.3 into Equation 2.1d and dividing by  $k_1$ , this leads to the

Michaelis-Menten equation:

$$v = \frac{V_{max}[S]}{K_m + [S]} \tag{2.4}$$

where  $V_{max} = k_2[E_0]$  the maximum achievable velocity of the reaction  $K_m = \frac{k_{-1} + k_2}{k_1}$  which is called the Michaelis constant

Although the Michaelis-Menten rate law is widely used, the equations become very complicated as the number of entities involved (substrates and modifiers) increases and so the analysis of such systems becomes mathematically intractable (Savageau, 1972). Therefore, alternative representations were sought for more complicated reactions and indeed for whole biochemical systems that are easier to mathematically analyse. This required re-examination of the underlying reaction dynamics and the search for suitable mathematical tools that could be utilised in their analysis.

# 2.3 Biochemical Systems Theory (BST)

Biochemical systems tend to be non-linear in nature and their behaviour correspondingly complex. Indeed, Wong and Hanes (1962) showed that the reaction rate of all enzyme-catalysed reactions could be written as a ratio of polynomials, an example of this is the Michaelis-Menten rate equation (Equation 2.4). However, analysis of such non-linear systems is a complicated procedure which is computationally intensive, if not impossible (Savageau, 1969b, 1970). To mitigate this, a standard mathematical technique was suggested as a way of approximating the system so that it could be more easily analysed. The technique is known as linearisation; whereby a linear function is computed that approximates the original function at a specific point (Savageau, 1972, 2009). The advantage of this method is that once the system is rewritten as a linear function, all the common mathematical tools that exist for the examination of linear functions can be utilised thus making the analysis far easier. However, this simplified version of the system is only an accurate representation of the underlying function at one point and

thus its use is limited, as obtaining useful information about the system as a whole is not possible due to the restricted range of validity of the approximation (Savageau, 1972, 2009).

Savageau (1969a,b, 1970) proposed an alternative method which still involved some linearisation, but the main novelty came from first recasting the system. This new framework involves the use of power-law approximations, which are based on the non-linearity of the system but they have the advantage of being relatively easy to mathematically analyse, even though they are non-linear functions. This power-law based system became known as Biochemical Systems Theory (BST), with several variants and extensions being added over time (Sorribas, 1988; Sorribas and Savageau, 1989a,b,c; Savageau, 1991). Indeed, those responsible for the establishment of BST consider various other mathematical representations of reaction kinetics to be specific versions of BST, including Michaelis-Menten, mass action and Metabolic Control Theory (MCT) (Savageau et al., 1987a,b; Sorribas and Savageau, 1989b; Savageau, 1996).

The principles of BST are underpinned by two key concepts in mathematics, namely Bode's analysis and Taylor's Theorem (Bode, 1945; Thomas and Finney, 1996); both of which are used widely throughout mathematics, physics and engineering. Bode's analysis allows for a change of coordinates to be performed on the system, whilst Taylor's Theorem is a classically used linearisation method.

Bode (1945) studied in the field of electrical engineering, where his work involved the examination of non-linear systems. His work became known as Bode's analysis and gave rise to a specific type of graph called Bode plots; which are ubiquitous throughout electrical engineering and control theory. Bode realised that if the non-linear system was transformed into logarithmic coordinates, the function could be approximated using piecewise linear approximations. This involves computing multiple linear functions that each approximate a different small section of the original function and collectively they provide an approximation for the whole function over its entire range (Bode, 1945). As these approximations are linear, the system is significantly easier to analyse, facilitating

a better understanding of the underlying problem.

Savageau (1969a,b, 1970) was able to appreciate the similarities between the systems studied by Bode and the rate laws of enzyme-catalysed reactions; namely, that both systems can be written as rational functions, specifically ratios of polynomials. In addition, the functions studied by Bode had a few other specific properties (Bode, 1945), thus for Bode's analysis to be applicable, the following criteria need to hold:

#### Criteria:

- 1. The function is a ratio of polynomials
- 2. The degree of the numerator is less than or equal to the degree of the denominator
- 3. All constants are real and positive

Indeed, in their work defining standard properties of reaction rate equations, Wong and Hanes (1962) also showed that by definition all of the above criteria hold. Therefore, equations representing enzyme-catalysed reaction rates are analogous to the functions studied by Bode thus allowing the techniques of Bode analysis to be directly applied in the study of these systems.

Once the change of coordinates had been performed, suitable linear functions needed to be identified that could approximate the system in logarithmic space; this is where Savageau utilised Taylor's Theorem (Savageau, 1969a,b, 1970).

**Taylor's Theorem.** Any continuous function, F(X), in an open interval that has n-continuously differentiable derivatives (i.e. the  $\frac{d^{n+1}F(X)}{dX^{n+1}}$  derivative of F(X) exists) over that interval, can be approximated at a specific point, op, in the interval by a polynomial. Namely,

$$F(X) = F(X_{op}) + \frac{dF(X_{op})}{dX}(X - X_{op}) + \frac{1}{2!}\frac{d^2F(X_{op})}{dX^2}(X - X_{op})^2 + \frac{1}{3!}\frac{d^3F(X_{op})}{dX^3}(X - X_{op})^3 + \dots + \frac{1}{n!}\frac{d^nF(X_{op})}{dX^n}(X - X_{op})^n$$

where 
$$X_{op} = X$$
 evaluated at the point op 
$$\frac{d^k F}{dX^k} = \text{the kth derivative of } F \text{ with respect to } X$$
 
$$k! = 1 \times 2 \times 3 \times \ldots \times k \text{ is } k \text{ factorial}$$

The specific point of the approximation is called the operating point, op.

The Taylor approximation can be linearised to the case where n = 1, whereby it is restricted to just the first two terms, the constant and first order term, and all other terms of higher order are discarded (Voit, 2000). Indeed, Taylor showed that after linearisation the approximation is still an exact match for the original function at the operating point, whilst close to the operating point the approximation is still very similar to F(X), but far from the operating point nothing can be said about the original function (Thomas and Finney, 1996; Voit, 2000).

In Bode's analysis multiple linear approximations are computed that provided a piecewise approximation of the original function. However, Savageau (1972) concluded that when dealing with enzyme reactions rates, it is in fact possible to use just one piece of Bode's piecewise approximation, i.e. just compute one linear approximation at a specific point (Torres and Voit, 2002). Although, this would seem counter-intuitive and it would appear that this method would then be limited in validity in the same way as the standard linearisation methods mentioned above, it is in fact a reasonable simplification due to the mathematical and biological context of these systems (Torres and Voit, 2002). Namely, as the linearisation is conducted in logarithmic space, the range of validity of the approximation is wider than it would be in rectangular coordinates and the physiological concentration ranges within which these biological systems operate is fairly narrow (Savageau, 1969b, 1972; Voit, 1992; Torres and Voit, 2002). Indeed, experimentation has shown that these models can accurately represent certain systems when input concentrations are increased by multiple-fold changes (Savageau, 1972; Voit, 1992). Moreover, as these approximations are themselves non-linear they are better able to capture the, often complex, non-linear reaction dynamics of the underlying system (Savageau, 1970).

Therefore, it is sufficient to compute a single linear function at one operating point as this is a suitable approximation of the original function over most conditions that are physiologically possible and plausible.

The method derived by Savageau (1969a,b, 1970) proceeds as outlined below; firstly for a one-variable system, then for the more general multivariable system.

### 2.3.1 BST formulation for a single variable system

For a reaction involving one metabolite  $X_1$ , the rate of reaction, or flux, v is a function of  $X_1$ , i.e.  $v = v(X_1)$ . Applying Bode's analysis, thereby transforming both the rate function and metabolites to logarithmic coordinates, gives  $log v = v(log X_1)^*$ .

Next applying Taylor's Theorem to this function yields:

$$logv = logv(X_{1,op}) + \frac{d\{logv(X_{1,op})\}}{d\{logX_{1}\}} (logX_{1} - logX_{1,op}) + \frac{1}{2!} \frac{d^{2}\{logv(X_{1,op})\}}{d\{logX_{1}\}^{2}} (logX_{1} - logX_{1,op})^{2} + \dots + \frac{1}{n!} \frac{d^{n}\{logv(X_{1,op})\}}{d\{logX_{1}\}^{n}} (logX_{1} - logX_{1,op})^{n} \quad (2.5)$$

where 
$$X_{1,op} = X_1$$
 evaluated at the operating point 
$$\frac{d^k \{logv\}}{d\{logX_1\}^k} = \text{the $kth$ derivative of $logv$ with respect to $logX_1$}$$
 
$$k! = 1 \times 2 \times 3 \times \ldots \times k \text{ is k factorial}$$

<sup>\*</sup>Whilst this notation may not necessarily conform to rigorous mathematical conventions, it shall be used here so as to align with the existing literature on BST (Savageau, 1972, 1988; Savageau et al., 1987a) which is approached from a bioengineering perspective. For example, the recasting of the function  $v = v(X_1)$  into logarithmic space yielding  $logv = v(logX_1)$  would not hold true in the strictest mathematical sense as the mapping of  $X_1$  to v is not the same as the mapping of  $logX_1$  to logv. However, for consistency with the relevant literature, the bioengineering approach shall be adopted throughout this thesis.

By performing linearisation on this function, i.e. restricting the function to n = 1, the following is obtained:

$$logv = logv(X_{1,op}) + \frac{d\{logv(X_{1,op})\}}{d\{logX_1\}}(logX_1 - logX_{1,op})$$
 (2.6)

If some of the terms are now redefined, then this equation becomes:

$$log v = log \alpha + f_1 log X_1$$
where 
$$log \alpha = log v(X_{1,op}) - \frac{d\{log v(X_{1,op})\}}{d\{log X_1\}} log X_{1,op}$$

$$f_1 = \frac{d\{log v(X_{1,op})\}}{d\{log X_1\}} = \frac{dv(X_{1,op})}{dX_1} \times \frac{X_{1,op}}{v(X_{1,op})}$$

Finally, converting back to rectangular coordinates, i.e. taking exponents of both sides gives:

$$v = \alpha X_1^{f_1} \tag{2.8}$$

where  $\alpha =$  the rate constant  $f_1 =$  the kinetic order

# 2.3.2 BST formulation for a multivariable system

In the more general case, with a system of r reactions involving n species  $X_1, X_2, \ldots, X_n$ , the flux  $v_i$  for the ith reaction is a function of all n metabolites, i.e.  $v_i = v_i(X_1, X_2, \ldots, X_n)$ . Applying the method of Bode and transforming both the rate function and metabolites to logarithmic coordinates, gives  $log v_i = v_i(log X_1, log X_2, \ldots, log X_n)$ . Next, using Taylor's Theorem in the new coordinate system and restricting to n = 1, yields:

$$log v_{i} = log v_{i}(X_{1,op}, X_{2,op}, ..., X_{n,op}) + \sum_{j=1}^{n} \frac{\partial \{log v_{i}(X_{1,op}, X_{2,op}, ..., X_{n,op})\}}{\partial \{log X_{j}\}} (log X_{j} - log X_{j,op})$$
(2.9)

where 
$$X_{j,op} = X_j$$
 evaluated at the operating point 
$$\sum_{j=1}^{n} Y_j = \text{the sum of the terms } Y_1, Y_2, \dots, Y_n$$
 
$$\frac{\partial^k \{log v_i\}}{\partial \{log X_i\}^k} = \text{the } kth \text{ partial derivative of } log v_i \text{ with respect to } log X_j$$

Redefining some of the terms, this becomes:

$$log v_{i} = log \alpha_{i} + f_{i1} log X_{1} + f_{i2} log X_{2} + \ldots + f_{in} log X_{n}$$
(2.10)
where 
$$log \alpha_{i} = log v_{i}(X_{1,op}, X_{2,op}, \ldots, X_{n,op}) - \sum_{j=1}^{n} \frac{\partial \{log v_{i}(X_{1,op}, X_{2,op}, \ldots, X_{n,op})\}}{\partial \{log X_{j}\}} log X_{j,op}$$

$$f_{ij} = \frac{\partial \{log v_{i}(X_{1,op}, X_{2,op}, \ldots, X_{n,op})\}}{\partial \{log X_{j}\}}$$

$$= \frac{\partial v_{i}(X_{1,op}, X_{2,op}, \ldots, X_{n,op})}{\partial X_{j}} \times \frac{X_{j,op}}{v_{i}(X_{1,op}, X_{2,op}, \ldots, X_{n,op})} \text{ for } j = 1, \ldots, n$$

Finally, converting back to rectangular coordinates gives:

$$v_i = \alpha_i X_1^{f_{i1}} X_2^{f_{i2}} \dots X_n^{f_{in}} = \alpha_i \prod_{j=1}^n X_j^{f_{ij}}$$
(2.11)

where  $\alpha_i$  = the rate constant for reaction i  $f_{ij} = \text{the kinetic order for metabolite } X_j \text{ in reaction } i$   $\prod_{j=1}^n Y_j = \text{the product of the terms } Y_1, Y_2, \dots, Y_n$ 

# 2.3.3 Generalised Mass Action (GMA)

Using the framework of BST, different mathematical variants were determined which differ in the way they deal with the aggregation of fluxes. The three variations being: Generalised Mass Action (GMA), S-systems and Half-system (Savageau, 1996; Voit, 2000, 2013). Each version has advantages and disadvantages, but the version that shall be considered here is GMA due to its better handling of branch-point dynamics, i.e. when

one metabolite is involved in the synthesis of two other metabolites through two distinct reactions, which is a common feature of the purine system being studied. Indeed, Curto et al. (1998b) and others (De Atauri et al., 1999) showed that the GMA model variant produces results that more closely reflect clinical findings compared to S-system formulations and that GMA models are better able to capture system dynamics further from the operating point. Therefore, GMA provides a framework that is more accurate over a wider range of physiological conditions.

The formulation of a GMA model for the above generalised reaction system proceeds thusly. Firstly, the rate of change of each metabolite  $X_k$  can be described in terms of the reaction rates, or fluxes, that produce it and those that consume it, such that:

$$\frac{dX_k}{dt} = \dot{X}_k = (c_1 v_1^+ + c_2 v_2^+ + \dots + c_p v_p^+) - (v_1^- + v_2^- + \dots + v_q^-)$$
(2.12)

where  $c_i$  = the stoichiometric coefficient for reaction  $v_i$   $v_i^+$  = is the flux of a reaction that synthesises  $X_k$   $v_i^-$  = is the flux of a reaction that degrades  $X_k$ 

Replacing each flux with its power-law approximation from Equation 2.11, gives:

$$\dot{X}_k = \sum_{i=1}^{r_k} \pm \alpha_i \prod_{j=1}^{n+m} X_j^{f_{ij}} \quad \text{for } k = 1, \dots, n$$
 (2.13)

where  $r_k \subseteq r$  the subset of reactions that affect the concentration of metabolite  $X_k$ 

r = the full set of reactions in the system

$$\sum_{j=1}^{n} Y_j = \text{the sum of the terms } Y_1, Y_2, \dots, Y_n$$

 $\alpha_i$  = the rate constant for reaction i

n = the number of dependent variables

m =the number of independent variables

$$\prod_{j=1}^{n} Y_j = \text{the product of the terms } Y_1, Y_2, \dots, Y_n$$

 $f_{ij}$  = the kinetic order for metabolite  $X_j$  in reaction i, which is defined as:

$$f_{ij} = \left(\frac{\partial v_i}{\partial X_j}\right)_{op} \times \frac{X_{j,op}}{(v_i)_{op}}$$
 (2.14)

where  $\left(\frac{\partial v_i}{\partial X_j}\right)_{op}$  = the partial derivative of  $v_i$  with respect to  $X_j$  evaluated at

 $X_{j,op}$  = the concentration of metabolite j at the operating point

 $(v_i)_{op}$  = the flux value of reaction i at the operating point

Finally, once the kinetic orders for all the metabolites involved in a reaction have been computed, the rate constant can be calculated using the fact that, by definition of Taylor's Theorem, the approximation is identical to the original function at the operating point, thus:

$$\alpha_{i} = \frac{(v_{i})_{op}}{\prod_{j=1}^{n+m} X_{j,op}^{f_{ij}}}$$
(2.15)

where  $(v_i)_{op}$  = the flux value of reaction i at the operating point  $X_{j,op}$  = the concentration of metabolite j at the operating point

As highlighted in the above derivation, certain information about the system needs to be known prior to the construction of a GMA model, namely the concentration of each metabolite at the operating point and the value of each flux at the operating point. This information is often obtained from experimental data and usually involves MichaelisMenten formulations of the reactions; thus kinetic parameters, such as  $K_m$ ,  $V_{max}$  and  $K_i$ , are often utilised as shown in the below example.

#### 2.3.3.1 GMA example system

To illustrate how to construct a GMA model, consider the following example system which consists of four dependent variables  $X_1$ ,  $X_2$ ,  $X_3$ ,  $X_4$  and three reactions, with fluxes defined as  $v_1$ ,  $v_2$ ,  $v_3$ , as shown in Figure 2.1. The synthesis of metabolite  $X_1$  and the degradation of species  $X_3$  and  $X_4$  are independent of all the metabolites in the system, thus  $X_1$  is produced at a constant rate  $k_1$ , whilst  $X_3$  and  $X_4$  are degraded at constant rates,  $k_2$  and  $k_3$ , respectively. Furthermore, metabolite  $X_3$  inhibits reaction 3.

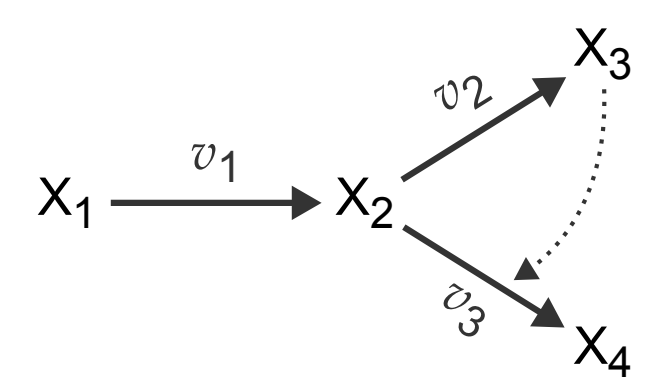


**Figure 2.1:** Schematic for GMA formulation example.  $X_1$ ,  $X_2$ ,  $X_3$ ,  $X_4$  are metabolites and  $v_1$ ,  $v_2$ ,  $v_3$  are the reaction fluxes. Solid arrows represent reactions, whilst dotted arrows indicate inhibitory regulations.

The reaction fluxes for the system are then given by:

$$v_1 = \alpha_1 X_1^{f_{11}}$$
  $v_2 = \alpha_2 X_2^{f_{22}}$   $v_3 = \alpha_3 X_2^{f_{32}} X_3^{f_{33}}$  (2.16)

where  $\alpha_i$  = the rate constant for reaction i $f_{ij}$  = the kinetic order for metabolite  $X_j$  in reaction i

The equation for the rate of change of concentration for each variable is thus defined as

follows:

$$\dot{X}_{1} = k_{1} - v_{1} = k_{1} - \alpha_{1} X_{1}^{f_{11}} 
\dot{X}_{2} = v_{1} - v_{2} - v_{3} = \alpha_{1} X_{1}^{f_{11}} - \alpha_{2} X_{2}^{f_{22}} - \alpha_{3} X_{2}^{f_{32}} X_{3}^{f_{33}} 
\dot{X}_{3} = v_{2} - k_{2} = \alpha_{2} X_{2}^{f_{22}} - k_{2} 
\dot{X}_{4} = v_{3} - k_{3} = \alpha_{3} X_{2}^{f_{32}} X_{3}^{f_{33}} - k_{3}$$
(2.17)

As an example, consider reaction 3 which produces  $X_4$ , along with appropriate kinetic and inhibitory data outlined below. Metabolite  $X_3$  at a concentration of 2000  $\mu$ M inhibits reaction 3 by 18 % therefore,

$$X_3^{f_{33}} = 1 - 0.18 \iff f_{33} = \frac{log(0.82)}{log(2000)} = -0.03$$

Also, using the standard Michaelis-Menten formulation as shown in Equation 2.4 along with Equation 2.14, the kinetic order for  $X_2$  in reaction 3 is given by:

$$f_{32} = \frac{V_{max}K_m}{(K_m + X_{2,op})^2} \times \frac{X_{2,op}}{(v_3)_{op}} = \frac{K_m}{K_m + X_{2,op}}$$

Taking a  $K_m$  value of 12  $\mu$ M for substrate  $X_2$  and a concentration of 33  $\mu$ M for  $X_2$  at the operating point gives:

$$f_{32} = \frac{12}{12 + 33} = 0.27$$

Finally, assuming a concentration of 12  $\mu$ M for metabolite  $X_3$  at the operating point and a flux value of 2.3  $\mu$ mol min<sup>-1</sup> (10<sup>9</sup> cells)<sup>-1</sup> for reaction 3 at the operating point then, the rate constant for reaction 3 can be calculated using Equation 2.15 as follows:

$$\alpha_3 = \frac{(v_3)_{op}}{X_{2,op}^{f_{32}} X_{3,op}^{f_{33}}} = \frac{2.3}{33^{0.27} \times 12^{-0.03}} = 0.97$$

Therefore, the equation for the flux  $v_3$  becomes:

$$v_3 = 0.97X_2^{0.27}X_3^{-0.03}$$

Using the same method for reactions 1 and 2, with a  $K_m$  of 21  $\mu$ M for  $X_1$  in reaction 1 plus a concentration of 25  $\mu$ M for  $X_1$  at the operating point and a  $K_m$  of 7.3  $\mu$ M for  $X_2$  in reaction 2, the kinetic orders  $f_{11}$  and  $f_{22}$  become:

$$f_{11} = 0.46$$
 and  $f_{22} = 0.18$ 

Taking these kinetic orders along with the operating point flux values of  $v_1$  equal to 8.7  $\mu$ mol min<sup>-1</sup> (10<sup>9</sup> cells)<sup>-1</sup> and  $v_2$  equal to 5.1  $\mu$ mol min<sup>-1</sup> (10<sup>9</sup> cells)<sup>-1</sup>, yields the rate constants:

$$\alpha_1 = 2.00$$
 and  $\alpha_2 = 2.71$ 

Thus the fluxes  $v_1$  and  $v_2$  are defined as:

$$v_1 = 2.00X_1^{0.46}$$
 and  $v_2 = 2.71X_2^{0.18}$ 

After substituting the equations for the three fluxes into Equation 2.17, the full system in GMA form is prescribed as below:

$$\dot{X}_1 = k_1 - 2.00X_1^{0.46} 
\dot{X}_2 = 2.00X_1^{0.46} - 2.71X_2^{0.18} - 0.97X_2^{0.27}X_3^{-0.03} 
\dot{X}_3 = 2.71X_2^{0.18} - k_2 
\dot{X}_4 = 0.97X_2^{0.27}X_3^{-0.03} - k_3$$
(2.18)

# 2.4 Mathematical model of purine metabolism

As previously mentioned, there already exists a mathematical model of human purine metabolism created by Curto et al. (1997, 1998b). Three different mathematical formulations for this model were described by Curto et al. (1998b): Complemented Michaelis-Menten (CMM), S-system and GMA. The latter is publicly available from the BioModels database (Li et al., 2010) under unique identifier BIOMD0000000015, where it can be

downloaded in Systems Biology Markup Language (SBML) format (Hucka et al., 2003).

This model describes the network from a single main input metabolite PRPP, through the production of nucleotides and deoxynucleotides, RNA and DNA synthesis and degradation, to waste product (uric acid) production and its final excretion from the system (see Appendix A for a schematic of the model). It consists of 16 dependent variables, two independent variables (see Table 2.1) and 37 metabolic reactions (see Table 2.2) prescribed by a set of 37 ODE equations. As shown in Table 2.1, several of the variables represent a group of metabolites, e.g. variable  $X_4$  corresponds to the collective pooled concentration of Ado, AMP, ADP and ATP. Moreover, there are multiple inbuilt regulatory controls within the system, in the form of internal inhibitory and activatory feedback mechanisms.

Although the models of Curto et al. (1997, 1998a,b) were tested, including against data for specific purine metabolic diseases, and they appear to be an accurate representation of the dynamics of the purine metabolic system; they do have some inherent limitations. Firstly, the pooling together of certain metabolites into one variable, means that their individual concentrations cannot be readily modelled. Secondly, they are whole body models and thus they may not be suitable for use in modelling purine metabolism in certain cell or tissue types. In particular, purine metabolism is crucial for many types of cancer cells, due to their high requirements for purines for DNA synthesis, but whether these models are appropriate for use in these cells remains to be determined.

Variable	Conc. (µM)	Metabolite(s)	Conc. (µM)	
Dependent variables				
$X_1$	5	PRPP	5	
$X_2$	100	IMP	100	
$X_3$	0.2	S-AMP	0.2	
$X_4$	2500	Ado, AMP, ADP, ATP	0.5, 200, 400, 1900	
$X_5$	4	SAM	4	
$X_6$	1	Ade	1	
$X_7$	25	XMP	25	
$X_8$	400	GMP, GDP, GTP	25, 75, 300	
$X_9$	6	dAdo, dAMP, dADP, dATP	0.1, 0.5, 1.4, 4	
$X_{10}$	3	dGMP, dGDP, dGTP	0.1, 0.5, 2.4	
$X_{11}$	28600	RNA	28600	
$X_{12}$	5160	DNA	5160	
$X_{13}$	10	HX, Ino, dIno	6.9, 3, 0.1	
$X_{14}$	5	Xa	5	
$X_{15}$	5	Gua, Guo, dGuo	0.5, 4.4, 0.1	
$X_{16}$	100	UA	100	
Independent variables				
X <sub>17</sub>	18	R5P	18	
X <sub>18</sub>	1400	Pi	1400	

**Table 2.1:** Metabolites from the Curto *et al.* (1998b) model of human purine metabolism. Metabolite name along with its corresponding variable annotation and initial concentration as defined by Curto *et al.* (1998b) are shown.

Abbreviation	Reaction		
PRPPS	$R5P + ATP \longrightarrow PRPP + AMP$		
DEN	$PRPP + glutamine + H_2O \longrightarrow b$ -5-phosphoribosyl-1-amine		
	$+\ glutamate + PPi$		
	(is a pathway, this is the first step)		
GPRT	$Gua + PRPP \longrightarrow GMP + PPi$		
HPRT	$HX + PRPP \longrightarrow IMP + PPi$		
APRT	$Ade + PRPP \longrightarrow AMP + PPi$		
PYR	Represents pyrimidine synthesis		
IMPDH	$IMP + NAD + H_2O \longrightarrow XMP + NADH$		
GMPS	$XMP + ATP + glutamine \longrightarrow GMP + AMP + PPi + glutamate$		
ASUC	$IMP + L$ -aspartate $+ GTP \longrightarrow S$ - $AMP + GDP + Pi$		
ASLI	$S$ - $AMP \longrightarrow AMP + fumarate$		
GMPR	$GMP + NADPH \Longrightarrow IMP + NADP + NH_3$		
AMPD	$AMP \longrightarrow IMP + NH_3$		
MAT	$methionine + ATP \longrightarrow SAM + Pi + PPi$		
TRANS	$protein + SAM \longrightarrow methylated \ protein + S-adenosyl-L-homocysteine$		
	(is a pathway, this is the first step)		
POLYAM	$SAM \longrightarrow decarboxylated SAM$		
	(is a pathway, this is the first step)		
INUC	$IMP + H_2O \longrightarrow Ino + Pi$		
GNUC	$GMP + H_2O \longrightarrow Guo + Pi$		

# continued on the next page

Abbreviation	Reaction
DGNUC	$dGMP + H_2O \longrightarrow dGuo + Pi$
GDRNR	$GDP + NADPH \longrightarrow dGDP + NADP + H_2O$
ADRNR	$ADP + NADPH \longrightarrow dADP + NADP + H_2O$
ADA	$Ado \longrightarrow Ino + NH_3$
DADA	$dAdo \longrightarrow dIno + NH_3$
ARNA	$ATP + RNA_n \longrightarrow PPi + RNA_{n+1}$
GRNA	$GTP + RNA_n \longrightarrow PPi + RNA_{n+1}$
RNAA	Hydrolysis of RNA into AMP
RNAG	Hydrolysis of RNA into GMP
ADNA	$dATP + DNA_n \longrightarrow PPi + DNA_{n+1}$
GDNA	$dGTP + DNA_n \longrightarrow PPi + DNA_{n+1}$
DNAA	Hydrolysis of DNA into dAMP
DNAG	Hydrolysis of DNA into dGMP
HXD	$HX + H_2O + (NAD \ or \ O_2) \longrightarrow Xa + (NADH \ or \ H_2O_2)$
XD	$Xa + H_2O + (NAD \ or \ O_2) \longrightarrow UA + (NADH \ or \ H_2O_2)$
GUA	$Gua + H_2O \longrightarrow Xa + NH_3$
ADE	oxidation of Ade to 2,8-dihydroxyadenine and excretion of both
HXE	excretion of HX
XE	excretion of Xa
UAE	excretion of UA

**Table 2.2:** Reactions from the Curto *et al.* (1998b) model of human purine metabolism. Each reaction along with its abbreviated name as defined by Curto *et al.* (1998b) is shown.

# Chapter 3: Model Adaptation

## 3.1 Model refinement

The GMA model of purine metabolism established by Curto et al. (1998b), was downloaded in SBML format (Hucka et al., 2003) from the BioModels database (Li et al., 2010) using the unique identifier BIOMD0000000015. This was initially imported into the modelling software COPASI (Hoops et al., 2006), but subsequently the model equations were coded directly into Matlab version R2015b (The MathWorks Inc., 2015). The following model adaptations and simulations were carried out using Matlab version R2015b (The MathWorks Inc., 2015), unless otherwise stated.

In order to more accurately examine the mode of action of IMPDH inhibitors on leukaemic cells, it was decided to examine the model to see if it was likely to be a true representation of purine metabolism in HL60 cells and adapt it as required. To do this I used RNAseq data, which detects transcript levels, as a proxy measure for enzyme abundance and activity, to determine whether the enzymes in the purine metabolic network and mathematical model were present in this cell type.

### 3.1.1 RNAseq analysis for ATRA treated HL60 cells

RNA sequencing (RNAseq) is a high throughput technique used to analyse gene expression. mRNA is isolated from cells and the enzyme reverse transcriptase is used to create complimentary DNA (cDNA). This cDNA is then cut into small fragments and special adapters are added to the ends which allow the fragments to be anchored in place. A DNA polymerase is then added along with fluorescently labelled nucleotides which are used to build a complementary copy of the cDNA. The fluorescence is read at each cycle of base incorporation, enabling the mRNA sequence to be determined.

I utilised a set of RNAseq data, obtained from the online database GEO (Edgar *et al.*, 2002) under accession number GSE28123, from a study involving brain tissue, liver tissue,

K562 cells and HL60 cells (Raz et al., 2011). The samples analysed were HL60 cells that either had been treated with ATRA or were untreated cells. The data, as normalised by Raz et al. (2011), from three biological replicates for each condition was used without further adjustment. Details of the sample identifiers from the GEO database (Edgar et al., 2002) for the six samples used are listed in Appendix B.

The list of enzymes used in the Curto *et al.* (1998b) model was converted to a list of gene symbols (see Appendix B for details) and the corresponding data was extracted from the RNAseq dataset, using the programming language R, version 2.14.1 (R Development Core Team, 2021).

To account for the fact that some enzymatic activities are performed by more than one gene product, the mRNA levels for each isozyme gene were summed to generate a single value for each enzymatic activity and these values were then averaged across the three replicate samples. The mean Reads Per Million (RPM) count for each enzyme for the three replicates was analysed to determine whether or not these enzymes were expressed. This analysis revealed that the majority of the enzymes included in the model are present in these cells (see Table 3.1); with only one gene under one experimental condition (GDA in ATRA treated cells) falling below the cut-off threshold of five RPM that was used by Raz et al. (2011).

Next, the log<sub>2</sub> fold change between the ATRA treated and untreated cells was calculated, i.e. log<sub>2</sub>(treated/untreated). These values were then used to generate a graphical picture of how the expression level of each enzyme changes upon treatment, using Cytoscape (Shannon et al., 2003). To do this, the KGML formatted version of the human purine metabolic network (reference: hsa00230) was downloaded from the KEGG database (Kanehisa and Goto, 2000) and imported into Cytoscape (Shannon et al., 2003). This generated a schematic for the network similar to that in KEGG which was hand curated to remove enzymes, metabolites and reactions that do not occur in humans. Moreover, the network was terminated at Uric acid to coincide with the network used by Curto et al. (1997, 1998b).

Gene	Untreated	ATRA	Gene	Untreated	ATRA
PRPS	109.666667	26.533333	GDA	7.533333	3.966667
HPRT	44.833333	20.966667	PPAT	53.033333	5.433333
APRT	13.666667	10.333333	GART	131.833333	33.366667
<i>ADSS</i>	91.433333	53.366667	PFAS	44.766667	25.900000
IMPDH	255.400000	84.433333	PAICS	284.100000	48.566667
<i>GMPS</i>	111.300000	34.066667	ATIC	90.166667	23.933333
AMPD	66.033333	98.133333	ITPA	21.666667	11.433333
GMPR	49.800000	60.700000	GUK1	19.566667	10.400000
XDH	6.233333	5.033333	NME	381.066667	179.266667
NT5	114.833333	144.066667	ADSL	84.666667	34.200000
POLR	1303.366667	947.200000	POL	983.333333	570.966667
ADA	37.300000	33.366667	ADK	84.333333	38.533333
RRM	320.900000	149.866667			

**Table 3.1:** Relevant Reads Per Million values from the Raz *et al.* (2011) RNAseq data set. RNAseq data from HL60 cells were utilised and Reads Per Million (RPM) values for genes corresponding to enzymes in the purine metabolic network were extracted to confirm their presence in this cell type.

The attributes list in Cytoscape includes a 'KEGG.label.first' field which is the attribute that is used to refer to the enzymes in the schematic produced (Shannon et al., 2003). Therefore, the log<sub>2</sub> fold-change values were assigned to the corresponding 'KEGG.label.first' name so they could be imported into Cytoscape. The enzyme nodes were then coloured according to these values; so that enzymes with mRNA levels that increase upon treatment with ATRA are blue, whilst those that decrease upon treatment are yellow. Enzymes that are not present in the purine network as defined by Curto et al. (1998b) are coloured grey (see Figure 3.1).

This comparison revealed that most of the enzymes in the network were down-regulated upon treatment with ATRA; with only three enzymes, namely adenosine monophosphate deaminase, guanosine monophosphate reductase and 5'-nucleotidase (AMPD, GMPR, and NT5, respectively), being up-regulated. The largest decrease in expression was observed within the *de novo* pathway (see Figure 3.1). This overall decrease in enzyme

expression in the network is consistent with the fact that administration of ATRA will cause these cells to stop proliferating and differentiate into granulocytes. Therefore, the cells' requirements for purine nucleotides will decrease as they will no longer be synthesising new DNA.

With the model now having been checked to ensure that it is appropriate for use in HL60 cells, attention then turned to investigating how the model could be used to examine the effect of IMPDH inhibitors on these cells. Specifically, how the model could be adapted so that the metabolites of interest could be independently assessed during simulations of IMPDH inhibition.

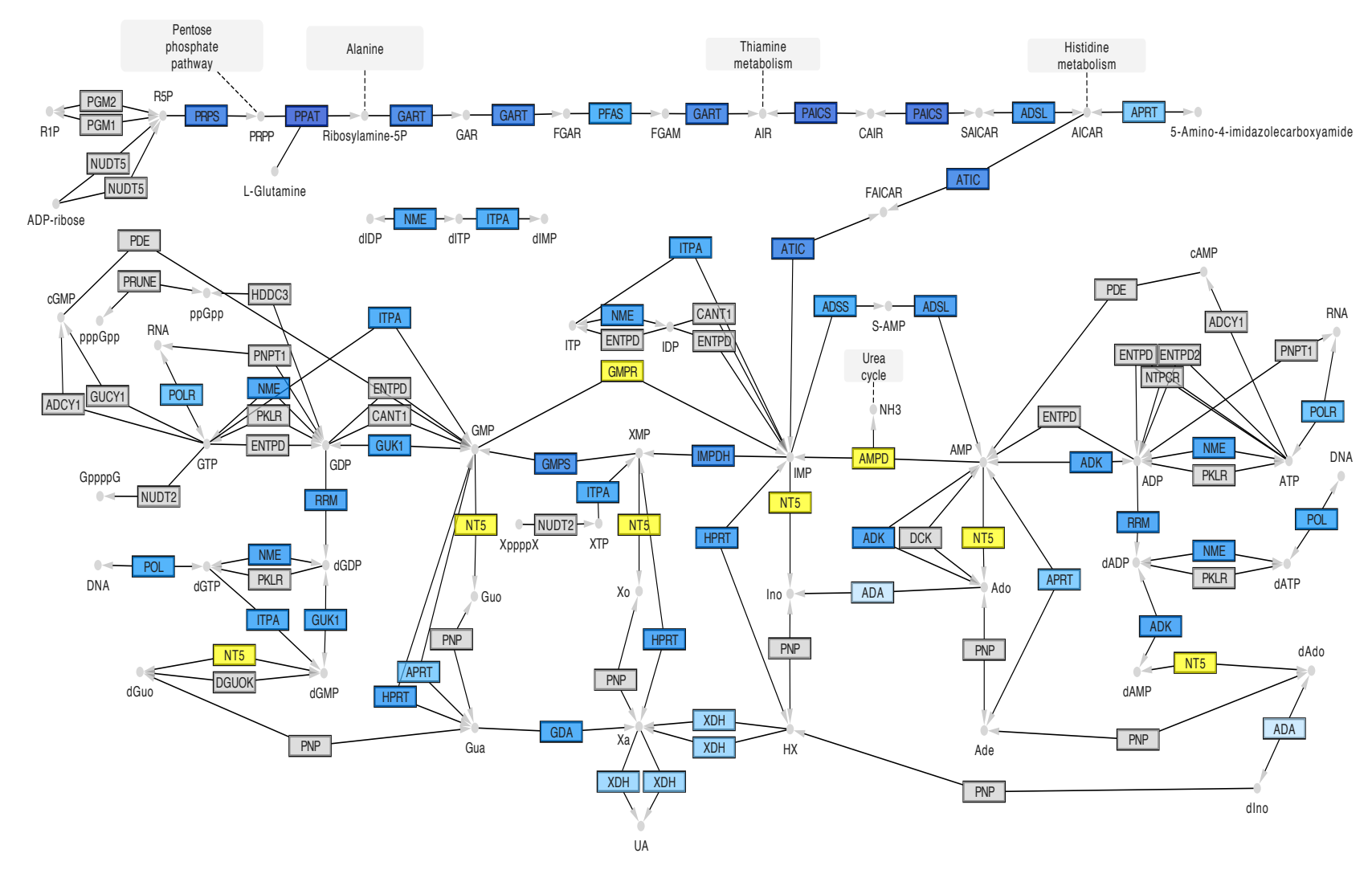


**Figure 3.1:** Comparison of mRNA expression levels between HL60 cells treated with ATRA and untreated cells. Boxes represent enzymes whilst circles represent metabolites. Blue indicates that mRNA expression decreases upon treatment with ATRA, whilst yellow represents an increase upon treatment. Grey denotes enzymes that are not present in the purine network as defined by Curto *et al.* (1998b). Data is from Raz *et al.* (2011) and visualisation was performed using Cytoscape (Shannon *et al.*, 2003).

### 3.2 Model version 1

As mentioned earlier, one of the limitations of the Curto et al. (1998b) model is that certain metabolites are pooled together into single variables. Importantly, the adenylate & adenosine and guanylate metabolites are grouped into variables  $X_4$  and  $X_8$ , respectively. This is problematic since I am interested in the absolute levels of many of these nucleotides, especially GTP, GDP and ATP. Therefore, the pooled variables  $X_4$  and  $X_8$  were removed from the model and replaced by separate variables for adenosine and each of the adenylate and guanylate nucleotides, as outlined in Table 3.2, thus allowing each species to be modelled separately and their individual concentrations to be examined.

Adenylate & adenosine pool $(X_4)$		Guanylate pool $(X_8)$	
Variable	Metabolite	Variable	Metabolite
$X_{4M}$	AMP	$X_{8M}$	GMP
$X_{4D}$	ADP	$X_{8D}$	GDP
$X_{4T}$	ATP	$X_{8T}$	GTP
$X_{4A}$	Adenosine		

**Table 3.2:** Variable nomenclature for previously pooled adenylate & adenosine and guanylate metabolites.

Full incorporation of these new variables into the existing model required both the replacement of the old pooled variables, from all equations, with the appropriate new variable that is the actual substrate, product or modulator in the reaction, and the creation of new equations that represent the biochemical reactions that exist between the newly defined variables. This firstly required redefining each existing kinetic order that involved either  $X_4$  or  $X_8$  so that the individual concentration of the precise species involved, rather than the pooled concentration, was used. This was achieved using in-

formation already present in Curto et al. (1998b) as the specific entity, from the pooled metabolites, that actually participates in each reaction is noted in the appendix (Curto et al., 1998b). Next, equations for the newly defined reactions needed to be established and kinetic orders determined. This required a database and literature search to identify the exact interconversion reactions that occur in humans between the previously pooled metabolites Ado, AMP, ADP and ATP and those that occur between the species GMP, GDP and GTP. Moreover, kinetic data was also acquired from the literature that was used to generate kinetic orders for these new reactions. Once both of these steps had been completed, steady state equations along with biochemically and experimentally derived constraints were utilised such that initial flux values for the system could be computed at the operating point. This then enabled the rate constant for each reaction in the amended system to be determined, as per the method used in Curto et al. (1998b), thus eventually producing a fully prescribed system of equations that can be used to model purine metabolism in HL60 cells and the effect of IMPDH inhibitors on the network.

### 3.2.1 Amendment of existing reactions

For both the adenylate & adenosine and guanylate pools, the specific metabolites which:

1) act as substrates for reactions beginning at the pools; 2) are products of reactions ending at the pools; and 3) are inhibitors or activators of reactions affected by the pools were determined, using information in Curto et al. (1998b). The kinetic orders for these reactions were recalculated using the values and enzymatic information in Curto et al. (1998b), correcting for individual metabolite concentrations, and are detailed in Appendix C.

#### 3.2.2 New interconversion reactions

New reactions for the interconversions between the metabolites within each pool were then determined. The full set of interconversion reactions between these metabolites in humans, as defined in the KEGG database (Kanehisa and Goto, 2000), was considered. Figure 3.2 shows the entire set of adenylate & adenosine interconversions, while Figure 3.3

details all of the guanylate interconversions; with enzymes represented by their Enzyme Commission (EC) number.

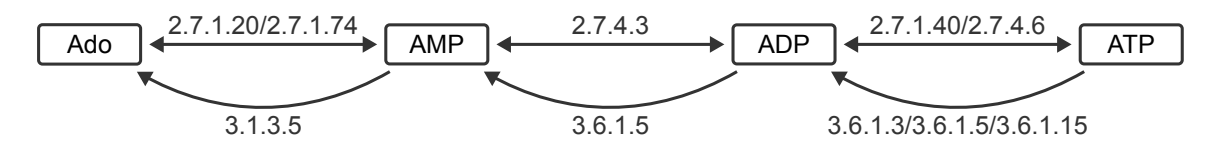


**Figure 3.2:** Interconversion reactions between Ado, AMP, ADP and ATP. Data is specific for humans and was obtained from the KEGG database (Kanehisa and Goto, 2000). Abbreviated metabolite names (boxes) and EC numbers are shown.

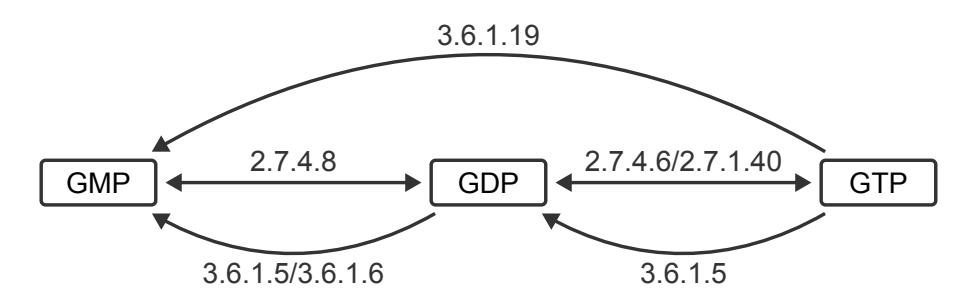


**Figure 3.3:** Interconversion reactions between GMP, GDP and GTP. Data is specific for humans and was obtained from the KEGG database (Kanehisa and Goto, 2000). Abbreviated metabolite names (boxes) and EC numbers are shown.

The enzymes responsible for these interconversion reactions were then examined to see if it was appropriate to include them in the model. Thus, enzymes EC 3.6.1.3, 3.6.1.5, 3.6.1.6, 3.6.1.15 and 3.6.1.19 were excluded as their sites of action are extracellular; EC 2.7.1.40 was discounted as it is a key glycolytic enzyme and its activity is regulated by other sources beyond the scope of this model; and finally EC 2.7.1.74 was discarded as it does not actually catalyse the reaction defined in the KEGG pathway (Lemmens et al., 1996; Kanehisa and Goto, 2000; Smith et al., 2002).

Since commencement of this project, several changes to the KEGG database have been implemented. Enzymes EC 2.7.1.74 and 2.7.1.40 have been removed from the KEGG purine network, thus confirming the validity of their exclusion from the model (Kanehisa and Goto (2000), accessed 2022). In addition, enzyme EC 3.6.1.19 has been renamed EC 3.6.1.9 and enzyme EC 3.6.1.3 has been removed and replaced by EC 3.6.1.-; nonethe-

less, both of these enzymes retain their extracellular sites of action. Lastly, enzyme EC 2.7.4.6 has been amended to remove the isozyme adenylate kinase 3, which received the new EC number 2.7.4.10. However, as adenylate kinase 3 has minimal catalytic activity with ATP as a substrate it was also excluded from the list of enzymes that was to be incorporated into the model (Noma et al., 2001).

Lastly, using the methodology used in Curto et al. (1998b), reversible reactions were replaced by their net flux, as observed in vivo. This applied to the reactions: EC 2.7.1.20, 2.7.4.3, 2.7.4.6 and 2.7.4.8, for which their net flux goes in the direction left to right as seen in Figures 3.2 and 3.3 Therefore, the refined interconversion schemes for the adenylate & adenosine and guanylate pools are shown in Figures 3.4 and 3.5, respectively, with the enzymes involved listed in Table 3.3.

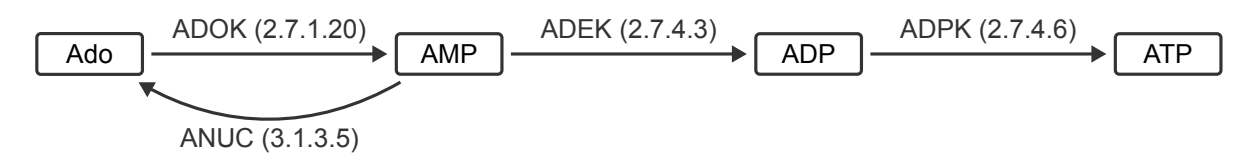


**Figure 3.4:** Hand curated adenylate & adenosine interconversion reactions. Abbreviated metabolite names (boxes), abbreviated enzyme names and EC numbers are shown.



**Figure 3.5:** Hand curated guanylate interconversion reactions. Abbreviated metabolite names (boxes), abbreviated enzyme names and EC numbers are shown.

EC number	Enzyme name	Abbreviation
2.7.1.20	Adenosine kinase	ADOK
2.7.4.3	Adenylate kinase	ADEK
2.7.4.6	Nucleoside-diphosphate kinase	ADPK/GDPK
2.7.4.8	Guanylate kinase	GUK
3.1.3.5	5'-Nucleotidase	ANUC

**Table 3.3:** List of hand curated adenylate & adenosine and guanylate interconversion reaction enzymes. Enzyme abbreviation and EC number corresponding to Figures 3.4 and 3.5 are shown along with each enzymes' full name.

### 3.2.3 ATP synthesis and degradation

Considering these two sets of interconversion reactions together and in the context of the existing model, a couple of points became evident. Firstly, as is apparent from their EC numbers, GDPK and ADPK are both catalysed by the same enzyme, nucleoside-diphosphate kinase (EC 2.7.4.6), and are in fact the forward and back steps of the same reaction, namely:

$$GDP + ATP \xrightarrow{GDPK} GTP + ADP$$

Secondly, whilst there are eight reactions (four new and four existing reactions) that result in ATP degradation, the only reaction that synthesises ATP is ADPK. ADPK uses GTP as a phosphate donor to produce ATP from ADP yet the only source of GTP in the network is from the opposing reaction GDPK, which is assumed to be predominant in vivo. Thus ATP production via ADPK will be negligible. Therefore, another source of ATP production seemed a necessary inclusion in the model. The main source of ATP production is through oxidative phosphorylation and can be modulated by many factors including external stimuli which are outside the scope of this model. Thus the reaction ATPSYN was incorporated into the model as a source of ATP, in the form of a simple mass action equation which converts its only substrate ADP into ATP. In addition, inclusion of a term for ATP degradation (called ATPDEG) via cellular processes outside of purine

metabolism; which are myriad and yield ADP as a byproduct, seemed prudent otherwise the incorporation of ATPSYN alone would artificially drive other reactions within the network that yield ADP to compensate for its use in ATP synthesis. The mass action equations for these new reactions are outlined below:

$$v_{atpsyn} = \alpha_{atpsyn}[ADP] = \alpha_{atpsyn}X_{4D}$$
  $v_{atpdeg} = \alpha_{atpdeg}[ATP] = \alpha_{atpdeg}X_{4T}$ 

Next, the kinetic orders for these newly defined reactions needed to be calculated. This was achieved using the same methodology as Curto et al. (1998b), along with Equation 2.14 and kinetic data sourced from appropriate literature, utilising human data wherever possible (Table 3.4 details this kinetic data). Appendix C provides more details about these calculations and the mathematical GMA equations used, along with the calculated kinetic orders for the new interconversion reactions.

Reaction	Metabolite	Туре	Substrate K <sub>m</sub> (μM)	K <sub>i</sub> (μM)	Source	
ADOK	Ado	Substrate	0.4		Palella <i>et al.</i> (1980)	
	ATP	Substrate	75		Palella <i>et al.</i> (1980)	
	AMP	Competitive inhibitor w.r.t Ado	0.4	140	Palella <i>et al.</i> (1980)	
	ADP	Non-competitive inhibitor	N/A	50	Palella <i>et al.</i> (1980)	
ADEK AMP	AMP	Substrate	80		Tsuboi and Chervenka (1975)	
ADLN	ATP	Substrate	90		Tsuboi and Chervenka (1975)	
ADPK GTP	ADP	Substrate	40		Mourad and Parks (1966)	
	GTP	Substrate	150		Mourad and Parks (1966)	
	GMP	Non-competitive inhibitor	N/A	650	Mourad and Parks (1966)	
	AMP	Substrate	31,000, h=1.5		Itoh and Oka (1985)	
ANUC Pi	D;	Competitive inhibitor w.r.t AMP	app 38,000		Itah and Oka (1005)	
	FI	at Pi=1000	h=1.7		Itoh and Oka (1985)	
GDPK (	ATP	Substrate	1330		Kimura and Shimada (1988)	
	GDP	Substrate	31		Kimura and Shimada (1988)	
	GMP	Non-competitive inhibitor	N/A	650	Mourad and Parks (1966)	
GUK	ATP	Substrate	190		Agarwal <i>et al.</i> (1978)	
GUN	GMP	Substrate	18		Agarwal <i>et al.</i> (1978)	

**Table 3.4:** Kinetic data for each of the adenylate & adenosine and guanylate interconversion reactions.  $K_m$  and  $K_i$  values for substates and inhibitors, respectively, are shown along with details of the relevant literature.

#### 3.2.4 Rate constant calculations

The final step to fully incorporate the newly separated variables and their interconversion reactions into the model, was to calculate a rate constant for each of the 45 reactions in the expanded system. This was achieved by first calculating the flux value for each reaction in the network at the operating point. These were determined utilising the methodology in Curto et al. (1998b), whereby a system of 45 simultaneous equations involving all of the 45 fluxes in the system was established and solved. The steady state equations for the dependent metabolites defined in Curto et al. (1998b), excluding those for  $X_4$  and  $X_8$ , were used without amendment. In addition to these 14 equations, the steady state equations for the individual adenylate & adenosine and guanylate metabolites were determined, as follows:

$$X_{4A}$$
:  $v_{trans} + v_{anuc} = v_{ada} + v_{adok}$ 
 $X_{4M}$ :  $v_{prpps} + v_{gmps} + v_{aprt} + v_{asli}$ 
 $+v_{rnaa} + v_{adok} = v_{ampd} + v_{adek} + v_{anuc}$ 
 $X_{4D}$ :  $v_{adok} + 2v_{adek} + v_{guk} + v_{gdpk}$ 
 $+v_{atpdeg} = v_{adrnr} + v_{adpk} + v_{atpsyn}$ 
 $X_{4T}$ :  $v_{adpk} + v_{atpsyn} = v_{prpps} + v_{gmps} + v_{mat} + v_{arna} + v_{adok}$ 
 $+v_{adek} + v_{guk} + v_{gdpk} + v_{atpdeg}$ 

$$X_{8M}$$
:  $v_{gprt} + v_{gmps} + v_{rnag} = v_{gmpr} + v_{gnuc} + v_{guk}$ 
 $X_{8D}$ :  $v_{asuc} + v_{guk} + v_{adpk} = v_{gdrnr} + v_{gdpk}$ 
 $X_{8T}$ :  $v_{gdpk} = v_{asuc} + v_{grna} + v_{adpk}$ 

The two RNA and two DNA constraints and the 17 experimentally based constraints

from Curto et al. (1998b) were also used without modification, except for the sixth constraint:  $v_{asuc} = 5 v_{impdh}$ . According to Snyder and Henderson (1973) and Hershfield and Seegmiller (1976), this relationship is appropriate for cells in stationary phase whereas the constraint  $v_{asuc} = v_{impdh}$  is more suitable for dividing cells. Since HL60 cells are continually proliferating, the latter condition was used.

In addition to these steady state equations and constraints, three additional flux relationships were required to produce a system of 45 simultaneous equations. The first of these was derived from the fact that the cellular levels of ATP and ADP remain roughly constant in HL60 cells at a ratio of 10:1 (Bradbury *et al.*, 2000), thus giving:

$$v_{atpsyn} = 10 v_{atpdeg}$$

Secondly, as previously mentioned, it was assumed that the reversible reaction

$$GDP + ATP \xrightarrow{GDPK} GTP + ADP$$

catalysed by the enzyme nucleoside-diphosphate kinase would tend to go in the forward direction; thus the following constraint was included:

$$v_{gdpk} = 10 v_{adpk}$$

Lastly, the literature search for kinetic data for the new interconversion reactions yielded the following constraint between the new reaction ANUC and the existing reaction INUC (Spychala *et al.*, 1988):

$$v_{inuc} \approx 15 v_{anuc}$$

This system of 45 simultaneous equations was solved using the computer program Mathematica (Wolfram Research Inc., 2010) to yield initial values for the 45 fluxes in the system. These values were then used with Equation 2.15 to calculate the rate constant for each of the 45 reactions in the system. The full system of simultaneous equations, the

flux values they yielded and the calculated rate constants are detailed in Appendix C.

With all the kinetic orders and rate constants now defined, the system of 45 ODE equations was coded into Matlab version R2015b (The MathWorks Inc., 2015) and analyses conducted to investigate the effect of IMPDH inhibition on the network. Data was obtained from the literature that suggests that MPA inhibits IMPDH by approximately 28 % (Ahmed and Weidemann, 1995). This level of inhibition was simulated by multiplying the rate constant for the reaction IMPDH by 0.72. These simulations resulted in the concentration of ATP increasing drastically: a percentage change of 392 % (see Figure 3.6). Therefore, a re-examination of the model was undertaken.

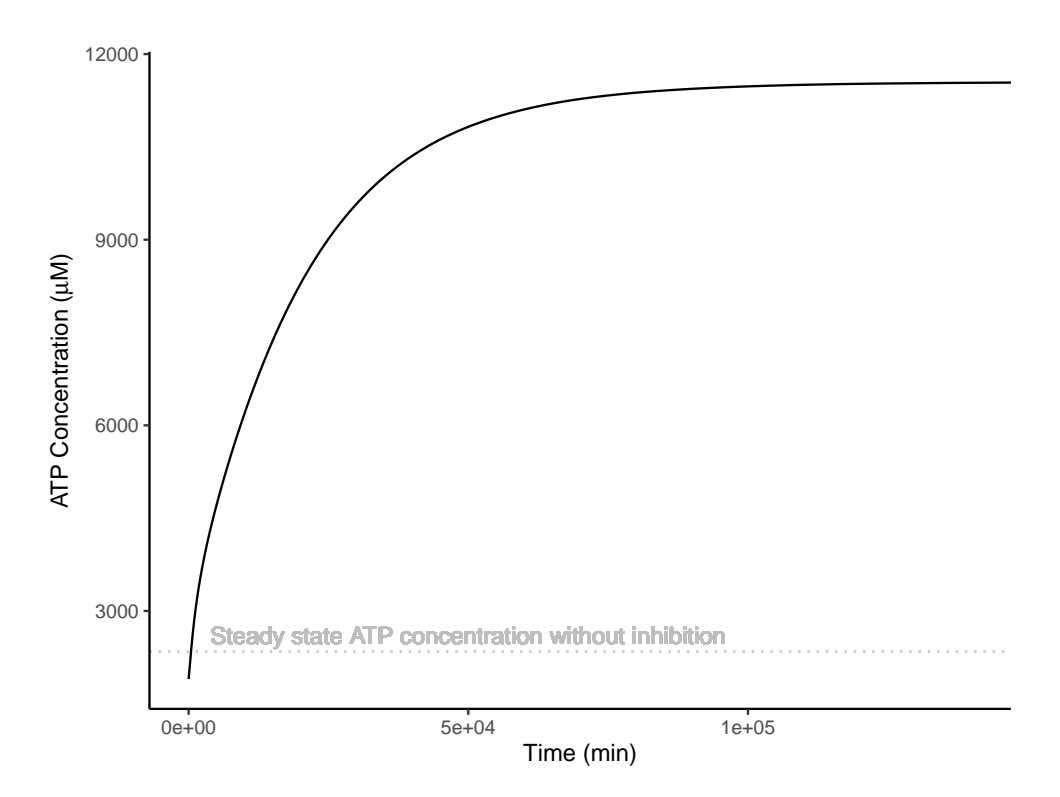


**Figure 3.6:** ATP concentration from model version 1 with simulation of 28 % IMPDH inhibition. The grey line shows the steady state concentration of ATP from the same model without inhibition.

# 3.3 Model version 2

The large increase in ATP concentration observed in the model upon IMPDH inhibition, suggested that the control of ATP (production and degradation) was not correct and so the new interconversion reactions including ATPSYN and ATPDEG were re-examined to determine if they could be modelled better.

#### 3.3.1 ATP synthesis and degradation revisited

Initially, it was decided to see if the ATPSYN and ATPDEG reactions could be removed. However, this resulted in the model crashing due to the level of ATP reaching zero within a few seconds of simulation. Next, examination of the adenylate & adenosine (and then guanylate) species as a separate group in isolation from the rest of the model was attempted. However, this could not be achieved as some of the flux out of the isolated system is recycled back in to it and, as this fraction is unknown, it is not possible to produce a closed system that can be examined.

Therefore, returning to the system as a whole, a logical simplification was to again adopt the procedure used by Curto et al. (1998b) and replace the two reactions catalysed by the enzyme nucleoside-diphosphate kinase, GDPK and ADPK, with the net flux for this reaction (termed NDPK) going in the forward, GDPK, direction resulting in synthesis of GTP. In addition, the separate synthesis and degradation reactions for ATP (ATPSYN and ATPDEG, respectively) were also replaced with one reaction, termed PHOSPHO, representing the net flux for ATP production. As this reaction covers a multitude of processes beyond the model's remit a simple mass action representation was again chosen, as shown below:

$$v_{\mathit{phospho}} = \alpha_{\mathit{phospho}} [ADP]^{f_{\mathit{phospho4D}}} [ATP]^{f_{\mathit{phospho4T}}} = \alpha_{\mathit{phospho}} X_{4D}^{f_{\mathit{phospho4D}}} X_{4T}^{f_{\mathit{phospho4T}}}$$

Thus, the final set of new reactions that were included in the model are detailed in Table 3.5

Abbreviation	Reaction		-
ADEK	$AMP + ATP \longrightarrow 2ADP$	)	
ADOK	$Ado + ATP \longrightarrow AMP + ADP$		Adenylate & adenosine
ANUC	$AMP + H_20 \longrightarrow Ado + Pi$		reactions
PHOSPHO	Net flux for ATP synthesis	J	_
NDPK	$GDP + ATP \longrightarrow GTP + ADP$	)	Guanylate
GUK	$GMP + ATP \longrightarrow GDP + ADP$	}	reactions

**Table 3.5:** Final set of new adenylate & adenosine and guanylate interconversion reactions. Enzyme abbreviations and corresponding reactions are shown.

To complete the amendments outlined above, the parameters for this new system were redefined as required. The kinetic orders for NDPK remained unchanged from those of GDPK whilst values of 0.5 and -0.1 were chosen for the kinetic orders  $f_{phospho4D}$  and  $f_{phospho4T}$ , respectively.

Next, the flux values were redefined by utilisation of the system of simultaneous equations described above (and in Appendix C) with the exclusion of the constraint involving  $v_{atpsyn}/v_{atpdeg}$  and the one involving  $v_{gdpk}/v_{adpk}$ , thus creating a system of 43 equations that was solved to provide initial flux values for the 43 reactions in this network. Lastly, the rate constants were calculated using these flux values and Equation 2.15. The flux values along with the rate constants for this system are detailed in Appendix C.

Again, this system of 43 ODE equations was coded into Matlab version R2015b (The MathWorks Inc., 2015) and simulations conducted. 28 % IMPDH inhibition was simulated, which again resulted in an extreme increase in ATP concentration (a percentage change of 520 %, see Figure 3.7) and thus another re-examination of the system was undertaken.

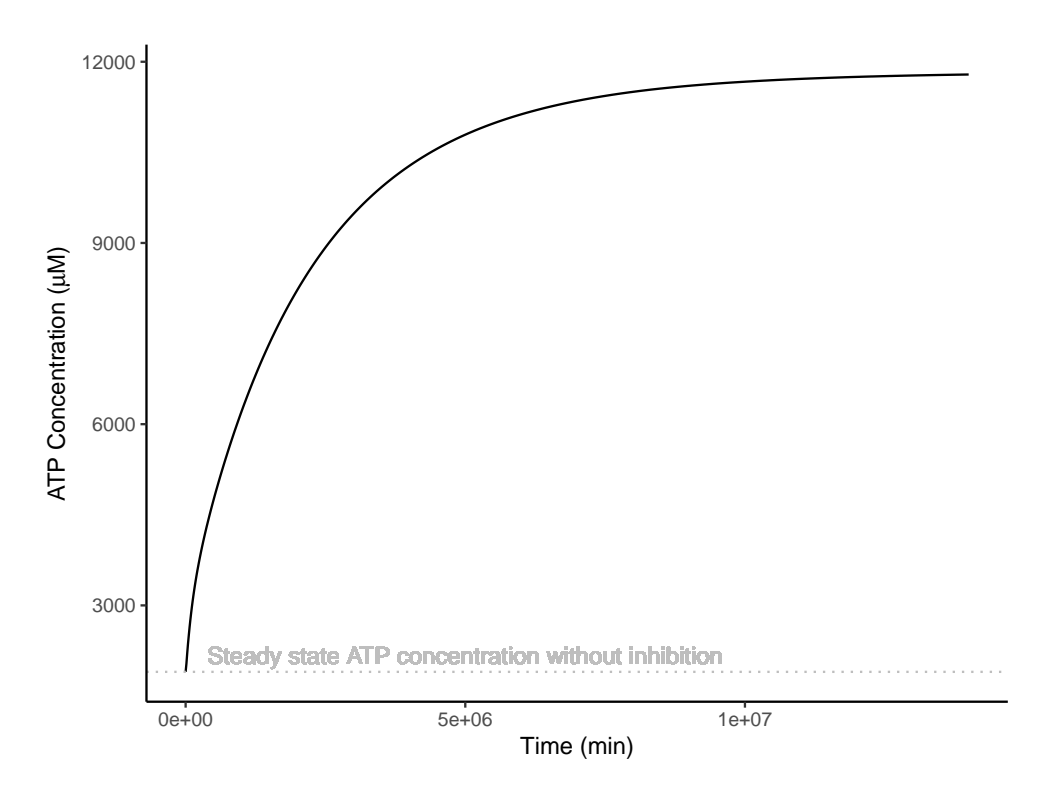


**Figure 3.7:** ATP concentration from model version 2 with simulation of 28 % IMPDH inhibition. The grey line shows the steady state concentration of ATP from the same model without inhibition.

# 3.4 Final model - version 3

Given that ATP concentration is still increasing greatly upon simulation of IMPDH inhibition, the next stage of model revision firstly focussed on the reaction PHOSPHO, specifically its kinetic orders. These had previously been defined as best approximations, as the processes that this reaction represents are complex and beyond the scope of this model. Therefore, in an attempt to more systematically define both of the kinetic orders for this reaction,  $f_{phospho4D}$  and  $f_{phospho4T}$ , it was decided to conduct a parameter sweep using the ranges outlined below:

$$0.3 \leq f_{phospho4D} \leq 0.6$$
 in increments of  $0.05$  
$$-0.16 \leq f_{phospho4T} \leq -0.1$$
 in increments of  $-0.01$ 

However, there appeared to be little difference between any of these possible combinations of values (see Appendix D) and thus the kinetic orders were maintained as before, i.e.  $f_{phospho4D} = 0.5$  and  $f_{phospho4T} = -0.1$ . Next, an inspection of the behaviour of the original Curto et al. (1998b) model was conducted and although ATP in this model is pooled together with the other adenylates & adenosine in the variable  $X_4$ , the increase seen with the new model upon IMPDH inhibition is not recapitulated with the Curto et al. (1998b) model; which only produced a percentage change of 5.8 % in the adenylate & adenosine pool (see Figure 3.8). Furthermore, the Curto et al. (1998b) model appears to produce a fairly robust steady state (Curto et al., 1997).

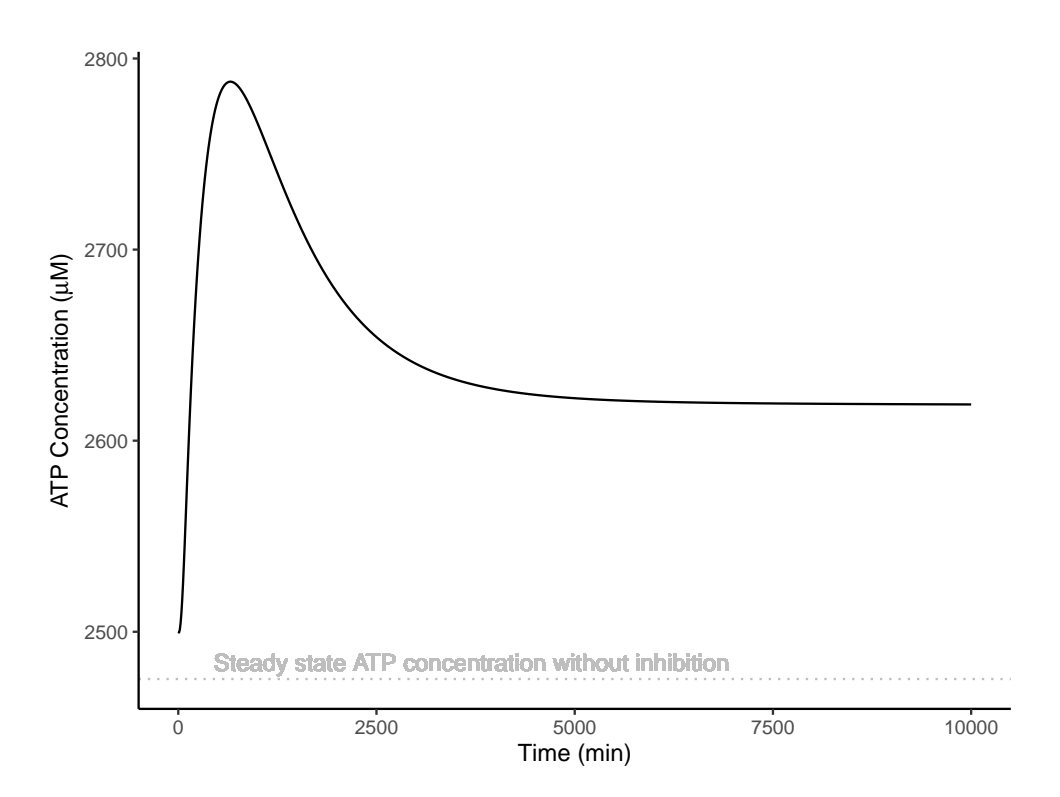


**Figure 3.8:** Adenylate & adenosine pool concentration from Curto *et al.* (1998b) model with simulation of 28 % IMPDH inhibition. The grey line shows the steady state concentration of ATP from the same model without inhibition.

# 3.4.1 Model tweaking towards the Curto et al. (1998b) model steady state

As the Curto et al. (1998b) model appears to produce a fairly robust steady state (Curto et al., 1997), it seemed appropriate to attempt to achieve a similar steady state with the new model. Therefore, the initial flux values for the existing reactions were set equal to the steady state flux values achieved by the Curto et al. (1998b) model (see Appendix D). This left just the flux values for the new interconversion reactions to be determined. This was achieved by solving two small systems of simultaneous equations, one for each of the split pools, comprised of steady state equations. An equation was constructed for each metabolite in the pool such that the net efflux of existing reactions was set equal to the net influx of new reactions. In addition, one extra constraint from the previous set of simultaneous equations was also needed to solve the adenylate & adenosine system. Figures 3.9 and 3.10 show the influx and efflux from each of these pools of metabolites and the sets of simultaneous equations are detailed in Table 3.6.

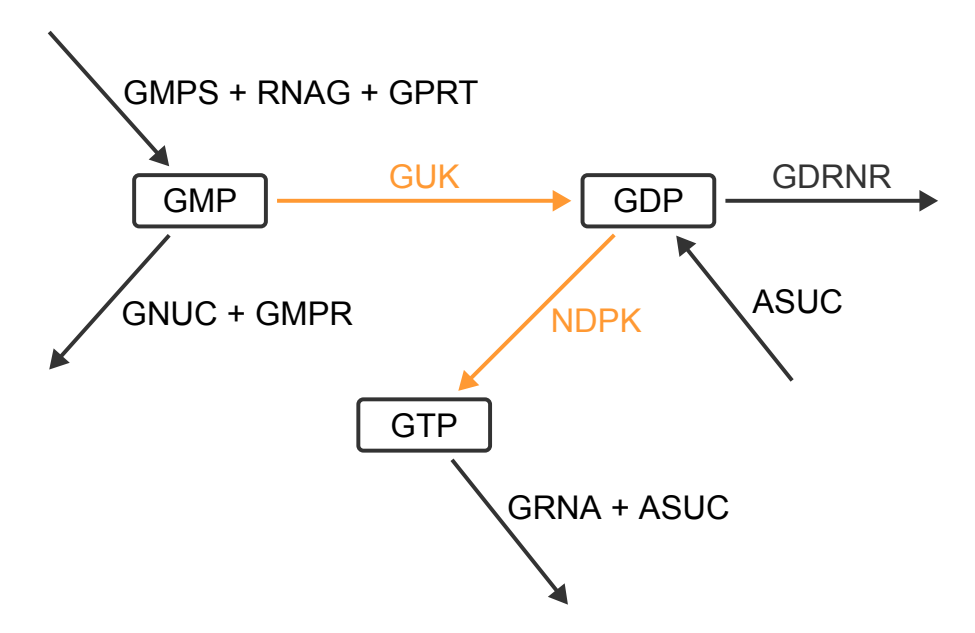


**Figure 3.9:** Influx and efflux from guanylate metabolites. Existing reactions from the Curto *et al.* (1998b) model are indicated with black arrows, whilst the new interconversion reactions are denoted with orange arrows.

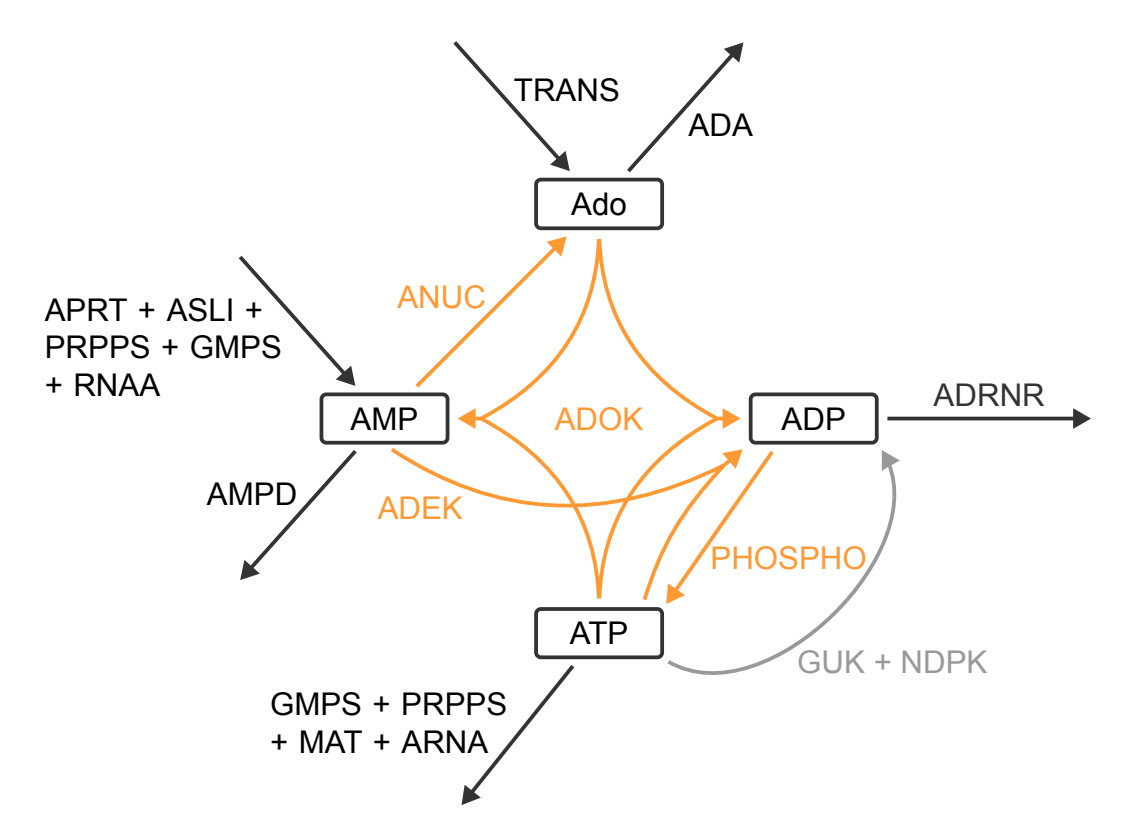


**Figure 3.10:** Influx and efflux from adenylate & adenosine metabolites. Existing reactions from the Curto *et al.* (1998b) model are indicated with black arrows, whilst the new interconversion reactions are denoted with orange arrows and the grey arrow represents reactions whose value was determined from the equivalent guanylate system, see Figure 3.9.

However, whilst solving these systems of simultaneous equations for the new reaction fluxes, it became apparent that the existing steady state flux values from the Curto et al. (1998b) model did not in fact result in an exact steady state, i.e. the sum of fluxes into a metabolite did not equal the sum of fluxes out of it. Although the differences were small, probably due to rounding errors, it was decided to correct for these small inaccuracies when calculating the new reaction flux values.

# 3.4.2 Flux value adjustments

To produce no change in the adenylate & adenosine pool concentration at steady state, the flux value for the reaction ADA was tweaked slightly and similarly for the guanylate pool the flux value for GNUC was tweaked accordingly. In addition, three further fluxes were altered from their steady state value in the Curto et al. (1998b) paper to account

Metabolite	Existing reaction net efflux	New reaction net influx
GMP	$v_{gnuc} + v_{gmpr} - v_{gmps} - v_{rnag} - v_{gprt}$	- v <sub>guk</sub>
GDP	$v_{gdrnr}-v_{asuc}$	$v_{guk}-v_{ndpk}$
GTP	$v_{grna} + v_{asuc}$	$v_{ndpk}$
Ado	$v_{ampd} - v_{aprt} - v_{asli} - v_{prpps} - v_{gmps} - v_{rnaa}$	$v_{adok} - v_{adek} - v_{anuc}$
AMP	$v_{ada}-v_{trans}$	$v_{anuc}-v_{adok}$
ADP	$v_{adrnr} - v_{ndpk} - v_{guk}$	$v_{adok} + 2v_{adek} - v_{phospho}$
ATP	$v_{prpps} + v_{gmps} + v_{mat} + v_{arna} + v_{ndpk} + v_{guk}$	$v_{phospho} - v_{adek} - v_{adok}$

Additional constraint:  $v_{inuc} = 15v_{anuc}$ 

**Table 3.6:** Guanylate and adenylate & adenosine steady state simultaneous equation systems. The additional constraint (taken from the set of equations used to yield flux values for previous versions of the model) is required in order to solve the set of simultaneous equations for the adenylate & adenosine system.

for this slight change in flux in the network. Therefore,  $v_{hxe}$  was amended to remove the extra flux from the network that was produced by tweaking  $v_{ada}$ , whilst  $v_{gua}$  and  $v_{xe}$  were adjusted to negate the effect of altering  $v_{gnuc}$ . The original steady state and tweaked flux values are detailed in Appendix D.

These amended flux values along with the remaining steady state flux values produced by the Curto *et al.* (1998b) model were then used to solve the two systems of simultaneous equations detailed in Table 3.6 to yield flux values for the new reactions (these are listed in Appendix D).

In addition, as the model defined by Curto *et al.* (1998b) is a whole body model and the new model will be used to represent the network in the HL60 cell line, it seemed appropriate to scale the model accordingly.

# 3.4.3 Better scaling

A literature search was undertaken to acquire enzymatic rate data for one reaction, from HL60 cells, from which all the flux values in the network could be scaled. The reaction PRPPS was chosen, as it is the first reaction in the network, and the data was used to scale the whole system to values appropriate for  $1\times10^9$  HL60 cells (Ahmed and Weidemann, 1994). Thus, the unit for flux values in the model is now  $\mu$ mol min<sup>-1</sup> ( $10^9$  HL60 cells)<sup>-1</sup>. Again, the rate constants for the whole system were recalculated using these new flux values and Equation 2.15. The kinetic orders for this final model version are detailed in Table 3.7, whilst the full set of flux values and rate constants for this system are listed in Tables 3.8 and 3.9, respectively. In addition, Figure 3.11 shows the model schematic for this final model. The system of 43 ODE equations for this model (version 3) are detailed in Table 3.10; these were again coded into Matlab version R2015b (The MathWorks Inc., 2015) and simulations were conducted (see Code Appendix for the Matlab code).

				-
$f_{ade6}=0.55$	$f_{adrnr9} = -0.3$	$f_{adrnr10} = 0.87$	)	
$f_{ampd18} = -0.1$	$f_{aprt1} = 0.5$	$f_{aprt6} = 0.75$		
$f_{asli3}=0.99$	$f_{asuc2}=0.4$	$f_{asuc18} = -0.05$		
$f_{dada9} = 1.0$	$f_{den1} = 2.0$	$f_{den2} = -0.06$		
$f_{den18} = -0.08$	$f_{dgnuc10} = 1.0$	$f_{dnan12} = 1.0$		
$f_{dnap9} = 0.42$	$f_{dnap10} = 0.33$	$f_{gdrnr9} = -1.2$		Reactions
$f_{gdrnr10} = -0.39$	$f_{gmpr2} = -0.15$	$f_{gmpr7} = -0.76$		present
$f_{gmps7} = 0.16$	$f_{gnuc18} = -0.34$	$f_{gprt1} = 1.2$		in original Curto <i>et al.</i> (1998b)
$f_{gprt15} = 0.42$	$f_{gua15} = 0.5$	$f_{hprt1} = 1.1$		model,
$f_{hprt2} = -0.89$	$f_{hprt13} = 0.48$	$f_{hxd13} = 0.65$		so value
$f_{hxe13} = 1.12$	$f_{impdh2} = 0.15$	$f_{impdh7} = -0.09$		unchanged
$f_{inuc2}=0.8$	$f_{inuc18} = -0.36$	$f_{mat5} = -0.6$		
$f_{polyam5} = 0.9$	$f_{prpps1} = -0.03$	$f_{prpps17} = 0.65$		
$f_{prpps18} = 0.7$	$f_{pyr1} = 1.27$	$f_{rnan11} = 1.0$		
$f_{trans5} = 0.33$	$f_{uae16} = 2.21$	$f_{xe14} = 2.0$		
$f_{xd14} = 0.55$			J	_
$f_{ada4A}=0.97$	$f_{adrnr4D} = 0.1$	$f_{ampd4M} = 0.81$	)	
$f_{ampd8T} = -0.03$	$f_{aprt4M} = -0.8$	$f_{asli4M} = -0.95$		Danations
$f_{asuc4M} = -0.24$	$f_{asuc8T} = 0.2$	$f_{den4M} = -0.17$		Reactions present
$f_{den4D} = -0.06$	$f_{den4T} = -0.028$	$f_{den8M} = -0.14$		in original
$f_{den8D} = -0.06$	$f_{den8T} = -0.016$	$f_{gdrnr8D} = 0.4$		Curto <i>et al.</i> (1998b)
$f_{gmpr4M} = -0.01$	$f_{gmpr4D} = -0.02$	$f_{gmpr4T} = -0.04$	}	model,
$f_{gmpr8M} = 0.23$	$f_{gmpr8D} = 0.18$	$f_{gmpr8T} = 0.29$		but redefined
$f_{gmps4T} = 0.12$	$f_{gnuc8M} = 0.9$	$f_{gprt8M} = -1.2.$		so specific metabolite
$f_{impdh8M} = -0.03$	$f_{mat4T} = 0.2$	$f_{prpps4M} = -0.1$		is used
$f_{prpps4D} = -0.36$	$f_{prpps4T} = 0.007$	$f_{prpps8M} = -0.004$		15 4564
$f_{prpps8D} = -0.04$	$f_{rnap4T} = 0.05$	$f_{rnap8T} = 0.13$	J	
$f_{adok4A} = 0.44$	$f_{adok4M} = -0.39$	$f_{adok4D} = -0.89$	)	
$f_{adok4T} = 0.038$	$f_{adek4M} = 0.29$	$f_{adek4T} = 0.045$		
$f_{anuc4M} = 1.37$	$f_{anuc18} = -0.21$	$f_{guk4T} = 0.091$	ļ	New
$f_{guk8M} = 0.42$	$f_{ndpk4T} = 0.41$	$f_{ndpk4T} = 0.41$		reactions
$f_{ndpk8M} = -0.037$	$f_{ndpk8D} = 0.29$	$f_{phospho4D} = 0.5$		
$f_{phospho4T} = -0.1$			J	-

**Table 3.7:** Kinetic order values for the final model. Values for kinetic orders for unchanged reaction and metabolite combinations are set equal to those from the Curto *et al.* (1998b) model. Kinetic order values for the existing reactions involving previously pooled metabolites were redefined using the appropriate individual metabolite concentration. Finally, kinetic orders for the new reactions were calculated using the kinetic data in Table 3.4, along with the GMA equations detailed in Appendix C.

$v_{ada}=0.023$	$v_{ade} = 0.00011$	$v_{adna} = 0.11$	)	
$v_{adrnr} = 0.0022$	$v_{ampd} = 0.062$	$v_{aprt} = 0.011$		
$v_{arna}=21.87$	$v_{asli} = 0.0881$	$v_{asuc}=0.088$		
$v_{dada} = 0.0022$	$v_{den}=0.026$	$v_{dgnuc} = 0.0011$		
$v_{dnaa} = 0.11$	$v_{dnag} = 0.075$	$v_{gdna} = 0.075$		Reactions
$v_{gdrnr} = 0.0011$	$v_{gmpr} = 0.0057$	$v_{gmps} = 0.018$		present
$v_{gnuc} = 0.053$	$v_{gprt} = 0.041$	$v_{grna} = 14.58$	}	in original
$v_{gua}=0.013$	$v_{hprt} = 0.041$	$v_{hxd} = 0.013$		Curto <i>et al.</i> (1998b)
$v_{hxe} = 0.00054$	$v_{impdh} = 0.018$	$v_{inuc}=0.029$		model
$v_{mat} = 0.17$	$v_{polyam} = 0.011$	$v_{prpps} = 0.23$		
$v_{pyr} = 0.11$	$v_{rnaa} = 21.87$	$v_{rnag} = 14.58$		
$v_{trans} = 0.15$	$v_{uae}=0.025$	$v_{xe} = 0.00032$		
$v_{xd} = 0.025$			J	
$v_{adek} = 22.28$	$v_{adok} = 0.13$	$v_{anuc}=0.0019$	)	New
$v_{guk} = 14.58$	$v_{ndpk} = 14.67$	$v_{phospho} = 73.94$		reactions

**Table 3.8:** Initial flux values for the final model. The values for existing fluxes were set equal to the steady state flux values produced by the Curto *et al.* (1998b) model and then scaled to  $10^9$  HL60 cells. The new interconversion fluxes were computed by solving the set of steady state equations for the adenylate & adenosine and guanylate pools and then scaled to  $10^9$  HL60 cells. All values are in µmol min $^{-1}$  ( $10^9$  HL60 cells) $^{-1}$ .

$\alpha_{ada} = 0.045$	$\alpha_{ade} = 0.00011$	$\alpha_{adna} = 0.036$	)	
$\alpha_{adrnr} = 0.00080$	$\alpha_{ampd} = 0.0022$	$\alpha_{aprt} = 0.34$		
$\alpha_{arna} = 7.14$	$\alpha_{asli} = 66.55$	$\alpha_{asuc} = 0.023$		
$\alpha_{dada} = 0.00037$	$\alpha_{den} = 0.024$	$\alpha_{dgnuc} = 0.00037$		
$\alpha_{dnaa} = 0.000021$	$\alpha_{dnag} = 0.000015$	$\alpha_{gdna} = 0.025$		Reactions
$\alpha_{gdrnr} = 0.0026$	$\alpha_{gmpr} = 0.0088$	$\alpha_{gmps} = 0.0042$		present
$\alpha_{gnuc} = 0.034$	$\alpha_{gprt} = 0.15$	$\alpha_{grna} = 4.76$	}	in original
$\alpha_{gua} = 0.0057$	$\alpha_{hprt} = 0.14$	$\alpha_{hxd} = 0.0029$		Curto <i>et al.</i> (1998b)
$\alpha_{hxe} = 0.000041$	$\alpha_{impdh} = 0.013$	$\alpha_{inuc} = 0.0099$		model
$\alpha_{mat} = 0.084$	$\alpha_{polyam} = 0.0032$	$\alpha_{prpps} = 0.0039$		
$\alpha_{pyr} = 0.0141$	$\alpha_{rnaa} = 0.00076$	$\alpha_{rnag} = 0.00051$		
$\alpha_{trans} = 0.097$	$\alpha_{uae} = 0.00000097$	$\alpha_{xe} = 0.000013$		
$\alpha_{xd} = 0.011$			J	
$\alpha_{adek} = 3.49$	$\alpha_{adok} = 218.61$	$\alpha_{anuc} = 0.0000062$	J	New
$\alpha_{guk} = 1.91$	$\alpha_{ndpk} = 0.21$	$\alpha_{phospho} = 7.87$		reactions

**Table 3.9:** Rate constants for the final model. Values were calculated using Equation 2.15, kinetic orders and flux values from Tables 3.7 and 3.8, respectively, and initial metabolite concentrations as detailed in Table 2.1.

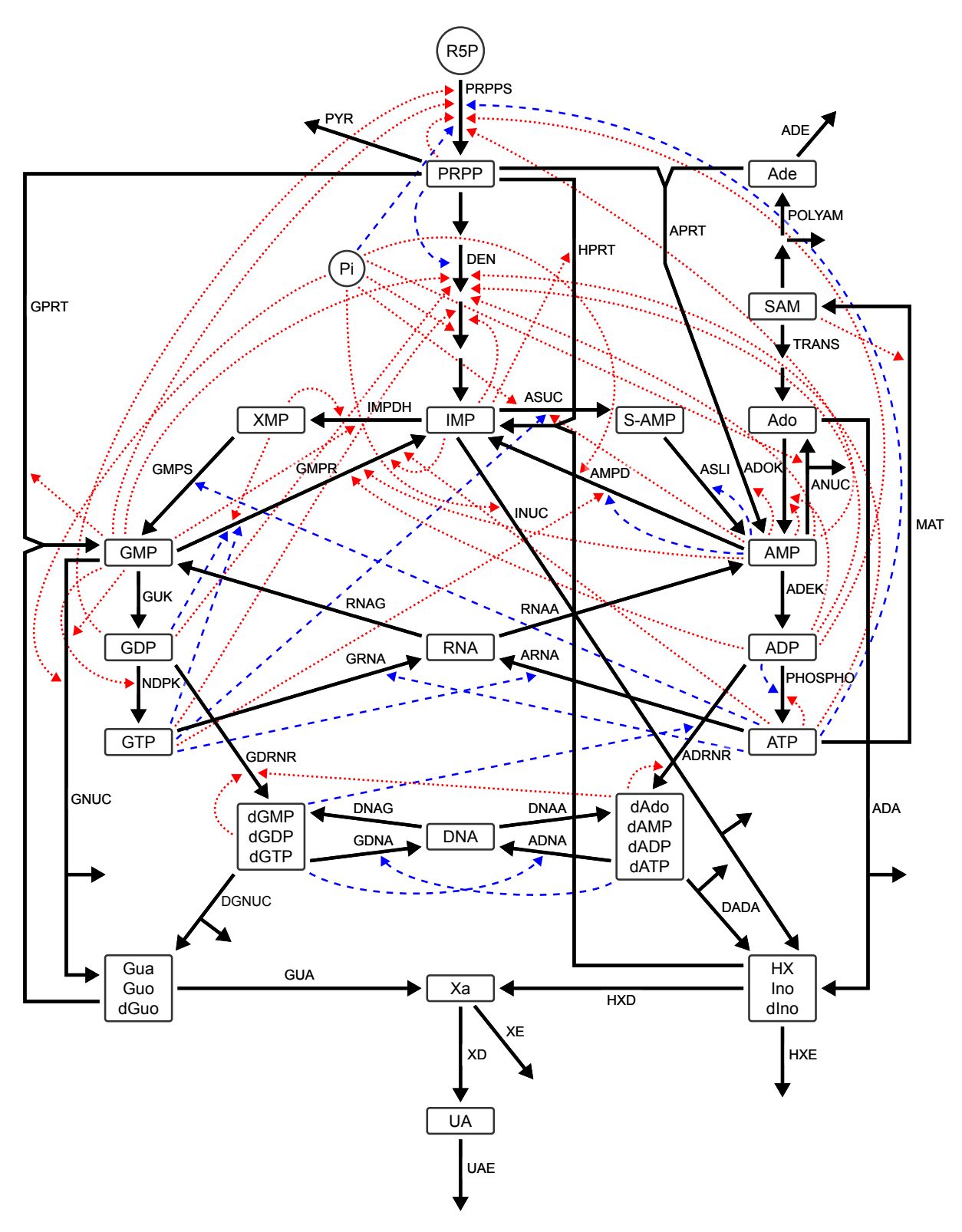


**Figure 3.11:** Network schematic of the final model. Dependent variables (metabolites) are shown in boxes whilst independent variables (R5P and Pi) are denoted by circles. Solid black arrows represent reactions, whilst dashed blue arrows indicate activatory regulations and dotted red arrows denote inhibitory modifications.

#### Metabolite ODE equation

#### continued on the next page

#### Metabolite ODE equation

#### continued on the next page

#### Metabolite ODE equation

**Table 3.10:** ODE equations for the final model. The ODE equation for each metabolite is defined as the sum of all the reactions that produce it minus all the reactions that degrade it, where fluxes are defined in GMA form. Variables consisting of pooled metabolites are defined as follows: dA pool represents dAdo, dAMP, dADP and dATP; dG pool refers to dGMP, dGDP and dGTP; HX pool encompasses HX, Ino and dIno; Guo pool equates to Gua, Guo and dGuo.

#### 3.5 Examination of the model

To asses the validity and accuracy of the final model, steady state analysis and sensitivity analysis were performed along with the re-creation of some of the model tests conducted by Curto *et al.* (1997). The steady state analysis was conducted in COPASI (Hoops *et al.*, 2006) and showed that the model is asymptotically stable, as all real parts of the systems' eigenvalues are negative (see Appendix E). The asymptotic stability of the final model (version 3) matches that seen with the original Curto *et al.* (1997, 1998b) model

(see Appendix E). Therefore similar to the Curto et al. (1997, 1998b) model, this new model is locally stable meaning it will return to its steady state after small perturbations in the system.

## 3.5.1 Sensitivity analysis

Sensitivity analysis investigates how sensitive the model is to its parameters and independent variables. If the sensitivity of the model is being computed with respect to the system's parameters, then the values computed are called (parameter) sensitivities, whilst the values calculated for the system with respect to its independent variables are referred to as logarithmic gains. Sensitivity analysis can be performed by simulating a 1 % change in each parameter (or independent variable) in turn and comparing the steady state value of each metabolite and flux to their steady state value in the unperturbed system (Sorribas and Savageau, 1989c). The sensitivity (or logarithmic gain) values produced can be interpreted in the following way: a value of 0.5 for metabolite or flux Y with respect to parameter (or independent variable) z, means that if z is altered by 1 % then this would result in a 0.5 % change in the value of Y. Usually the lower the absolute value of the sensitivities and logarithmic gains the more robust the model.

From the above description of sensitivity analysis it would appear to be a purely mathematical concept, however it does have a meaningful biological interpretation. Namely, parameter sensitivities represent response to an inherent change within the organism being modelled, e.g. a genetic mutation, and show how the organism responds to this permanent system change (Voit, 2000). In contrast, logarithmic gains can be considered to model a change in environmental conditions and show how the system responds to the altered stimuli, resources, etc. that are present within this new environment (Voit, 2000). Thus, sensitivity analysis provides useful insights into the model being studied as well as being a useful tool to measure system robustness.

To compare the new model's sensitivities to those of the Curto *et al.* (1997, 1998b) model, parameter sensitivities were calculated for all the model's kinetic orders; these are

shown in Appendix E. Most of these sensitivities were evaluated using COPASI (Hoops et al., 2006), except for kinetic orders that are common to multiple reactions (e.g.  $f_{rnap4T}$  for reactions ARNA and GRNA) for which sensitivities were computed using Matlab, as COPASI is unable to correctly deal with such parameter sensitivities. These results reveal that 99 % of the 6016 sensitivities have an absolute value of less than five, with 89 % being less than one. Of the remaining values, only 14 sensitivities have an absolute value greater than 10 (see Figure 3.12). Of these, some are related to marginal metabolites such as the HX pool which Curto et al. (1998b) considered to be inconsequential. In addition, Curto et al. (1997) note that higher sensitivities associated with the reaction PRPPS are to be expected as this is a crucial reaction within purine metabolism. Overall, the fact that the vast majority of the model's sensitivities are less than one indicates that the steady state is robust.

In addition to sensitivities, logarithmic gains for the independent metabolites were also computed using COPASI (Hoops *et al.*, 2006); these are shown in Appendix E. All of the 128 logarithmic gains have an absolute value of less than 2.5, with 89 % being less than one, again indicating that the model is robust.

As the results from the steady state analysis and sensitivity analysis are very similar to those seen with the Curto *et al.* (1997, 1998b) model this indicates that, like the Curto *et al.* (1998b) model, this new model has a robust steady state but is still able to respond to physiological perturbations (Curto *et al.*, 1997, 1998b).

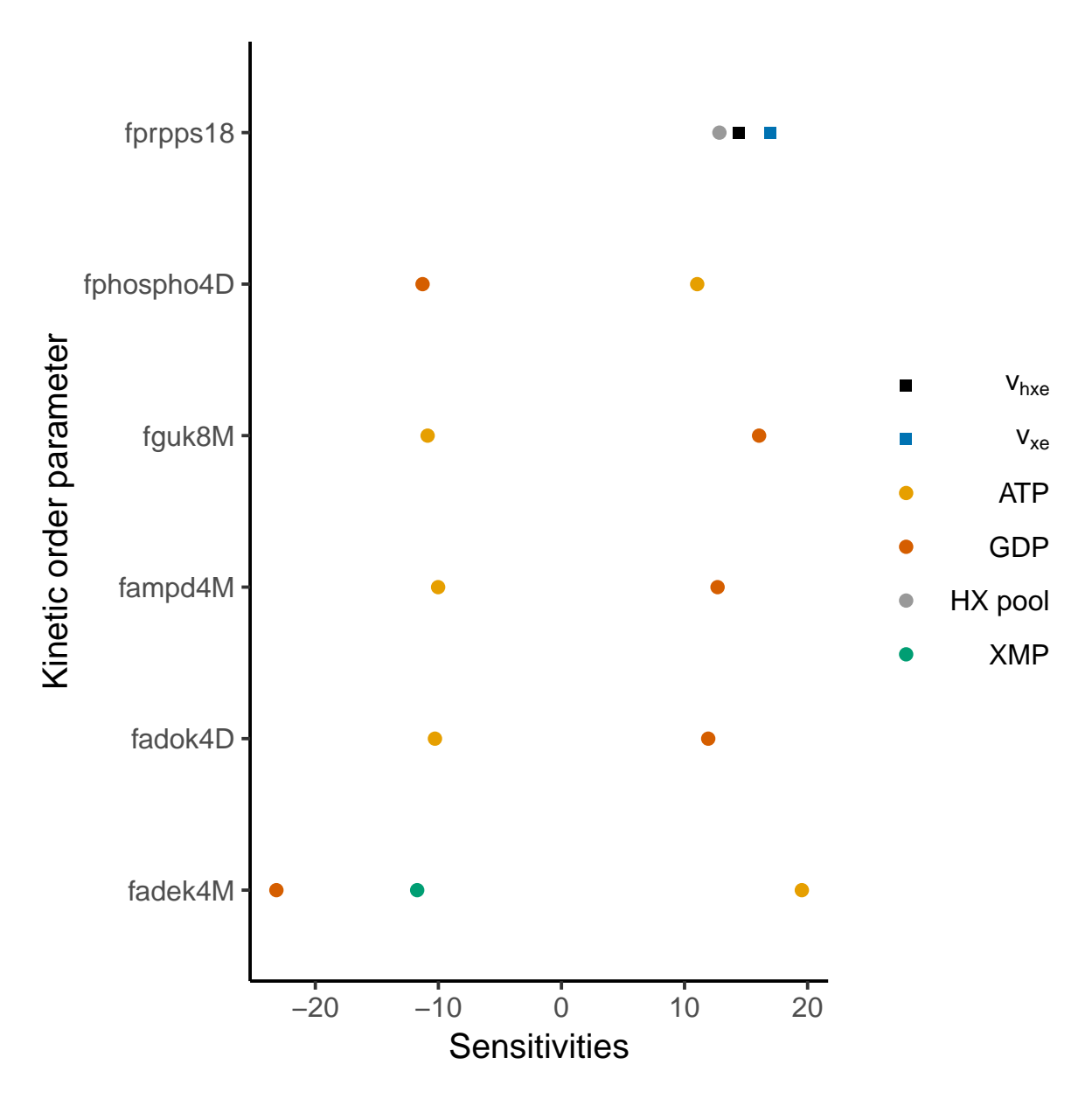


**Figure 3.12:** Parameter sensitivities with values greater than 10. Sensitivities were calculated for all fluxes and metabolites with respect to all kinetic order parameters. Values greater than 10 are shown for fluxes (squares) and metabolites (circles).

#### 3.5.2 Model simulation tests

As well as comparing the final model (version 3) to the Curto *et al.* (1998b) model in terms of their steady states and sensitivities, some of the model tests conducted by Curto *et al.* (1997, 1998b) were also performed on this new model, using the same methods of simulation as Curto *et al.* (1997, 1998b). Firstly, the ability of the model to maintain

consistent levels of the adenylate & adenosine pool and the guanylate pool was assessed. As noted by Curto et~al.~(1997), the concentrations of these pools remain relatively constant over different conditions and thus this was tested by separately altering the initial concentration of each dependent variable ( $\pm 100~\mu M$ ) and recording the largest deviation produced in each of the pools before the system returned to its steady state. These simulations were performed using the new final model with the concentration of the previously pooled metabolites added together (see Table 3.11) to enable comparison with the Curto et~al.~(1997) model output.

C	-	7
	_	_

Variable	Metabolite	Normal conc. (µM)	Adjusted conc. (μM)	A pool	conc. (µM)	G pool	conc. (µM)
Without	alteration to	any variable		Initial	Steady state	Initial	Steady state
				2500.5	2780.7371	400.0	386.0210
With alte	eration to des	scribed variable		Minimum	Maximum	Minimum	Maximum
$X_1$	PRPP	5	105	2500.5	2780.7386	386.1694	400.0
$X_2$	IMP	100	1	2475.4074	2780.7384	385.3423	400.3190
$X_2$	IMP	100	200	2500.5	2780.7370	386.5106	400.0
$X_3$	S-AMP	0.2	100.2	2500.5	2780.7368	386.3928	400.0
$X_5$	SAM	4	104	2500.5	2780.7364	386.3028	400.0
$X_6$	Ade	1	101	2500.5	2780.7368	385.8138	400.0
$X_7$	XMP	25	125	2398.1829	2780.7386	387.0713	430.4710
$X_9$	dA pool	6	106	2500.5	2780.7380	386.1965	400.0
$X_{10}$	dG pool	3	103	2415.9524	2780.7427	387.6541	411.6959
$X_{11}$	RNA	28600	28500	2500.5	2780.7372	384.0632	400.0
$X_{11}$	RNA	28600	28700	2500.5	2780.7370	387.2792	404.9020
$X_{12}$	DNA	5160	5060	2500.5	2780.7450	384.8607	400.0
$X_{12}$	DNA	5160	5260	2500.5	2780.7375	387.1420	400.0
$X_{13}$	HX pool	10	110	2500.5	2780.7372	385.9720	400.0
$X_{14}$	Xa	5	105	2500.5	2780.7374	386.0082	400.0
$X_{15}$	Guo pool	5	105	2447.6989	2780.7389	386.7472	415.2938
$X_{16}$	UA	100	1	2500.5	2780.7369	385.9571	400.0
$X_{16}$	UA	100	200	2500.5	2780.7364	385.9860	400.0

**Table 3.11:** Consistency of previously pooled metabolite concentrations. Simulations were performed using the final model. Initial concentrations of the dependent variables were increased or decreased (where appropriate) by  $100 \,\mu\text{M}$ . The concentrations of the previously pooled adenylate & adenosine and guanylate metabolites were summed and the largest deviation produced in these concentrations before the system returned to its steady state was recorded. dA pool represents the pooled metabolites dAdo, dAMP, dADP and dATP, whilst dG pool indicates the grouping: dGMP, dGDP and dGTP. HX pool equates to the collective species HX, Ino and dIno, whilst Guo pool refers to the group consisting of Gua, Guo and dGuo.

Comparing these results to those produced by the Curto et al. (1997) model (see Appendix E) shows that the new model is able to maintain relatively consistent levels of the adenylate & adenosine and guanylate pools and, similar to the Curto et al. (1997) model, the largest deviations from the steady state values are produced when the level of XMP, the dG pool or the Guo pool is altered.

Next, PRPPS superactivity was simulated by doubling the value of the rate constant for the reaction PRPPS and lastly, HGPRT deficiency was modelled by reducing the rate of this reaction to 1 % of its original level; this was achieved by reducing the rate constants for both of the reactions HPRT and GPRT, which are both catalysed by the enzyme HGPRT, to 1 % of their original values.

The results from both of these analyses show that the new model performs in a similar way to the Curto et al. (1997, 1998b) model, both in terms of the percentage change in metabolites and fluxes monitored and in the closeness of these simulated results to available data from patients with diseases that cause these metabolic changes. The results from both test simulations from the new model are shown in Table 3.12, along with both clinical data and model results from Curto et al. (1997, 1998b).

Collectively, these three tests show that the new model (version 3) is able to match the performance of the Curto et al. (1998b) model in its ability to re-create experimental and clinical data, and together with the steady state and sensitivity analyses highlight that the new model is robust and should hopefully provide a useful tool to model purine metabolism in HL60 cells.

٩	
$\circ$	

Metabolite	Curto	Curto PRPPS	%	Clinic data	Model 3	Model 3 PRPPS	%	Clinic data
or flux	at <i>op</i>	superactivity	change	from Curto	at <i>op</i>	superactivity	change	scaled
$\overline{X_1}$	5	7.8	156	13–29	5	7.8	157	13–29
$X_{13}$	10	41	410	30	10	44.5	445	30
$X_{14}$	5	15	300	10	5	14.7	295	10
$X_{16}$	100	131	131	300	100	130.9	131	300
$v_{den}$	2.39	4.7	197	4.7-12.4	0.026	0.052	196	0.052-0.14

Metabolite	Curto	Curto 1 %	%	Clinic data	Model 3	Model 3 1 %	%	Clinic data
or flux	at op	HGPRT	change	from Curto	at <i>op</i>	HGPRT	change	scaled
$\overline{X_{13}}$	10	70.6	706	71	10	89.3	893	71
$X_{14}$	5	22.5	450	15	5	26.7	534	15
$X_{16}$	100	145.7	146	150	100	151.7	152	150
$v_{den}$	2.39	6.3	264	40	0.027	0.080	302	0.4406
$v_{hxe}$	0.05	0.4	880	0.45	0.00054	0.0063	1162	0.0050
$v_{uae}$	2.30	5.3	230	7–14	0.025	0.064	251	0.077-0.15
$v_{xe}$	0.03	0.6	2000	0.27	0.00032	0.0091	2853	0.0030

Table 3.12: PRPPS superactivity and HGPRT deficiency simulation results. PRPPS superactivity (top panel) was simulated by doubling the rate constant for the reaction PRPPS, whilst HGPRT deficiency (bottom panel) was simulated by reducing the rate constants for the reactions HPRT and GPRT; concentrations and fluxes shown are for metabolites and reactions that are affected by PRPPS (top panel) and HGPRT (bottom panel) activity and for which there is clinical data available. Simulation results are shown for both the new model (version 3) and the Curto *et al.* (1997, 1998b) model. Clinical data is taken from Curto *et al.* (1997, 1998b), where appropriate references can be found. op is the operating point. All clinical data for metabolites has units μM, whilst flux data from Curto *et al.* (1997, 1998b) has units: μmol min<sup>-1</sup> (Body weight<sup>-1</sup>) and scaled flux data has units: μmol min<sup>-1</sup> (10<sup>9</sup> HL60 cells)<sup>-1</sup>.

# 3.6 Issues with the model

Simulations of 28 % IMPDH inhibition were conducted with this final model (version 3), which again resulted in a large increase in the concentration of ATP; a percentage change of 528 % (see Figure 3.13). Therefore, a search of the literature was undertaken to find purine data for IMPDH inhibited cells. This yielded concentration data for certain metabolites in HL60 cells after treatment with MPA. In addition, fluxes for some reactions in the network were also obtained from MPA treated HL60 cells; this along with the aforementioned metabolite data are detailed in Table 3.13.

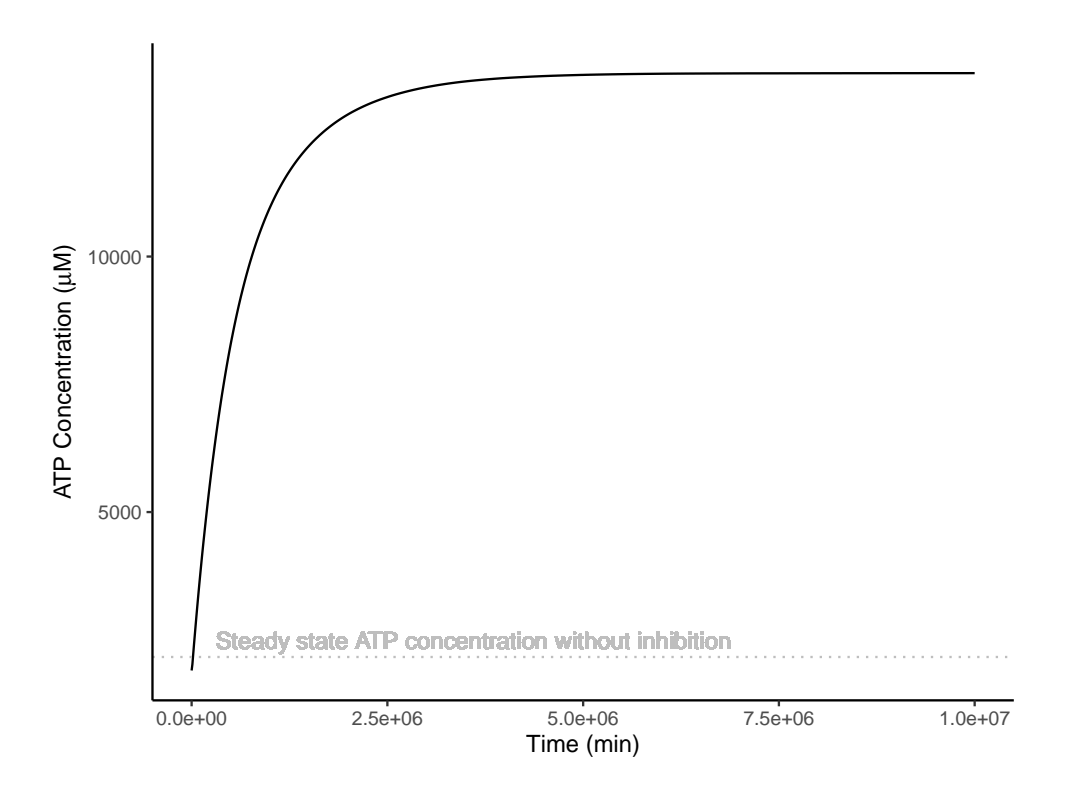


**Figure 3.13:** ATP concentration from the final model with simulation of 28 % IMPDH inhibition. The grey line shows the steady state concentration of ATP from the same model without inhibition.

Metabolite change (% of control)					Experimental	Experimental details			
PRPP	IMP	ADP	ATP	GTP	Conc. (µM)	Time (h)	Source		
150	103				5	72	Ahmed and Weidemann (1995)		
		58	71	23	1	72	Lucas <i>et al.</i> (1983a)		
			$\approx 70$	$\approx 25$	3	48	Collart and Huberman (1990)		
			$\approx 85$	$\approx 15$	10	24	Sokoloski <i>et al.</i> (1986)		
				20-24	1-10	24	Inai <i>et al.</i> (2000)		
			No change	23	2	96	Inai <i>et al.</i> (2000)		

Flux cha	nge (% of	control	)	Experimental details					
IMPDH	PRPPS	DEN	ASUC	GMPS	HGPRT	APRT	Conc. (µM)	Time (h)	Source
72	91	28	82	71	302	100	5	72	Ahmed and Weidemann (1995)

**Table 3.13:** Literature data for MPA treated HL60 cells. Values shown are percentage of control (untreated cells). Time is period of exposure to the IMPDH inhibitor MPA.

With this newly acquired data, it was decided to perform a search of the model parameter space in an attempt to find parameters which could better re-create this experimental data.

## 3.6.1 Grid search parameter simulations

Due to the large number of parameters that are present in the model, it was decided to target specific reactions in the network in the parameter grid search. Firstly, the reactions involved in degrading ATP and IMP were chosen as it was noted that upon simulation of IMPDH inhibition the level of HX was not increasing as much as expected; intuitively, a build up of IMP should have led to an increased rate of degradation of IMP to HX. In addition, the enzymatic data in Table 3.13 suggested that IMPDH inhibitors affect other enzymes in the network, albeit perhaps only as a knock-on effect via gene regulation. Therefore, two simulations were conducted; one whereby the ATP and IMP degradation enzymes along with a few others related to the other adenylate & adenosine and guanylate species were altered, and the second where reactions with kinetic data upon IMPDH inhibition (see Table 3.13) were adjusted.

For each enzyme that was perturbed, a factor, p, was multiplied by the rate constant value for that reaction, where p took the following values: 1/3, 0.5, 0.8, 1.5, 2, 3. For the analysis without literature data, a level of IMPDH inhibition of 28 % was used; whilst for the analysis of enzymes with data, the rate constant for the reaction IMPDH was also multiplied by the factor p. Some of the selected reactions are catalysed by an enzyme that also catalyses other reactions in the network, thus the corresponding rate constants for all these enzymes are altered by the same multiplication factor. The list of reactions in each set of simulations is outlined below; reactions that are catalysed by the same enzyme are grouped together:

- ADA/DADA, GMPR, INUC/ANUC/GNUC, ADRNR/GDRNR, MAT, TRANS, AMPD, ASLI
- 2. IMPDH, PRPPS, DEN, ASUC, GMPS, HPRT/GPRT, APRT

The new steady state concentration values from these simulations were compared to those from the literature and suitable parameter sets were defined as those that produced metabolic concentrations that lay within reasonable ranges that encompassed the literature values, as outlined in Table 3.14.

Metabolite	% change from data	Acceptable % range
PRPP	150	140–160
IMP	103	90–110
ADP	58	45–65
ATP	82	65–85
GTP	22	18–27

**Table 3.14:** Metabolite concentration ranges for parameter grid search. Values shown are percentage of control (untreated cells) and are the average value for each metabolite from the available literature data, see Table 3.13. Also detailed are parameter ranges for use in determining acceptable parameter sets.

The results from the first set of simulations showed that it is possible to reduce the level of ATP upon IMPDH inhibition and still match with most of the other data. There were 54 sets of these parameters that were able to match with four of the five concentration ranges (IMP, ADP, ATP and GTP), these are detailed in Appendix F.

The results from the second set of simulations showed that no sets of parameters were able to match to the metabolite data ranges when any level of IMPDH inhibition was present.

As the results from both of these simulations show, it was not possible to find parameter values that were able to match to the concentration range set for PRPP. Indeed, this metabolite is a special case as it is the first dependent metabolite in the system as it is synthesised from the independent species R5P. Therefore, it was suggested that the level of R5P be raised as this should only serve to increase the level of PRPP and not affect the model in any other way, as R5P is an independent metabolite and thus does not have any regulatory control within the model. It was therefore decided to expand the scope of these grid search analyses by combining both of the above simulations and

to also include the level of R5P within the parameter search.

# 3.6.2 Combined large-scale parameter simulations

As in the previous simulations, p was used as a multiplication factor for the reaction rate constants, but this time the actual values of p were determined by sampling from one of two uniform distributions; the first covering the range 1/3–1 and the second spanning the range 1–3; such that each distribution was sampled an equal number of times. In addition, the concentration of R5P was altered by a multiplication factor whose values were selected by sampling from a uniform distribution in the range 1.2–2.

Two different simulations were conducted using this method, each with 1,000,000 simulations. The first had a fixed level of 28 % IMPDH inhibition, whilst the second allowed IMPDH inhibition to vary between 0–70 %, i.e. the range of the multiplication factor for the IMPDH rate constant was 0.3–1, with values again being determined by sampling from a uniform distribution over this range.

The results from these simulations showed that it was possible to produce metabolite concentrations that satisfied the predefined ranges for all five metabolites (as outlined in Table 3.14), however the number of parameter sets which achieved this was very small. Only four sets of parameters from the first simulation were able to produce concentration matches, whilst only two parameter sets matched from the second set of simulations; all six parameter sets are detailed in Appendix F.

Therefore, using the first type of simulation (i.e. with the level of IMPDH inhibition set to 28 %), a larger parameter search with 4,000,000 simulations was undertaken. This resulted in more parameter sets which could achieve concentrations within the predefined ranges for all five metabolites; there were 22 sets in total and these are outlined in Appendix F. Closer examination of these 22 parameter sets revealed a number of consistent patterns for certain reactions, these are shown in Figure 3.14 and detailed below:

- INUC/ANUC/GNUC rates are always increased
- DEN rate is always decreased

- GMPS rate is always decreased
- HPRT/GPRT rates are always decreased

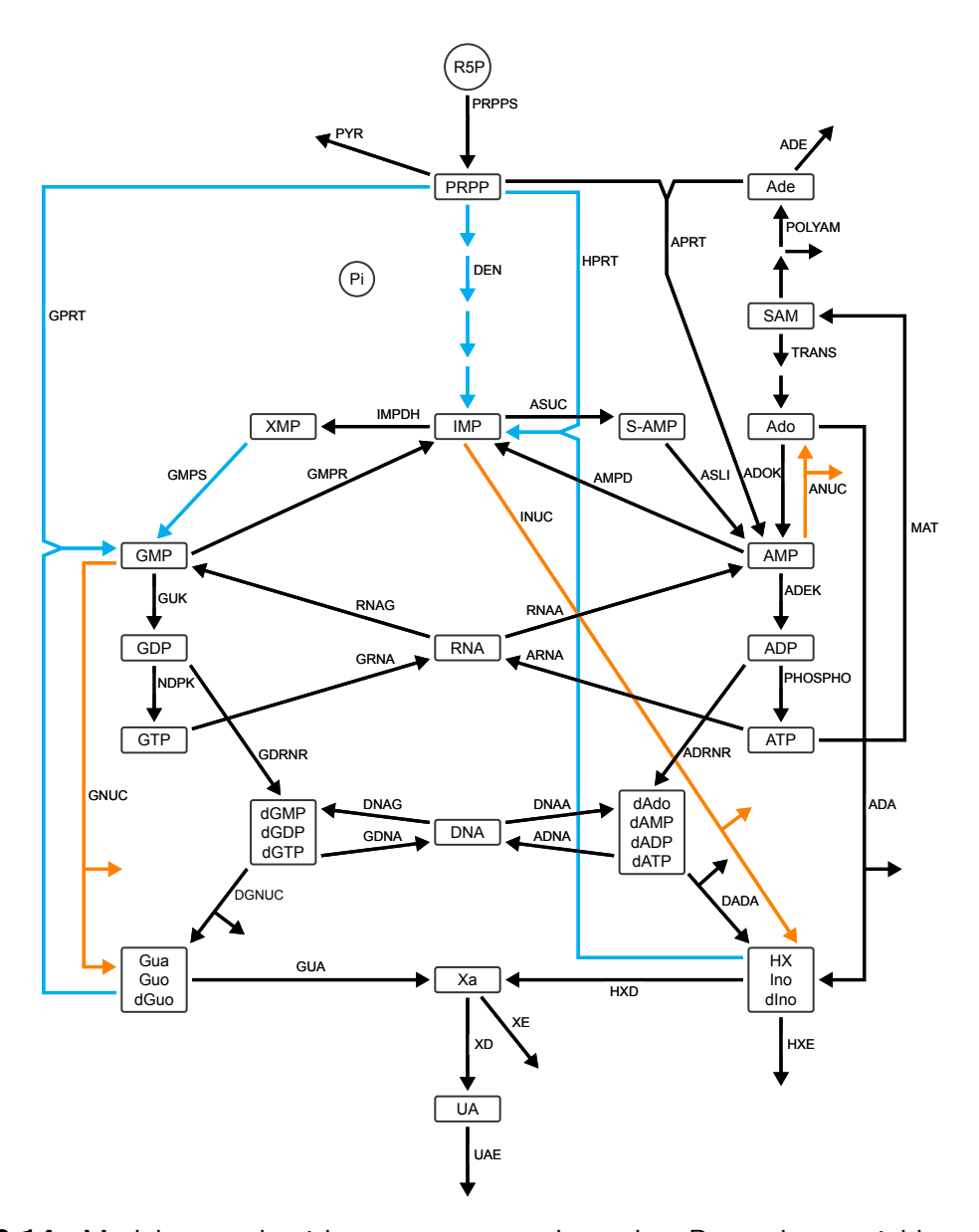


**Figure 3.14:** Model network with parameter search results. Dependent variables are shown in boxes whilst independent variables are denoted by circles. Arrows represent reactions; with cyan arrows indicating reaction rates that are always decreased in the parameter search results, whilst orange arrows indicate reaction rates that are always increased in those simulations. Activatory and inhibitory modifications are omitted for simplicity.

The consistent decrease in the *de novo* pathway (DEN) is expected due to product inhibition by IMP, which accumulates in the presence of IMPDH inhibitors. Similarly,

the flux through GMPS would be lowered due to a lack of XMP. In contrast, the other patterns involve enzymes that catalyse multiple reactions within the network; some with GMP and others with IMP, as a product or substrate. As such the behaviour seen is more complicated to decipher, as one would anticipate the system to enhance mechanisms that degrade IMP, whilst decreasing those that synthesise it, whereas the opposite would be expected for GMP. Therefore, the decrease seen in the salvage pathways (HPRT/G-PRT) is probably due to decreased HX salvage via HPRT, which obscures the anticipated increase in guanine salvage (GPRT). Similarly, the increase in 5'-nucleotidease activity (INUC/ANUC/GNUC) is likely to represent an increased flux through INUC, and perhaps ANUC, which is masking the expected decrease in GMP hydrolysis (GNUC). In light of these results, in future analyses of this type, it would seem prudent to uncouple INUC, ANUC and GNUC as well as HPRT and GPRT, given that the substrate/product concentrations for their individual reactions vary greatly upon IMPDH inhibition and thus their reaction rates are unlikely to respond in a similar manner.

Nevertheless, these results show that it is possible for the model to match the experimental observations; however, the sparsity of data available limits the ability to determine whether the model is fully recapitulating the effect of IMPDH inhibitors on purine metabolism. Therefore, experimentation was conducted to broaden the scope of metabolite data available for HL60 cells to facilitate further testing of the model to improve its accuracy.

# Chapter 4: Experimental Methods and Results

# 4.1 Materials and methods

#### 4.1.1 Purine standards

All HPLC purine standards (all from Sigma, except XMP which was from Santa Cruz) were made as 100 mM stock solutions in 100 mM Tris pH 8.7, except adenosine and guanosine which were dissolved in DMSO and hypoxanthine which was dissolved in DMSO to produce a 50 mM stock solution. All standards were stored in aliquots at -20 °C until needed. All purine standards for HPLC were used at a final concentration of 1 mM unless otherwise stated.

Guanosine and a denosine for use in differentiation experiments were both dissolved in cell culture media immediately before use at a concentration of 100  $\mu$ M and used at a final concentration of 50  $\mu$ M.

The adenylate kinase inhibitor P<sup>1</sup>, P<sup>5</sup>-diadenosine pentaphosphate, Ap5A (Sigma), was prepared as a stock solution of 10 mM by dissolving in 100 mM Tris pH 8.7 and stored at -20 °C until needed.

Ribose 5-phosphate, R5P (Sigma), was prepared as a 10 mM stock solution by dissolving in 100 mM Tris pH 8.7 and was stored at -20 °C until needed.

# 4.1.2 Differentiating agents

All-trans Retinoic acid, ATRA (Sigma), was prepared as a 100 mM stock solution in absolute ethanol. Mycophenolic Acid, MPA (Sigma), was prepared as a 20 mM stock solution by dissolving in absolute ethanol. Mizoribine, MZ (MedChemExpress), was prepared as a 25 mM stock solution in PBS. All were stored at -80 °C until needed with

ATRA stored in the dark and handled with minimal exposure to light.

## 4.1.3 HPLC procedure

HPLC experiments were conducted using two different systems: a Waters system and an Agilent machine. The Waters system comprised a 1525 dual pump, a 717+ Autosampler and a 2487 dual wavelength UV/Visible light detector. Breeze software (version 3.3) was used to control the system and collect and process the data. The Agilent machine was an Agilent Infinity II 1260 machine with Agilent ChemStation software, used to operate the machine and analyse the data.

Purines were separated using ion-pair RP-HPLC with a gradient elution method. A Supelcosil LC-18-T column of 5 µm particle size was used together with the ion-pair reagent Tetrabutylammonium hydrogen sulphate, TBAHS (Fisher Chemical, Laboratory reagent grade). Various gradient elution methods were tried, with the following producing acceptable resolution and reproducibility:

Protocol 1		Protoco	Protocol 2		Protocol 3	
Time (min)	%A	Time (min)	%A	Time (min)	%A	
0.0	100	0	100	0	100	
2.5	100	3.0	100	9.0	80	
10.0	80	17.0	80	10.0	60	
21.0	60	41.0	60	30.0	0	
27.0	0	48.5	0	35.0	0	
32.0	0	55.0	0	40.0	95	
32.1	100	55.1	100	80.0	95	
37.0	100	60.0	100	85	100	
Flow rate: 1.5 ml/min		Flow rate: 1.25	Flow rate: $1.25 \text{ ml/min}$		Flow rate: 1.0 ml/min	
Temperature: Not set		Temperature	Temperature: 19 °C		Temperature: 35 °C	

**Table 4.1:** HPLC gradient methods and specifications. Described are the alternative gradient methods utilised, along with details of the flow rate and temperature settings used.

HPLC buffers were made fresh before use, from stock solutions of 100 mM TBAHS, 1 M KH<sub>2</sub>PO<sub>4</sub> (Sigma, ≥98 %) and Methanol (LiChrosolv, hypergrade for LC-MS) with pH adjusted with concentrated HCl, as below:

Buffer A:  $100 \text{ mM KH}_2\text{PO}_4 + 4 \text{ mM TBAHS}, \text{ pH } 4$ 

Buffer B:  $70 \text{ mM KH}_2\text{PO}_4 + 4 \text{ mM TBAHS} + 30 \% \text{ Methanol, pH } 5.5$ 

All samples and standards were filtered before analysis using a 0.2  $\mu$ m HPLC syringe filter (Whatman) and buffers were filtered and de-gassed using a vacuum filtration pump before use.

For some analyses the temperature of the column was fixed and maintained throughout, either by immersing the column in a temperature controlled water bath or an oven, see Table 4.1 for details of temperatures used.

Purines were detected by measuring absorbance at 254 nm. Integration of the area under the peak corresponding to each metabolite was computed using either the Breeze or Agilent ChemStation software to yield the absorbance for each purine.

#### 4.1.4 Calibration curves

HPLC calibration was conducted using serial dilutions for each standard such that a range of concentrations was produced for each metabolite. These spanned a central value that estimated the concentration of each purine present in an HL60 cell extract, as determined by HPLC analysis. The range spanned a  $\log_{10}$  fold change above and below this central value, in half- $\log_{10}$  increments, thus creating a series of five concentrations from which the calibration curves were constructed. Some metabolites were not detected, or were present at very low levels, in the HL60 cell extract thus their central value was estimated based on other metabolite levels. However, when all 11 sets of standards were initially analysed via HPLC all of the lowest concentrations were undetectable, therefore this calibration standard was dropped from each set and replaced by an additional higher concentration. See Appendix G for details of the ranges used for each calibration curve and the concentration of each species in untreated HL60 cells as determined by HPLC. Calibration curves were plotted and the line of best fit was determined for each metabolite using the programming language R, version 4.0.3 (R Development Core Team, 2021). See

Appendix G for the full set of eleven purine calibration curves and calibration equations.

#### 4.1.5 Cell culture

HL60 cells, obtained from Public Health England (catalogue number: ECACC 98070106), were maintained in RPMI 1640 plus GlutaMAX<sup>TM</sup> (Gibco, Life Technologies) supplemented with 10 % (v/v) Foetal Bovine Serum, FBS (Gibco, Life Technologies), plus 100 units/ml Penicillin and 100  $\mu$ g/ml Streptomycin (Sigma), at 37 °C in a 5 % v/v CO<sub>2</sub> atmosphere. 50 ml cultures in T75 plastic cell culture flasks (Thermo Fisher Scientific) were maintained at a density between  $2\times10^5$  and  $1\times10^6$  with passaging every 42 h to 72 h.

# 4.1.6 Phosphoribosylpyrophosphate synthetase (PRPPS) assay

HL60 cells were centrifuged at  $200 \times g$  for 5 min at 4 °C and the supernatant aspirated. The pellet was resuspended in PBS and washed twice by centrifugation. The resulting pellet was resuspended in 1 ml of 1 mM EDTA, 1 mM DTT in PBS (Buffer A) and placed on ice. A small volume was removed for cell counting. The sample was sonicated on ice using a probe sonicator on 50 % duty cycle, power setting 4 for 10 s. The sample was mixed gently and the process repeated twice. The cell lysate was then centrifuged in a TLA-45 rotor to remove debris at  $40,000 \times g$  for 40 min at 4 °C. The supernatant was passed through a NAP<sup>TM</sup>-10 column (previously equilibrated with Buffer A) and the protein was eluted with 1.5 ml Buffer A. The protein concentration in the eluate was estimated by measuring optical absorbance at 280 nm using a NanoDrop<sup>TM</sup> instrument (Thermo Fisher Scientific). Protein extracts were incubated at 37 °C, for varying time periods, with an equal volume of reaction mixture: 50 mM Tris pH 7.4, 5 mM MgCl, 1 mM EDTA, 1 mM DTT, 32 mM NaH<sub>2</sub>PO<sub>4</sub>, 0.5 mM MgATP, 0.15 mM R5P, 0.25 mM Ap5A. After the required time period, the reaction was stopped by adding an excess of EDTA and the sample was placed on ice. Control samples already containing an excess of EDTA prior to the addition of the protein extract, were placed straight on ice without incubation. The resulting solutions were transferred to YM-10 Centricon® centrifugal

filter devices (Millipore) and centrifuged in a J2-20 rotor at  $9770 \times g$  for >12 h at 4 °C to remove protein and other large molecules. The recovered filtrates were stored at -80 °C until analysis via HPLC. The area under the curve corresponding to AMP on each chromatogram was determined and was converted to a concentration using the HPLC calibration curve and equation for AMP (see Appendix G, for the calibration curve plot and equation).

## 4.1.7 Flow cytometry analysis of HL60 cell differentiation

Six or 12 well plates were seeded with  $2\times10^5$  HL60 cells/ml (final volume: 3 ml or 1 ml, respectively) in the presence or absence of differentiating agents and/or guanosine or adenosine, as a negative control. In most cases cells were maintained for three days before analysis by flow cytometry, however initial experiments were conducted on each of one to seven days after set-up. The final concentration of agents added were as follows: ATRA 1 μM; MPA 1 μM (2 μM also tried initially); MZ 50 μM (100 μM also tried initially); guanosine 50 µM; adenosine 50 µM. Cells were collected and centrifuged at 200 × g for 5 min at 4 °C. The pellet was resuspended in PBS and the cells were washed once. The supernatant was aspirated and the pellet resuspended in a 2 % anti-CD11b antibody (Bio-Rad, Rat anti-Mouse CD11b:Alexa Fluor® 488, Clone number: M1/70.15, Catalogue number: MCA74GA488, also cross-reactive with Human CD11b), 5 % FBS solution in PBS. The sample was left on ice for 30 min in the dark, after which time it was washed with PBS. The pellet was resuspended in PBS and the sample was analysed by flow cytometry on an Attune<sup>TM</sup> NxT Acoustic Focusing Cytometer (Thermo Fisher Scientific). Alexa Fluor® 488 was excited by the blue laser and detected using a 530/30 nm bandpass filter. An unstained sample of control (untreated) HL60 cells that were not incubated with the anti-CD11b antibody was used to set the gate. The programming language R, version 4.0.3 (R Development Core Team, 2021), along with the package CytoExploreR (Hammill, 2021) were used to analyse the data.

#### 4.1.7.1 Effects of combining ATRA and IMPDH inhibitors

The above experimental procedure for analysing HL60 cell differentiation was followed except that cells were maintained in media containing various combinations of the differentiating drugs for four days (three days in initial experiments). In addition, varying concentrations of the drugs were used: MPA at 0.1  $\mu$ M, MZ at 5  $\mu$ M and ATRA ranging from 1 nM to 1  $\mu$ M.

# 4.1.8 HL60 cell reactive oxygen species detection experiments

Twelve well plates were seeded with  $2\times10^5$  HL60 cells/ml (final volume 1 ml) in the presence or absence of differentiating agents and were maintained for three days. Cells were then stimulated with 200 nM phorbol 12-myristate 13-acetate (PMA) for 30 min at 37 °C in a 5 % v/v CO<sub>2</sub> atmosphere to induce reactive oxygen species (ROS) production. The reagent from the Deep Red Cellular ROS Assay Kit (abcam: ab186029) was added to the cells as per the manufacturer's instructions and incubated for 45 min at 37 °C in a 5 % v/v CO<sub>2</sub> atmosphere. Cells were then harvested and centrifuged at 200  $\times$  g for 5 min at 4 °C. The pellet was resuspended in PBS and the cells were washed once. The supernatant was aspirated and the pellet resuspended in a 2 % anti-CD11b antibody (Bio-Rad, Rat anti-Mouse CD11b:Alexa Fluor® 488, Clone number: M1/70.15, Catalogue number: MCA74GA488, also cross-reactive with Human CD11b), 5 % FBS solution in PBS. The sample was left on ice for 30 min in the dark, and then washed with PBS. The pellet was resuspended in PBS and the sample was analysed by flow cytometry on an Attune<sup>TM</sup> NxT Acoustic Focusing Cytometer (Thermo Fisher Scientific). Alexa Fluor® 488 was excited by the blue laser and detected using a 530/30 nm bandpass filter and Deep Red Cellular ROS detection reagent was excited by the red laser and detected in the 670/14 nm channel. Cells labelled with either anti-CD11b or Deep Red Cellular ROS detection reagent alone were used to set the gate for the other fluorophore. In addition, an unstained sample of control (untreated) HL60 cells that were not incubated with the anti-CD11b antibody or the Deep Red Cellular ROS detection reagent was used as an additional negative control. The programming language R, version 4.0.3 (R Development Core Team, 2021), along with the package CytoExploreR (Hammill, 2021) were used to analyse the data.

#### 4.1.9 HL60 cell purine extraction

HL60 cells were centrifuged at  $200 \times g$  for 5 min at 4 °C. The cell pellet was washed twice with PBS (Sigma) and then resuspended in PBS to give a total volume of  $300 \mu l$ . A small volume was removed for cell counting. An equal volume of ice cold 6 % (w/v) trichloroacetic acid (TCA) was added before vortexing for 20 s and then placing on ice for 10 min. The sample was then centrifuged at  $300 \times g$  for 10 min at 4 °C. 0.5 ml of supernatant was recovered and neutralised with the addition of 5 M K<sub>2</sub>CO<sub>3</sub> to approx. pH 6 (checked with high resolution pH indicator paper).

Samples prepared for HPLC calibration curves and peak assignment were stored at -20 °C until needed. In addition, samples obtained from cell cultures treated with differentiating reagents were also stored at -20 °C until HPLC analysis.

## 4.1.10 HPLC analysis of HL60 cell purine levels

T75 cell culture flasks (Thermo Fisher Scientific) were seeded with  $2\times10^5$  HL60 cells/ml (final volume 50 ml) in the presence or absence of differentiating agents and/or guanosine. The concentration of agents added were as follows: ATRA 1  $\mu$ M; MPA 1  $\mu$ M; MZ 50  $\mu$ M; guanosine 50  $\mu$ M. Cells were maintained for three days at 37 °C in a 5 % v/v CO<sub>2</sub> atmosphere; with control cells, i.e. those without any differentiation agents present, being passaged as required. The cells were then lysed as per the extraction method detailed in 4.1.9 and the resulting solution analysed via HPLC, as outlined in 4.1.3. In each chromatogram, the area under the curve corresponding to each metabolite was determined and converted to a concentration using the relevant calibration curve and equation (see Appendix G, for the calibration curve plots and equations).

#### 4.1.11 Statistical analysis

To analyse the statistical significance of drug treatments on HL60 cell differentiation, a Kruskal–Wallis test followed by pairwise comparisons using a Conover post-hoc test, with Benjamini–Hochberg correction for multiple comparisons, was conducted using the R package PMCMRplus (Pohlert, 2021). Differences with a p-value < 0.05 were considered significant.

## 4.2 Results

### 4.2.1 Phosphoribosylpyrophosphate synthetase (PRPPS) assay

As the refined mathematical model of purine metabolism is to be used to investigate the network in HL60 cells, part of the refinement process was to scale the model from a whole body model to one appropriate for 10<sup>9</sup> HL60 cells. Data from HL60 cells for the reaction rate of the first enzyme in the network, PRPPS, was obtained from the literature (Ahmed and Weidemann, 1994) and used to scale the model accordingly. However, it was decided to perform an enzyme assay using HL60 cells to determine the reaction rate for PRPPS in order to either confirm the rate obtained by Ahmed and Weidemann (1994) or provide an alternative value with which to scale the model. Therefore, utilising a protocol adapted from that used by Torres et al. (1996) the reaction rate of PRPPS was determined from HL60 cell extracts. The reaction was assessed over a time course consisting of the time points: 0, 5, 10, 20, 30, and 40 min, with metabolite concentrations from each time point being analysed via HPLC (see Appendix H for chromatograms). The reaction catalysed by PRPPS is as follows:

$$R5P + ATP \xrightarrow{PRPPS} PRPP + AMP$$

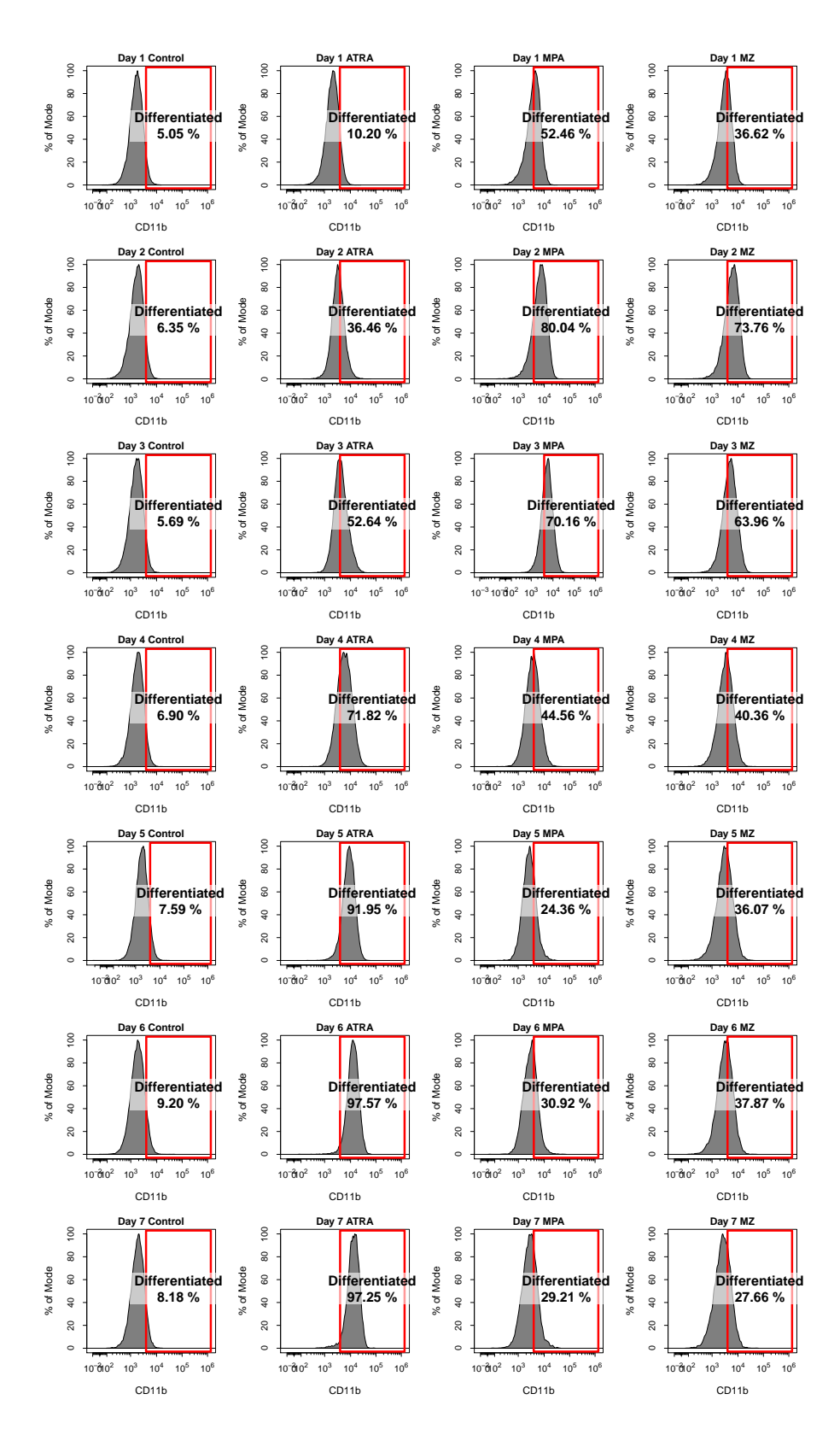
Therefore, the reaction rate can be determined by calculating the rate of AMP production. As shown in Appendix H, AMP production, and thus the rate of reaction, is

linear for the first 20 min or so, therefore the reaction rate was calculated using data from within this time period. This experiment was performed twice; one yielded a value greater than the value from Ahmed and Weidemann (1994) and the other produced a value less than the value from the literature;  $3.49 \, \mu \text{mol} \, \text{min}^{-1} \, (10^9 \, \text{HL}60 \, \text{cells})^{-1}$  and  $0.08 \, \mu \text{mol} \, \text{min}^{-1} \, (10^9 \, \text{HL}60 \, \text{cells})^{-1}$ , respectively. Therefore, it was decided to continue to use the value of  $0.23 \, \mu \text{mol} \, \text{min}^{-1} \, (10^9 \, \text{HL}60 \, \text{cells})^{-1}$  from Ahmed and Weidemann (1994) as a reasonable estimate for this reaction rate. This produced a scaling factor of 0.011, with which all the model's fluxes were adjusted.

#### 4.2.2 Flow cytometry analysis of HL60 cell differentiation

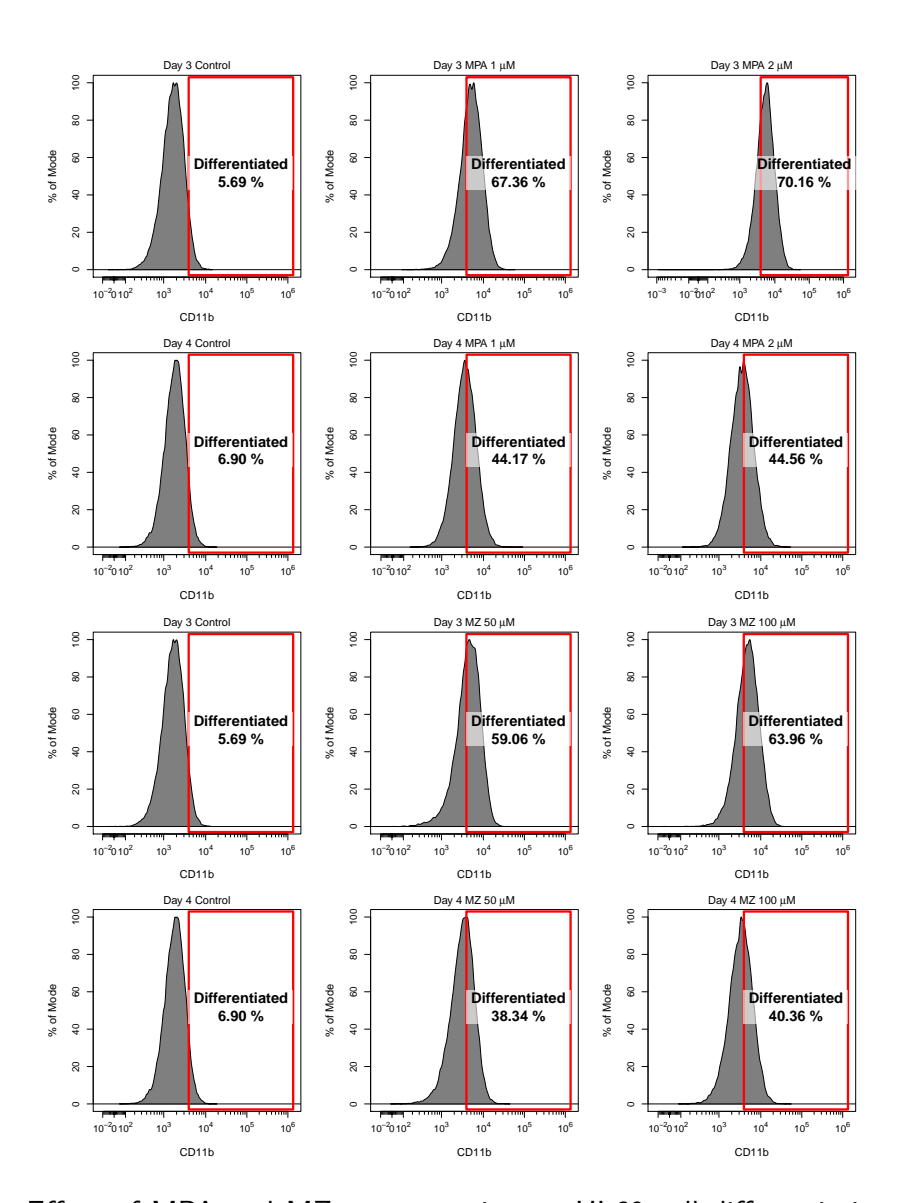
To assess the differentiating ability of IMPDH inhibitors, HL60 cells were incubated with either MPA, MZ or ATRA and analysed via flow cytometry (example gating strategy shown in Appendix H) for expression of CD11b; a cell surface marker present on differentiated myeloid cells of the innate immune system. In previous investigations into the effect of MPA or MZ on HL60 cells, a variety of both incubation periods and concentrations of IMPDH inhibitors were used (Ahmed and Weidemann, 1995; Inai et al., 1997, 2000). To identify the optimal length of incubation and the ideal concentration for the two IMPDH inhibitors, initial experiments were conducted on each of days one to seven with ATRA at a final concentration of 1  $\mu$ M and MPA at both 1  $\mu$ M & 2  $\mu$ M and MZ at both 50  $\mu$ M & 100  $\mu$ M.

Figure 4.1 shows the percentage of differentiated cells in each sample and indicates that ATRA driven differentiation increases over the time course. However, differentiation mediated by the IMPDH inhibitors MPA and MZ peaks at day two, with the level decreasing substantially from day four. Therefore, although the optimal length of incubation for ATRA appears to be four days or more, as the level of differentiation produced by both MPA and MZ decreases notably from day four, day three was chosen as a compromise for use in future flow cytometry and HPLC differentiation experiments.



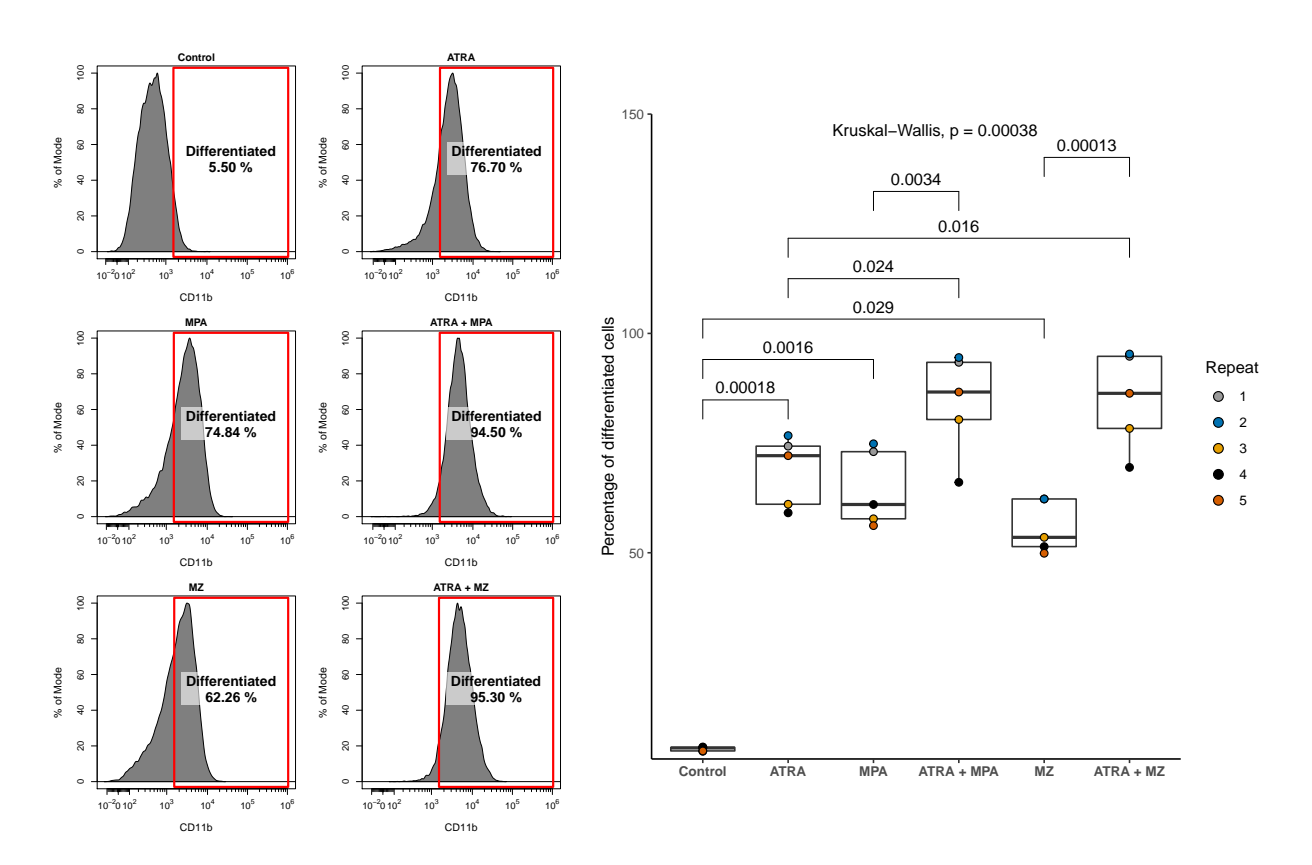
**Figure 4.1:** Time course of HL60 cell differentiation. HL60 cells were incubated with ATRA, MPA or MZ or were left untreated for the number of days indicated and the percentage of differentiated cells was determined via expression of CD11b, as assessed via flow cytometry. Results from n=1 experiments are shown.

In addition, Figure 4.2 indicates there was little difference in the level of differentiation between the two concentrations of MPA and the two concentrations of MZ at both three and four days, thus all subsequent experiments were conducted with MPA at a final concentration of 1  $\mu$ M and MZ at 50  $\mu$ M.



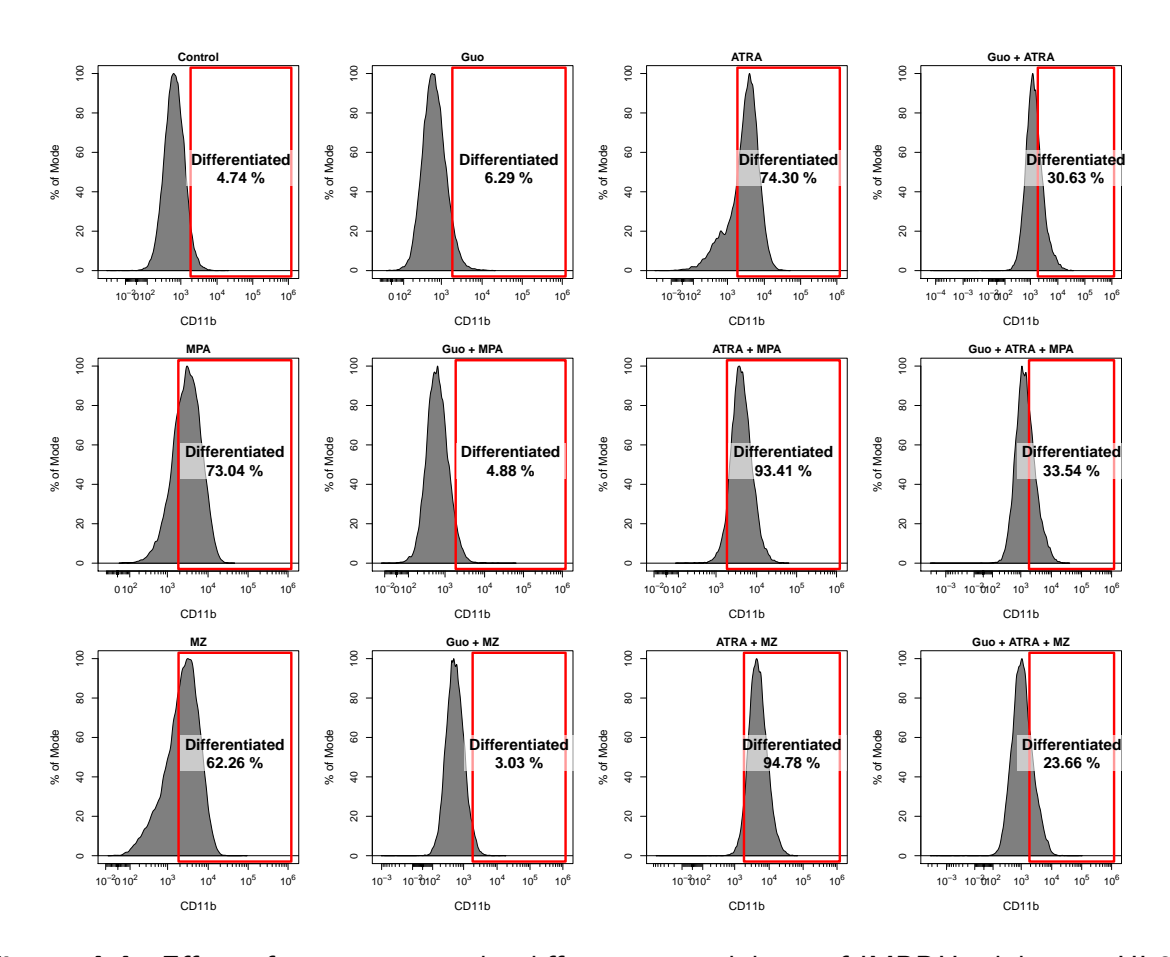
**Figure 4.2:** Effect of MPA and MZ concentration on HL60 cell differentiation. HL60 cells were incubated with MPA at either 1  $\mu$ M or 2  $\mu$ M or MZ at either 50  $\mu$ M or 100  $\mu$ M for either three or four days and the percentage of differentiated cells was determined via expression of the cell surface marker CD11b, as assessed via flow cytometry. Results from n=1 experiments are shown.

Figure 4.3 shows that differentiation of HL60 cells is significantly increased upon treatment with either ATRA, MPA or MZ. Furthermore, combinations of ATRA with either MPA or MZ were also assessed and as indicated in Figure 4.3 the level of HL60 cell differentiation was further significantly increased when a combination of ATRA and an IMPDH inhibitor was used compared to either drug alone.



**Figure 4.3:** Statistical significance of drug treatments on HL60 cell differentiation. HL60 cells were incubated with 1 μM ATRA and/or 1 μM MPA or 50 μM MZ for three days and the percentage of differentiated cells was determined via expression of CD11b, as assessed via flow cytometry. Representative results from n=5 experiments are shown in the left panel, whilst a statistical analysis of this data is shown in the right panel. Data were analysed using a Kruskal-Wallis test, followed by a Conover post-hoc test with Benjamini-Hochberg correction for multiple comparisons; p-values < 0.05 were considered significant.

To assess the preventative effects of guanosine on IMPDH inhibitor driven differentiation, cells were incubated with guanosine along with ATRA, MPA or MZ or combinations thereof. In addition, adenosine was used instead of guanosine in some experiments to confirm that the effect seen is specific to guanosine and is not common to other nucleosides. Figure 4.4 highlights that the cellular differentiation observed with MPA and MZ is reduced when guanosine is present, whilst differentiation seen with ATRA alone or in combination with either MPA or MZ is less affected by the addition of guanosine. Moreover, the addition of adenosine had no affect on the differentiating ability of MPA, MZ or ATRA, as shown in Figure 4.5.



**Figure 4.4:** Effect of guanosine on the differentiating abilities of IMPDH inhibitors. HL60 cells were incubated with 1 μM ATRA and/or 1 μM MPA or 50 μM MZ for three days. 50 μM guanosine (Guo) was also added where indicated and the percentage of differentiated cells was determined via expression of CD11b, as assessed via flow cytometry. Results from n=1 experiments are shown.

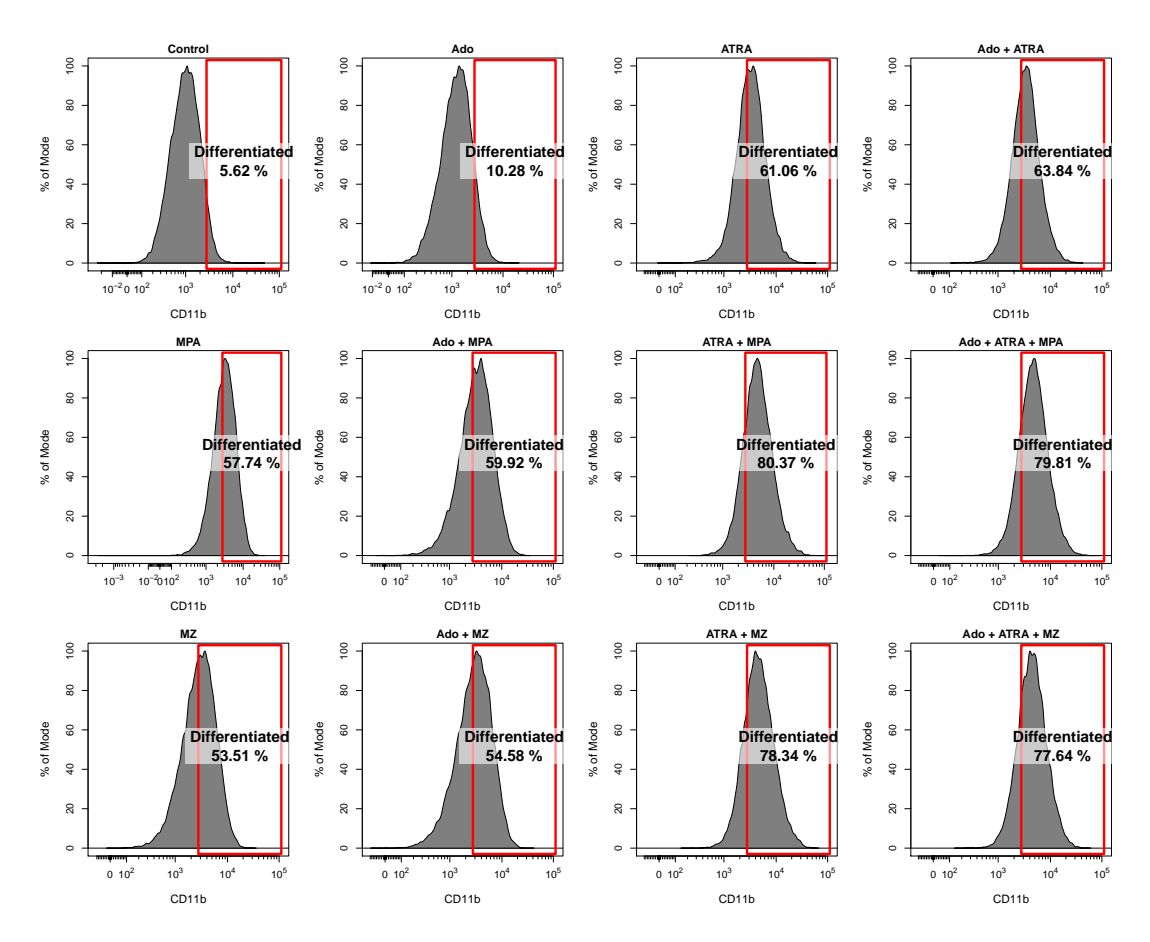


**Figure 4.5:** Effect of adenosine on the differentiating abilities of IMPDH inhibitors. HL60 cells were incubated with 1  $\mu$ M ATRA and/or 1  $\mu$ M MPA or 50  $\mu$ M MZ for three days. 50  $\mu$ M adenosine (Ado) was also added where indicated and the percentage of differentiated cells was determined via expression of CD11b, as assessed via flow cytometry. Results from n=1 experiments are shown.

#### 4.2.2.1 Effects of combining ATRA and IMPDH inhibitors

It had previously been shown that the use of ATRA in combination with an IMPDH inhibitor had a synergistic effect on HL60 cell differentiation compared to using ATRA or an IMPDH inhibitor alone (unpublished data, G. Thomas, see Appendix H). However, as shown in Figure 4.3, this effect was not observed with ATRA and MPA or MZ at the concentrations used. Therefore, to investigate this further, it was decided to reduce the concentration of ATRA, in the range 1 nM to 1  $\mu$ M, and use MPA and MZ at 10 % of their previous levels (0.1  $\mu$ M and 5  $\mu$ M, respectively). Figure 4.6 shows that with ATRA at a concentration of 10 nM and MZ at 5  $\mu$ M, the effect on differentiation was more than

additive compared to when the two drugs were used separately. However, this effect was not seen with ATRA in combination with MPA and thus, as the level of differentiation increases with increasing length of incubation with ATRA (as shown in Figure 4.1) it was decided to increase the length of exposure of HL60 cells to the reduced concentrations of ATRA plus an IMPDH inhibitor to four days. Figure 4.7 illustrates that with a four day incubation period and when using 10 nM ATRA, 0.1  $\mu$ M MPA and 5  $\mu$ M MZ, ATRA plus either MPA or MZ has a more than additive effect on cellular differentiation compared to incubation with either drug alone.

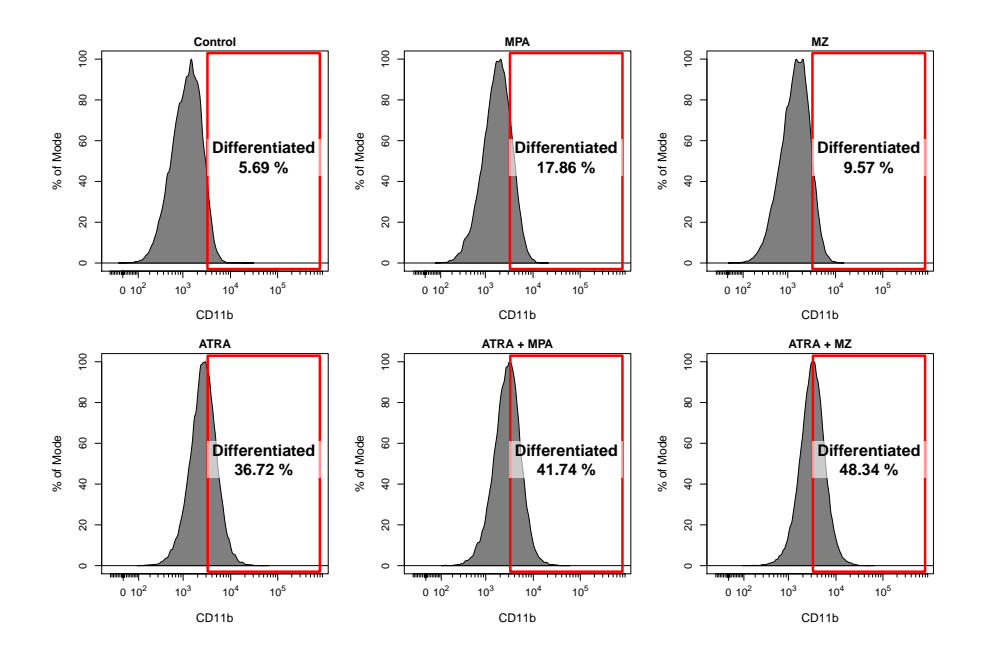


**Figure 4.6:** Synergistic effect of low dose ATRA plus low dose MZ. HL60 cells were incubated with 10 nM ATRA and/or 0.1  $\mu$ M MPA or 5  $\mu$ M MZ for three days. The percentage of differentiated cells was determined via expression of CD11b, as assessed via flow cytometry. Results from n=1 experiments are shown.

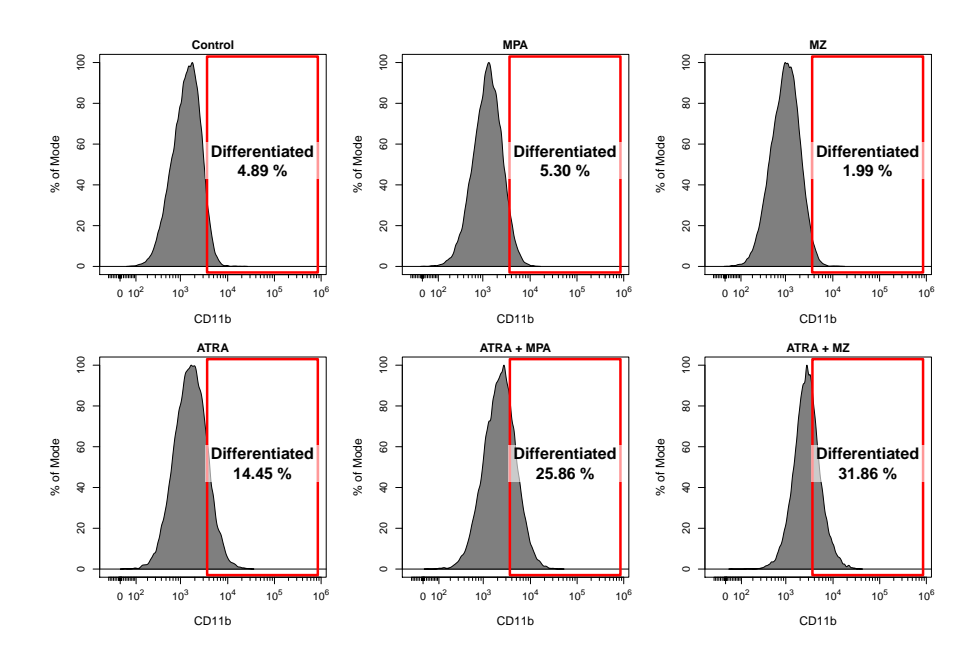


**Figure 4.7:** Synergistic effect of low dose ATRA plus low dose IMPDH inhibitor. HL60 cells were incubated with 10 nM ATRA and/or 0.1  $\mu$ M MPA or 5  $\mu$ M MZ for four days. The percentage of differentiated cells was determined via expression of CD11b, as assessed via flow cytometry. Results from n=1 experiments are shown.

### 4.2.3 HL60 cell reactive oxygen species detection experiments

In addition to expression of CD11b, differentiated myeloid cells of the innate immune system produce ROS in response to appropriate stimuli. To assess whether ATRA, MPA and MZ are able to induce HL60 cells to acquire this ability, a ROS assay was performed. Cells were incubated with either ATRA, MPA, MZ or combinations of these for three days before stimulation with PMA. As illustrated in Figure 4.8 ATRA and/or MPA or MZ again induced HL60 cells to express CD11b whilst the addition of PMA further increased this expression. ROS were not detected in any of the unstimulated cells or the stimulated control cells. In contrast, treatment with PMA and ATRA and/or an IMPDH inhibitor resulted in high levels of ROS production (see Figure 4.8).

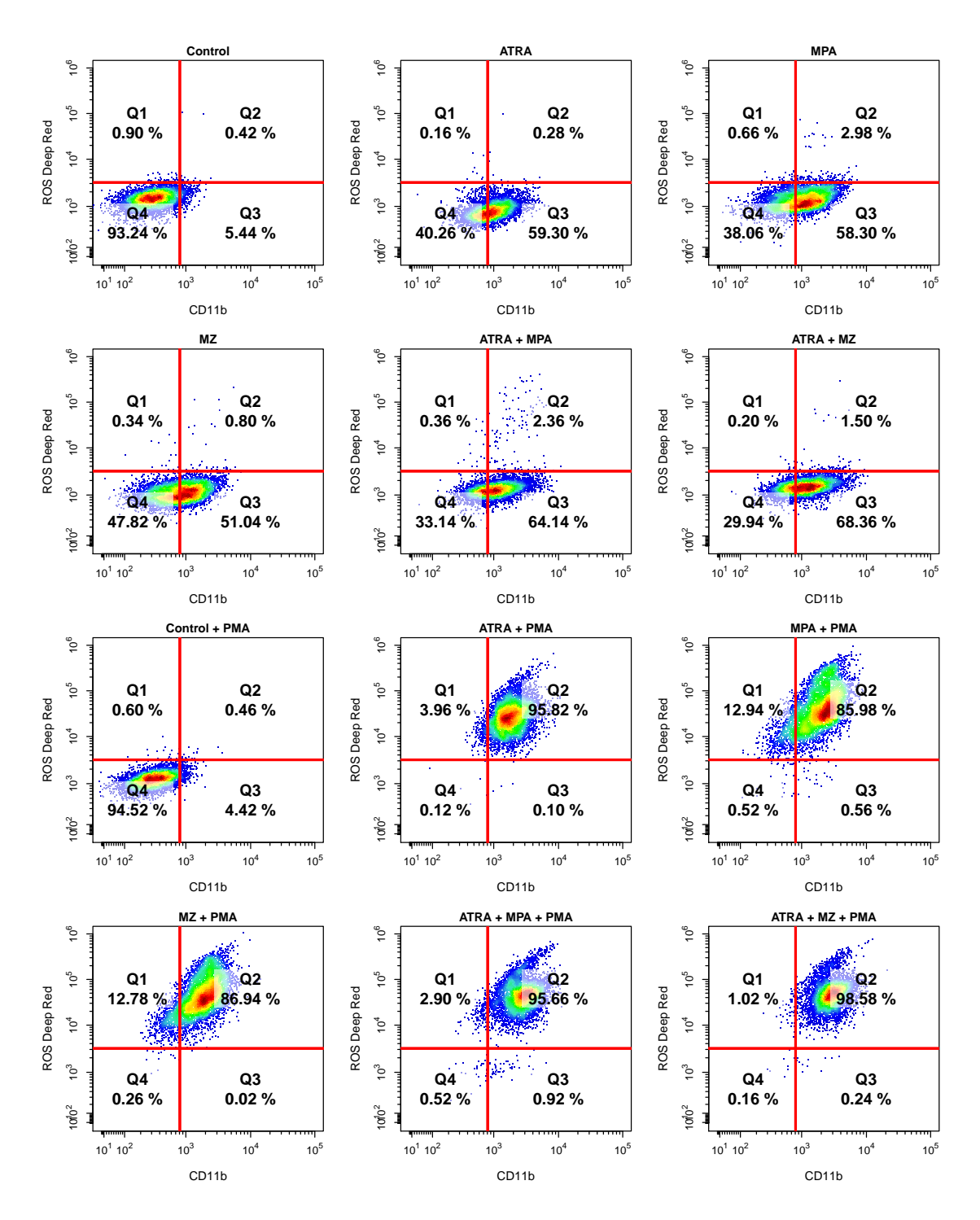


**Figure 4.8:** Production of ROS by stimulated ATRA and/or IMPDH inhibitor treated HL60 cells. HL60 cells were incubated with 1  $\mu$ M ATRA and/or 1  $\mu$ M MPA or 50  $\mu$ M MZ for three days. Cells were then stimulated with PMA for 30 min where indicated and CD11b expression and ROS production were assessed via flow cytometry. Results from n=1 experiments are shown.

#### 4.2.4 HPLC analysis of HL60 cell purine levels

To investigate the change in purine concentrations after differentiation, HL60 cells were incubated with either ATRA, MPA, or MZ +/- guanosine for three days and the purine levels were assessed via HPLC (see Appendix H for example chromatograms). Many of the purine concentrations in these samples were very low or below the level of detection. This was the case for IMP across the full set of experimental conditions and interestingly for HX in all samples except those where guanosine was present. In addition, the peaks corresponding to AMP and Ado could not be consistently resolved, similarly the elution times for GMP and Guo were very similar and thus the levels of these four metabolites could not be reliably determined. Furthermore, the peak corresponding to XMP could not be reliably determined across the entire set of experiments. Therefore, IMP, HX, AMP, Ado, GMP, Guo and XMP were all excluded from further analysis.

Concentration data for ATP, ADP, GTP and GDP were analysed and the results, as a percentage of the control (untreated) condition, are shown in Figure 4.9 for those samples without the addition of guanosine.

The levels of the adenylates from cells treated with either MPA or MZ were fairly consistent, whereas there was more variation in guanylate levels between these two conditions. There was also variation between the results for ATRA treated and IMPDH inhibitor treated cells. In addition, the data for MPA treated cells also failed to match the existing comparable (1  $\mu$ M MPA for 72 h) literature data (Lucas *et al.*, 1983a) for the metabolites ADP, ATP and GTP.

Comparison of data from IMPDH inhibitor treated HL60 cells with model simulations showed concordance between the level of GTP from MZ treated cells and the model results. However, the data for the other nucleotides and that from MPA failed to match the model output.

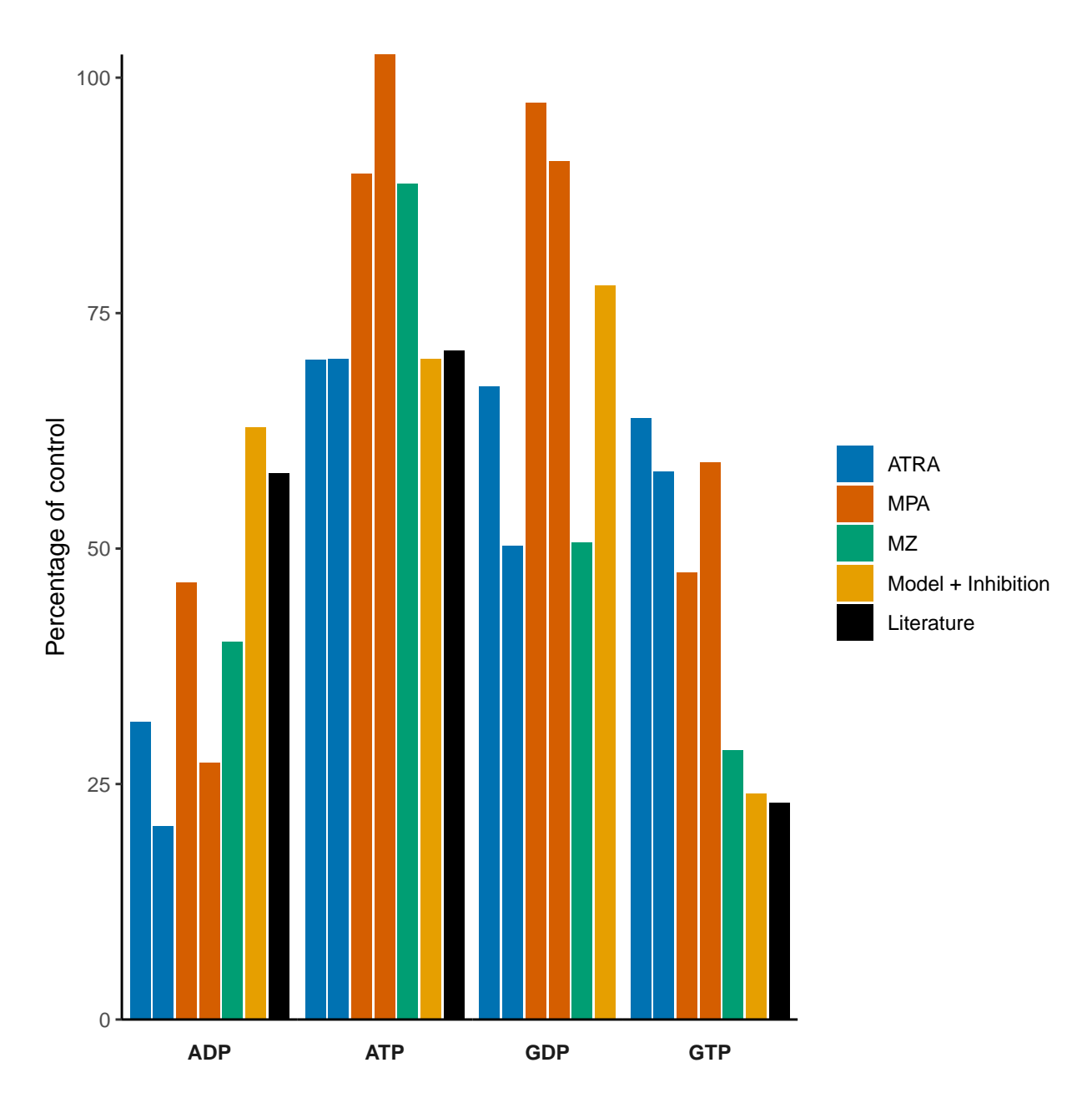


**Figure 4.9:** Percentage change in purine concentrations after differentiation. HL60 cells were incubated with either 1 μM ATRA, 1 μM MPA or 50 μM MZ for three days and purine levels were assessed via HPLC. Percentage change was calculated using control cells which were incubated in the absence of differentiating agents. Percentage change values for Model + Inhibition were computed using purine levels from the model with 28 % IMPDH inhibition simulated along with steady state purine levels without simulation of inhibition. Lastly, also included are the percentage change values for three of the nucleotides as determined by Lucas et al. (1983a) for HL60 cells treated with 1 μM MPA for 72 h relative to untreated cells. Data from two experiments is shown, except for MZ.

Next, ratios for specific nucleotide combinations were then computed from both the experimental data and the model results; these are shown in Figure 4.10. These showed a reduction in the GTP:GDP ratio upon IMPDH inhibition, whereas the ATP:ADP and ATP:GTP ratios both increased after treatment. However, the absolute values of these ratios were markedly different between the model results and the experimental data.

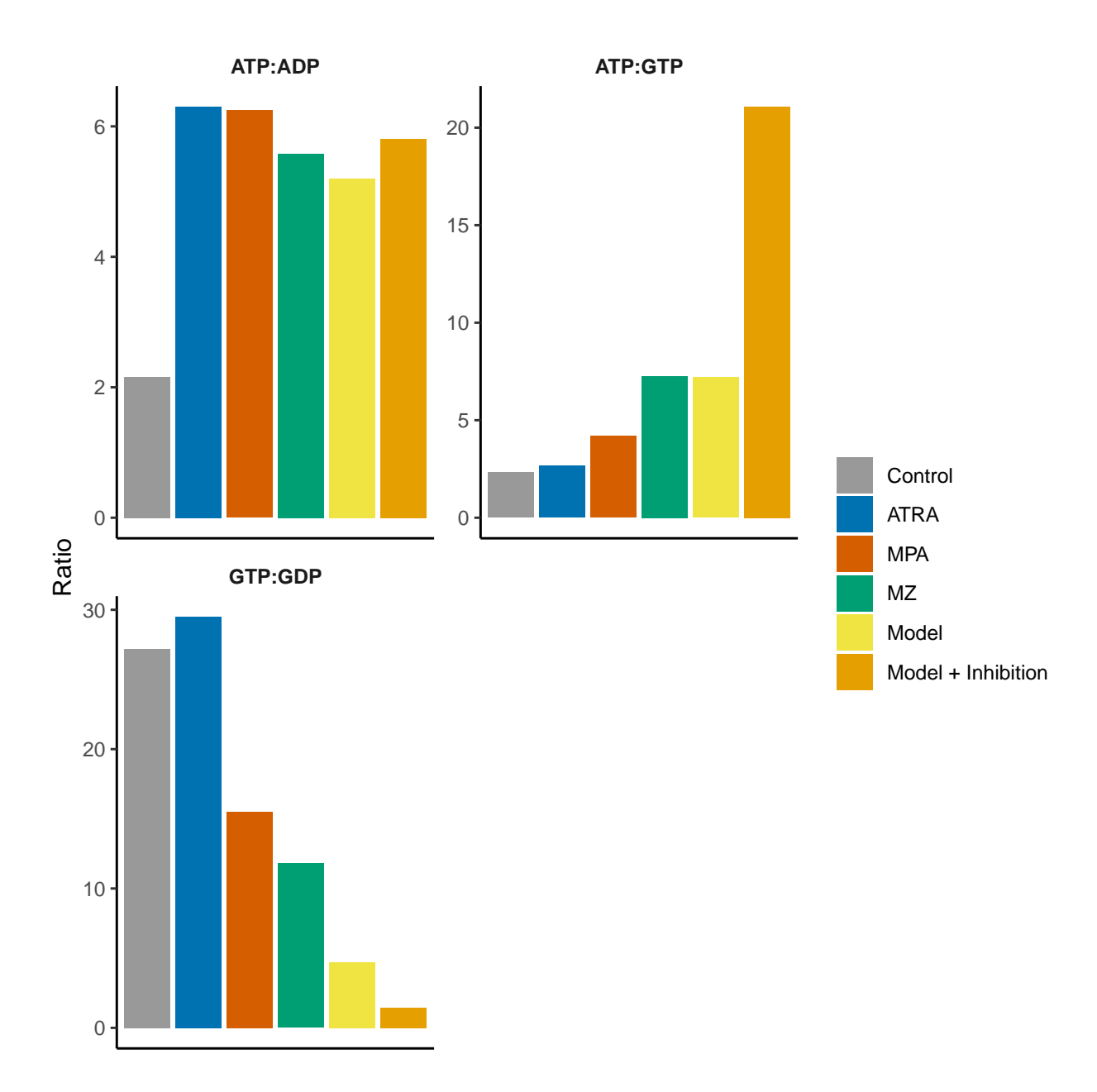
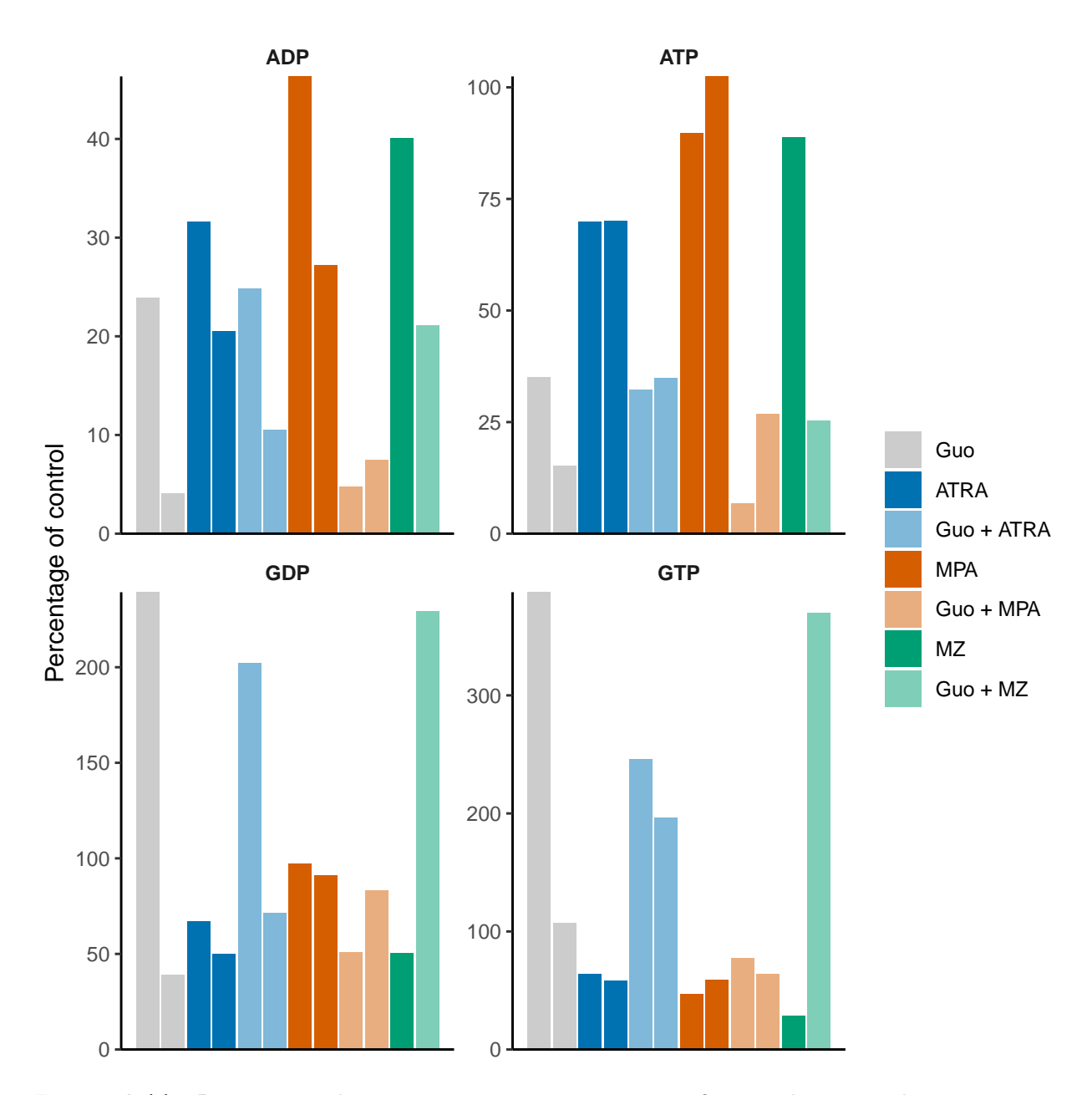


Figure 4.10: HL60 cell nucleotide ratios after differentiation. HL60 cells were incubated with either 1  $\mu$ M ATRA, 1  $\mu$ M MPA or 50  $\mu$ M MZ for three days and purine levels were assessed via HPLC. Ratios for the Model were determined from steady state levels, whilst ratios for Model + Inhibition were computed using nucleotide levels from the model with 28 % IMPDH inhibition simulated. For experimental data, ratios were calculated using the mean values from two experiments, with the exception of MZ where data from a single experiment was used.

To assess the effect of the addition of guanosine on purine levels, cells incubated in the presence of guanosine were compared to those cultured without guanosine for each differentiating agent (see Figure 4.11). These comparisons highlight that the addition of guanosine results in a decrease in the level of both adenylates, whilst the levels of both guanylates increase when guanosine is present, except for the MPA treated cells. In this case, the levels of both guanylates fail to be rescued by the addition of guanosine; with GTP only increasing slightly and GDP decreasing in the presence of guanosine.

Finally, the effect of combining ATRA with an IMPDH inhibitor on purine levels was examined by comparing cells treated with the two drugs to those treated with a single differentiating agent. As shown in Figure 4.12, when cells were treated with ATRA plus MPA or MZ the levels of adenylates were further decreased compared to cells treated with each drug separately. However, as seen in the rest of the data, the change in guanylate levels was more variable. The level of guanylates from ATRA plus MPA treated cells was lower than from cells incubated with either drug alone. However, cells treated with ATRA plus MZ had higher levels of GDP than cells incubated with either of those drugs separately, whilst the level of GTP was higher than the level in cells solely exposed to MZ.



**Figure 4.11:** Percentage change in purine concentrations after incubation with guanosine. HL60 cells were incubated with either 1  $\mu$ M ATRA, 1  $\mu$ M MPA or 50  $\mu$ M MZ for three days either in the presence or in the absence of guanosine and purine levels were assessed via HPLC. Percentage change was calculated using control cells which were incubated in the absence of differentiating agents and guanosine. Data from two experiments is shown, except for MZ and Guo + MZ.

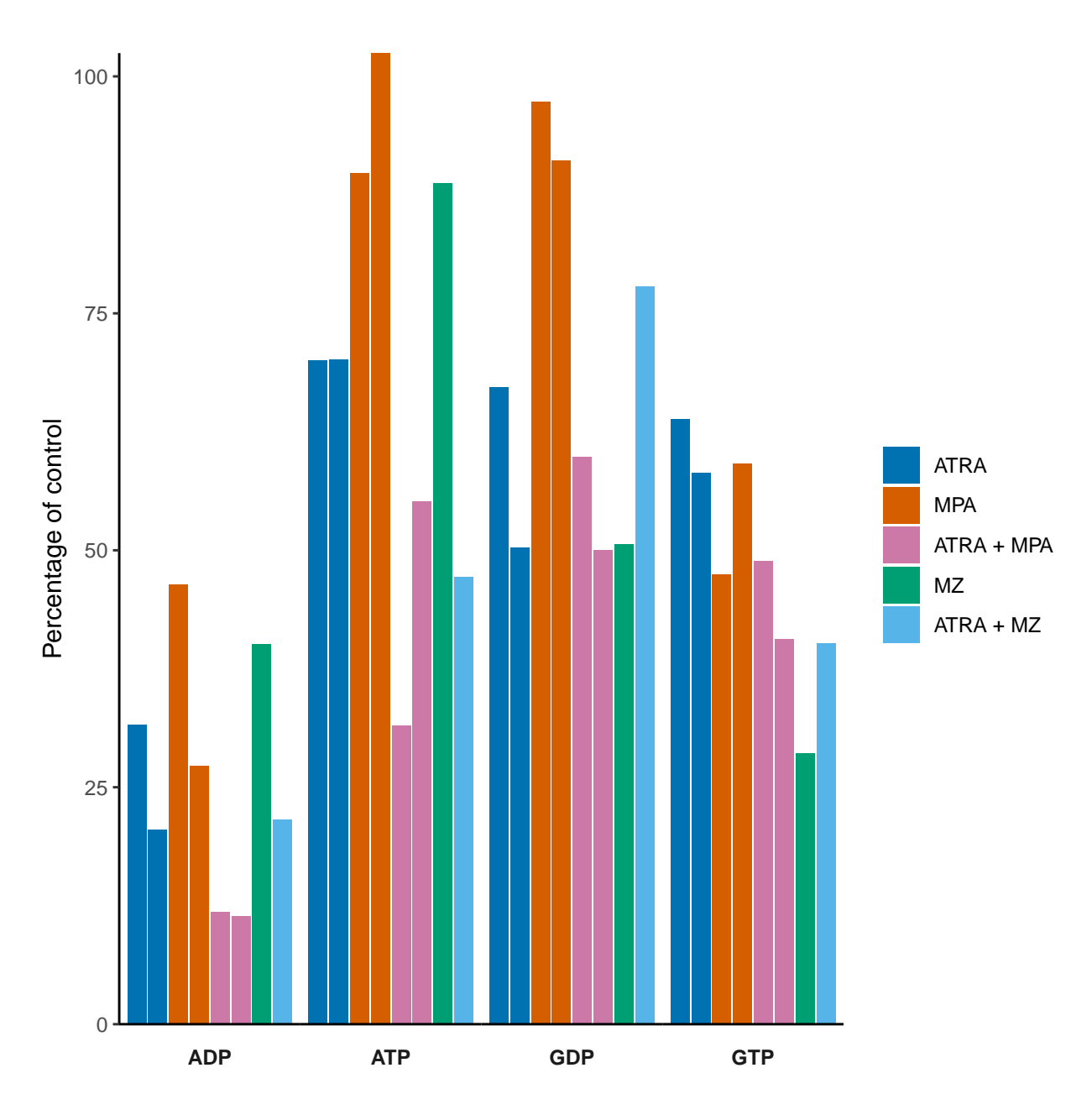


**Figure 4.12:** Percentage change in purine concentrations after combination treatment. HL60 cells were incubated with 1  $\mu$ M ATRA, 1  $\mu$ M MPA or 50  $\mu$ M MZ or combinations thereof for three days and purine levels were assessed via HPLC. Percentage change was calculated using control cells which were incubated in the absence of differentiating agents. Data from two experiments is shown, except for MZ and ATRA + MZ.

# Chapter 5: Discussion and Conclusions

# 5.1 Data interpretation and model comparison

#### 5.1.1 Model scaling

In order to make this new mathematical model of purine metabolism more specific to HL60 cells, it was decided to scale the system based on an HL60 cell specific value for the first enzyme in the model: PRPPS. Although experimentation was conducted to obtain such a value, as these produced values either side of the available literature data (Ahmed and Weidemann, 1994), it was decided to continue using the value from Ahmed and Weidemann (1994) as a reasonable estimate and scale the model accordingly. Together with the RNAseq analysis, this scaling allowed the model to be adapted to one that is specifically tailored to HL60 cells which should help ensure any predictions are more reliable and relevant to this cell type.

## 5.1.2 Cellular changes upon IMPDH inhibition

#### 5.1.2.1 Phenotypic markers

The flow cytometry data clearly highlights that incubation of HL60 cells with either an IMPDH inhibitor or ATRA results in cellular differentiation, as seen by the increased expression of CD11b; a cell surface marker present on differentiated myeloid cells of the innate immune system. Moreover, an interesting observation from these experiments was the apparent increased level of cell death seen when certain differentiating agents were used, particularly MZ. Although cell number was not measured immediately prior to flow cytometry analysis, given that each condition was seeded with the same number of cells, an examination by eye of the size of each cell pellet during the washing steps appeared to reveal increased cellular toxicity by MZ. Indeed, the inclusion of a cell viability marker would have allowed for a more quantitative examination of cellular survival and drug

toxicity.

In addition, the increase in expression of CD11b was also seen in cells treated with both ATRA and guanosine, but to a lesser extent. Indeed, the expression of CD11b by cells treated with both ATRA and guanosine was approximately 41 % of that seen with cells incubated with ATRA alone, a phenomenon previously seen by Wright (1987). In contrast, in line with earlier studies (Inai et al., 2000), the expression of CD11b did not increase in cells that were incubated with guanosine and an IMPDH inhibitor. Moreover, when HL60 cells were incubated with adenosine and either an IMPDH inhibitor or ATRA, CD11b expression was unchanged from cells treated with the differentiating agent alone, in concordance with previous findings (Ahmed and Weidemann, 1995). Collectively, these results therefore indicate that guanylate levels appear to be an important factor in IMPDH inhibitor driven differentiation and to a lesser extent ATRA driven differentiation.

#### 5.1.2.2 Functional assay

Results from the functional assay involving detection of ROS indicate that treatment with either ATRA, MPA or MZ results in cells that possess the ability to produce ROS after appropriate stimulation; a property inherent to mature myeloid cells of the innate immune system. Taken together with the results from the flow cytometric analysis of CD11b expression, these data confirm that treatment with either MPA or MZ induces differentiation of HL60 cells towards a neutrophil-like phenotype, as shown previously (Inai et al., 1997, 2000).

#### 5.1.2.3 Purine levels

HPLC analysis of HL60 cell purine levels yielded reliable results for only four metabolites: ATP, ADP, GTP and GDP. This data showed fairly good consistency in the change in both adenylate levels between HL60 cells treated with MPA and those incubated with MZ. However, this was not the case for either of the guanylate levels. These data suggest that perhaps there is some difference between these two IMPDH inhibitors in terms of

their effect on the purine metabolic network that was previously uncharacterised. Indeed, there is little data available on the purine levels of MZ treated HL60 cells.

A comparison of the results for MPA treated cells with the most comparable literature data set (Lucas et al., 1983a) showed poor concordance. However, other studies suggest that ATP levels after treatment with MPA remain very similar to control levels, which more closely matches the experimental data obtained here, although the experimental conditions were slightly different (see Table 3.13 and Inai et al. (2000)). Furthermore, as Lucas et al. (1983a) was the main source of literature data for adenylate and guanylate levels that was used in the model parameter search simulations (see 3.6.1), the experimental data from this study also failed to match the equivalent model output.

Nucleotide ratio comparisons showed that the ATP:ADP ratio increases after treatment and that this increase is similar regardless of the differentiating agent used. Furthermore, the results from the model with 28 % IMPDH inhibition simulated also showed a slight increase in this ratio with the value being very similar to those seen experimentally, although the ATP:ADP ratio for the steady state model without inhibition simulated was quite different to the experimental control value. The ATP:GTP ratio also increased after HL60 cell differentiation and the same pattern was seen with the model results when IMPDH inhibition was simulated; however the level of these increases was not consistent between any of the experimental conditions or the model. Lastly, the GTP:GDP ratio decreased upon treatment with an IMPDH inhibitor and simulation of IMPDH inhibition in the model but increased slightly in ATRA treated cells.

Therefore, from this data, it would appear that differentiation of HL60 cells causes a fairly consistent increase in the ATP:ADP ratio regardless of the differentiating agent used. However, given the inconsistent values observed in the data for the other ratios and the difference in ratios between the control sample and the steady state model, it is difficult to ascertain whether the model is responding appropriately.

Examination of purine nucleotide levels from cells incubated in the presence of guanosine revealed that once again the change in adenylate levels was more consistent across the set of samples compared to guanylate levels. Intuitively, an increase in guanylate levels would be expected when cells are incubated in the presence of guanosine as the free base will be converted to GMP via the salvage pathway. Indeed, guanylate levels were higher than in control cells for all samples except MPA plus guanosine, again highlighting the inconsistency in the results from MPA treated samples. In contrast to the results for guanylate levels, the addition of guanosine produced a uniform decrease in adenylate levels in all cells. This may be due to inhibition of the *de novo* pathway by salvaged guanylates, resulting in reduced adenylate synthesis.

Throughout the HPLC nucleotide data it was apparent that there were discrepancies between the guanylate levels in MPA treated cells and those in MZ incubated cells. This was somewhat unexpected as it had been assumed that the effects of MPA and MZ on purine levels would be similar, especially given the dearth of data available on purine levels from MZ treated cells. Instead these data suggest that perhaps there is a difference in the underlying biology of these two drugs. Indeed, they differ in their inhibitory mechanism; MZ is a competitive inhibitor with respect to IMP, whilst MPA is uncompetitive with respect to both substrates (Wu, 1994; Hager et al., 1995; Link and Straub, 1996; Allison and Eugui, 2000); but whether this difference can explain the observed discrepancies in purine levels is unclear.

The decrease in nucleotide levels seen here in all differentiated cells, regardless of differentiating agent used, coupled with the decrease in expression levels of enzymes involved in the de novo and salvage pathways in ATRA treated cells, as shown in the RNAseq data (see Figure 3.1), indicates a decrease in purine synthesis in differentiated cells. These results raise the question: does differentiation subsequently lead to a decrease in purine production, or can these cells be forced to differentiate just by decreasing their purine synthesis? The fact that IMPDH inhibitors induce differentiation of HL60 cells supports the latter hypothesis, however these two hypotheses may not be mutually exclusive. Nevertheless, the fact that the addition of guanosine partly prevented the differentiation of ATRA treated cells, indicates that the purine metabolic network plays

a role, at least in part, in differentiation of these cells. This therefore raises the question of whether targeting other enzymes within the purine metabolic network might also result in differentiation of HL60 cells; this could be a novel exploratory avenue for the development of new drug therapies to treat APL.

#### 5.1.3 Effects of combining ATRA and IMPDH inhibitors

As indicated in the flow cytometry results, there is a synergistic effect on HL60 cell differentiation when using ATRA and an IMPDH inhibitor together, but only when the incubation time is increased to four days and the two drugs are used at lower concentrations.

Furthermore, purine nucleotide analysis of cells differentiated using a combination of ATRA and an IMPDH inhibitor showed similar trends to the rest of the HPLC data, with the effect on adenylate levels being more consistent than the effect on guanylate levels. Specifically, the levels of adenylates decrease further in cells treated with both ATRA and MPA or MZ, compared to cells treated with any of the differentiating agents alone, whereas the pattern for guanylate levels differs depending upon which IMPDH inhibitor is used alongside ATRA; further supporting the hypothesis that there are some inherent mechanistic differences between the actions of MPA and MZ.

It would have been interesting to compare these data with simulations from the model, however this was not possible as there is no way within the modelling system to simulate the effects of ATRA. Nevertheless, analysis of this data indicates that combining ATRA and an IMPDH inhibitor generally increases the effect on purine nucleotide levels compared to using a single differentiating agent alone.

This intriguing observation of synergy between ATRA and IMPDH inhibitors raises the possibility of using the two drugs together clinically at lower doses to treat APL in the hope that it may reduce some of the unfavourable side effects often seen with these drugs, whilst still being able to cause differentiation of immature neutrophils.

#### 5.2 Model evaluation

Using published RNAseq data (Raz et al., 2011) and rate of reaction data for the enzyme PRPPS (Ahmed and Weidemann, 1994), the Curto et al. (1998b) purine metabolic model was adapted to create a version specific to HL60 cells, which was then expanded to allow the levels of key metabolites to be modelled separately. Further refinement of the model was undertaken, via parameter search simulations, which revealed that the model was capable of reproducing available literature data of purine nucleotide concentrations after IMPDH inhibition. This model is robust with a stable steady state, thus facilitating comparison of the new experimental data with model output. However, as discussed above, concordance of the data and model was generally low. As noted, this will partly be due to the source of data for the parameter search simulations; which also failed to match the data acquired here.

Furthermore, the model could only be assessed against a limited set of four purines due to the inability to reliably measure the concentrations of seven other metabolites experimentally. This meant a thorough evaluation of model validity could not be performed. Nevertheless, the model is a useful tool and with further work could provide useful insights into the effects of IMPDH inhibitors on the purine metabolic network.

#### 5.3 Future work

To expand the current available data, the next logical step would be to further optimise the HPLC method to allow resolution of all purine metabolites of interest. Although substantial effort was made to achieve this, it is hoped that amendments to the protocol and/or the addition of a mass spectrometry based detection method may be able to resolve this key issue.

If this data could be obtained, then the model could be further refined using a subset of this data as an alternative source for new parameter search simulations, with the remainder of this data being used to validate the newly refined model. As mentioned earlier, it would seem prudent to uncouple certain reactions that are catalysed by a common enzyme in these new parameter search simulations, namely HPRT & GPRT; and INUC, ANUC & GNUC. This is because one would expect IMPDH inhibition to have opposing effects on those reactions involving GMP and those involving IMP (and perhaps AMP). Once the model had been further refined using the new data and parameter search results, it could then be used to explore other potential drug targets within the purine metabolic network, with model predictions then being tested experimentally, to try to identify potential new drug treatments for use in AML therapy.

In addition, it would have been interesting to be able to compare the model with the newly acquired data for purine nucleotide levels in guanosine treated cells. One way to achieve this would be to make guanosine an independent variable in the model so that its concentration remains constant. However, guanosine is currently grouped together into a pool with guanine and deoxyguanosine and as such the validity and feasibility of such an approach is unclear. Therefore, extending the model to separate this pool (as done here for the guanylate and adenylate pools) seems like a logical next step to allow the effect of the addition of guanosine, both in the presence and absence of IMPDH inhibition, to be modelled.

As mentioned above, it would be interesting to repeat some of the flow cytometry analysis with the inclusion of a cell viability marker to assess cell death and investigate drug toxicity effects.

As the publicly available RNAseq data used in this study was from ATRA treated HL60 cells only, it would be useful to have equivalent data for IMPDH inhibitor treated cells so that further assessment of the differences and similarities between these two classes of drug could be assessed. Moreover, with the recent advances in metabolomics techniques since commencement of this project, an examination of proteomics or metabolomics data from both HL60 cells treated with ATRA and from those treated with an IMPDH inhibitor would provide a more accurate picture of purine levels in these cell after differentiation.

Finally, as the purine nucleotide analysis from cells treated with a combination of ATRA and an IMPDH inhibitor was conducted at three days and using the original concentrations of differentiating agents, it would seem appropriate to repeat this analysis using the increased time frame and with ATRA, MPA and MZ at the lower concentrations which were shown to produce a synergistic effect on HL60 cell differentiation.

# 5.4 Conclusions

Refinement and expansion of an existing mathematical model of purine metabolism was undertaken resulting in the creation of an HL60 cell specific model of this network, which allowed for the examination of key metabolites during simulations of IMPDH inhibition. The model is robust, with a stable steady state and performed in a similar manner to the original Curto et al. (1998b) model during various test simulations. The sparsity of available literature data hampered efforts to further refine the model, thus necessitating the need to generate additional purine metabolite concentrations to continue this work.

Experimentation was undertaken to better understand the effects of IMPDH inhibitors on HL60 cells and consisted of three parts: 1) an assessment of differentiation; 2) a functional study; and 3) determination of metabolite concentrations. Flow cytometric analyses of CD11b expression and ROS production showed that treatment with either MPA or MZ resulted in HL60 cell differentiation and acquisition of both phenotypic and functional properties of mature myeloid cells of the innate immune system; confirming that the HPLC analysis conducted provides data on purine levels from differentiated cells. This HPLC data highlights a general decrease in purine nucleotide levels upon differentiation, for both IMPDH inhibitor and ATRA treated cells. Furthermore, the addition of guanosine was shown to prevent the differentiating abilities of IMPDH inhibitors, and to a lesser extent ATRA, whilst assessment of purine nucleotide levels from these samples provides insights into these conditions which were previously uncharacterised.

A comparison of the experimentally obtained purine concentration data with the model output was undertaken. However, discrepancies between this new data and that in the literature resulted in low concordance between the model and this experimental data. Nevertheless it is hoped that, with further experimentation and possible refinement, this model may prove useful for further investigation of IMPDH inhibition and purine metabolism in the HL60 cell line, which may yield predictions that provide insights into potential novel treatments for APL and perhaps other forms of AML.

# **Bibliography**

- Aarbakke, J., Miura, G. A., Prytz, P. S., Bessesen, A., Slørdal, L., Gordon, R. K., and Chiang, P. K. Induction of HL-60 cell differentiation by 3-deaza-(+/-)-aristeromycin, an inhibitor of S-adenosylhomocysteine hydrolase. *Cancer research*, 46(11):5469–72, 1986.
- Agarwal, K., Miech, R., and Parks, R. Guanylate kinases from human erythrocytes, hog brain, and rat liver. *Methods in enzymology*, LI:483–490, 1978.
- Ahmed, N. and Weidemann, M. J. Purine metabolism in promyelocytic HL60 and dimethylsulphoxide-differentiated HL60 cells. *Leukemia research*, 18(6):441–451, 1994.
- Ahmed, N. and Weidemann, M. J. Biochemical effect of three different inhibitors of purine/pyrimidine metabolism on differentiation in HL60 cells. *Leukemia research*, 19 (4):263–73, 1995.
- Alcalay, M., Zangrilli, D., Pandolfi, P. P., Longo, L., Mencarelli, A., Giacomucci, A., Rocchi, M., Biondi, A., Rambaldi, A., Lo Coco, F., Diverio, D., Donti, E., Grignani, F., and Pelicci, P. G. Translocation breakpoint of acute promyelocytic leukemia lies within the retinoic acid receptor α locus. *Proceedings of the National Academy of Sciences of the United States of America*, 88(5):1977–1981, 1991.
- Alcalay, M., Zangrilli, D., Fagioli, M., Pandolfi, P. P., Mencarelli, A., Lo Coco, F., Biondi, A., Grignani, F., and Pelicci, P. G. Expression pattern of the RARα-PML fusion gene in acute promyelocytic leukemia. *Proceedings of the National Academy of Sciences of the United States of America*, 89(11):4840–4844, 1992.
- Allison, A. C. and Eugui, E. M. Mycophenolate mofetil and its mechanisms of action. *Immunopharmacology*, 47(2-3):85–118, 2000.
- Arber, D. A., Orazi, A., Hasserjian, R., Thiele, J., Borowitz, M. J., Le Beau, M. M., Bloomfield, C. D., Cazzola, M., and Vardiman, J. W. The 2016 revision to the World Health Organization classification of myeloid neoplasms and acute leukemia. *Blood*, 127(20):2391–2405, 2016.
- Balasubramaniam, S., Duley, J. A., and Christodoulou, J. Inborn errors of purine metabolism: clinical update and therapies. *Journal of Inherited Metabolic Disease*, 37(5):669–686, 2014.
- Bartel, T. and Holzhütter, H.-G. Mathematical modelling of the purine metabolism of the rat liver. *Biochimica et Biophysica Acta (BBA) General Subjects*, 1035(3):331–339, 1990.
- Bennett, J. M., Catovsky, D., Daniel, M. ., Flandrin, G., Galton, D. A., Gralnick, H. R., and Sultan, C. Proposals for the Classification of the Acute Leukaemias French-American-British (FAB) Co-operative Group. *British Journal of Haematology*, 33(4):451–458, 1976.

- Bentley, R. Mycophenolic acid: A one hundred year odyssey from antibiotic to immuno-suppressant. *Chemical Reviews*, 100(10):3801–3825, 2000.
- Beutler, B. Innate immunity: an overview. *Molecular Immunology*, 40(12):845–859, 2004.
- BloodCancerUK. Facts and information about blood cancer, 2019. URL https://bloodcancer.org.uk/news/blood-cancer-facts/.
- Bode, H. W. Network Analysis and Feedback Amplifier Design. Bell Telephone Laboratories series. D. Van Nostrand Company, Incorporated, 1945. ISBN 0882752421. URL https://books.google.co.uk/books?id=kSYhAAAAMAAJ.
- Bonilla, F. A. and Oettgen, H. C. Adaptive immunity. *Journal of Allergy and Clinical Immunology*, 125(2):S33–S40, 2010.
- Bonnet, D. Normal and leukaemic stem cells. *British Journal of Haematology*, 130(4): 469–479, 2005.
- Borrow, J., Goddard, A. D., Sheer, D., and Solomon, E. Molecular analysis of acute promyelocytic leukemia breakpoint cluster region on chromosome 17. *Science*, 249 (4976):1577–1580, 1990.
- Bradbury, D. A., Simmons, T. D., Slater, K. J., and Crouch, S. P. Measurement of the ADP:ATP ratio in human leukaemic cell lines can be used as an indicator of cell viability, necrosis and apoptosis. *Journal of Immunological Methods*, 240(1-2):79–92, 2000.
- Breitman, T. R., Selonick, S. E., and Collins, S. J. Induction of differentiation of the human promyelocytic leukemia cell line (HL-60) by retinoic acid. *Proceedings of the National Academy of Sciences of the United States of America*, 77(5):2936–40, 1980.
- Briggs, G. E. and Haldane, J. B. A Note on the Kinetics of Enzyme Action. *The Biochemical journal*, 19(2):338–339, 1925.
- Bullingham, R. E., Nicholls, A. J., and Kamm, B. R. Clinical pharmacokinetics of mycophenolate mofetil. *Clinical pharmacokinetics*, 34(6):429–55, 1998.
- Carr, S. F., Papp, E., Wu, J. C., and Natsumeda, Y. Characterization of human type I and type II IMP dehydrogenases. *Journal of Biological Chemistry*, 268(36):27286–27290, 1993.
- Chaplin, D. D. Overview of the immune response. *Journal of Allergy and Clinical Immunology*, 125(2):1–45, 2010.
- Chiang, P., Lucas, D., and Wright, D. Induction of Differentiation of HL-60 Human Promyelocytic Leukemia Cells by 3-Deaza Purines. *Annals of the New York Academy of Sciences*, 435(1):126–128, 1984.
- Cholewiński, G., Iwaszkiewicz-Grześ, D., Prejs, M., Głowacka, A., and Dzierzbicka, K. Synthesis of the inosine 5 -monophosphate dehydrogenase (IMPDH) inhibitors. *Journal of Enzyme Inhibition and Medicinal Chemistry*, 30(4):550–563, 2015.

- Collart, F. R. and Huberman, E. Expression of IMP dehydrogenase in differentiating HL-60 cells. *Blood*, 75(3):570–6, 1990.
- Collins, S. J., Gallo, R. C., and Gallagher, R. E. Continuous growth and differentiation of human myeloid leukaemic cells in suspension culture. *Nature*, 270(5635):347–9, 1977.
- CRUK. Leukaemia Types, 2019. URL https://www.cancerresearchuk.org/about-cancer/chronic-myeloid-leukaemia-cml/types.
- CRUK. Leukaemia (all subtypes combined) statistics, 2022. URL https://www.cancerresearchuk.org/health-professional/cancer-statistics/statistics-by-cancer-type/leukaemia.
- Cuny, G. D., Suebsuwong, C., and Ray, S. S. Inosine-5'-monophosphate dehydrogenase (IMPDH) inhibitors: a patent and scientific literature review (2002-2016). *Expert Opinion on Therapeutic Patents*, 27(6):677–690, 2017.
- Curto, R., Voit, E. O., Sorribas, A., and Cascante, M. Validation and steady-state analysis of a power-law model of purine metabolism in man. *The Biochemical journal*, 324:761–75, 1997.
- Curto, R., Voit, E. O., and Cascante, M. Analysis of abnormalities in purine metabolism leading to gout and to neurological dysfunctions in man. *The Biochemical journal*, 329 (pt 3):477–87, 1998a.
- Curto, R., Voit, E. O., Sorribas, A., and Cascante, M. Mathematical models of purine metabolism in man. *Mathematical biosciences*, 151(1):1–49, 1998b.
- Dalton, W. T., Ahearn, M. J., McCredie, K. B., Freireich, E. J., Stass, S. A., and Trujillo, J. M. HL-60 cell line was derived from a patient with FAB-M2 and not FAB-M3. *Blood*, 71(1):242–7, 1988.
- De Atauri, P., Curto, R., Puigjaner, J., Cornish-Bowden, A., and Cascante, M. Advantages and disadvantages of aggregating fluxes into synthetic and degradative fluxes when modelling metabolic pathways. *European Journal of Biochemistry*, 265(2):671–9, 1999.
- De Kouchkovsky, I. and Abdul-Hay, M. 'Acute myeloid leukemia: a comprehensive review and 2016 update'. *Blood Cancer Journal*, 6(7):1–10, 2016.
- de Thé, H., Chomienne, C., Lanotte, M., Degos, L., and Dejean, A. The t(15;17) translocation of acute promyelocytic leukaemia fuses the retinoic acid receptor alpha gene to a novel transcribed locus. *Nature*, 347(6293):558–61, 1990.
- de Thé, H., Lavau, C., Marchio, A., Chomienne, C., Degos, L., and Dejean, A. The PML-RAR $\alpha$  fusion mRNA generated by the t(15;17) translocation in acute promyelocytic leukemia encodes a functionally altered RAR. *Cell*, 66(4):675–684, 1991.
- Dembitz, V. and Gallipoli, P. The Role of Metabolism in the Development of Personalized Therapies in Acute Myeloid Leukemia. *Frontiers in Oncology*, 11(May):1–9, 2021.

- Dilworth, F. J. and Chambon, P. Nuclear receptors coordinate the activities of chromatin remodeling complexes and coactivators to facilitate initiation of transcription. *Oncogene*, 20(24 REV. ISS. 3):3047–3054, 2001.
- Döhner, H., Weisdorf, D. J., and Bloomfield, C. D. Acute Myeloid Leukemia. *New England Journal of Medicine*, 373(12):1136–1152, 2015.
- Edgar, R., Domrachev, M., and Lash, A. E. Gene Expression Omnibus: NCBI gene expression and hybridization array data repository. *Nucleic acids research*, 30(1):207–10, 2002.
- Elgemeie, G. Thioguanine, Mercaptopurine: Their Analogs and Nucleosides as Antimetabolites. Current Pharmaceutical Design, 9(31):2627–2642, 2005.
- Eugui, E. M., Almquist, S. J., Muller, C. D., and Allison, A. C. Lymphocyte-Selective Cytostatic and Immunosuppressive Effects of Mycophenolic Acid in Vitro: Role of Deoxyguanosine Nucleotide Depletion. *Scandinavian Journal of Immunology*, 33(2): 161–173, 1991.
- Franco, R. and Canela, E. I. Computer simulation of purine metabolism. *European Journal of Biochemistry*, 144(2):305–315, 1984.
- Frank Starmer, C., Sperling, O., and Wyngaarden, J. B. A kinetic model for the intramolecular distribution of 15N in uric acid in patients with primary gout fed 15N-glycine. *Mathematical Biosciences*, 25(1-2):105–123, 1975.
- Gallagher, R., Collins, S., Trujillo, J., McCredie, K., Ahearn, M., Tsai, S., Metzgar, R., Aulakh, G., Ting, R., Ruscetti, F., and Gallo, R. Characterization of the continuous, differentiating myeloid cell line (HL-60) from a patient with acute promyelocytic leukemia. *Blood*, 54(3):713–33, 1979.
- Gallagher, R. E. Retinoic acid resistance in acute promyelocytic leukemia. *Leukemia*, 16 (10):1940–1958, 2002.
- García-Alvarez-Coque, M. C., Ramis-Ramos, G., and Ruiz-Angel, M. J. Liquid Chromatography | Ion Pair. In Worsfold, P., Poole, C., Townshend, A., and Miró, M., editors, *Encyclopedia of Analytical Science (Third Edition)*, pages 117–126. Academic Press, Oxford, third edit edition, 2015. ISBN 978-0-08-101984-9. doi: https://doi.org/10.1016/B978-0-12-409547-2.11687-7. URL https://www.sciencedirect.com/science/article/pii/B9780124095472116877.
- Garcia-Manero, G., Pemmaraju, N., Alvarado, Y., Naqvi, K., Ravandi, F., Jabbour, E., De Lumpa, R., Kantarjian, H., Advani, A., Mukherjee, S., Gerds, A., Carraway, H. E., Nazha, A., Iwamura, H., Murase, M., Bavisotto, L., Kurman, M., Maier, G., Johansen, M., and Sekeres, M. A. Results of a Phase 1/2a dose–escalation study of FF-10501-01, an IMPDH inhibitor, in patients with acute myeloid leukemia or myelodysplastic syndromes. *Leukemia & Lymphoma*, 61(8):1943–1953, 2020.
- Goldsby, R. A., Kindt, T. J., Kuby, J., and Osborne, B. A. *Immunology, Fifth Edition*. W. H. Freeman, 2002. ISBN 9781493990047.

- Goldstein, B. M., Risal, D., and Strickler, M. *IMPDH Structure and Ligand Binding*, chapter 7, pages 140–168. American Chemical Society, 2003. ISBN 9780841237803. doi: 10.1021/bk-2003-0839.ch007. URL https://pubs.acs.org/doi/abs/10.1021/bk-2003-0839.ch007.
- Gordon, S. Elie Metchnikoff: Father of natural immunity. European Journal of Immunology, 38(12):3257–3264, 2008.
- Grisolano, J. L., Wesselschmidt, R. L., Pelicci, P. G., and Ley, T. J. Altered myeloid development and acute leukemia in transgenic mice expressing PML-RAR alpha under control of cathepsin G regulatory sequences. *Blood*, 89(2):376–87, 1997.
- Grønningsæter, I. S., Reikvam, H., Aasebø, E., Bartaula-Brevik, S., Tvedt, T. H., Bruserud, Ø., and Hatfield, K. J. Targeting Cellular Metabolism in Acute Myeloid Leukemia and the Role of Patient Heterogeneity. *Cells*, 9(5):1155, 2020.
- Häger, M., Cowland, J. B., and Borregaard, N. Neutrophil granules in health and disease. *Journal of Internal Medicine*, 268(1):25–34, 2010.
- Hager, P. W., Collart, F. R., Huberman, E., and Mitchell, B. S. Recombinant human inosine monophosphate dehydrogenase type I and type II proteins. Purification and characterization of inhibitor binding. *Biochemical pharmacology*, 49(9):1323–9, 1995.
- Hammill, D. CytoExploreR: Interactive Analysis of Cytometry Data, 2021. URL https://github.com/DillonHammill/CytoExploreR.
- Harper, J. W., Adami, G. R., Wei, N., Keyomarsi, K., and Elledge, S. J. The p21 Cdk-interacting protein Cip1 is a potent inhibitor of G1 cyclin-dependent kinases. Cell, 75 (4):805–816, 1993.
- Hartman, S. C. and Buchanan, J. M. Nucleic acids, purines, pyrimidines (nucleotide synthesis). *Annual review of biochemistry*, 28:365–410, 1959.
- He, L. Z., Guidez, F., Tribioli, C., Peruzzi, D., Ruthardt, M., Zelent, A., and Pandolfi, P. P. Distinct interactions of PML-RARalpha and PLZF-RARalpha with co-repressors determine differential responses to RA in APL. *Nature genetics*, 18(2):126–35, 1998.
- Hedstrom, L. IMP dehydrogenase: Structure, mechanism, and inhibition. *Chemical Reviews*, 109(7):2903–2928, 2009.
- Heinmets, F. Supercomputer analysis of purine and pyrimidine metabolism leading to DNA synthesis. *Cell Biophysics*, 14(3):283–323, 1989.
- Henri, V. Lois générales de l'action des diastases. Librairie Scientifique A. Hermann, Paris, 1903.
- Hershfield, M. S. and Seegmiller, J. E. Regulation of de novo purine biosynthesis in human lymphoblasts. *The Journal of biological chemistry*, 251(23):7348–7354, 1976.
- Hillestad, L. Aciite Proin yelocytic. *Acta Medica Scandinavica*, CLIX(1951):159–189, 1957.

- Holmes, E. W., Pehlke, D. M., and Kelley, W. N. Human IMP dehydrogenase. Kinetics and regulatory properties. *Biochimica et biophysica acta*, 364(2):209–17, 1974.
- Hoops, S., Sahle, S., Gauges, R., Lee, C., Pahle, J., Simus, N., Singhal, M., Xu, L., Mendes, P., and Kummer, U. COPASI–a COmplex PAthway SImulator. *Bioinformatics*, 22(24):3067–74, 2006.
- Hospital, M.-A., Green, A. S., Maciel, T. T., Moura, I. C., Leung, A. Y., Bouscary, D., and Tamburini, J. FLT3 inhibitors: clinical potential in acute myeloid leukemia. *OncoTargets and Therapy*, 10:607–615, 2017.
- Huang, D., Zhang, Y., and Chen, X. Analysis of intracellular nucleoside triphosphate levels in normal and tumor cell lines by high-performance liquid chromatography. *Journal of Chromatography B: Analytical Technologies in the Biomedical and Life Sciences*, 784 (1):101–109, 2003.
- Hucka, M., Finney, A., Sauro, H. M., Bolouri, H., Doyle, J. C., Kitano, H., Arkin, A. P., Bornstein, B. J., Bray, D., Cornish-Bowden, A., Cuellar, A. A., Dronov, S., Gilles, E. D., Ginkel, M., Gor, V., Goryanin, I. I., Hedley, W. J., Hodgman, T. C., Hofmeyr, J. H., Hunter, P. J., Juty, N. S., Kasberger, J. L., Kremling, A., Kummer, U., Le Novère, N., Loew, L. M., Lucio, D., Mendes, P., Minch, E., Mjolsness, E. D., Nakayama, Y., Nelson, M. R., Nielsen, P. F., Sakurada, T., Schaff, J. C., Shapiro, B. E., Shimizu, T. S., Spence, H. D., Stelling, J., Takahashi, K., Tomita, M., Wagner, J., and Wang, J. The systems biology markup language (SBML): A medium for representation and exchange of biochemical network models. Bioinformatics, 19(4):524–531, 2003.
- Inai, K., Tsutani, H., Yamauchi, T., Huberman, E., Nakamura, T., and Ueda, T. Differentiation induction in non-lymphocytic leukemia cells upon treatment with mizoribine. *International journal of hematology*, 66(3):335–44, 1997.
- Inai, K., Tsutani, H., Yamauchi, T., Fukushima, T., Iwasaki, H., Imamura, S., Wano, Y., Nemoto, Y., Naiki, H., and Ueda, T. Differentiation induction in non-lymphocytic leukemia cells upon treatment with mycophenolate mofetil. *Leukemia research*, 24(9): 761–8, 2000.
- Ishikawa, H., Tsuchiya, M., and Itoh, H. *Mizoribine: Experimental and Clinical Experience*, chapter 15, pages 294–327. American Chemical Society, 2003. ISBN 9780841237803. doi: 10.1021/bk-2003-0839.ch015. URL https://pubs.acs.org/doi/abs/10.1021/bk-2003-0839.ch015.
- Itoh, R. and Oka, J. Evidence for existence of a cytosol 5'-nucleotidase in chicken heart: comparison of some properties of heart and liver enzymes. *Comparative biochemistry and physiology. B, Comparative biochemistry*, 81(1):159–63, 1985.
- Jackson, R. C., Weber, G., and Morris, H. P. IMP dehydrogenase, an enzyme linked with proliferation and malignancy. *Nature*, 256(5515):331–3, 1975.
- Jackson, S. H., Gallin, J. I., and Holland, S. M. The p47phox mouse knock-out model of chronic granulomatous disease. *Journal of Experimental Medicine*, 182(3):751–758, 1995.

- Janeway, C. A. and Medzhitov, R. Innate Immune Recognition. *Annual Review of Immunology*, 20(1):197–216, 2002.
- Johnson, K. A. and Goody, R. S. The original Michaelis constant: Translation of the 1913 Michaelis-Menten Paper. *Biochemistry*, 50(39):8264–8269, 2011.
- Juda, P., Šmigová, J., Kováčik, L., Bártová, E., and Raška, I. Ultrastructure of Cytoplasmic and Nuclear Inosine-5'-Monophosphate Dehydrogenase 2 "Rods and Rings" Inclusions. *Journal of Histochemistry and Cytochemistry*, 62(10):739–750, 2014.
- Kakizuka, A., Miller, W. H., Umesono, K., Warrell, R. P., Frankel, S. R., Murty, V. V., Dmitrovsky, E., and Evans, R. M. Chromosomal translocation t(15;17) in human acute promyelocytic leukemia fuses RAR alpha with a novel putative transcription factor, PML. *Cell*, 66(4):663–74, 1991.
- Kanehisa, M. and Goto, S. KEGG: kyoto encyclopedia of genes and genomes. *Nucleic acids research*, 28(1):27–30, 2000.
- Kastner, P., Perez, A., Lutz, Y., Rochette-Egly, C., Gaub, M. P., Durand, B., Lanotte, M., Berger, R., and Chambon, P. Structure, localization and transcriptional properties of two classes of retinoic acid receptor α fusion proteins in acute promyelocytic leukemia (APL): Structural similarities with a new family of oncoproteins. *EMBO Journal*, 11 (2):629–642, 1992.
- Kastner, P., Mark, M., and Chambon, P. Nonsteroid nuclear receptors: what are genetic studies telling us about their role in real life? *Cell*, 83(6):859–69, 1995.
- Kim, H. K., Son, S. Y., Oh, J. S., Song, Y. N., Byun, J. M., Koh, Y., Hong, J., Yoon, S.-S., Lee, C. H., Shin, D.-Y., and Lee, M. R. Metabolic Profiling during Acute Myeloid Leukemia Progression Using Paired Clinical Bone Marrow Serum Samples. *Metabolites*, 11(9):586, 2021.
- Kimura, N. and Shimada, N. Membrane-associated nucleoside diphosphate kinase from rat liver. *The Journal of biological chemistry*, 263(10):4647–4653, 1988.
- Knight, R. D., Mangum, J., Lucas, D. L., Cooney, D. a., Khan, E. C., and Wright, D. G. Inosine monophosphate dehydrogenase and myeloid cell maturation. *Blood*, 69 (2):634–9, 1987.
- Kondo, K. and Sasaki, M. Cytogenetic studies in four cases of Acute Promyelocytic Leukemia (APL). Cancer Genetics and Cytogenetics, 1(2):131–138, 1979.
- Kondo, K. and Sasaki, M. Further cytogenetic studies on acute promyelocytic leukemia. Cancer Genetics and Cytogenetics, 6(1):39–46, 1982.
- Konno, Y., Natsumeda, Y., Nagai, M., Yamaji, Y., Ohno, S., Suzuki, K., and Weber, G. Expression of human IMP dehydrogenase types I and II in Escherichia coli and distribution in human normal lymphocytes and leukemic cell lines. *Journal of Biological Chemistry*, 266(1):506–509, 1991.

- Koudriavtsev, A., Jameson, R. F., and Linert, W. *The Law of Mass Action*. Springer Berlin Heidelberg, Berlin, Heidelberg, 2001. ISBN 978-3-642-62494-0. doi: 10.1007/978-3-642-56770-4. URL https://pubs.acs.org/doi/10.1021/ja015294ihttp://link.springer.com/10.1007/978-3-642-56770-4.
- Kozhevnikova, E. N., van der Knaap, J. A., Pindyurin, A. V., Ozgur, Z., van Ijcken, W. F. J., Moshkin, Y. M., and Verrijzer, C. P. Metabolic enzyme IMPDH is also a transcription factor regulated by cellular state. *Molecular cell*, 47(1):133–9, 2012.
- Lawson, N. D. and Berliner, N. Neutrophil maturation and the role of retinoic acid. *Experimental Hematology*, 27(9):1355–1367, 1999.
- Leid, M., Kastner, P., Lyons, R., Nakshatri, H., Saunders, M., Zacharewski, T., Chen, J. Y., Staub, A., Garnier, J. M., Mader, S., and Chambon, P. Purification, cloning, and RXR identity of the HeLa cell factor with which RAR or TR heterodimerizes to bind target sequences efficiently. *Cell*, 68(2):377–395, 1992.
- Lemmens, R., Vanduffel, L., Teuchy, H., and Culic, O. Regulation of proliferation of LLC-MK2 cells by nucleosides and nucleotides: the role of ecto-enzymes. *Biochemical Journal*, 316(2):551–557, 1996.
- Li, C., Donizelli, M., Rodriguez, N., Dharuri, H., Endler, L., Chelliah, V., Li, L., He, E., Henry, A., Stefan, M. I., Snoep, J. L., Hucka, M., Le Novère, N., and Laibe, C. BioModels Database: An enhanced, curated and annotated resource for published quantitative kinetic models. *BMC systems biology*, 4:92, 2010.
- Link, J. and Straub, K. Trapping of an IMP dehydrogenase-substrate covalent intermediate by mycophenolic acid. *Journal of the American Chemical Society*, 118:2091–2092, 1996.
- Liquori, A., Ibañez, M., Sargas, C., Sanz, M. Á., Barragán, E., and Cervera, J. Acute promyelocytic leukemia: A constellation of molecular events around a single PML-RARA fusion gene. *Cancers*, 12(3), 2020.
- Lo-Coco, F., Ammatuna, E., Montesinos, P., and Sanz, M. A. Acute promyelocytic leukemia: recent advances in diagnosis and management. *Seminars in oncology*, 35(4): 401–9, 2008.
- Lo Presti, C., Fauvelle, F., Jacob, M.-C., Mondet, J., and Mossuz, P. The metabolic reprogramming in acute myeloid leukemia patients depends on their genotype and is a prognostic marker. *Blood Advances*, 5(1):156–166, 2021.
- Lucas, D. L., Webster, H. K., and Wright, D. G. Purine metabolism in myeloid precursor cells during maturation. Studies with the HL-60 cell line. *The Journal of clinical investigation*, 72(6):1889–900, 1983a.
- Lucas, D., Robins, R., Knight, R., and Wright, D. Induced maturation of the human promyelocytic leukemia cell, HL-60, by 2-B-D-ribofuranosylselenazole-4- carboxamide. *Biochemical and biophysical research communications*, 115(3):971–980, 1983b.

- Marshall, J. S., Warrington, R., Watson, W., and Kim, H. L. An introduction to immunology and immunopathology. *Allergy, Asthma & Clinical Immunology*, 14(S2):49, 2018.
- Martin, A. J. and Synge, R. L. A new form of chromatogram employing two liquid phases: 1. A theory of chromatography. 2. Application to the micro-determination of the higher monoamino-acids in proteins. *The Biochemical journal*, 35(12):1358–68, 1941.
- Mathur, P., Kottilil, S., and Wilson, E. Use of ribavirin for hepatitis c treatment in the modern direct-acting antiviral era. *Journal of Clinical and Translational Hepatology*, 6 (4):431–437, 2018.
- McMaster, M. C. Advantages and Disadvantages of HPLC. In *HPLC: A Practical User's Guide, Second Edition*, chapter 1, pages 1–13. John Wiley & Sons, Ltd, 2nd ed edition, 2007a. ISBN 9780470079096. doi: 10.1002/9780470079096.ch1. URL https://onlinelibrary.wiley.com/doi/abs/10.1002/9780470079096.ch1.
- McMaster, M. C. Partition Chromatography Modifications. In *HPLC: A Practical User's Guide*, *Second Edition*, chapter 7, pages 89–94. John Wiley & Sons, Ltd, 2nd ed edition, 2007b. ISBN 9780470079096. doi: 10.1002/9780470079096.ch7. URL https://onlinelibrary.wiley.com/doi/abs/10.1002/9780470079096.ch7.
- Mesbahi, Y., Trahair, T. N., Lock, R. B., and Connerty, P. Exploring the Metabolic Landscape of AML: From Haematopoietic Stem Cells to Myeloblasts and Leukaemic Stem Cells. *Frontiers in Oncology*, 12(February):1–17, 2022.
- Meyer, V. R. Practical High-Performance Liquid Chromatography. John Wiley & Sons, Ltd, Chichester, UK, 2010. ISBN 9780470688427. doi: 10.1002/9780470688427. URL http://doi.wiley.com/10.1002/9780470688427.
- Michaelis, L. and Menten, M. L. Die kinetik der invertinwirkung.  $Biochem\ Z,\ 49:333-369,\ 1913.$
- Mitelman, F. Catalogue of Chromosome Aberrations in Cancer: Chromosome 15. Cytogenetic and Genome Research, 36(1-2):294–309, 1983a.
- Mitelman, F. Catalogue of Chromosome Aberrations in Cancer: Chromosome 17. Cytogenetic and Genome Research, 36(1-2):323–349, 1983b.
- Mourad, N. and Parks, R. E. Erythrocytic nulceoside diphosphokinase. *The Journal of biological chemistry*, 241(2):271–278, 1966.
- Murray, A. W. The biological significance of purine salvage. *Annual review of biochemistry*, 40:811–826, 1971.
- Nagai, M., Natsumeda, Y., Konno, Y., Hoffman, R., Irino, S., and Weber, G. Selective Up-Regulation of Type II Inosine 5-Monophosphate Dehydrogenase Messenger RNA Expression in Human Leukemias. *Cancer Research*, 51(15):3886–3890, 1991.

- Nagai, M., Natsumeda, Y., and Weber, G. Proliferation-linked Regulation of Type II IMP Dehydrogenase Gene in Human Normal Lymphocytes and HL-60 Leukemic Cells. *Cancer Research*, 52(2):258–261, 1992.
- Natsumeda, Y., Ohno, S., Kawasaki, H., Konno, Y., Weber, G., and Suzuki, K. Two distinct cDNAs for human IMP dehydrogenase. *Journal of Biological Chemistry*, 265 (9):5292–5295, 1990.
- Nesterenko, P. N. and Palamareva, M. D. Liquid Chromatography | Overview. In Worsfold, P., Poole, C., Townshend, A., and Miró, M., editors, *Encyclopedia of Analytical Science (Third Edition)*, pages 174–181. Academic Press, Oxford, third edit edition, 2019. ISBN 978-0-08-101984-9. doi: https://doi.org/10.1016/B978-0-12-409547-2.14214-3. URL https://www.sciencedirect.com/science/article/pii/B9780124095472142143.
- Newell, L. F. and Cook, R. J. Advances in acute myeloid leukemia. BMJ, 375:1–20, 2021.
- Noma, T., Fujisawa, K., Yamashiro, Y., Shinohara, M., Nakazawa, A., Gondo, T., Ishihara, T., and Yoshinobu, K. Structure and expression of human mitochondrial adenylate kinase targeted to the mitochondrial matrix. *The Biochemical journal*, 358(Pt 1): 225–32, 2001.
- O'Dwyer, P. J., Shoemaker, D. D., Jayaram, H. N., Johns, D. G., Cooney, D. A., Marsoni, S., Malspeis, L., Plowman, J., Davignon, J. P., and Davis, R. D. Tiazofurin: a new antitumor agent. *Investigational new drugs*, 2(1):79–84, 1984.
- Palella, T. D., Andres, C. M., and Fox, I. H. Human placental adenosine kinase. *The Journal of biological chemistry*, 255(11):5264–5269, 1980.
- Pandolfi, P. P., Alcalay, M., Fagioli, M., Zangrilli, D., Mencarelli, A., Diverio, D., Biondi, A., Lo Coco, F., Rambaldi, A., Grignani, F., Rochette-Egly, C., Gaube, M. P., Chambon, P., and Pelicci, P. G. Genomic variability and alternative splicing generate multiple PML/RARα transcripts that encode aberrant PML proteins and PML/RARα isoforms in acute promyelocytic leukaemia. EMBO Journal, 11(4):1397–1407, 1992.
- Pankiewicz, K. W. and Goldstein, B. M. Inosine Monophosphate Dehydrogenase and Its Inhibitors: An Overview, chapter 1, pages 1–17. American Chemical Society, 2003. ISBN 9780841237803. doi: 10.1021/bk-2003-0839.ch001. URL https://pubs.acs.org/doi/abs/10.1021/bk-2003-0839.ch001.
- Perez, A., Kastner, P., Sethi, S., Lutz, Y., Reibel, C., and Chambon, P. PMLRAR homodimers: Distinct DNA binding properties and heteromeric interactions with RXR. *EMBO Journal*, 12(8):3171–3182, 1993.
- Petkovich, M., Brand, N. J., Krust, A., and Chambon, P. A human retinoic acid receptor which belongs to the family of nuclear receptors. *Nature*, 330(6147):444–50, 1987.
- Pilz, R. B., Huvar, I., Scheele, J. S., Van den Berghe, G., and Boss, G. R. A decrease in the intracellular guanosine 5'-triphosphate concentration is necessary for granulocytic

- differentiation of HL-60 cells, but growth cessation and differentiation are not associated with a change in the activation state of Ras, the transformin. Cell growth & differentiation: the molecular biology journal of the American Association for Cancer Research, 8(1):53–9, 1997.
- Pohlert, T. PMCMRplus: Calculate Pairwise Multiple Comparisons of Mean Rank Sums Extended, 2021. URL https://cran.r-project.org/package=PMCMRplus.
- R Development Core Team. R: A Language and Environment for Statistical Computing. R Foundation for Statistical Computing, Vienna, Austria, 2021.
- Rashkovan, M. and Ferrando, A. Metabolic dependencies and vulnerabilities in leukemia. Genes & Development, 33(21-22):1460–1474, 2019.
- Raz, T., Kapranov, P., Lipson, D., Letovsky, S., Milos, P. M., and Thompson, J. F. Protocol dependence of sequencing-based gene expression measurements. *PloS one*, 6 (5):e19287, 2011.
- Roboz, G. J. Current treatment of acute myeloid leukemia. Current Opinion in Oncology, 24(6):711–719, 2012.
- Rosales, C. Neutrophil: A Cell with Many Roles in Inflammation or Several Cell Types? *Frontiers in Physiology*, 9(FEB):1–17, 2018.
- Sak, K. and Everaus, H. Established Human Cell Lines as Models to Study Anti-leukemic Effects of Flavonoids. *Current Genomics*, 18(1):3–26, 2016.
- Savageau, M. A. Introduction to s-systems and the underlying power-law formalism. *Mathematical and Computer Modelling*, II:546–551, 1988.
- Savageau, M. A. Biochemical systems theory: operational differences among variant representations and their significance. *Journal of theoretical biology*, 151(4):509–30, 1991.
- Savageau, M. A. Biochemical systems analysis. I. Some mathematical properties of the rate law for the component enzymatic reactions. *Journal of theoretical biology*, 25(3): 365–9, 1969a.
- Savageau, M. A. Biochemical systems analysis. II. The steady-state solutions for an n-pool system using a power-law approximation. *Journal of theoretical biology*, 25(3): 370–9, 1969b.
- Savageau, M. A. Biochemical systems analysis. III. Dynamic solutions using a power-law approximation. *Journal of theoretical biology*, 26(2):215–26, 1970.
- Savageau, M. A. The Behavior of Intact Biochemical Control Systems. In **Topics** Cellular Regulation, Currentinvolume 6, pages 63–130. DEMIC PRESS, INC., 1972. doi: 10.1016/B978-0-12-152806-5.50010-2. http://dx.doi.org/10.1016/B978-0-12-152806-5.50010-2https: URL //linkinghub.elsevier.com/retrieve/pii/B9780121528065500102.

- Savageau, M. A. Power-law formalism: A canonical nonlinear approach to modeling and analysis. In Lakshmikantham, V., editor, World Congress of Nonlinear Analysts '92: Proceedings of the First World Congress of Nonlinear Analysts, Tampa, Florida, August 19-26, 1992, pages 3323-3334. De Gruyter, 1996. doi: 10.1515/9783110883237. 3323. URL https://www.degruyter.com/document/doi/10.1515/9783110883237. 3323/html.
- Savageau, M. A. Biochemical systems analysis. A study of function and design in molecular biology. Addison Wesley Publ., 2009.
- Savageau, M. A., Voit, E. O., and Irvine, D. H. Biochemical systems theory and metabolic control theory: 1. fundamental similarities and differences. *Mathematical Biosciences*, 86(2):127–145, 1987a.
- Savageau, M. A., Voit, E. O., and Irvine, D. H. Biochemical systems theory and metabolic control theory: 2. the role of summation and connectivity relationships. *Mathematical Biosciences*, 86(2):147–169, 1987b.
- Schalm, S. W., Hansen, B. E., Chemello, L., Bellobuono, A., Brouwer, J. T., Weiland, O., Cavalletto, L., Schvarcz, R., Ideo, G., and Alberti, A. Ribavirin enhances the efficacy but not the adverse effects of interferon in chronic hepatitis C. Meta-analysis of individual patient data from European centers. *Journal of hepatology*, 26(5):961–6, 1997.
- Shannon, P., Markiel, A., Ozier, O., Baliga, N. S., Wang, J. T., Ramage, D., Amin, N., Schwikowski, B., and Ideker, T. Cytoscape: a software environment for integrated models of biomolecular interaction networks. *Genome research*, 13(11):2498–504, 2003.
- Shephard, E. A., Neal, R. D., Rose, P. W., Walter, F. M., and Hamilton, W. Symptoms of adult chronic and acute leukaemia before diagnosis: large primary care case-control studies using electronic records. *British Journal of General Practice*, 66(644):e182–e188, 2016.
- Sheshachalam, A., Srivastava, N., Mitchell, T., Lacy, P., and Eitzen, G. Granule protein processing and regulated secretion in neutrophils. *Frontiers in Immunology*, 5(SEP): 1–11, 2014.
- Shu, Q. and Nair, V. Inosine monophosphate dehydrogenase (IMPDH) as a target in drug discovery. *Medicinal Research Reviews*, 28(2):219–232, 2008.
- Sidwell, R. W., Huffman, J. H., Khare, G. P., Allen, L. B., Witkowski, J. T., and Robins, R. K. Broad-spectrum antiviral activity of virazole:  $1-\beta$ -D-ribofuranosyl-1, 2,4-triazole-3-carboxamide. *Science*, 177(4050):705-706, 1972.
- Smith, T. M., Hicks-Berger, C. A., Kim, S., and Kirley, T. L. Cloning, expression, and characterization of a soluble calcium-activated nucleotidase, a human enzyme belonging to a new family of extracellular nucleotidases. *Archives of Biochemistry and Biophysics*, 406(1):105–115, 2002.

- Snyder, F. F. and Henderson, J. F. Alternative Pathways of Deoxyadenosine and Adenosine Metabolism. *The Journal of biological chemistry*, 248(16):5899–5904, 1973.
- Sokoloski, J. A., Blair, O. C., and Sartorelli, A. C. Alterations in glycoprotein synthesis and guanosine triphosphate levels associated with the differentiation of HL-60 leukemia cells produced by inhibitors of inosine 5'-phosphate dehydrogenase. *Cancer research*, 46(5):2314–9, 1986.
- Sokoloski, J. A., Beardsley, G. P., and Sartorelli, A. C. Induction of HL-60 leukemia cell differentiation by the novel antifolate 5,10-dideazatetrahydrofolic acid. *Cancer research*, 49(17):4824–8, 1989.
- Soliven, A., Kayillo, S., and Shalliker, R. A. Liquid Chromatography | Reversed Phase. In Worsfold, P., Poole, C., Townshend, A., and Miró, M., editors, Encyclopedia of Analytical Science (Third Edition), pages 238-243. Academic Press, Oxford, third edit edition, 2013. ISBN 978-0-08-101984-9. doi: https://doi.org/10.1016/B978-0-12-409547-2.00305-X. URL https://www.sciencedirect.com/science/article/pii/B978012409547200305X.
- Sorribas, A. Alternative s-system representations for reversible biochemical pathways. *Mathematical and Computer Modelling*, 11:129–133, 1988.
- Sorribas, A. and Savageau, M. a. Strategies for representing metabolic pathways within biochemical systems theory: reversible pathways. *Mathematical biosciences*, 94(2): 239–69, 1989a.
- Sorribas, A. and Savageau, M. A. A comparison of variant theories of intact biochemical systems. II. flux-oriented and metabolic control theories. *Mathematical Biosciences*, 94 (2):195–238, 1989b.
- Sorribas, A. and Savageau, M. A. A comparison of variant theories of intact biochemical systems. I. enzyme-enzyme interactions and biochemical systems theory. *Mathematical Biosciences*, 94(2):161–193, 1989c.
- Spychala, J., Madrid-Marina, V., and Fox, I. High Km Soluble 5'-nucleotidase from human placenta (1988). *The Journal of biological chemistry*, 263(35):18759–18765, 1988.
- Srivastava, P. C., Pickering, M. V., Allen, L. B., Streeter, D. G., Campbell, M. T., Witkowski, J. T., Sidwell, R. W., and Robins, R. K. Synthesis and Antiviral Activity of Certain Thiazole C-Nucleosides. *Journal of Medicinal Chemistry*, 20(2):256–262, 1977.
- Stahl, M. and Tallman, M. S. Differentiation syndrome in acute promyelocytic leukaemia. British Journal of Haematology, 187(2):157–162, 2019.
- Stone, K. D., Prussin, C., and Metcalfe, D. D. IgE, mast cells, basophils, and eosinophils. Journal of Allergy and Clinical Immunology, 125(2):S73–S80, 2010.

- Stuani, L., Sabatier, M., and Sarry, J.-E. Exploiting metabolic vulnerabilities for personalized therapy in acute myeloid leukemia. *BMC Biology*, 17(1):57, 2019.
- Sweeney, M. J., Hoffman, D. H., and Poore, G. A. Possible in Situ Activation of Mycophenolic Acid by  $\beta$ -Glucuronidase. Cancer Research, 31(4):477–478, 1971.
- Sweeney, M. J., Hoffman, D. H., and Esterman, M. A. Metabolism and biochemistry of mycophenolic acid. *Cancer Research*, 32(9):1803–1809, 1972.
- Tasseff, R., Jensen, H. A., Congleton, J., Dai, D., Rogers, K. V., Sagar, A., Bunaciu, R. P., Yen, A., and Varner, J. D. An Effective Model of the Retinoic Acid Induced HL-60 Differentiation Program. *Scientific Reports*, 7(1):1–21, 2017.
- Tebbi, C. K. Etiology of Acute Leukemia: A Review. Cancers, 13(9):1–19, 2021.
- The MathWorks Inc. MATLAB. Natick, Massachusetts, 8.6.0.2672 edition, 2015.
- Thomas, D. and Majeti, R. Biology and relevance of human acute myeloid leukemia stem cells. *Blood*, 129(12):1577–1585, 2017.
- Thomas, G. B. and Finney, R. L. Calculus and Analytic Geometry. Addison-Wesley world student series. Addison-Wesley Publishing Company, 1996. ISBN 0-201-400015-4. URL https://books.google.co.uk/books?id=LJWKSQAACAAJ.
- Thomas, X. Acute Promyelocytic Leukemia: A History over 60 Years—From the Most Malignant to the most Curable Form of Acute Leukemia. *Oncology and Therapy*, 7(1): 33–65, 2019.
- Torres, N. V. and Voit, E. O. Pathway Analysis and Optimization in Metabolic Engineering. Cambridge University Press, 2002. ISBN 9780521800389. doi: 10.1017/CBO9780511546334. URL https://www.cambridge.org/core/product/identifier/9780511546334/type/book.
- Torres, R. J., Mateos, F. A., Puig, J. G., and Becker, M. A. Determination of phosphoribosylpyrophosphate synthetase activity in human cells by a non-isotopic, one step method. *Clinica Chimica Acta*, 245(1):105–112, 1996.
- Tricot, G. J., Jayaram, H. N., Lapis, E., Natsumeda, Y., Nichols, C. R., Kneebone, P., Heerema, N., Weber, G., and Hoffman, R. Biochemically directed therapy of leukemia with tiazofurin, a selective blocker of inosine 5'-phosphate dehydrogenase activity. Cancer research, 49(13):3696–701, 1989.
- Tsuboi, K. K. and Chervenka, C. H. Adenylate kinase of human erythrocyte. *The Journal of biological chemistry*, 250(1):132–140, 1975.
- Turvey, S. E. and Broide, D. H. Innate immunity. *Journal of Allergy and Clinical Immunology*, 125(2):S24–S32, 2010.
- Voit, E. O. Optimization in integrated biochemical systems. *Biotechnology and bioengineering*, 40(5):572–82, 1992.

- Voit, E. O. Computational analysis of biochemical systems: a practical guide for biochemists and molecular biologists. Cambridge University Press, 2000.
- Voit, E. O. Biochemical Systems Theory: A Review. *ISRN Biomathematics*, 2013:1–53, 2013.
- Voit, E. O., Martens, H. A., and Omholt, S. W. 150 Years of the Mass Action Law. *PLoS Computational Biology*, 11(1):e1004012, 2015.
- von Vietinghoff, S. and Ley, K. Homeostatic Regulation of Blood Neutrophil Counts. *The Journal of Immunology*, 181(8):5183–5188, 2008.
- Waage, P. and Gulberg, C. M. Studies concerning affinity. *Journal of Chemical Education*, 63(12):1044–1047, 1986.
- Warburg, O. On the Origin of Cancer Cells. Science, 123(3191):309–314, 1956.
- Warburg, O., Wind, F., and Negelein, E. The Metabolism of Tumors in the Body. *Journal of General Physiology*, 8(6):519–530, 1927.
- Werner, A., Schneider, W., Siems, W., Grune, T., and Schreiter, C. Ion-pair reversed phase HPLC determination of nucleotides, nucleosides and nucleobases Application to nucleotide metabolism in hepatocytes. *Chromatographia*, 27(11-12):639–643, 1989.
- Westervelt, P., Lane, A. A., Pollock, J. L., Oldfather, K., Holt, M. S., Zimonjic, D. B., Popescu, N. C., DiPersio, J. F., and Ley, T. J. High-penetrance mouse model of acute promyelocytic leukemia with very low levels of PML-RARα expression. *Blood*, 102(5): 1857–1865, 2003.
- Wolfram Research Inc. Mathematica, 2010.
- Wong, J. T.-F. and Hanes, C. S. Kinetic formulations for enzymic reactions involving two substrates. *Canadian Journal of Biochemistry and Physiology*, 40(6):763–804, 1962.
- Wright, D. A role for guanine ribonucleotides in the regulation of myeloid cell maturation. *Blood*, 69:334–337, 1987.
- Wu, J. C. Mycophenolate mofetil: Molecular mechanisms of action. *Perspectives in Drug Discovery and Design*, 2:185–204, 1994.
- Yang, H., Fang, Z., Wei, Y., Bohannan, Z. S., Gañán-Gómez, I., Pierola, A. A., Paradiso, L. J., Iwamura, H., and Garcia-Manero, G. Preclinical activity of FF-10501-01, a novel inosine-5'-monophosphate dehydrogenase inhibitor, in acute myeloid leukemia. Leukemia research, 59:85–92, 2017.
- Yatim, K. M. and Lakkis, F. G. A Brief Journey through the Immune System. *Clinical Journal of the American Society of Nephrology*, 10(7):1274–1281, 2015.
- Yu, V. C., Delsert, C., Andersen, B., Holloway, J. M., Devary, O. V., Näär, A. M., Kim, S. Y., Boutin, J. M., Glass, C. K., and Rosenfeld, M. G. RXRβ: A coregulator that enhances binding of retinoic acid, thyroid hormone, and vitamin D receptors to their cognate response elements. Cell, 67(6):1251–1266, 1991.

- Zelent, A., Guidez, F., Melnick, A., Waxman, S., and Licht, J. D. Translocations of the RAR $\alpha$  gene in acute promyelocytic leukemia. *Oncogene*, 20(49 REV. IIS. 6):7186–7203, 2001.
- Zhu, J., Lallemand-Breitenbach, V., and De Thé, H. Pathways of retinoic acid- or arsenic trioxide-induced PML/RAR $\alpha$  catabolism, role of oncogene degradation in disease remission. *Oncogene*, 20(49 REV. IIS. 6):7257–7265, 2001.

# Appendices

# Appendix A

This appendix contains the network schematic for the Curto et al. (1998b) model.

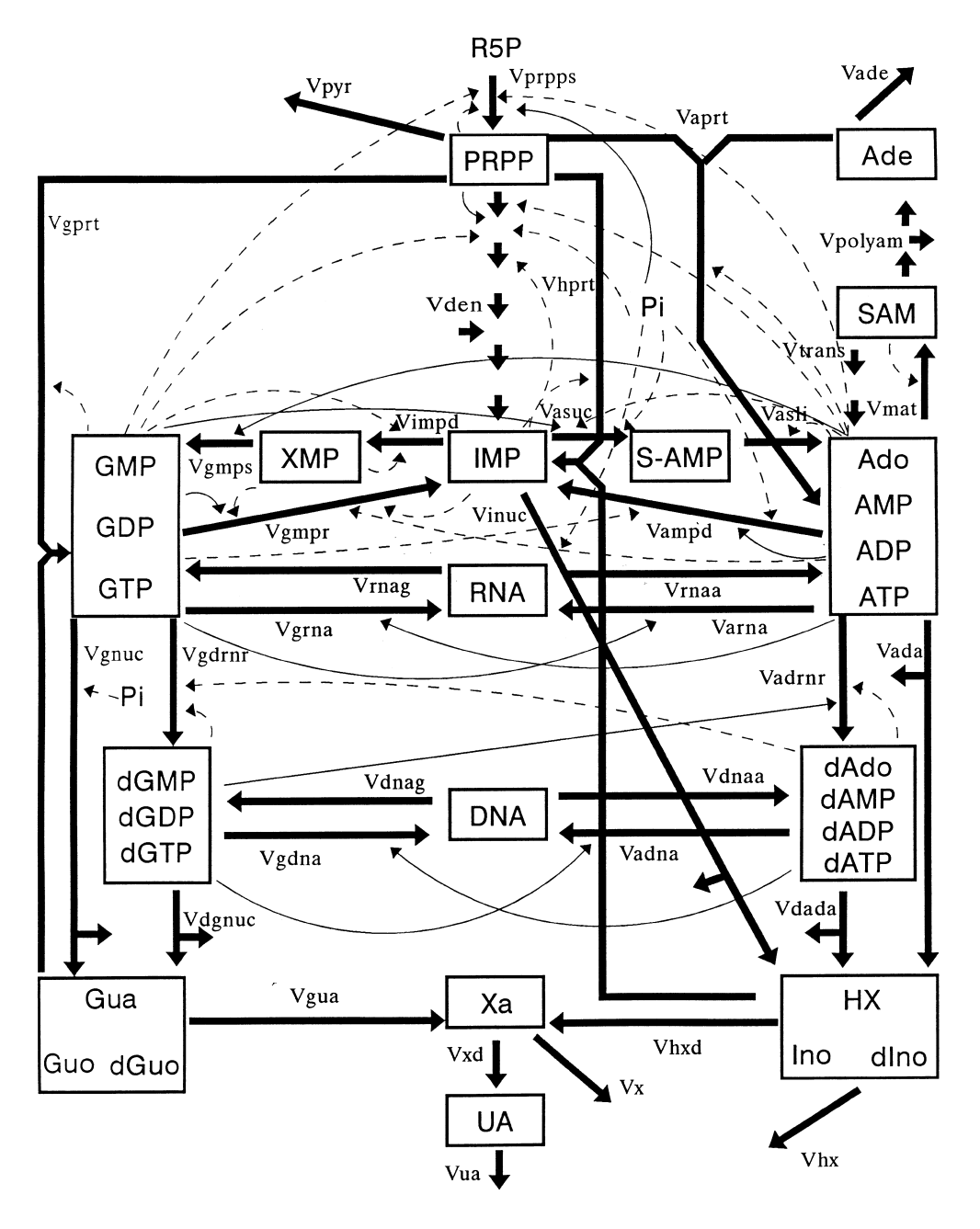


**Figure A.1:** Network schematic from the Curto *et al.* (1998b) model. Dependent variables (metabolites) are shown in boxes, whilst independent variables (R5P and Pi) are depicted without boxes. Thick solid arrows represent fluxes, whilst activatory regulations are indicated by thin arrows and inhibitory controls are denoted by dashed arrows.

# Appendix B

Contained in this appendix are two tables relating to the RNAseq data analysis. The first details the sample information, whilst the second provides information on the gene symbols relating to the purine metabolic enzymes investigated in the analysis.

Untreated	Treated with ATRA					
RPM2_1_12fc1ch9	RPM2_1_12_FC1CH7					
RPM2_1_12fc1ch10	RPM2_1_12_FC1CH8					
RPM11_12_11fc2ch15	RPM11_12_11_FC2CH14					

**Table B.1:** HL60 cell samples used in RNAseq data analysis. Samples are listed using their unique identifier from the GEO database (Edgar *et al.*, 2002).

Enzyme abbreviation	Gene symbol
ADA/DADA	ADA
ADE/HXD/XD	XDH
ADEK	AK1
ADNA/GDNA	POL_MU, POLA1, POLA2, POLB, POLD1,
	POLD2, POLD3, POLD4, POLDS, POLE,
	POLE2, POLE3, POLE4, POLG, POLG2,
	POLH, POLI, POLK, POLL, POLM,
	POLN, POLQ, POLS
ADOK	ADK
ADPK/GDPK	NME1, NME2, NME3, NME4,
	NME5, NME6, NME7
ADRNR/GDRNA	RRM1, RRM2, RRM2B
AMPD	AMDP1, AMDP2, AMPD3
APRT	APRT
ARNA/GRNA	POLR1A, POLR1B, POLR1C, POLR1D, POLR1E,
	POLR2A, POLR2B, POLR2C, POLR2D, POLR2E,
	POLR2F, POLR2G, POLR2H, POLR2I, POLR2J,
	POLR2J2, POLR2J3, POLR2K, POLR2L, POLR3A,
	POLR3B, POLR3C, POLR3D, POLR3E, POLR3F,
	POLR3G, POLR3H, POLR3K
ASLI	ADSL
ASUC	ADSS
continued on the next	t page

Enzyme abbreviation	Gene symbol
DEN	PPAT, GART, PFAS, PAICS, ATIC
DGNUC	NT5C
DNAA/DNAG	DNASE1, DNASE2
GMPR	GMPR, GMPR2
GMPS	GMPS
GUA	GDA
GUK	GUK1
HPRT/GPRT	HPRT1
IMPDH	IMPDH1, IMPDH2
INUC/ANUC/GNUC	NT5C1A, NT5C1B, NT5C2, NT5C3
MAT	MAT1A, MAT2A
NTPP	ITPA
POLYAM	AMD1
PRPPS	PRPS1, PRPS2
RNAA/RNAG	RNASE1, RNASE2, RNASE3, RNASE4,
	RNASE6, RNASE7, RNASE8
TRANS	PCMT1, ICMT

**Table B.2:** List of purine enzyme abbreviations with corresponding gene names. These were used to extract data from the Raz *et al.* (2011) RNAseq data set corresponding to enzymes present in the purine metabolic network.

# Appendix C

This appendix provides information on the derivation of the GMA kinetic orders and equations for the new interconversion reactions as well as details of the sets of simultaneous equations used to calculate the initial flux values for model versions 1 and 2. Also included here are six tables detailing the kinetic orders, initial flux values and rate constants for model versions 1 and 2.

# $f_{ij}$ equations used for interconversion reactions

#### Substrates

$$f_{ij} = \frac{K_m}{K_m + [S]}$$
 derivative of  $v_{ij} = \frac{V_{max}[S]}{K_m + [S]}$  w.r.t. [S]

Used for substrates of reactions: ADOK, ADEK, ADPK, ANUC (plus Hill coefficient), GDPK/NDPK and GUK.

### Competitive inhibition

$$f_{ij} = \frac{-[I]K_m}{K_i \left(K_m \left(1 + \frac{[I]}{K_i}\right) + [S]\right)} \quad \text{derivative of} \quad v_{ij} = \frac{V_{max}[S]}{K_m \left(1 + \frac{[I]}{K_i}\right) + [S]} \quad \text{w.r.t.} \quad [I]$$

Used for inhibitors of reactions: AMP for ADOK and Pi for ANUC (plus Hill coefficient).

### Non-competitive inhibition

$$f_{ij} = \frac{-[I]}{K_i \left(1 + \frac{[I]}{K_i}\right)} \quad \text{derivative of} \quad v_{ij} = \frac{V_{max}[S]}{\left(1 + \frac{[I]}{K_i}\right) \left(K_m + [S]\right)} \quad \text{w.r.t.} \quad [I]$$

Used for inhibitors of reactions: ADP for ADOK, GMP for ADPK and GMP for GDPK.

#### Hill's functions

Raise [S] to the power of n in the above Michaelis-Menten equations. Used for reaction: ANUC

### Apparent $K_m$

$$K_m^{app} = K_m \left( 1 + \frac{[I]}{K_i} \right)$$

Used for inhibitor of reaction: Pi for ANUC.

## GMA equations for the interconversion reactions

#### **ADEK**

$$AMP + ATP \longrightarrow 2ADP$$

 $K_m$  for AMP = 80  $\mu$ M and  $K_m$  for ATP = 90  $\mu$ M, giving  $f_{adek4M} = 0.286$  and  $f_{adek4T} = 0.0452$ . No inhibition or activation.

$$v_{adek} = \alpha_{adek} X_{4M}^{f_{adek4M}} X_{4T}^{f_{adek4T}}$$

### **ADOK**

$$Ado + ATP \longrightarrow AMP + ADP$$

 $K_m$  for Ado = 0.4  $\mu$ M and  $K_m$  for ATP = 75  $\mu$ M, giving  $f_{adok4A} = 0.444$  and  $f_{adok4T} = 0.038$ . Product inhibition by AMP and ADP. AMP inhibits competitively w.r.t. Ado, with  $K_i = 140 \ \mu$ M, giving  $f_{adok4M} = -0.388$  whilst ADP inhibits non-competitively, with  $K_i = 50 \ \mu$ M, giving  $f_{adok4D} = -0.889$ . Initially ignoring Ado inhibition as only seen at high concentrations of Ado.

$$v_{adok} = lpha_{adok} X_{4A}^{f_{adok4A}} X_{4M}^{f_{adok4M}} X_{4D}^{f_{adok4D}} X_{4T}^{f_{adok4T}}$$

#### **ADPK**

$$ADP + GTP \longrightarrow ATP + GDP$$

 $K_m$  for ADP = 40  $\mu$ M and  $K_m$  for GTP = 150  $\mu$ M, giving  $f_{adpk4D}$  = 0.0909 and  $f_{adpk8T}$  = 0.333. GMP inhibits non-competitively with,  $K_i$  = 650  $\mu$ M, giving  $f_{adpk8M}$  = -0.0370. Initially ignoring GDP inhibition so as to follow the method adopted by Curto et al. (1998b) whereby the kinetic orders for substrates are calculated using the standard Michaelis-Menten equation, without inhibition. In the equation for substrate inhibition, the  $K_m$  for the non-inhibiting substrate is modified by the inhibitor (see above).

$$v_{adpk} = \alpha_{adpk} X_{4D}^{f_{adpk4D}} X_{8M}^{f_{adpk8M}} X_{8T}^{f_{adpk8T}}$$

#### ANUC

$$AMP + H_20 \longrightarrow Ado + Pi$$

This reaction exhibits cooperativity w.r.t. the substrate AMP, with  $K_m$  for AMP = 31,000  $\mu$ M and a Hill coefficient of n=1.5, giving  $f_{anuc4M}=1.375$ . The product Pi inhibits competitively w.r.t. AMP altering both the  $K_m$  and n values. A concentration of 1000  $\mu$ M of Pi produces  $K_m^{app}=38,000~\mu$ M (implying  $K_i=4428.57~\mu$ M) and n=1.7, giving  $f_{anuc18}=-0.212$ . Initially ignoring alternative substrate inhibition (e.g. by GMP and IMP etc.) and activation as done by Curto et al. (1998b), so only including inhibition by Pi.

$$v_{anuc} = \alpha_{anuc} X_{4M}^{f_{anuc4M}} X_{18}^{f_{anuc18}}$$

### GDPK/NDPK

$$GDP + ATP \longrightarrow GTP + ADP$$

 $K_m$  for ATP = 1330 µM and  $K_m$  for GDP = 31 µM, giving  $f_{gdpk4T} = 0.412$  and  $f_{gdpk8D} = 0.292$ . GMP inhibits non-competitively with  $K_i = 650$  µM, giving  $f_{gdpk8M} = -0.0370$ . Initially ignoring ADP inhibition so as to follow the method adopted by Curto et al. (1998b) whereby the kinetic orders for substrates are calculated using the standard Michaelis-Menten equation, without inhibition. In the equation for substrate inhibition, the  $K_m$  for the non-inhibiting substrate is modified by the inhibitor (see above).

$$v_{gdpk} = \alpha_{gdpk} X_{4T}^{f_{gdpk4T}} X_{8M}^{f_{gdpk8M}} X_{8D}^{f_{gdpk8D}}$$

**GUK** 

$$GMP + ATP \longrightarrow GDP + ADP$$

 $K_m$  for ATP = 190  $\mu$ M and  $K_m$  for GMP = 18  $\mu$ M, giving  $f_{guk4T} = 0.0909$  and  $f_{guk8M} = 0.419$ . No inhibition or activation.

$$v_{guk} = \alpha_{guk} X_{4T}^{f_{guk4T}} X_{8M}^{f_{guk8M}}$$

#### **ATPDEG**

$$ATP \longrightarrow ADP$$

Reaction for the generic degradation of ATP, via multiple enzymes. No inhibition or activation.

$$v_{atpdeg} = \alpha_{atpdeg} X_{4T}$$

#### **ATPSYN**

$$ADP \longrightarrow ATP$$

Reaction for the generic synthesis of ATP, via multiple enzymes. No inhibition or activation.

$$v_{atpsyn} = \alpha_{atpsyn} X_{4D}$$

#### **PHOSPHO**

$$ADP \longrightarrow ATP$$

Reaction for the net synthesis of ATP, via multiple processes. ADP is an activator, whilst ATP inhibits the reaction. However, as this reaction represents multiple processes, no kinetic data is available thus the kinetic orders are set at:  $f_{phospho4D} = 0.5$  and  $f_{phospho4T} = -0.1$ .

$$v_{phospho} = \alpha_{phospho} X_{4D}^{f_{phospho4D}} X_{4T}^{f_{phospho4T}}$$

# Set of simultaneous flux equations for models 1 and 2

### Steady state equations

$$X_1: v_{prpps} = v_{gprt} + v_{hprt} + v_{aprt} + v_{den} + v_{pyr}$$

$$X_2: v_{den} + v_{gmpr} + v_{ampd} + v_{hprt} = v_{impdh} + v_{asuc} + v_{inuc}$$

$$X_3: v_{asuc} = v_{asli}$$

$$X_5: v_{mat} = v_{trans} + v_{polyam}$$

$$X_6: v_{polyam} = v_{aprt} + v_{ade}$$

$$X_7: v_{impdh} = v_{gmps}$$

$$X_9: v_{adrnr} + v_{dnaa} = v_{adna} + v_{dada}$$

$$X_{10}: v_{gdrnr} + v_{dnag} = v_{gdna} + v_{dgnuc}$$

$$X_{11}: v_{arna} + v_{grna} = v_{rnag} + v_{rnaa}$$

$$X_{12}: v_{adna} + v_{gdna} = v_{dnag} + v_{dnaa}$$

$$X_{13}: v_{ada} + v_{dada} + v_{inuc} = v_{hprt} + v_{hxd} + v_{hxe}$$

$$X_{14}: \quad v_{hxd} + v_{gua} = v_{xd} + v_{xe}$$

$$X_{15}: v_{dgnuc} + v_{gnuc} = v_{gprt} + v_{gua}$$

$$X_{16}: v_{xd} = v_{uae}$$

$$X_{4A}: v_{trans} + v_{anuc} = v_{ada} + v_{adok}$$

$$X_{4M}: v_{prpps} + v_{gmps} + v_{aprt} + v_{asli} + v_{rnaa} + v_{adok} = v_{ampd} + v_{adek} + v_{anuc}$$

$$X_{4D}: v_{adok} + 2v_{adek} + v_{guk} + v_{gdpk} + v_{atpdeg} = v_{adrnr} + v_{adpk} + v_{atpsyn}$$

$$X_{4T}: \quad v_{adpk} + v_{atpsyn} = v_{prpps} + v_{gmps} + v_{mat} + v_{arna} + v_{adok} + v_{adek} + v_{guk} + v_{gdpk} + v_{atpdeg}$$

$$X_{8M}: v_{gprt} + v_{gmps} + v_{rnag} = v_{gmpr} + v_{gnuc} + v_{guk}$$

$$X_{8D}: v_{asuc} + v_{guk} + v_{adpk} = v_{gdrnr} + v_{gdpk}$$

$$X_{8T}: v_{gdpk} = v_{asuc} + v_{grna} + v_{adpk}$$

### RNA and DNA constraints

$$v_{arna} = \frac{3}{2}v_{grna}$$

$$v_{rnaa} = \frac{3}{2}v_{rnag}$$

$$v_{adna} = \frac{3}{2}v_{gdna}$$

$$v_{dnaa} = \frac{3}{2}v_{dnag}$$

### Experimentally based constraints

```
v_{uae} \approx 2.27 \ \mu mol \ min^{-1} \ (Body \ weight)^{-1}
 v_{hxd} + v_{hprt} \approx 4.9 \; \mu mol \; min^{-1} \; (Body \; weight)^{-1}
 v_{hprt} \approx 3 v_{hxd}
 v_{hprt} \approx v_{gprt}
 v_{gdrnr} + v_{gnuc} \approx 9 v_{gmpr}
 v_{aprt} \approx 1 \ \mu mol \ min^{-1} \ (Body \ weight)^{-1}
\frac{v_{ada}}{v_{dada}} \approx \frac{[Ado]}{[dAdo]} \approx 10
\frac{v_{gnuc}}{v_{dgnuc}} \approx \frac{[GMP]}{[dGMP]} \approx 250
 v_{trans} \approx 14 \ \mu mol \ min^{-1} \ (Body \ weight)^{-1}
 v_{pyr} \approx 10 \ \mu mol \ min^{-1} \ (Body \ weight)^{-1}
 v_{ade} \approx 0.01 \ \mu mol \ min^{-1} \ (Body \ weight)^{-1}
 v_{hxe} \approx 0.05 \ \mu mol \ min^{-1} \ (Body \ weight)^{-1}
 v_{xe} \approx 0.03 \ \mu mol \ min^{-1} \ (Body \ weight)^{-1}
 v_{ampd} \approx 3 v_{ada}
 v_{adna} + v_{gdna} = 17 \; \mu mol \; min^{-1} \; (Body \; weight)^{-1}
 v_{arna} + v_{grna} = 3300 \; \mu mol \, min^{-1} \, (Body \, weight)^{-1}
                                     Altered from value in Curto et al. (1998b)
 v_{asuc} \approx v_{imvdh}
 v_{inuc} \approx 15 v_{anuc}
 v_{atpsyn} = 10 \, v_{atpdeg}
                                         For model 1 only
v_{gdpk} = 10 \, v_{adpk}
```

				_
$f_{ade6} = 0.55$	$f_{adrnr9} = -0.3$	$f_{adrnr10} = 0.87$	)	
$f_{ampd18} = -0.1$	$f_{aprt1} = 0.5$	$f_{aprt6} = 0.75$		
$f_{asli3}=0.99$	$f_{asuc2}=0.4$	$f_{asuc18} = -0.05$		
$f_{dada9} = 1.0$	$f_{den1} = 2.0$	$f_{den2} = -0.06$		
$f_{den18} = -0.08$	$f_{dgnuc10} = 1.0$	$f_{dnan12} = 1.0$		
$f_{dnap9} = 0.42$	$f_{dnap10} = 0.33$	$f_{gdrnr9} = -1.2$		Reactions
$f_{gdrnr10} = -0.39$	$f_{gmpr2} = -0.15$	$f_{gmpr7} = -0.76$		present
$f_{gmps7} = 0.16$	$f_{gnuc18} = -0.34$	$f_{gprt1} = 1.2$	l	in original Curto <i>et al.</i> (1998b)
$f_{gprt15} = 0.42$	$f_{gua15} = 0.5$	$f_{hprt1} = 1.1$		model,
$f_{hprt2} = -0.89$	$f_{hprt13} = 0.48$	$f_{hxd13} = 0.65$		so value
$f_{hxe13} = 1.12$	$f_{impdh2} = 0.15$	$f_{impdh7} = -0.09$		unchanged
$f_{inuc2}=0.8$	$f_{inuc18} = -0.36$	$f_{mat5} = -0.6$		
$f_{polyam5} = 0.9$	$f_{prpps1} = -0.03$	$f_{prpps17} = 0.65$		
$f_{prpps18} = 0.7$	$f_{pyr1} = 1.27$	$f_{rnan11} = 1.0$		
$f_{trans5} = 0.33$	$f_{uae16} = 2.21$	$f_{xe14} = 2.0$		
$f_{xd14} = 0.55$			J	
$f_{ada4A} = 0.97$	$f_{adrnr4D} = 0.1$	$f_{ampd4M} = 0.81$	)	
$f_{ampd8T} = -0.03$	$f_{aprt4M} = -0.8$	$f_{asli4M} = -0.95$		D
$f_{asuc4M} = -0.24$	$f_{asuc8T} = 0.2$	$f_{den4M} = -0.17$		Reactions present
$f_{den4D} = -0.06$	$f_{den4T} = -0.028$	$f_{den8M} = -0.14$		in original
$f_{den8D} = -0.06$	$f_{den8T} = -0.016$	$f_{gdrnr8D} = 0.4$		Curto <i>et al.</i> (1998b)
$f_{gmpr4M} = -0.01$	$f_{gmpr4D} = -0.02$	$f_{gmpr4T} = -0.04$	}	model,
$f_{gmpr8M} = 0.23$	$f_{gmpr8D} = 0.18$	$f_{gmpr8T} = 0.29$		but redefined
$f_{gmps4T} = 0.12$	$f_{gnuc8M} = 0.9$	$f_{gprt8M} = -1.2.$		so specific metabolite
$f_{impdh8M} = -0.03$	$f_{mat4T} = 0.2$	$f_{prpps4M} = -0.1$		is used
$f_{prpps4D} = -0.36$	$f_{prpps4T} = 0.007$	$f_{prpps8M} = -0.004$		4004
$f_{prpps8D} = -0.04$	$f_{rnap4T} = 0.05$	$f_{rnap8T} = 0.13$		-

**Table C.1:** Kinetic order values for existing reactions for model versions 1 and 2. Values for kinetic orders for unchanged reaction and metabolite combinations are set equal to those from the Curto *et al.* (1998b) model. Kinetic order values for existing reactions involving previously pooled metabolites were redefined using the appropriate individual metabolite concentration.

·				
$f_{adok4A} = 0.44$	$f_{adok4M} = -0.39$	$f_{adok4D} = -0.89$	)	
$f_{adok4T} = 0.038$	$f_{adek4M} = 0.29$	$f_{adek4T} = 0.045$	Į	Reactions in
$f_{anuc4M} = 1.37$	$f_{anuc18} = -0.21$	$f_{guk4T} = 0.091$		models 1 & 2
$f_{guk8M} = 0.42$			J	
$f_{adpk4D} = 0.091$	$f_{adpk8M} = -0.037$	$f_{adpk8T} = 0.33$	)	Reactions in
$f_{gdpk4T} = 0.41$	$f_{gdpk8M} = -0.037$	$f_{gdpk8D} = 0.29$	5	model 1
$f_{ndpk4T} = 0.41$	$f_{ndpk8M} = -0.037$	$f_{ndpk8D} = 0.29$	)	Reactions in
$f_{phospho4D} = 0.5$	$f_{phospho4T} = -0.1$			model 2

**Table C.2:** Kinetic order values for the new interconversion reactions for model versions 1 and 2. Values were calculated using the kinetic data in Table 3.4, along with the GMA equations detailed above.

$v_{ada} = 0.39$	$v_{ade} = 0.01$	$v_{adna} = 10.2$	)	
$v_{adrnr} = 0.039$	$v_{ampd} = 1.17$	$v_{aprt} = 1.0$		
$v_{arna}=1980.0$	$v_{asli} = 1.6$	$v_{asuc}=1.6$		
$v_{dada} = 0.039$	$v_{den} = 2.36$	$v_{dgnuc} = 0.019$		
$v_{dnaa} = 10.2$	$v_{dnag} = 6.8$	$v_{gdna} = 6.8$		Reactions
$v_{gdrnr} = 0.019$	$v_{gmpr} = 0.53$	$v_{gmps} = 1.60$		present
$v_{gnuc} = 4.73$	$v_{gprt} = 3.68$	$v_{grna} = 1320.0$	}	in original
$v_{gua}=1.075$	$v_{hprt} = 3.68$	$v_{hxd} = 1.23$		Curto <i>et al.</i> (1998b)
$v_{hxe}=0.05$	$v_{impdh} = 1.60$	$v_{inuc} = 4.52$		model
$v_{mat} = 15.01$	$v_{polyam} = 1.01$	$v_{prpps} = 20.71$		
$v_{pyr} = 10.0$	$v_{rnaa} = 1980.0$	$v_{rnag} = 1320.0$		
$v_{trans} = 14.0$	$v_{uae} = 2.27$	$v_{xe} = 0.03$		
$v_{xd} = 2.27$			J	
$v_{adek} = 2017.36$	$v_{adok} = 13.91$	$v_{adpk} = 146.85$	)	Na
$v_{anuc}=0.302$	$v_{atpdeg} = 743.36$	$v_{atpsyn} = 7433.58$	}	New reactions
$v_{gdpk} = 1468.45$	$v_{guk} = 1320.02$		J	

**Table C.3:** Initial flux values for model version 1. These were calculated using the full set of 45 simultaneous equations listed above. Values are in  $\mu$ mol min<sup>-1</sup> (Body weight)<sup>-1</sup>.

$\alpha_{ada} = 0.76$	$\alpha_{ade} = 0.01$	$\alpha_{adna} = 3.34$	)	-
$\alpha_{adrnr} = 0.014$	$\alpha_{ampd} = 0.039$	$\alpha_{aprt} = 31.0$		
$\alpha_{arna} = 646.7$	$\alpha_{asli} = 1210.13$	$\alpha_{asuc} = 0.42$		
$\alpha_{dada} = 0.0065$	$\alpha_{den} = 2.13$	$\alpha_{dgnuc} = 0.0063$		
$\alpha_{dnaa} = 0.002$	$\alpha_{dnag} = 0.0013$	$\alpha_{gdna} = 2.23$		Reactions
$\alpha_{gdrnr} = 0.044$	$\alpha_{gmpr} = 0.82$	$\alpha_{gmps} = 0.39$		present
$\alpha_{gnuc} = 3.07$	$\alpha_{gprt} = 12.9$	$\alpha_{grna} = 431.13$	}	in original
$\alpha_{gua} = 0.48$	$\alpha_{hprt} = 12.49$	$\alpha_{hxd} = 0.27$		Curto <i>et al.</i> (1998b)
$\alpha_{hxe}=0.0038$	$\alpha_{impdh} = 1.18$	$\alpha_{inuc} = 1.54$		model
$\alpha_{mat} = 7.62$	$\alpha_{polyam} = 0.29$	$\alpha_{prpps} = 0.35$		
$\alpha_{pyr} = 1.30$	$\alpha_{rnaa}=0.069$	$\alpha_{rnag} = 0.046$		
$\alpha_{trans} = 8.86$	$\alpha_{uae} = 0.000086$	$\alpha_{xe}=0.0012$		
$\alpha_{xd} = 0.94$			J	_
$\alpha_{adek} = 315.55$	$\alpha_{adok} = 22869.1$	$\alpha_{adpk} = 14.33$	)	Now
$\alpha_{anuc} = 0.00096$	$\alpha_{atpdeg} = 0.39$	$\alpha_{atpsyn} = 18.58$	}	New reactions
$\alpha_{gdpk} = 20.90$	$\alpha_{guk} = 172.71$		J	-

**Table C.4:** Rate constants for model version 1. Values were calculated using Equation 2.15, flux values from Table C.3, appropriate kinetic orders from Tables C.1 and C.2 and initial metabolite concentrations as detailed in Table 2.1.

$v_{ada}=0.39$	$v_{ade} = 0.01$	$v_{adna} = 10.2$	)	
$v_{adrnr} = 0.039$	$v_{ampd} = 1.17$	$v_{aprt} = 1.0$		
$v_{arna}=1980.0$	$v_{asli} = 1.6$	$v_{asuc} = 1.6$		
$v_{dada} = 0.039$	$v_{den} = 2.36$	$v_{dgnuc} = 0.019$		
$v_{dnaa} = 10.2$	$v_{dnag} = 6.8$	$v_{gdna} = 6.8$		Reactions
$v_{gdrnr} = 0.019$	$v_{gmpr} = 0.53$	$v_{gmps} = 1.6$		present
$v_{gnuc} = 4.73$	$v_{gprt} = 3.68$	$v_{grna} = 1320.0$	}	in original
$v_{gua} = 1.08$	$v_{hprt} = 3.68$	$v_{hxd} = 1.23$		Curto <i>et al.</i> (1998b)
$v_{hxe}=0.05$	$v_{impdh} = 1.6$	$v_{inuc}=4.52$		model
$v_{mat} = 15.01$	$v_{polyam} = 1.01$	$v_{prpps} = 20.71$		
$v_{pyr} = 10.0$	$v_{rnaa}=1980.0$	$v_{rnag} = 1320.0$		
$v_{trans} = 14.0$	$v_{uae} = 2.27$	$v_{xe}=0.03$		
$v_{xd} = 2.27$			J	
$v_{adek} = 2017.36$	$v_{adok} = 13.91$	$v_{anuc}=0.30$	)	New
$v_{guk} = 1320.02$	$v_{ndpk} = 1321.6$	$v_{phospho} = 6690.22$		reactions

**Table C.5:** Initial flux values for model version 2. These were calculated using the set of 43 simultaneous equations listed above. Values are in  $\mu$ mol min<sup>-1</sup> (Body weight)<sup>-1</sup>.

$\alpha_{ada} = 0.0084$	$\alpha_{ade} = 0.00011$	$\alpha_{adna} = 0.037$	)	
$\alpha_{adrnr} = 0.00015$	$\alpha_{ampd} = 0.00045$	$\alpha_{aprt} = 0.34$		
$\alpha_{arna} = 7.121$	$\alpha_{asli} = 13.33$	$\alpha_{asuc} = 0.0046$		
$\alpha_{dada} = 0.000071$	$\alpha_{den} = 0.023$	$\alpha_{dgnuc} = 0.000069$		
$\alpha_{dnaa} = 0.000022$	$\alpha_{dnag} = 0.000015$	$\alpha_{gdna} = 0.025$		Reactions
$\alpha_{gdrnr} = 0.00049$	$\alpha_{gmpr} = 0.0090$	$\alpha_{gmps} = 0.0047$		present
$\alpha_{gnuc} = 0.034$	$\alpha_{gprt} = 0.14$	$\alpha_{grna} = 4.75$	}	in original
$\alpha_{gua} = 0.0053$	$\alpha_{hprt} = 0.14$	$\alpha_{hxd} = 0.0030$		Curto <i>et al.</i> (1998b)
$\alpha_{hxe} = 0.000042$	$\alpha_{impdh} = 0.013$	$\alpha_{inuc} = 0.017$		model
$\alpha_{mat} = 0.084$	$\alpha_{polyam} = 0.0032$	$\alpha_{prpps} = 0.0038$		
$\alpha_{pyr} = 0.014$	$\alpha_{rnaa}=0.00076$	$\alpha_{rnag} = 0.00051$		
$\alpha_{trans} = 0.098$	$\alpha_{uae} = 0.00000095$	$\alpha_{xe}=0.000013$		
$\alpha_{xd} = 0.010$			J	
$\alpha_{adek} = 3.48$	$\alpha_{adok} = 251.88$	$\alpha_{anuc} = 0.000011$	)	New
$\alpha_{guk} = 1.90$	$\alpha_{ndpk} = 0.21$	$\alpha_{phospho} = 7.84$	5	reactions

**Table C.6:** Rate constants for model version 2. Values were calculated using Equation 2.15, flux values from Table C.5, appropriate kinetic orders from Tables C.1 and C.2 and initial metabolite concentrations as detailed in Table 2.1.

# Appendix D

Contained in this appendix are five tables related to parameter simulations and values. The first two detail the effect of changing the kinetic orders for the reaction PHOSPHO, whilst the next two tables contain the steady state flux values from the Curto et al. (1998b) model and the adjustments made to ensure a zero net flux in the system. The last table shows the initial flux values for the new interconversion reactions.

$f_{phosphoADP}$	$f_{phosphoATP}$	PRPPS	IMP	S-AMP	SAM	Ade	XMP	dA pool	dG pool	RNA	DNA
0.30	-0.10	4.93	95.01	0.19	4.08	1.03	23.16	5.92	2.92	28,692.83	5,087.59
0.30	-0.11	4.93	94.94	0.19	4.08	1.03	23.20	5.92	2.93	28,681.02	5,089.85
0.30	-0.12	4.93	94.88	0.19	4.08	1.03	23.23	5.92	2.93	28,670.09	5,091.94
0.30	-0.13	4.93	94.82	0.19	4.07	1.02	23.26	5.93	2.93	28,659.95	5,093.88
0.30	-0.14	4.93	94.77	0.19	4.07	1.02	23.28	5.93	2.93	28,650.52	5,095.68
0.30	-0.15	4.93	94.72	0.19	4.07	1.02	23.31	5.93	2.93	28,641.73	5,097.37
0.30	-0.16	4.93	94.67	0.19	4.07	1.02	23.33	5.93	2.94	28,633.51	5,098.94
0.35	-0.10	4.94	95.16	0.20	4.09	1.03	23.09	5.91	2.92	28,719.15	5,082.57
0.35	-0.11	4.94	95.09	0.20	4.09	1.03	23.12	5.91	2.92	28,706.63	5,084.96
0.35	-0.12	4.93	95.02	0.19	4.08	1.03	23.16	5.92	2.92	28,695.03	5,087.17
0.35	-0.13	4.93	94.96	0.19	4.08	1.03	23.19	5.92	2.93	28,684.25	5,089.23
0.35	-0.14	4.93	94.91	0.19	4.08	1.03	23.22	5.92	2.93	28,674.20	5,091.15
0.35	-0.15	4.93	94.85	0.19	4.07	1.02	23.24	5.93	2.93	28,664.82	5,092.95
0.35	-0.16	4.93	94.80	0.19	4.07	1.02	23.27	5.93	2.93	28,656.04	5,094.63
0.40	-0.10	4.94	95.31	0.20	4.10	1.04	23.02	5.91	2.92	28,744.13	5,077.81
0.40	-0.11	4.94	95.23	0.20	4.09	1.03	23.06	5.91	2.92	28,731.00	5,080.31
0.40	-0.12	4.94	95.16	0.20	4.09	1.03	23.09	5.91	2.92	28,718.80	5,082.64
0.40	-0.13	4.94	95.10	0.20	4.09	1.03	23.12	5.91	2.92	28,707.44	5,084.80
0.40	-0.14	4.93	95.04	0.19	4.08	1.03	23.15	5.92	2.92	28,696.84	5,086.82
0.40	-0.15	4.93	94.98	0.19	4.08	1.03	23.18	5.92	2.93	28,686.93	5,088.72
0.40	-0.16	4.93	94.92	0.19	4.08	1.03	23.21	5.92	2.93	28,677.63	5,090.49
0.45	-0.10	4.94	95.44	0.20	4.10	1.04	22.95	5.90	2.91	28,767.88	5,073.29
0.45	-0.11	4.94	95.36	0.20	4.10	1.04	22.99	5.90	2.91	28,754.19	5,075.90
0.45	-0.12	4.94	95.29	0.20	4.10	1.04	23.03	5.91	2.92	28,741.47	5,078.32
0.45	-0.13	4.94	95.22	0.20	4.09	1.03	23.06	5.91	2.92	28,729.60	5,080.58
0.45	-0.14	4.94	95.16	0.20	4.09	1.03	23.09	5.91	2.92	28,718.50	5,082.69
0.45	-0.15	4.94	95.10	0.20	4.09	1.03	23.12	5.91	2.92	28,708.11	5,084.67
0.45	-0.16	4.93	95.04	0.19	4.08	1.03	23.15	5.92	2.92	28,698.35	5,086.54
0.50	-0.10	4.94	95.57	0.20	4.11	1.04	22.89	5.89	2.91	28,790.47	5,069.01
0.50	-0.11	4.94	95.49	0.20	4.10	1.04	22.93	5.90	2.91	28,776.31	5,071.69
0.50	-0.12	4.94	95.42	0.20	4.10	1.04	22.97	5.90	2.91	28,763.11	5,074.20
0.50	-0.13	4.94	95.34	0.20	4.10	1.04	23.00	5.90	2.91	28,750.79	5,076.54
0.50	-0.14	4.94	95.28	0.20	4.09	1.04	23.03	5.91	2.92	28,739.25	5,078.74
0.50	-0.15	4.94	95.22	0.20	4.09	1.03	23.06	5.91	2.92	28,728.43	5,080.80
0.50	-0.16	4.94	95.16	0.20	4.09	1.03	23.09	5.91	2.92	28,718.26	5,082.74
0.55	-0.10	4.95	95.70	0.20	4.11	1.05	22.83	5.89	2.90	28,811.99	5,064.93
0.55	-0.11	4.94	95.61	0.20	4.11	1.04	22.87	5.89	2.91	28,797.41	5,067.69
0.55	-0.12	4.94	95.53	0.20	4.11	1.04	22.91	5.90	2.91	28,783.80	5,070.27
0.55	-0.13	4.94	95.46	0.20	4.10	1.04	22.95	5.90	2.91	28,771.07	5,072.69
0.55	-0.14	4.94	95.39	0.20	4.10	1.04	22.98	5.90	2.91	28,759.14	5,074.95
0.55	-0.15	4.94	95.33	0.20	4.10	1.04	23.01	5.90	2.92	28,747.93	5,077.09
0.55	-0.16	4.94	95.27	0.20	4.09	1.04	23.04	5.91	2.92	28,737.38	5,079.09
0.60	-0.10	4.95	95.81	0.20	4.12	1.05	22.78	5.88	2.90	28,832.52	5,061.04
0.60	-0.11	4.95	95.73	0.20	4.12	1.05	22.82	5.89	2.90	28,817.57	5,063.87
0.60	-0.12	4.94	95.65	0.20	4.11	1.05	22.86	5.89	2.91	28,803.60	5,066.52
0.60	-0.13	4.94	95.57	0.20	4.11	1.04	22.89	5.89	2.91	28,790.51	5,069.00
0.60	-0.14	4.94	95.50	0.20	4.11	1.04	22.93	5.90	2.91	28,778.23	5,071.33
0.60	-0.15	4.94	95.44	0.20	4.10	1.04	22.96	5.90	2.91	28,766.67	5,073.52
0.60	-0.16	4.94	95.37	0.20	4.10	1.04	22.99	5.90	2.91	28,755.78	5,075.59

**Table D.1:** Effect of changing PHOSPHO kinetic orders 1. Simulations were performed with slight changes to the kinetic order parameters  $f_{phospho4D}$  and  $f_{phospho4T}$  for the reaction PHOSPHO. Metabolite steady state values, in  $\mu$ M, for each of these simulations is shown. dA pool represents the pooled metabolites dAdo, dAMP, dADP and dATP, whilst dG pool refers to the group consisting of dGMP, dGDP and dGTP.

$f_{phosphoADP}$	$f_{phosphoATP}$	HX pool	Xa	Guo pool	UA	Ado	AMP	ADP	ATP	GMP	GDP	GTP
0.30	-0.10	9.68	4.84	4.86	99.21	0.53	199.09	417.70	2,096.67	24.66	65.87	296.14
0.30	-0.11	9.67	4.84	4.86	99.19	0.53	198.92	417.92	2,088.67	24.66	66.13	295.64
0.30	-0.12	9.66	4.84	4.86	99.18	0.53	198.77	418.11	2,081.30	24.65	66.37	295.17
0.30	-0.13	9.65	4.83	4.85	99.16	0.53	198.63	418.30	2,074.48	24.65	66.60	294.74
0.30	-0.14	9.64	4.83	4.85	99.15	0.53	198.50	418.47	2,068.15	24.65	66.81	294.34
0.30	-0.15	9.63	4.83	4.85	99.14	0.53	198.38	418.63	2,062.27	24.64	67.00	293.97
0.30	-0.16	9.62	4.83	4.85	99.13	0.53	198.26	418.78	2,056.78	24.64	67.19	293.62
0.35	-0.10	9.70	4.85	4.86	99.25	0.53	199.45	417.22	2,114.59	24.67	65.29	297.26
0.35	-0.11	9.69	4.85	4.86	99.23	0.53	199.28	417.45	2,106.05	24.67	65.56	296.73
0.35	-0.12	9.68	4.84	4.86	99.21	0.53	199.12	417.66	2,098.16	24.66	65.82	296.23
0.35	-0.13	9.67	4.84	4.86	99.20	0.53	198.97	417.86	2,090.85	24.66	66.06	295.77
0.35	-0.14	9.66	4.84	4.86	99.18	0.53	198.83	418.04	2,084.07	24.66	66.28	295.35
0.35	-0.15	9.65	4.84	4.85	99.17	0.53	198.70	418.21	2,077.75	24.65	66.49	294.95
0.35	-0.16	9.64	4.83	4.85	99.16	0.53	198.57	418.37	2,071.85	24.65	66.68	294.58
0.40	-0.10	9.72	4.86	4.86	99.28	0.53	199.80	416.77	2,131.72	24.68	64.75	298.33
0.40	-0.11	9.71	4.85	4.86	99.27	0.53	199.62	417.01	2,122.69	24.67	65.03	297.77
0.40	-0.12	9.70	4.85	4.86	99.25	0.53	199.45	417.23	2,114.34	24.67	65.30	297.25
0.40	-0.13	9.69	4.85	4.86	99.23	0.53	199.29	417.44	2,106.60	24.67	65.55	296.76
0.40	-0.14	9.68	4.84	4.86	99.22	0.53	199.14	417.63	2,099.39	24.66	65.78	296.31
0.40	-0.15	9.67	4.84	4.86	99.20	0.53	199.00	417.81	2,092.67	24.66	66.00	295.89
0.40	-0.16	9.66	4.84	4.86	99.19	0.53	198.88	417.98	2,086.38	24.66	66.20	295.49
0.45	-0.10	9.74	4.86	4.86	99.32	0.53	200.14	416.34	2,148.12	24.69	64.24	299.34
0.45	-0.11	9.73	4.86	4.86	99.30	0.53	199.94	416.59	2,138.65	24.68	64.53	298.76
0.45	-0.12	9.72	4.86	4.86	99.28	0.53	199.77	416.82	2,129.88	24.68	64.80	298.21
0.45	-0.13	9.71	4.85	4.86	99.26	0.53	199.60	417.03	2,121.73	24.67	65.06	297.71
0.45	-0.14	9.70	4.85	4.86	99.25	0.53	199.45	417.23	2,114.14	24.67	65.30	297.23
0.45	-0.15	9.69	4.85	4.86	99.23	0.53	199.30	417.42	2,107.05	24.67	65.53	296.79
0.45	-0.16	9.68	4.84	4.86	99.22	0.53	199.16	417.60	2,100.42	24.66	65.75	296.37
0.50	-0.10	9.76	4.87	4.86	99.35	0.53	200.45	415.93	2,163.83	24.69	63.75	300.32
0.50	-0.11	9.75	4.87	4.86	99.33	0.53	200.25	416.19	2,153.97	24.69	64.06	299.71
0.50	-0.12	9.74	4.86	4.86	99.31	0.53	200.07	416.43	2,144.82	24.68	64.34	299.14
0.50	-0.13	9.73	4.86	4.86	99.29	0.53	199.90	416.65	2,136.30	24.68	64.60	298.61
0.50	-0.14	9.72	4.86	4.86	99.28	0.53	199.74	416.86	2,128.36	24.68	64.85	298.12
0.50	-0.15	9.71	4.85	4.86	99.26	0.53	199.58	417.05	2,120.93	24.67	65.09	297.66
0.50	-0.16	9.70	4.85	4.86	99.25	0.53	199.44	417.24	2,113.97	24.67	65.31	297.22
0.55	-0.10	9.78	4.88	4.86	99.38	0.53	200.75	415.54	2,178.89	24.70	63.30	301.24
0.55	-0.11	9.77	4.87	4.86	99.36	0.53	200.75	415.80	2,168.68	24.69	63.61	300.61
0.55	-0.11	9.76	4.87	4.86	99.34	0.53	200.36	416.05	2,159.18	24.69	63.90	300.01
0.55	-0.12	9.75	4.87	4.86	99.32	0.53	200.30	416.28	2,150.34	24.69	64.17	299.48
0.55	-0.13	9.73	4.86	4.86	99.32	0.53	200.18	416.50	2,130.34	24.68	64.42	298.97
0.55	-0.14	9.74	4.86	4.86	99.31	0.53	199.86	416.70	2,134.34	24.68	64.66	298.49
0.55	-0.16	9.73	4.86	4.86	99.29	0.53	199.71	416.70	2,127.08	24.68	64.89	298.49
0.60	-0.10 -0.10	9.72	4.88	4.86	99.27	0.53	201.04	415.17	2,127.08	24.08	62.87	302.13
0.60	-0.10 -0.11	9.80	4.88	4.86	99.41	0.53	201.04	415.17	2,193.35	24.71	63.18	302.13
0.60	-0.11 -0.12	9.79 9.78	4.88	4.86	99.39	0.53	200.83	415.44	2,182.81	24.70	63.47	301.48
	-0.12 -0.13											
0.60		9.76	4.87	4.86	99.35	0.53	200.45 200.28	415.93	2,163.86	24.69 24.69	63.75	300.32 299.79
0.60	-0.14	9.75	4.87	4.86	99.33	0.53		416.15	2,155.30		64.01	
0.60	-0.15	9.74	4.86	4.86	99.32	0.53	200.12	416.36	2,147.28	24.68	64.26	299.29
0.60	-0.16	9.73	4.86	4.86	99.30	0.53	199.97	416.56	2,139.75	24.68	64.50	298.83

**Table D.2:** Effect of changing PHOSPHO kinetic orders 2. Simulations were performed with slight changes to the kinetic order parameters  $f_{phospho4D}$  and  $f_{phospho4T}$  for the reaction PHOSPHO. Metabolite steady state values, in  $\mu$ M, for each of these simulations is shown. HX pool represents the pooled metabolites HX, Ino and dIno, whilst Guo pool refers to the group consisting of Gua, Guo and dGuo.

$v_{ada}=2.079$	$v_{ade}=0.0099$	$v_{adna} = 10.04$	$v_{adrnr} = 0.2$
$v_{ampd} = 5.64$	$v_{aprt} = 1.0$	$v_{arna}=1985.63$	$v_{asli} = 8.0$
$v_{asuc} = 8.0$	$v_{dada} = 0.2$	$v_{den}=2.4$	$v_{dgnuc} = 0.1$
$v_{dnaa} = 10.04$	$v_{dnag} = 6.83$	$v_{gdna} = 6.83$	$v_{gdrnr} = 0.1$
$v_{gmpr} = 0.51$	$v_{gmps} = 1.6$	$v_{gnuc} = 4.81$	$v_{gprt} = 3.75$
$v_{grna}=1323.54$	$v_{gua}=1.15$	$v_{hprt} = 3.68$	$v_{hxd} = 1.19$
$v_{hxe} = 0.047$	$v_{impdh} = 1.6$	$v_{inuc}=2.64$	$v_{mat} = 14.99$
$v_{polyam} = 1.0$	$v_{prpps} = 20.88$	$v_{pyr} = 10.04$	$v_{rnaa}=1985.56$
$v_{rnag} = 1323.61$	$v_{trans} = 13.98$	$v_{uae} = 2.31$	$v_{xe}=0.031$
$v_{xd} = 2.31$			

**Table D.3:** Steady state flux values from the Curto *et al.* (1998b) model. Values are in  $\mu$ mol min<sup>-1</sup> (Body weight)<sup>-1</sup>.

Flux	Value in Curto et al. (1998b) model	Adjusted value
$v_{ada}$	2.07949	2.08137
$v_{gnuc}$	4.80719	4.8053
$v_{gua}$	1.15436	1.15246
$v_{hxe}$	0.0473136	0.049198
$v_{xe}$	0.0307238	0.028825

**Table D.4:** Adjusted flux values from the Curto *et al.* (1998b) model. Listed are the steady state Curto *et al.* (1998b) model flux values and the adjusted values that ensure zero net flux in and out of the adenylate & adenosine and guanylate pools at steady state, as determined by solving the two sets of simultaneous equations as detailed in Table 3.6. Values are in  $\mu$ mol min<sup>-1</sup> (Body weight)<sup>-1</sup>.

$v_{adek} = 2023.3$	$v_{adok} = 12.075$	$v_{anuc}=0.18$
$v_{guk} = 1323.64$	$v_{ndpk} = 1331.54$	$v_{phospho} = 6713.65$

**Table D.5:** Unscaled initial flux values for the new reactions for the final model. Values were computed by solving the two sets of steady state equations for the adenylate & adenosine and guanylate pools, as detailed in Table 3.6. All values are in  $\mu$ mol min<sup>-1</sup> (Body weight)<sup>-1</sup>.

# Appendix E

This appendix contains two tables relating to model output and nine sensitivity analysis figures. The first table details the eigenvalues for the new model (version 3) along with those from the Curto et al. (1998b) model, whilst the second table shows the consistency in concentration of certain variables in the Curto et al. (1998b) model. The first five graphs show the parameter sensitivities for each flux in the system with respect to the kinetic orders, whilst the next three graphs show the equivalent sensitivities for each of the dependent variables in the network. Lastly, the final figure details the logarithmic gains for all the metabolites and fluxes in the system with respect to both independent variables.

Final mo	del (version 3)	Curto et al. (1998b) model
Real part	Imaginary part	Real part Imaginary part
-1.440E-06	0	-5.080E-02 0
-6.027E-06	-2.482E-06	-2.890E-03 0
-6.027E-06	2.482E-06	-1.380E-04 0
-2.037E-04	0	-1.240E-03 0
-5.382E-04	0	-1.62E-02 0
-5.470E-04	0	-4.950E-02 3.170E-04
-5.591E-04	0	-4.950E-02 -3.170E-04
-2.743E-03	0	-2.650E-01 0
-2.962E-03	0	-2.440E-01 0
-4.393E-03	0	-3.710E-01 0
-8.003E-03	0	-6.160E-01 0
-8.847E-03	0	-7.430E-01 0
-1.660E-02	0	-1.491E+00 0
-3.167E-02	0	-5.533E+00 0
-3.928E-02	0	-3.630E+00 0
-6.129E-02	-2.476E-03	-3.960E+01 0
-6.129E-02	2.476E-03	
-1.029E-01	0	
-1.554E-01	0	
-2.534E-01	0	
-4.358E-01	0	

**Table E.1:** Model eigenvalues. Eigenvalues for the new model were calculated using COPASI (Hoops *et al.*, 2006), whilst those from the Curto *et al.* (1998b) model were detailed in Curto *et al.* (1997).

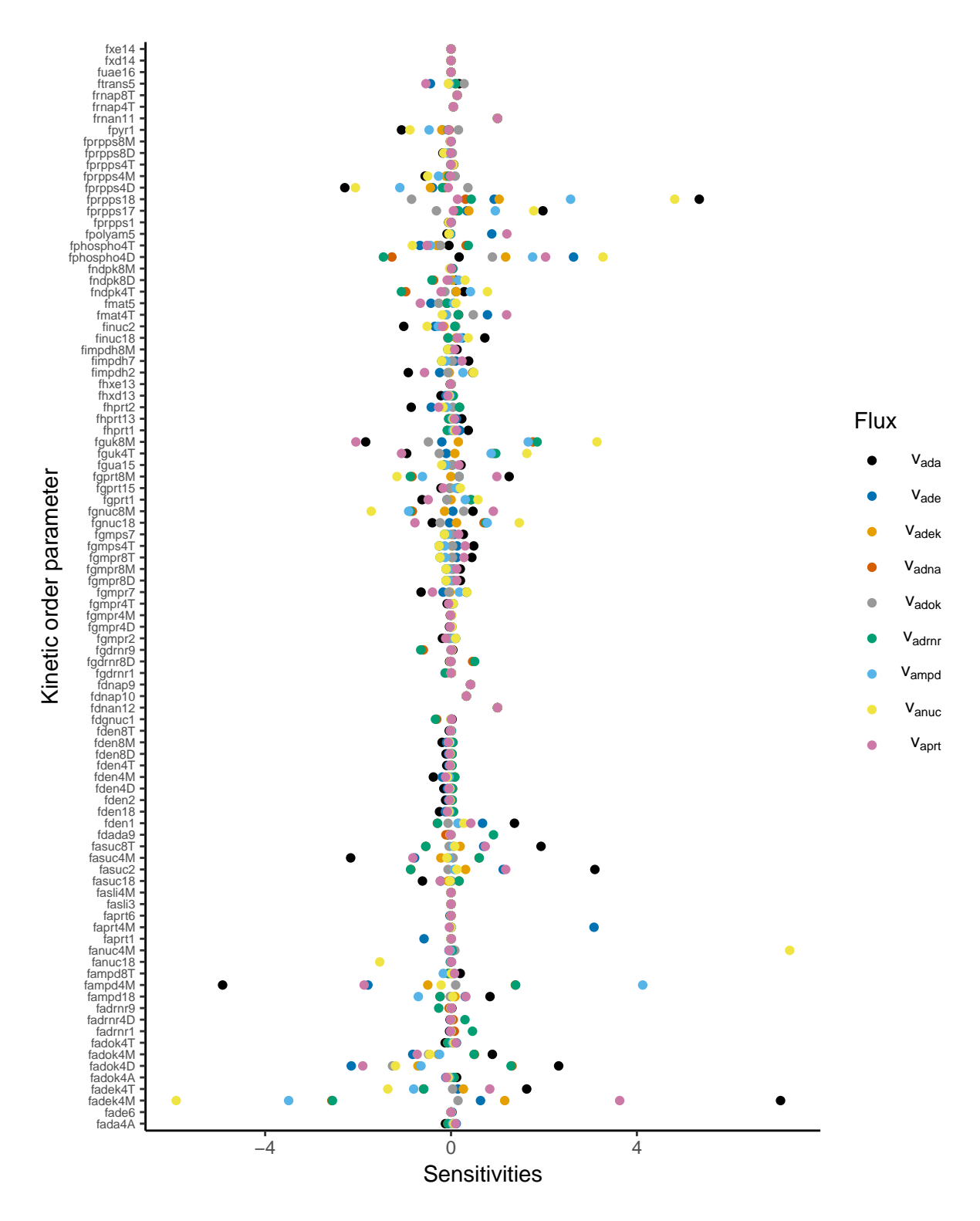


**Figure E.1:** Parameter sensitivities for fluxes 1. Sensitivities were calculated for all fluxes with respect to all kinetic order parameters.

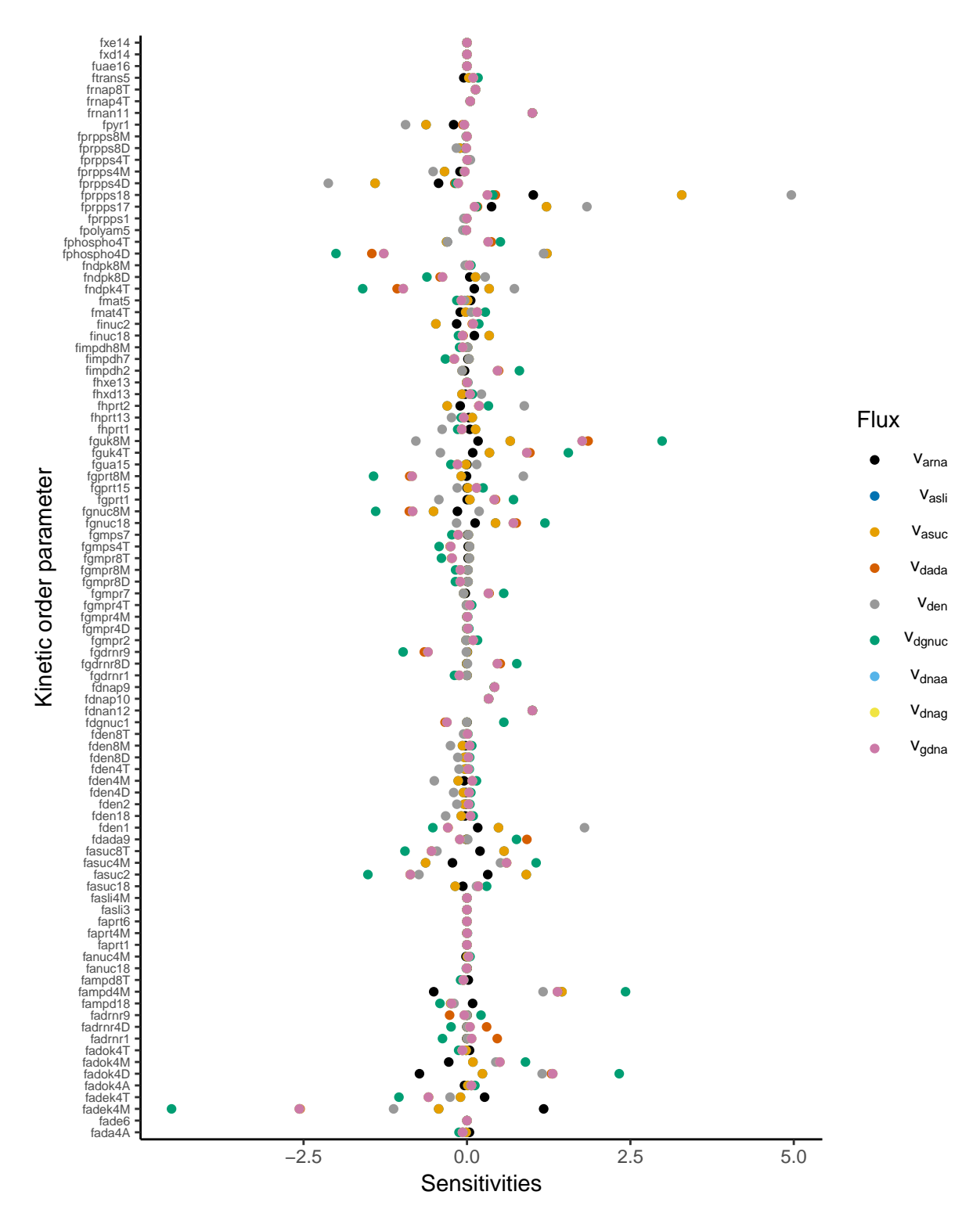


**Figure E.2:** Parameter sensitivities for fluxes 2. Sensitivities were calculated for all fluxes with respect to all kinetic order parameters.

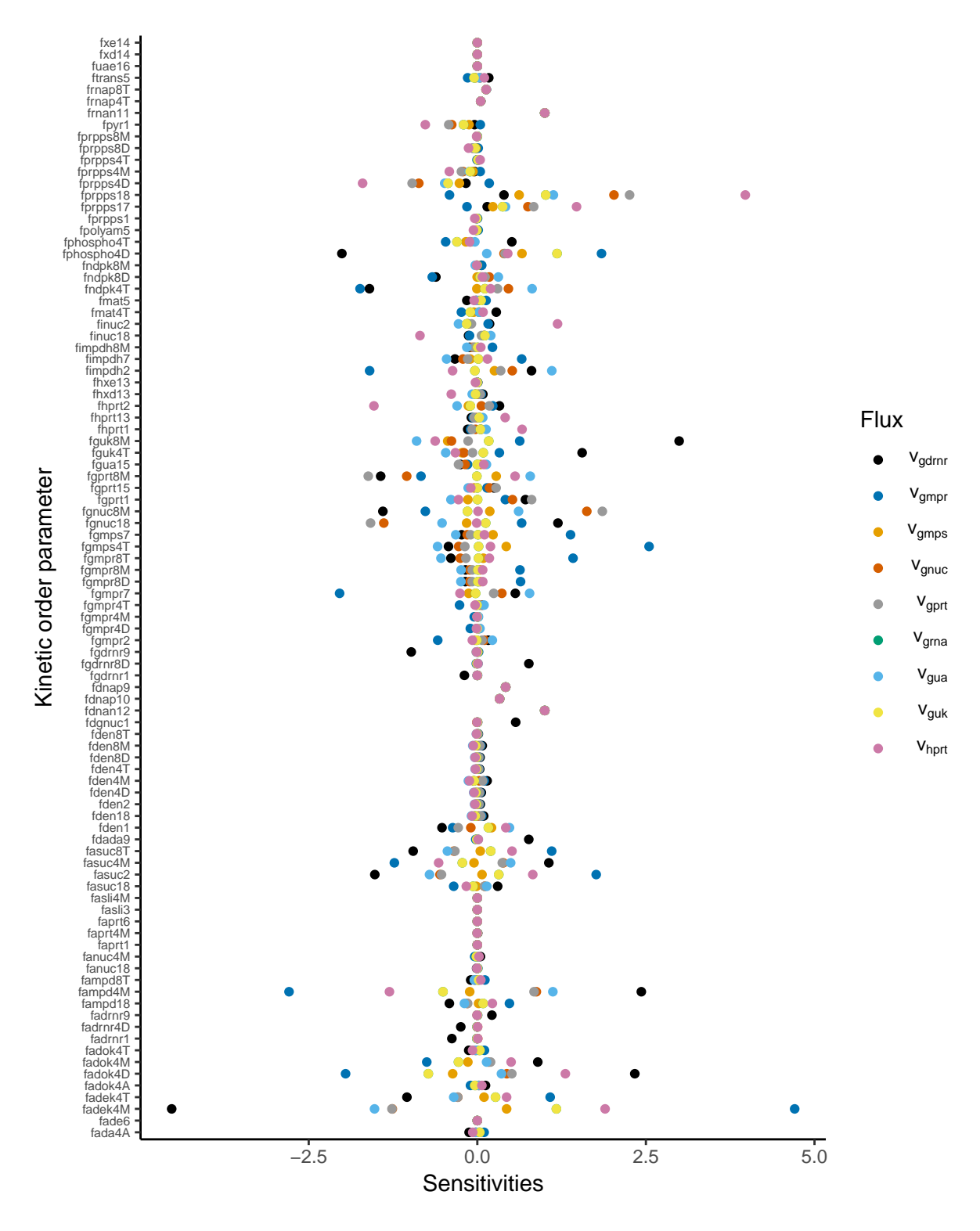


**Figure E.3:** Parameter sensitivities for fluxes 3. Sensitivities were calculated for all fluxes with respect to all kinetic order parameters.

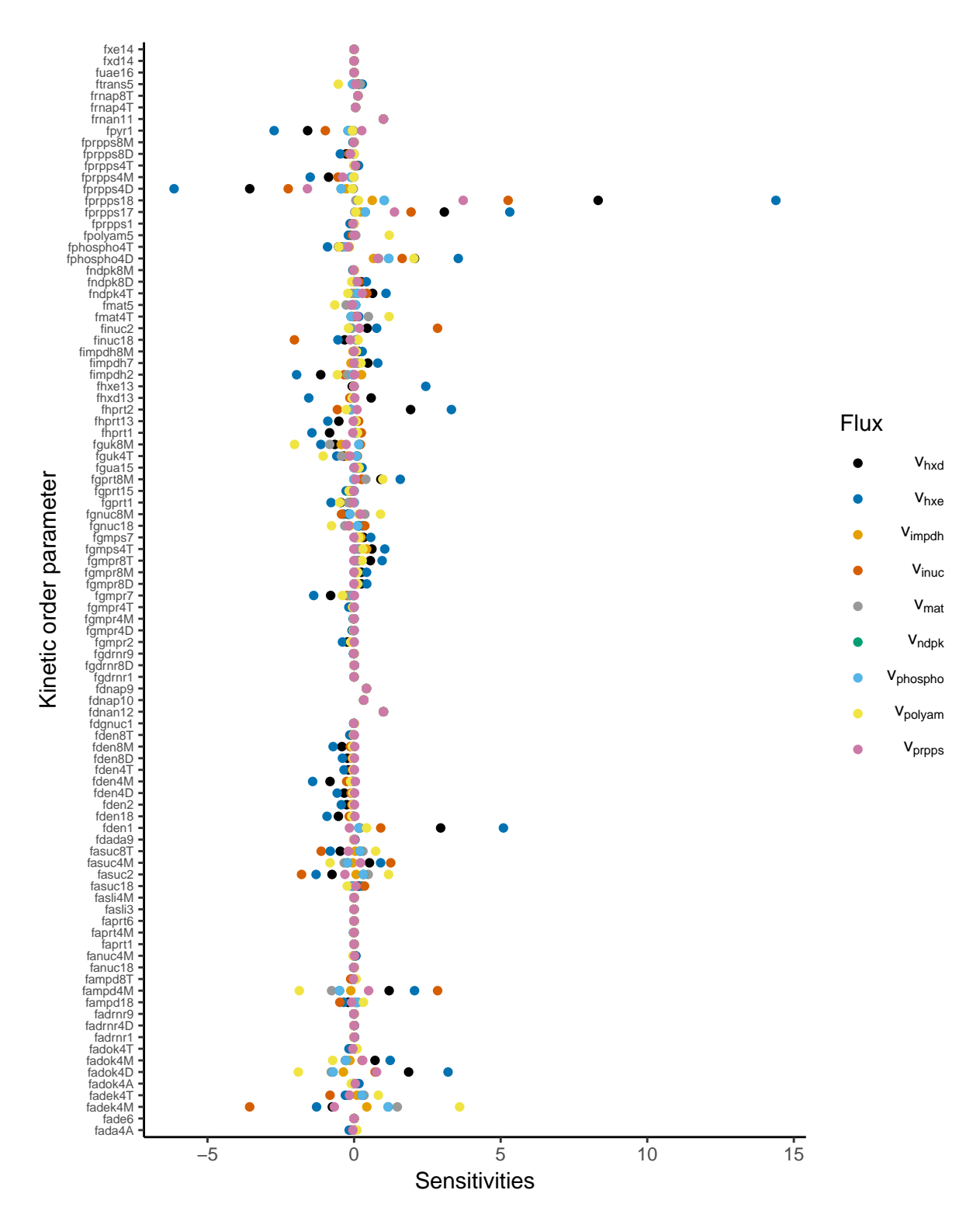


**Figure E.4:** Parameter sensitivities for fluxes 4. Sensitivities were calculated for all fluxes with respect to all kinetic order parameters.

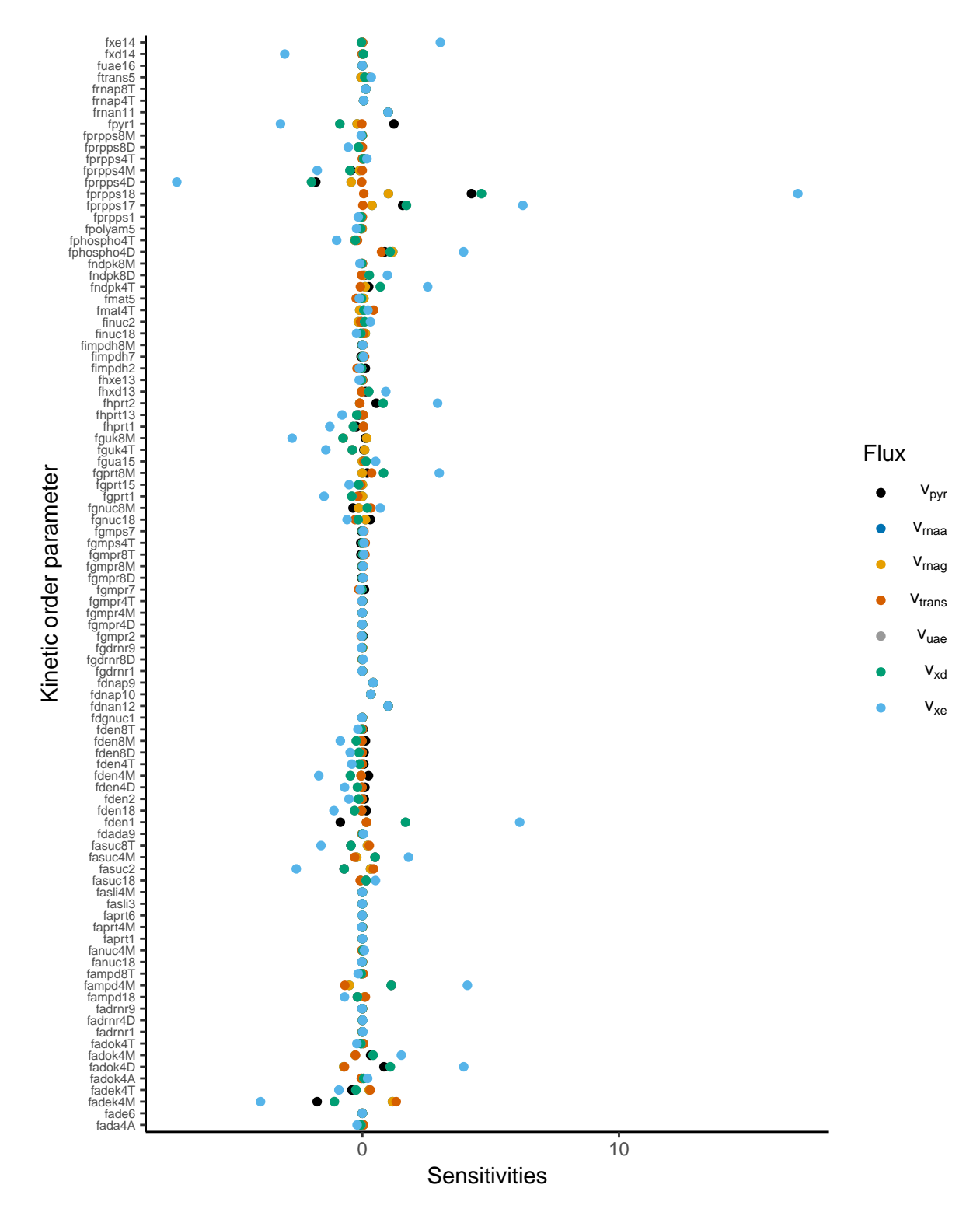


**Figure E.5:** Parameter sensitivities for fluxes 5. Sensitivities were calculated for all fluxes with respect to all kinetic order parameters.

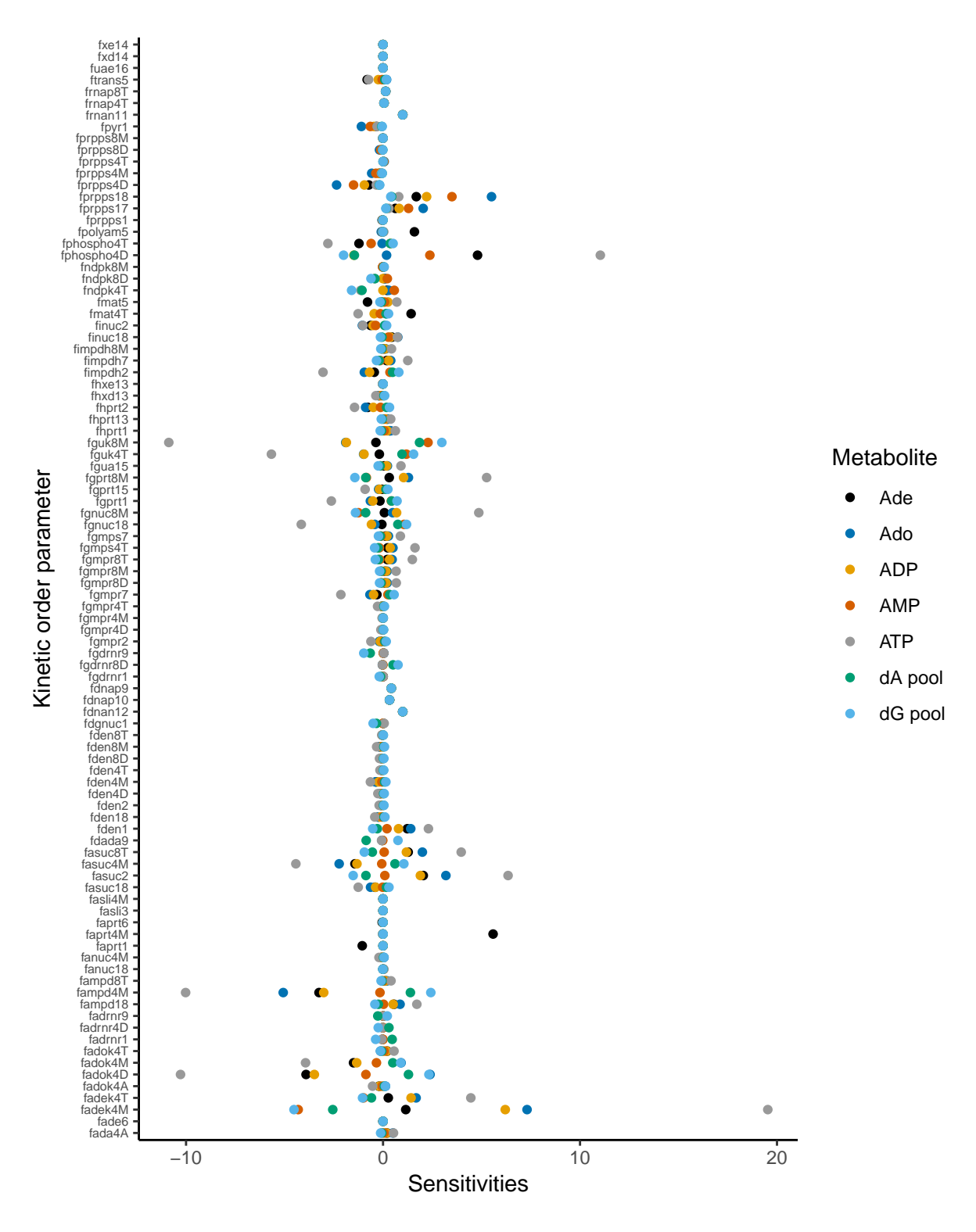


**Figure E.6:** Parameter sensitivities for metabolites 1. Sensitivities were calculated for all metabolites with respect to all kinetic order parameters. dA pool represents the pooled metabolites dAdo, dAMP, dADP and dATP, whilst dG pool refers to the group consisting of dGMP, dGDP and dGTP.

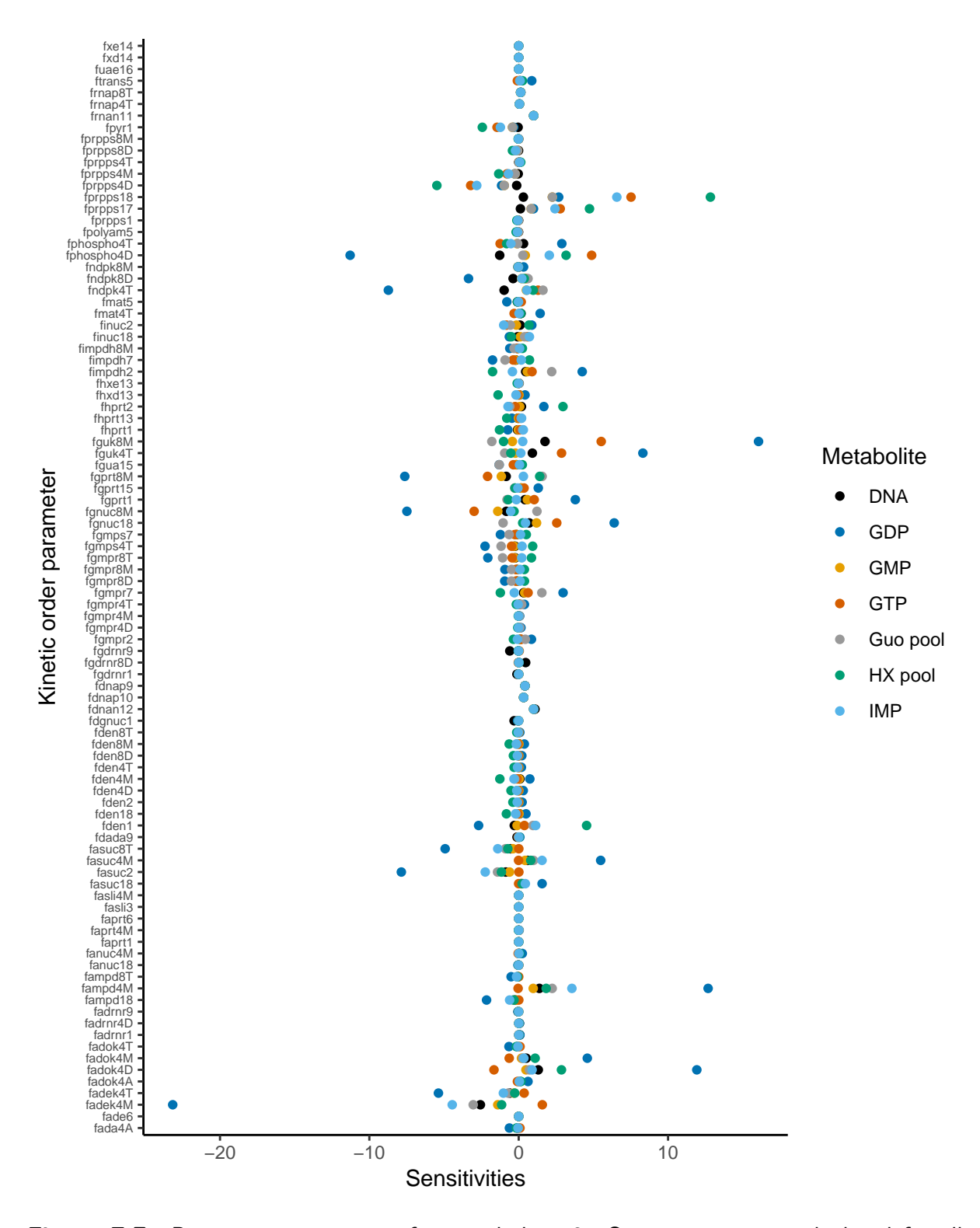


**Figure E.7:** Parameter sensitivities for metabolites 2. Sensitivities were calculated for all metabolites with respect to all kinetic order parameters. Guo pool represents the pooled metabolites Gua, Guo and dGuo, whilst HX pool refers to the group consisting of HX, Ino and dIno.

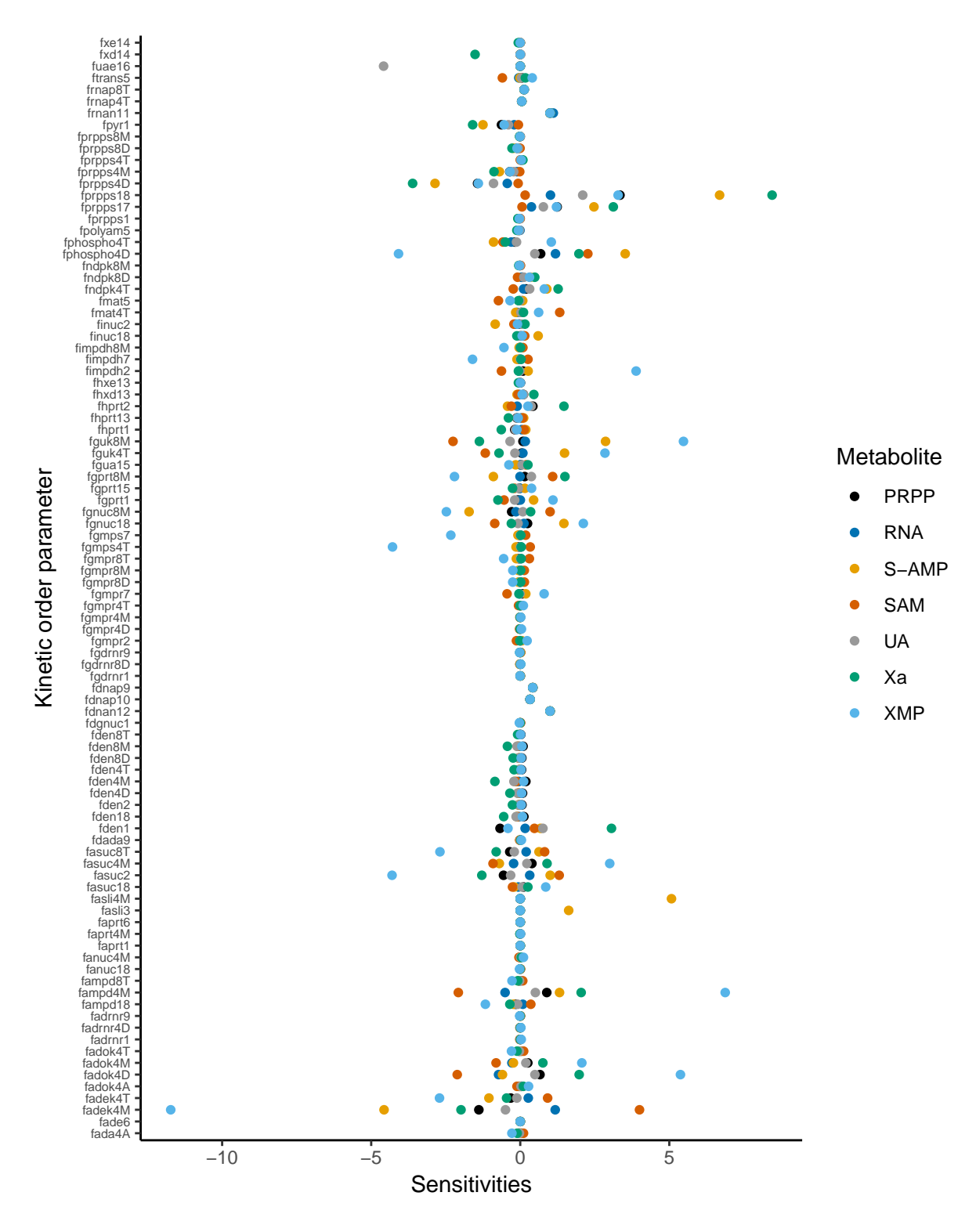


**Figure E.8:** Parameter sensitivities for metabolites 3. Sensitivities were calculated for all metabolites with respect to all kinetic order parameters.

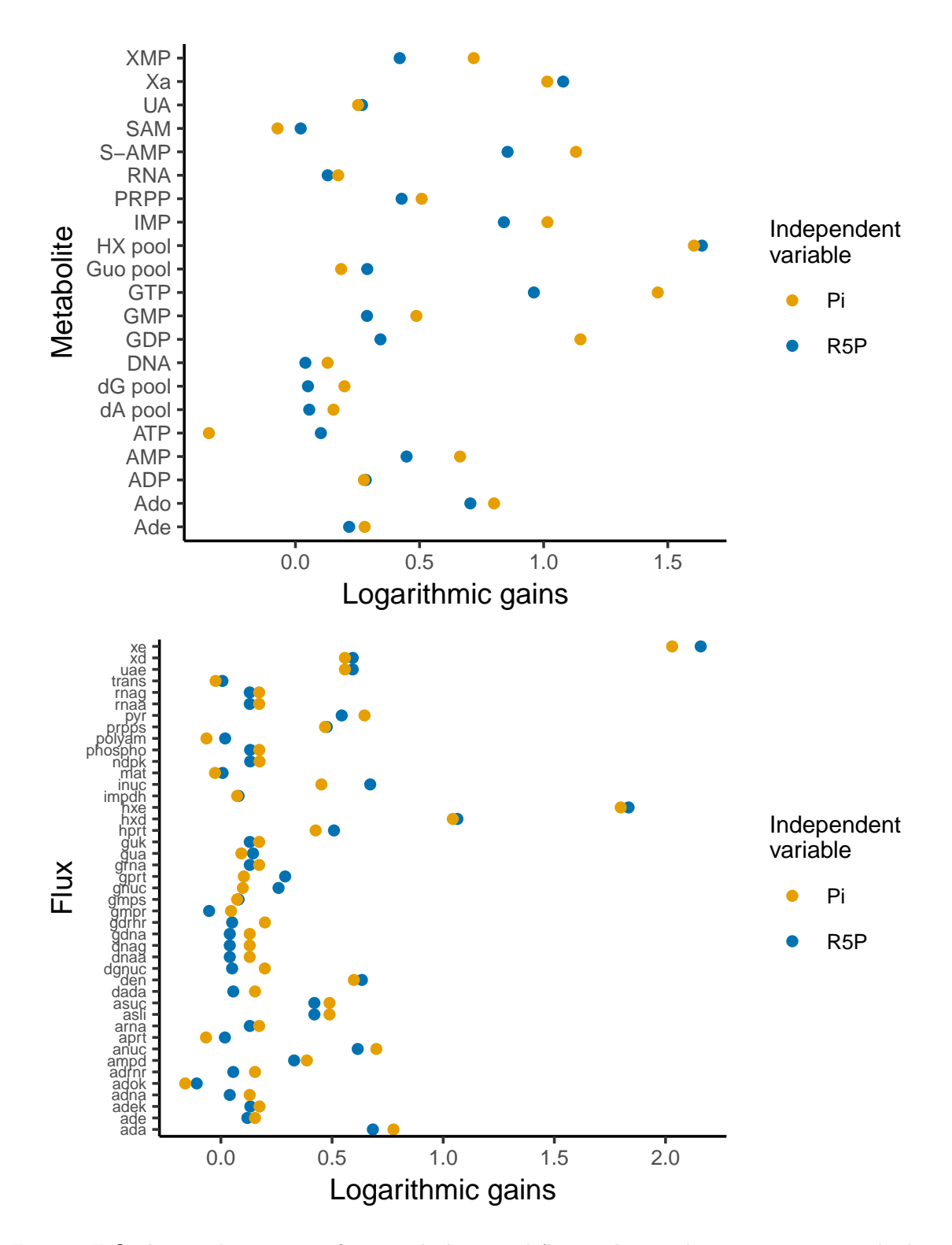


**Figure E.9:** Logarithmic gains for metabolites and fluxes. Logarithmic gains were calculated for all metabolites (top panel) and fluxes (bottom panel) with respect to all independent variables. HX pool equates to the collective species HX, Ino and dIno, whilst Guo pool refers to the group consisting of Gua, Guo and dGuo. dG pool indicates the grouping: dGMP, dGDP and dGTP, whilst dA pool represents the pooled metabolites dAdo, dAMP, dADP and dATP.

Variable	Metabolite	Normal	Externally set	Transitional extreme	Transitional extreme
name		concentration	concentration	value of adenylates	value of guanylates
		(μM)	(μM)	(X4) (μM)	(X8) (µM)
$X_1$	PRPP	5	105	2504 (max)	405 (max)
$X_2$	IMP	100	200	2536 (max)	401 (max)
$X_2$	IMP	100	1	2454 (min)	400
$X_3$	S-AMP	0.2	100.2	2595 (max)	397 (min)
$X_5$	SAM	4	104	2589 (max)	401 (max)
$X_6$	Ade	1	101	2591 (max)	394 (min)
$X_7$	XMP	25	125	2416 (min)	425 (max)
$X_9$	dA pool	6	106	2524 (max)	399 (min)
$X_{10}$	dG pool	3	103	2402 (min)	410 (max)
$X_{11}$	RNA	28600	28700	2514 (max)	409 (max)
$X_{11}$	RNA	28600	28500	2478 (min)	393 (min)
$X_{13}$	HX pool	10	110	2515 (max)	399 (min)
$X_{15}$	Guo pool	5	105	2432 (min)	417 (max)

**Table E.2:** Consistency of  $X_4$  and  $X_8$  metabolites in the Curto *et al.* (1998b) model. Initial concentrations of the dependent variables were increased or decreased (where appropriate) by 100  $\mu$ M and the largest deviation produced in these concentrations before the system returned to its steady state was recorded. Data is from Curto *et al.* (1997). dA pool represents the pooled metabolites dAdo, dAMP, dADP and dATP, whilst dG pool indicates the grouping: dGMP, dGDP and dGTP. HX pool equates to the collective species HX, Ino and dIno, whilst Guo pool refers to the group consisting of Gua, Guo and dGuo.

# Appendix F

Contained in this appendix are two tables that detail parameter sets that produced acceptable metabolite concentrations in the parameter search simulations.

		ion factors							lite concent			
(D)ADA	GMPR	I/A/GNUC	A/GDRNR	MAT	TRANS	AMPD	ASLI	PRPP	IMP	ADP	ATP	GTP
0.333	3.0	2.0	1.5	2.0	0.5	1.5	0.333	4.640	87.617	263.769	1,534.740	75.798
0.333	3.0	2.0	1.5	2.0	0.5	1.5	0.5	4.640	87.617	263.769	1,534.732	75.798
0.333	3.0	2.0	1.5	2.0	0.5	1.5	8.0	4.640	87.617	263.769	1,534.739	75.798
0.333	3.0	2.0	1.5	2.0	0.5	1.5	1.5	4.640	87.617	263.769	1,534.729	75.798
0.333	3.0	2.0	1.5	2.0	0.5	1.5	2.0	4.640	87.617	263.769	1,534.741	75.798
0.333	3.0	2.0	1.5	2.0	0.5	1.5	3.0	4.640	87.617	263.769	1,534.739	75.798
0.333	3.0	2.0	3.0	1.5	0.333	1.5	0.333	4.630	87.293	265.311	1,585.201	75.743
0.333	3.0	2.0	3.0	1.5	0.333	1.5	0.5	4.630	87.293	265.311	1,585.209	75.743
0.333	3.0	2.0	3.0	1.5	0.333	1.5	0.8	4.630	87.293	265.311	1,585.201	75.743
0.333	3.0	2.0	3.0	1.5	0.333	1.5	1.5	4.630	87.293	265.311	1,585.201	75.743
0.333	3.0	2.0	3.0	1.5	0.333	1.5	2.0	4.630	87.293	265.311	1,585.213	75.743
0.333	3.0	2.0	3.0	1.5	0.333	1.5	3.0	4.630	87.293	265.311	1,585.208	75.743
0.5	3.0	2.0	0.333	2.0	0.5	1.5	0.333	4.614	87.199	270.042	1,659.730	75.853
0.5	3.0	2.0	0.333	2.0	0.5	1.5	0.5	4.614	87.199	270.042	1,659.731	75.853
0.5	3.0	2.0	0.333	2.0	0.5	1.5	0.8	4.614	87.199	270.042	1,659.731	75.853
0.5	3.0	2.0	0.333	2.0	0.5	1.5	1.5	4.614	87.199	270.042	1,659.730	75.853
0.5	3.0	2.0	0.333	2.0	0.5	1.5	2.0	4.614	87.199	270.042	1,659.730	75.853
0.5	3.0	2.0	0.333	2.0	0.5	1.5	3.0	4.614	87.199	270.042	1,659.729	75.853
0.5	3.0	2.0	0.55	2.0	0.5	1.5	0.333	4.633	87.491	265.266	1,565.595	75.726
0.5	3.0	2.0	0.5	2.0	0.5	1.5	0.55	4.633	87.491	265.266	1,565.596	75.720
0.5	3.0	2.0	0.5	2.0	0.5	1.5	0.8	4.633	87.491	265.266		75.720
											1,565.594	
0.5	3.0	2.0	0.5	2.0	0.5	1.5	1.5	4.633	87.491	265.266	1,565.594	75.720
0.5	3.0	2.0	0.5	2.0	0.5	1.5	2.0	4.633	87.491	265.266	1,565.595	75.726
0.5	3.0	2.0	0.5	2.0	0.5	1.5	3.0	4.633	87.491	265.266	1,565.595	75.72
0.5	3.0	2.0	0.8	2.0	0.5	1.5	0.333	4.665	87.992	257.335	1,417.745	75.50
0.5	3.0	2.0	8.0	2.0	0.5	1.5	0.5	4.665	87.992	257.335	1,417.739	75.50
0.5	3.0	2.0	8.0	2.0	0.5	1.5	8.0	4.665	87.992	257.335	1,417.740	75.50
0.5	3.0	2.0	8.0	2.0	0.5	1.5	1.5	4.665	87.992	257.335	1,417.743	75.50
0.5	3.0	2.0	8.0	2.0	0.5	1.5	2.0	4.665	87.992	257.335	1,417.732	75.50
0.5	3.0	2.0	8.0	2.0	0.5	1.5	3.0	4.665	87.992	257.335	1,417.740	75.50
0.5	3.0	2.0	1.5	1.5	0.5	1.5	0.333	4.757	91.091	259.918	1,415.972	79.08
0.5	3.0	2.0	1.5	1.5	0.5	1.5	0.5	4.757	91.091	259.918	1,415.972	79.08
0.5	3.0	2.0	1.5	1.5	0.5	1.5	8.0	4.757	91.091	259.918	1,415.977	79.08
0.5	3.0	2.0	1.5	1.5	0.5	1.5	1.5	4.757	91.091	259.918	1,415.980	79.08
0.5	3.0	2.0	1.5	1.5	0.5	1.5	2.0	4.757	91.091	259.918	1,415.981	79.08
0.5	3.0	2.0	1.5	1.5	0.5	1.5	3.0	4.757	91.091	259.918	1,415.977	79.08
0.5	3.0	2.0	2.0	1.5	0.333	1.5	0.333	4.630	87.258	265.213	1,585.545	75.61
0.5	3.0	2.0	2.0	1.5	0.333	1.5	0.5	4.630	87.258	265.212	1,585.551	75.61
0.5	3.0	2.0	2.0	1.5	0.333	1.5	0.8	4.630	87.258	265.212	1,585.556	75.61
0.5	3.0	2.0	2.0	1.5	0.333	1.5	1.5	4.630	87.258	265.212	1,585.562	75.61
0.5	3.0	2.0	2.0	1.5	0.333	1.5	2.0	4.630	87.258	265.212	1,585.549	75.61
0.5	3.0	2.0	2.0	1.5	0.333	1.5	3.0	4.630	87.258	265.212	1,585.564	75.61
0.8	3.0	2.0	0.333	1.5	0.5	1.5	0.333	4.740	90.803	264.221	1,496.044	79.10
0.8	3.0	2.0	0.333	1.5	0.5	1.5	0.5	4.740	90.803	264.221	1,496.045	79.10
0.8	3.0	2.0	0.333	1.5	0.5	1.5	0.8	4.740	90.803	264.221	1,496.045	79.10
0.8	3.0	2.0	0.333	1.5	0.5	1.5	1.5	4.740	90.803	264.221	1,496.046	79.10
0.8	3.0	2.0	0.333	1.5	0.5	1.5	2.0	4.740	90.803	264.221	1,496.046	79.10
0.8	3.0	2.0	0.333	1.5	0.5	1.5	3.0	4.740	90.803	264.221	1,496.045	79.10
	3.0	2.0	0.333		0.5	1.5		4.740	90.803 87.509	258.912		75.02
1.5				1.5			0.333				1,473.071	
1.5	3.0	2.0	0.333	1.5	0.333	1.5	0.5	4.652	87.509	258.912	1,473.071	75.02
1.5	3.0	2.0	0.333	1.5	0.333	1.5	0.8	4.652	87.509	258.912	1,473.071	75.02
1.5	3.0	2.0	0.333	1.5	0.333	1.5	1.5	4.652	87.509	258.912	1,473.071	75.02
1.5	3.0	2.0	0.333	1.5	0.333	1.5	2.0	4.652	87.509	258.912	1,473.071	75.02
1.5	3.0	2.0	0.333	1.5	0.333	1.5	3.0	4.652	87.509	258.912	1,473.071	75.02

**Table F.1:** Parameter grid search results. Simulations were conducted whereby the rate constants for specific reactions were multiplied by multiplication factors and the resulting concentrations of specific metabolites were examined. The parameter sets shown are those that produce metabolite concentrations that lie within predefined ranges as detailed in Table 3.14. Parameter multiplication factors for the respective rate constants are shown along with the relevant resultant metabolite concentrations, in  $\mu M$ .

-	
$\alpha$	
$\overline{}$	-

Parameter	multiplicat	ion factors														Metabo	lite concenti	rations		
(D)ADA	GMPR	I/A/GNUC	A/GDRNR	MAT	TRANS	AMPD	ASLI	PRPPS	DEN	ASUC	GMPS	H/GPRT	APRT	IMPDH	R5P	PRPP	IMP	ADP	ATP	GTP
Parameter	grid search	ı large-scale sim	ulation run 1																	
2.328	0.919	1.973	0.696	1.420	1.487	2.441	1.135	0.804	0.452	1.704	0.343	0.607	2.962	0.720	1.960	7.647	98.109	259.983	1587.868	64.547
2.679	2.913	2.466	0.417	1.301	1.977	0.624	2.172	0.894	0.456	0.952	0.513	0.954	0.570	0.720	1.850	7.329	99.097	245.400	1315.577	63.303
1.568	1.981	0.676	2.186	2.644	1.679	1.598	2.843	0.801	0.306	1.463	0.873	0.638	1.885	0.720	1.440	7.334	100.365	256.963	1336.293	74.719
0.813	2.272	1.870	2.933	2.398	1.539	2.001	2.401	0.750	0.335	1.307	0.600	0.629	1.107	0.720	1.858	7.500	91.076	236.140	1296.789	55.328
Parameter	grid search	ı large-scale sim	ulation run 2																	
0.402	1.310	1.872	2.090	0.710	2.382	1.506	0.384	0.816	0.508	0.903	0.749	0.447	1.698	0.955	1.667	7.557	104.825	259.136	1410.293	73.836
0.369	1.601	1.984	0.763	0.447	1.908	0.896	2.141	0.912	0.379	0.469	1.304	0.610	0.990	0.975	1.262	7.445	109.664	232.730	1247.919	57.536
Parameter	grid search	ı large-scale sim	ulation run 3																	
2.602	0.931	1.414	0.476	1.759	0.957	1.010	0.808	0.868	0.549	0.818	0.574	0.466	0.607	0.720	1.363	6.943	100.526	261.428	1517.520	72.130
2.405	0.504	2.863	0.934	2.030	0.804	0.952	1.852	1.066	0.511	0.779	0.776	0.842	2.589	0.720	1.431	6.944	91.314	265.882	1811.106	61.421
2.170	1.584	1.265	0.742	2.454	2.840	2.443	0.379	1.078	0.821	2.672	0.710	0.487	0.678	0.720	1.276	7.160	87.419	264.705	1539.762	66.627
2.692	0.970	2.182	0.463	0.960	0.436	0.713	0.813	1.042	0.346	0.463	0.671	0.690	0.868	0.720	1.238	7.349	90.219	269.510	1815.656	67.701
0.400	0.755	2.209	2.942	1.645	1.667	0.615	1.786	0.880	0.306	0.509	0.346	0.758	1.101	0.720	1.782	7.825	91.625	269.227	1551.474	75.838
1.796	1.753	1.474	1.422	0.692	1.746	1.419	2.981	0.916	0.321	0.976	0.650	0.441	2.131	0.720	1.254	7.906	90.590	244.699	1448.498	58.348
0.741	0.650	1.747	2.670	0.633	2.832	2.536	0.418	0.882	0.501	1.522	0.507	0.578	2.809	0.720	1.343	7.013	98.938	257.668	1430.181	70.555
1.794	0.512	1.514	2.491	2.855	2.168	1.839	1.804	0.948	0.836	1.862	0.506	0.454	2.029	0.720	1.530	7.197	99.164	257.297	1418.493	67.002
2.526	1.088	1.786	0.511	1.381	1.760	0.533	0.845	0.865	0.542	0.850	0.356	0.549	0.916	0.720	1.716	7.501	99.267	267.666	1739.216	65.137
2.053	0.919	1.970	0.980	2.146	2.331	0.778	2.898	0.995	0.743	1.283	0.703	0.555	2.234	0.720	1.611	7.489	103.410	261.954	1618.411	61.841
2.328	0.456	1.812	2.125	0.766	0.984	1.276	2.615	0.763	0.502	0.854	0.647	0.505	0.373	0.720	1.804	7.282	100.684	263.293	1662.029	67.429
0.857	0.944	1.559	2.044	1.371	1.399	0.879	0.753	0.750	0.477	0.639	0.595	0.466	0.306	0.720	1.663	7.137	100.480	261.369	1607.521	66.678
1.382	0.350	2.634	2.876	1.830	0.861	1.455	0.639	0.893	0.384	0.997	0.830	0.732	1.986	0.720	1.975	7.786	89.767	259.895	1507.294	69.336
0.939	0.362	2.417	2.518	0.312	0.996	1.863	2.719	0.934	0.303	0.998	0.310	0.751	2.640	0.720	1.500	7.762	93.291	255.832	1617.714	62.535
2.068	0.392	2.484	1.678	2.608	2.150	2.501	0.475	0.994	0.679	2.339	0.740	0.738	1.879	0.720	1.798	7.243	88.429	260.156	1477.886	65.802
1.614	0.307	2.811	0.417	1.195	2.443	0.927	0.379	1.165	0.648	0.998	0.996	0.773	0.634	0.720	1.337	7.278	101.930	258.379	1529.448	63.769
1.193	1.245	2.591	0.904	2.894	1.862	0.477	2.288	0.956	0.535	0.789	0.337	0.797	2.989	0.720	1.797	7.442	103.058	259.885	1663.115	58.167
1.649	1.491	1.830	1.779	1.033	1.275	2.503	2.137	0.782	0.397	1.461	0.392	0.505	0.683	0.720	1.756	7.611	95.086	259.746	1773.156	57.865
1.473	0.940	1.971	0.943	1.154	1.844	0.575	1.764	0.977	0.334	0.722	0.824	0.690	2.854	0.720	1.481	7.839	88.273	269.989	1629.361	72.871
2.784	0.992	2.975	0.752	0.430	1.857	0.990	0.301	1.167	0.362	0.793	0.503	0.864	0.654	0.720	1.283	7.827	91.656	244.335	1409.786	59.164
0.570	1.222	2.450	0.790	2.208	2.980	0.789	1.323	0.959	0.370	0.894	0.893	0.833	2.854	0.720	1.720	7.841	98.278	266.968	1785.779	57.794
1.234	0.639	2.182	1.329	1.718	2.350	1.404	2.009	0.933	0.541	1.219	0.718	0.594	2.757	0.720	1.489	7.284	91.479	245.407	1432.942	56.063

**Table F.2:** Parameter grid search large-scale simulation results. Simulations were conducted whereby the rate constants for specific reactions were multiplied by multiplication factors and the resulting concentrations of specific metabolites were examined. The parameter sets shown are those that produce metabolite concentrations that lie within predefined ranges as detailed in Table 3.14. Parameter multiplication factors for the respective rate constants are shown along with the relevant resultant metabolite concentrations, in  $\mu$ M.

## Appendix G

This appendix contains two tables and two figures relating to HPLC calibration. The first table details the concentration ranges used for each metabolite from which the calibration curves were constructed. These calibration curves are shown in the following two figures, whilst the final table shows the calibration equations obtained from these curves.

Metabolite	Concentration range (μM) Cell est. (μM)					
Adenosine	2.0	6.3	20.0	63.2	200.0	†
AMP	10.0*	31.6	100.0	316.2	1000.0	24.0
ADP	10.0	31.6*	100.0	316.2	1000.0	23.0
ATP	50.0	158.1	499.9	1581.0	5000.0	135.0
HX	3.0*	9.5	30.0	94.9	300.0	11.0
IMP	2.0	6.3	20.0	63.2	200.0	4.0
Guanosine	2.0	6.3	20.0	63.2	200.0	†
GMP	0.7*	2.4	7.5	23.7	75.0	2.0
GDP	3.0	9.5	30.0	94.9	300.0	10.0
GTP	20.0	63.2	200.0	632.4	2000.0	69.0
XMP	2.0	6.3	20.0	63.2	200.0	0.4‡

**Table G.1:** Metabolite concentration ranges used for HPLC calibration curves. Metabolite concentrations (as determined via HPLC) from extracts of HL60 cells were used to estimate suitable concentration ranges for the construction of calibration curves. \* These samples had technical issues so results from these were excluded from the calibration curves. † Concentrations for these metabolites were not detectable via HPLC in the HL60 cell extract whereas ‡ was barely detectable in this sample, thus calibration standards for these three metabolites were selected based upon reasonable estimates.

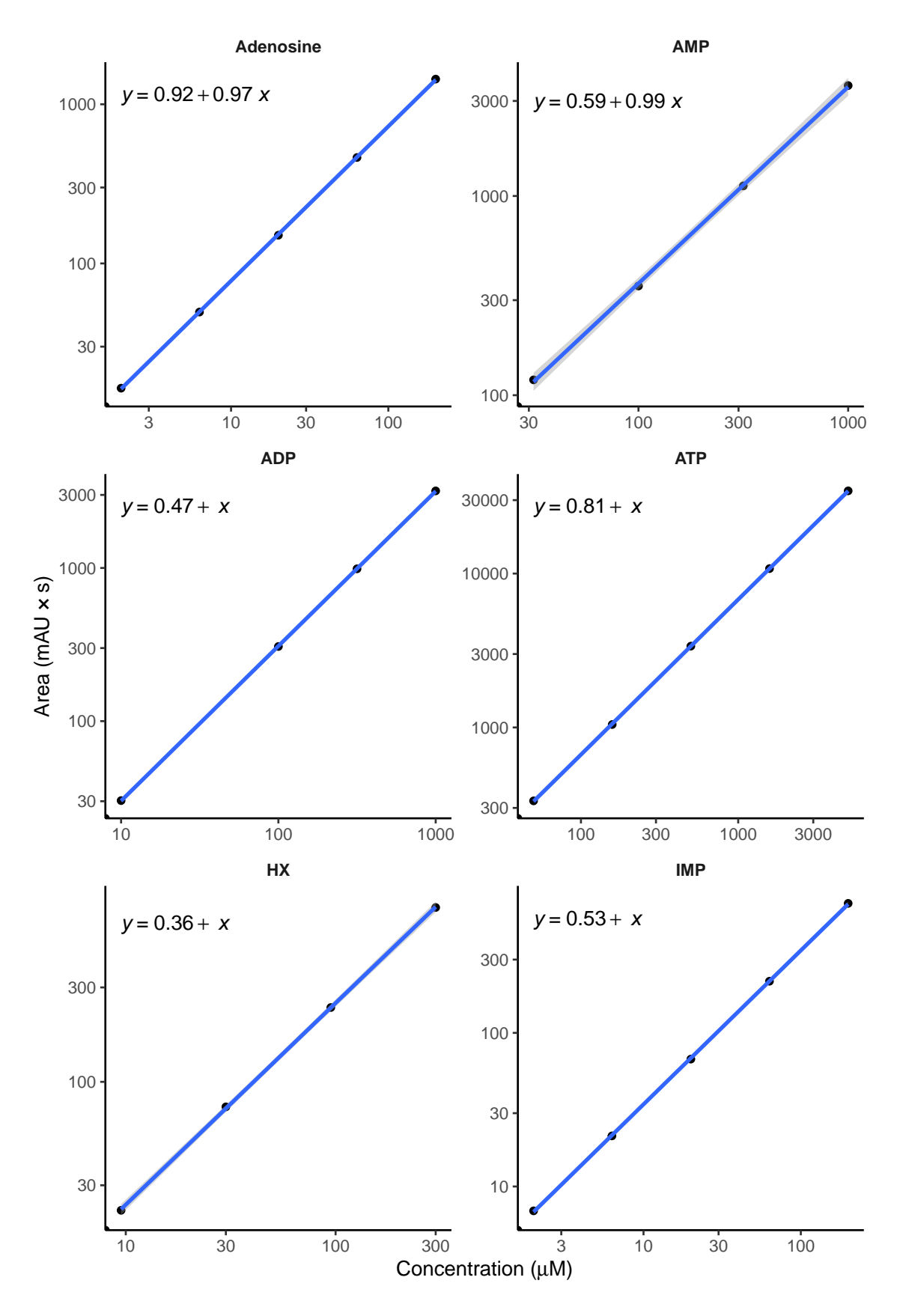


**Figure G.1:** HPLC calibration curves for Ado, AMP, ADP, ATP, HX and IMP. The curves were constructed via HPLC analysis of the calibration standards as shown in Table G.1.

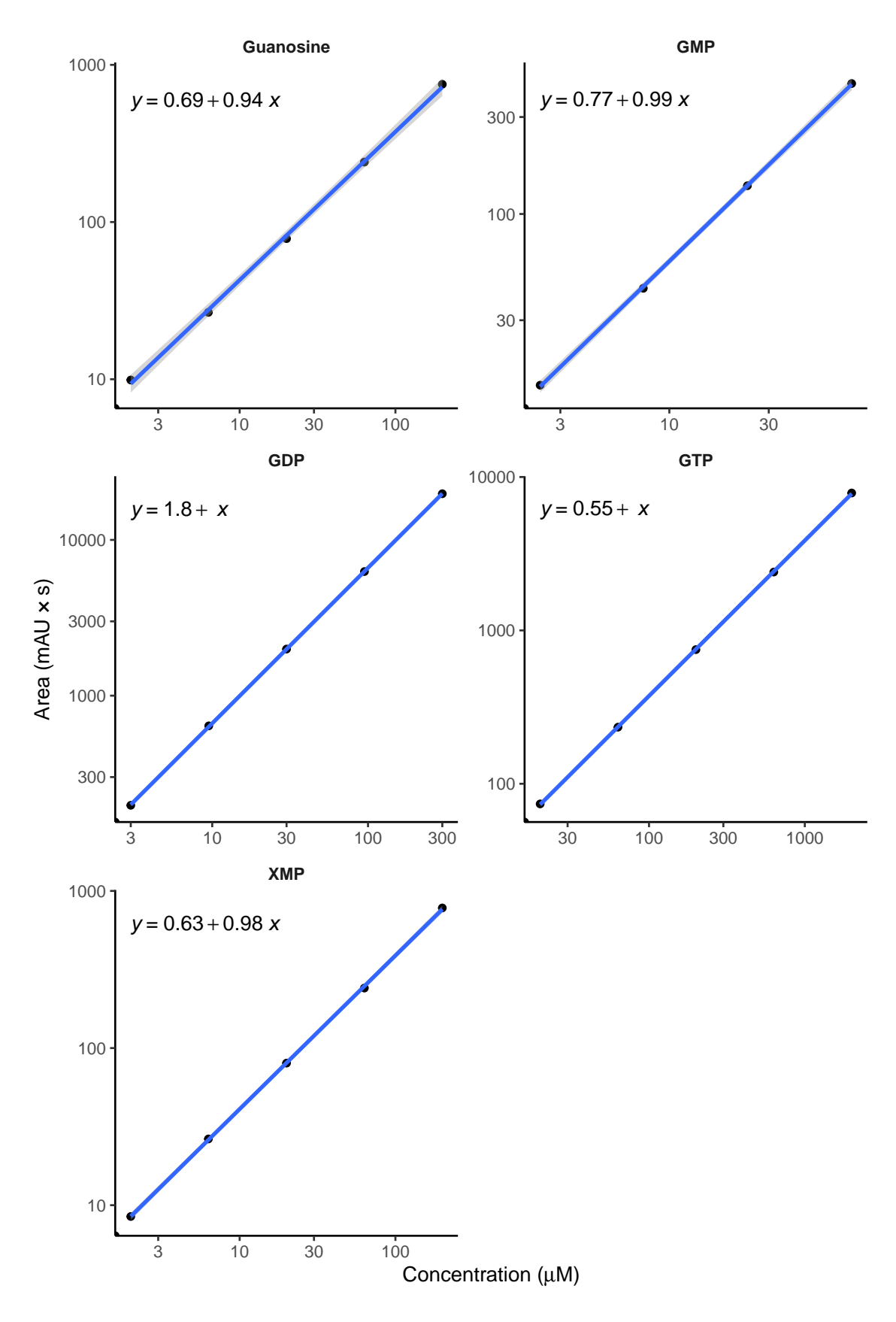


**Figure G.2:** HPLC calibration curves for Guo, GMP, GDP, GTP and XMP. The curves were constructed via HPLC analysis of the calibration standards as shown in Table G.1.

Metabolite	Calibration equation
Adenosine	y = 0.92 + 0.97x
AMP	y = 0.59 + 0.99x
ADP	y = 0.47 + x
ATP	y = 0.81 + x
HX	y = 0.36 + x
IMP	y = 0.53 + x
Guanosine	y = 0.69 + 0.94x
GMP	y = 0.77 + 0.99x
GDP	y = 1.8 + x
GTP	y = 0.55 + x
XMP	y = 0.63 + 0.98x

**Table G.2:** HPLC calibration equations. The equation of the line of best fit for the calibration curve for each purine (see Figures G.1 and G.2) is shown. Calibration standards as shown in Table G.1 were analysed via HPLC and equations were calculated using the programming language R, version 4.0.3 (R Development Core Team, 2021).

## Appendix H

Contained in this appendix are five figures of experimental data. The first shows the HPLC chromatograms for the PRPPS assay time course, whilst the second shows the change in AMP concentration over this time course. The third figure is the gating strategy used for the flow cytometry analysis, whilst the fourth figure shows the effect of adding ATRA and MZ on HL60 cells. The last figure shows the HPLC chromatograms for the HL60 cell differentiation experiments.

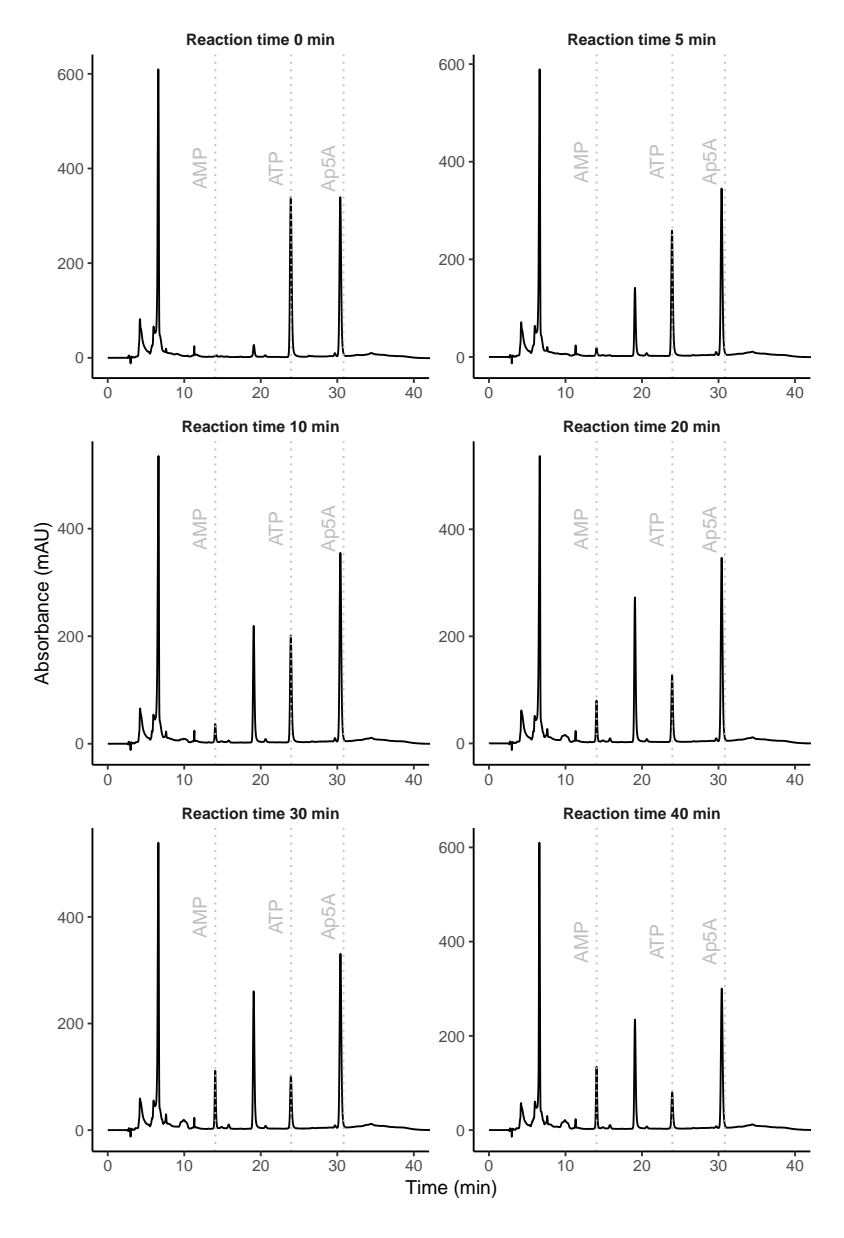


**Figure H.1:** Chromatograms for PRPPS assay time course. To determine the rate of reaction for the enzyme PRPPS, HL60 cell protein extracts were incubated with the reaction substrates for the time periods 0, 5, 10, 20, 30, and 40 min. AMP production was then assessed via HPLC and used to determine the rate of reaction. AMP, ATP and Ap5A standards were used to determine peak assignment as shown in grey.

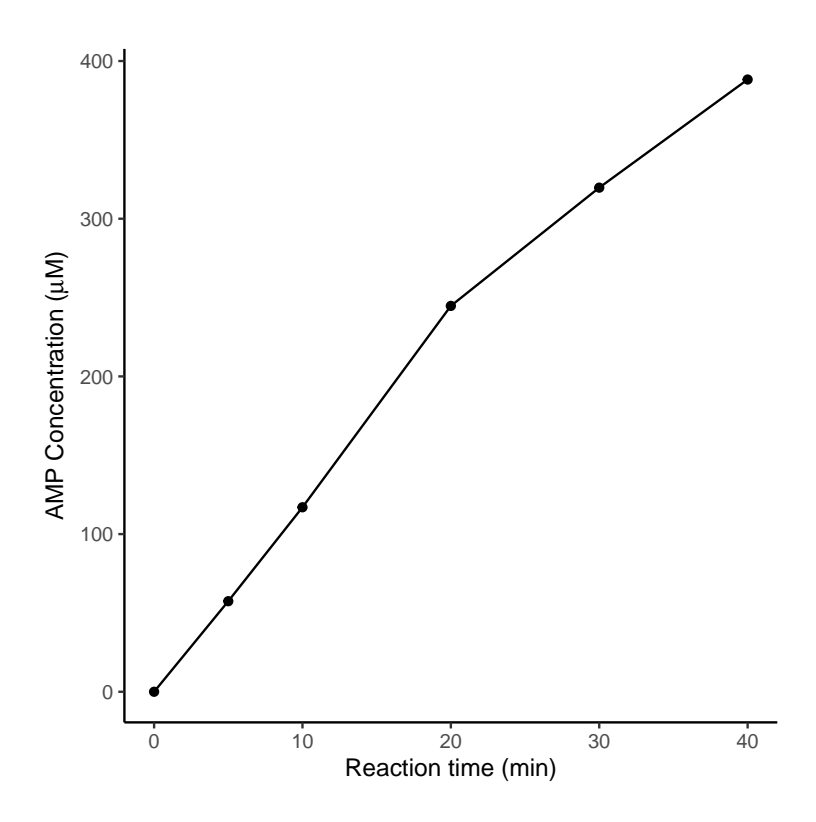


**Figure H.2:** Change in AMP concentration over PRPPS assay time course. The concentration of AMP was assessed via HPLC over the time course which consisted of the time points: 0, 5, 10, 20, 30, and 40 min.

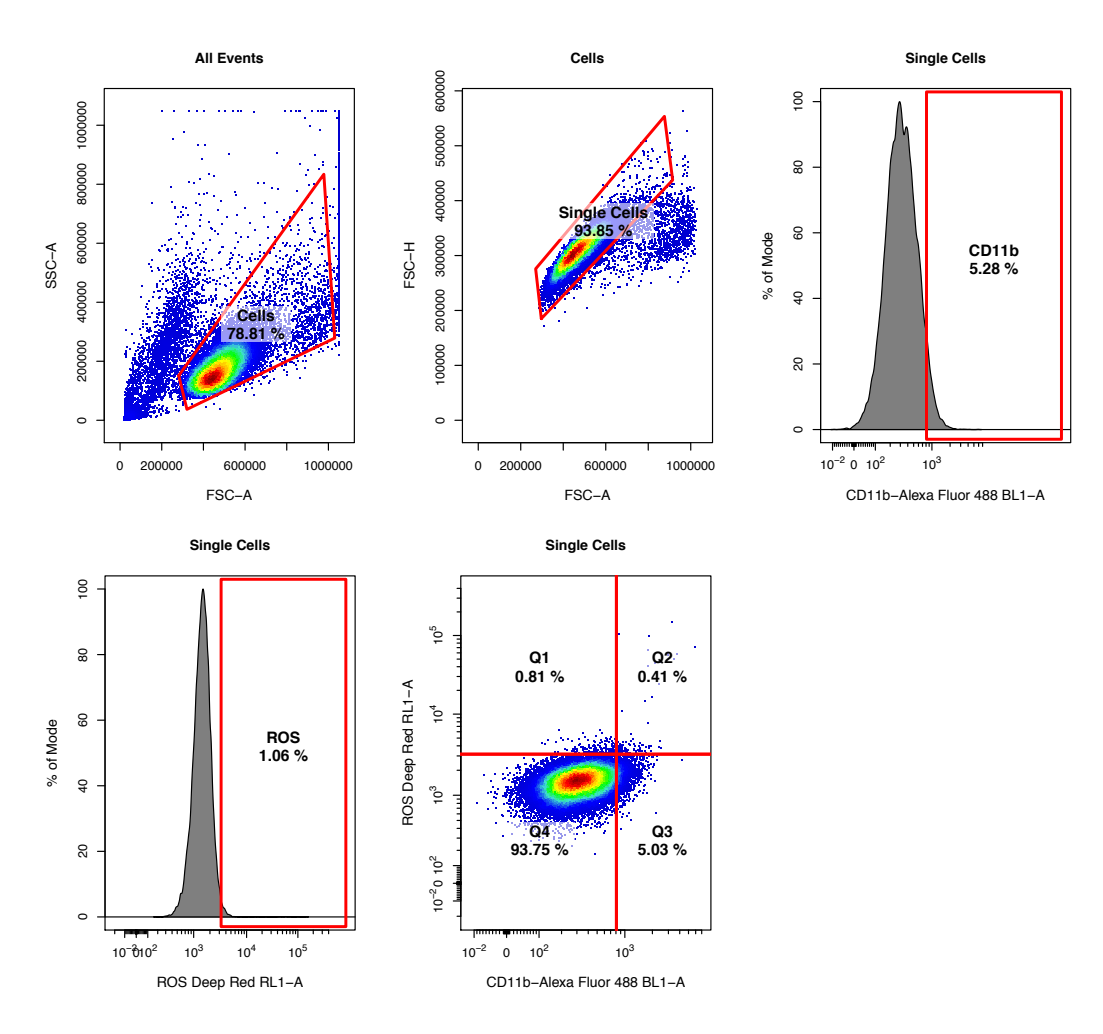


**Figure H.3:** Example flow cytometry gating strategy. Cells were gated as indicated to remove debris and doublets.

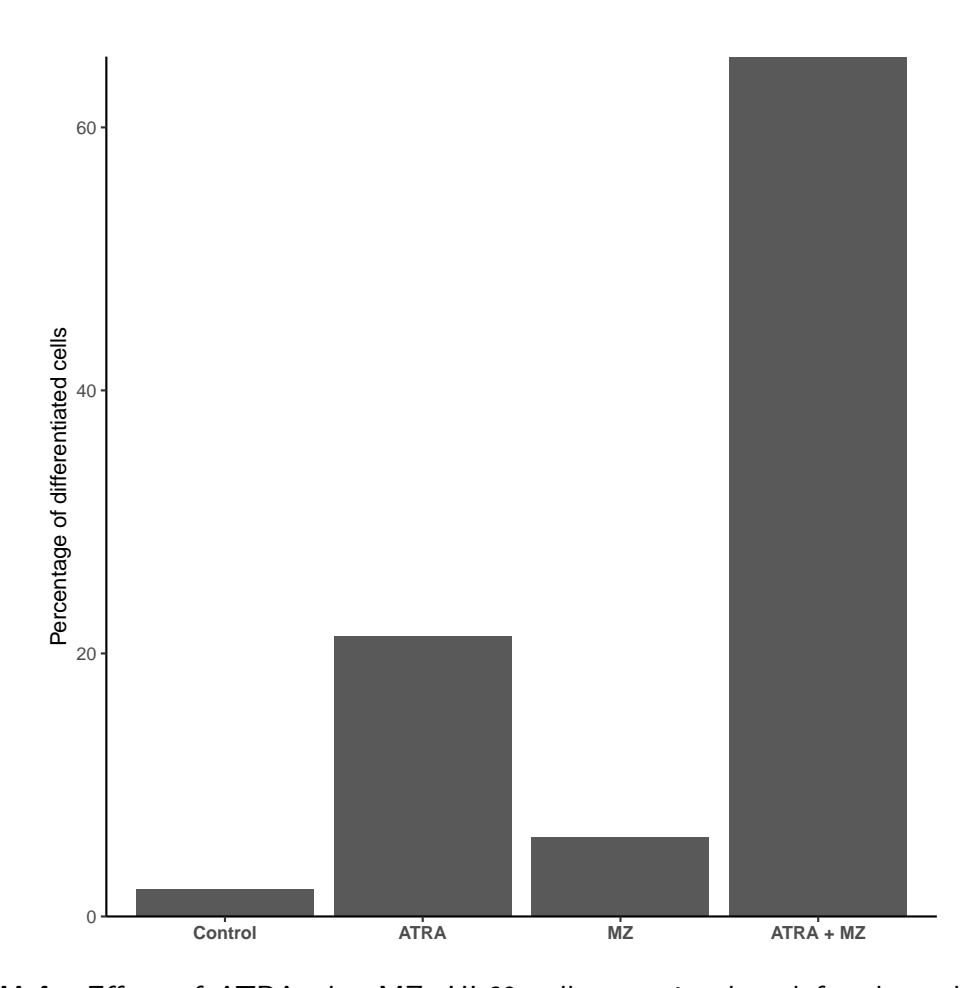


**Figure H.4:** Effect of ATRA plus MZ. HL60 cells were incubated for three days in the presence of either 1  $\mu$ M ATRA, 17  $\mu$ M MZ or both, or left untreated. The percentage of differentiated cells was determined via expression of CD11b, as assessed via flow cytometry. Results courtesy of G. Thomas (unpublished data) from n=1 experiments are shown.

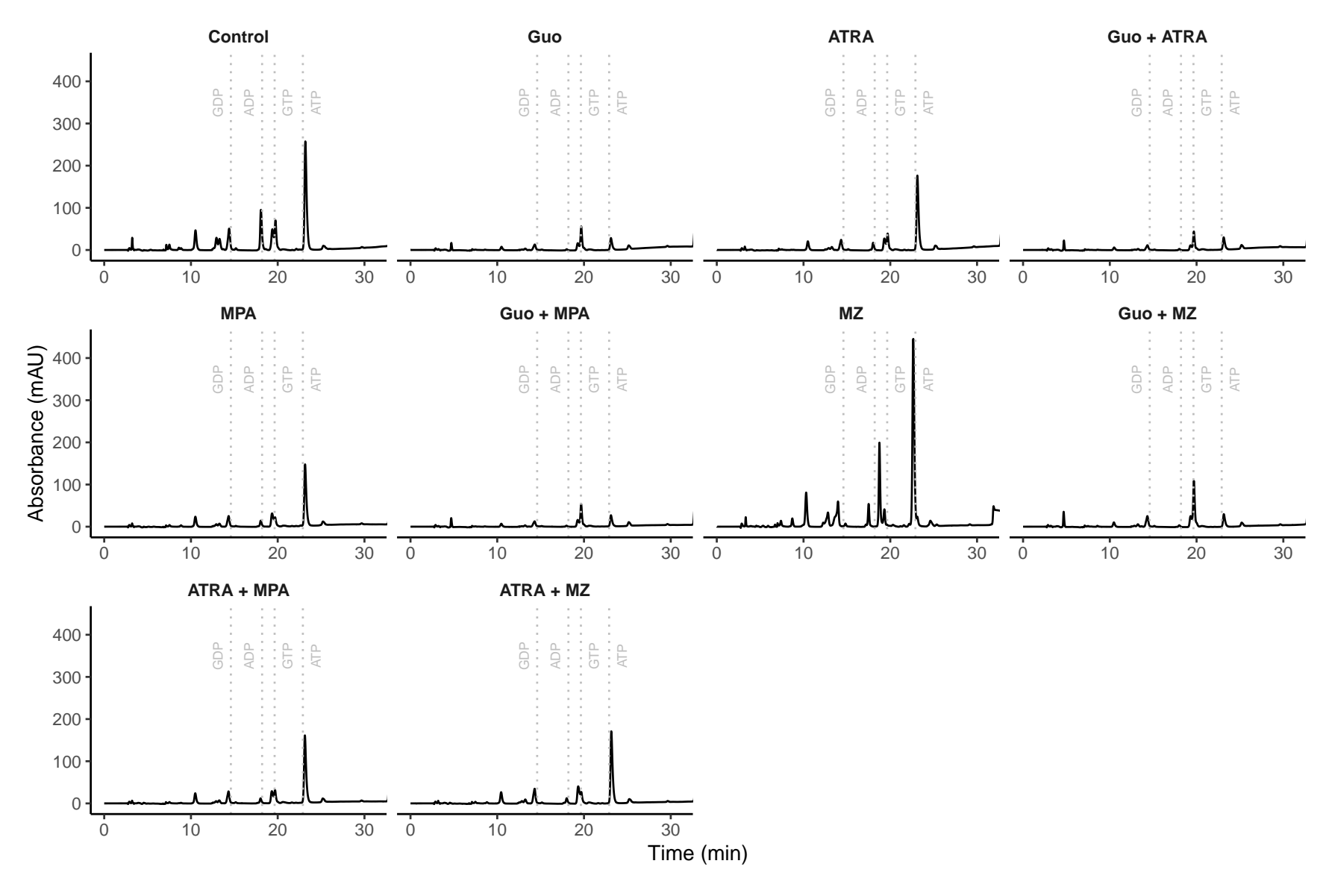


**Figure H.5:** HPLC chromatograms from HL60 cell differentiation experiments. Cells were incubated for three days in the presence of 1 μM ATRA, 1 μM MPA or 50 μM MZ or combinations, or left untreated. 50 μM guanosine was added where indicated. Purine nucleotide levels were assessed via HPLC, with purine standards used to determine peak assignment as shown in grey.

## Code Appendix

This appendix contains the Matlab code for the final model that was used for simulations.

```
function Model 3() %GMA version of expanded model with PRPPS scalability
%Time
t0 = 0;
tf = 10000000;
step = tf/1000;
tspan = [t0:step:tf];
%Initial concentrations
%The entries 4 and 8 have been left blank, as these corresponded to the
%A and T pools in the original model, thus the same indexing is retained
XO(1,1) = 5;
                    %PRPP
XO(2,1) = 100;
                    %IMP
XO(3,1) = 0.2;
                    %S-AMP
XO(5,1) = 4;
                    %SAM
XO(6,1) = 1;
                    %Ade
XO(7,1) = 25;
                    %XMP
XO(9,1) = 6;
                    %dAdo dAMP dADP dATP
XO(10,1) = 3;
                    %dGMP dGDP dGTP
XO(11,1) = 28600;
                    %RNA
XO(12,1) = 5160;
                    %DNA
XO(13,1) = 10;
                    %HX Ino dIno
XO(14,1) = 5;
                    %Xa
XO(15,1) = 5;
                    %Gua Guo dGuo
XO(16,1) = 100;
                    %Uric Acid
XO(17,1) = 18;
                    %R5P
XO(18,1) = 1400;
                    %Pi
XO(19,1) = 0.5;
                    %Ado
XO(20,1) = 200;
                    %AMP
XO(21,1) = 400;
                    %ADP
XO(22,1) = 1900;
                    %ATP
XO(23,1) = 25;
                    %GMP
XO(24,1) = 75;
                    %GDP
X0(25,1) = 300;
                    %GTP
```

## %Reaction parameters

%a is a vector of the rate constants - scaled based on PRPPS assay %and to umol  $min^-1$  (10^9 cells)^-1. prpps scaling = 0.23/20.8826 %f is a matrix of kinetic orders

```
a(1,1) = 0.0449046;
                        %ada
f(1,19) = 0.97;
                        %fada4A
a(2,1) = 0.000109213; %ade
f(2,6) = 0.55;
                        %fade6
a(3,1) = 0.0362616;
                        %adna
f(3,9) = 0.42;
                        %fdnap9
f(3,10) = 0.33;
                        %fdnap10
a(4,1) = 0.000800949; %adrnr
f(4,21) = 0.1;
                        %fadrnr4D
f(4,9) = -0.3;
                        %fadrnr9
f(4,10) = 0.87;
                        %fadrnr10
a(5,1) = 0.00208149; %ampd
                        %fampd4M
f(5,20) = 0.8;
f(5,25) = -0.03;
                        %fampd8T
f(5,18) = -0.1;
                        %fampd18
a(6,1) = 0.340758;
                        %aprt
f(6,1) = 0.5;
                        %faprt1
f(6,20) = -0.8;
                        %faprt4M
f(6,6) = 0.75;
                        %faprt6
a(7,1) = 7.14296;
                        %arna
f(7,22) = 0.05;
                        %frnap4T
f(7,25) = 0.13;
                        %frnap8T
                        %asli
a(8,1) = 66.5529;
f(8,3) = 0.99;
                        %fasli3
                        %fasli4M
f(8,20) = -0.95;
a(9,1) = 0.0228738;
                        %asuc
f(9,2) = 0.4;
                        %fasuc2
                        %fasuc4M
f(9,20) = -0.24;
                        %fasuc8T
f(9,25) = 0.2;
f(9,18) = -0.05;
                        %fasuc18
a(10,1) = 0.00036816; %dada
f(10,9) = 1;
                        %fdada9
```

```
a(11,1) = 0.0238581; %den
f(11,1) = 2;
                        %fden1
f(11,2) = -0.06;
                        %fden2
f(11,20) = -0.1675;
                        %fden4M
f(11,21) = -0.06;
                        %fden4D
f(11,22) = -0.028;
                        %fden4T
f(11,23) = -0.14;
                        %fden8M
f(11,24) = -0.06;
                        %fden8D
f(11,25) = -0.016;
                        %fden8T
f(11,18) = -0.08;
                        %fden18
a(12,1) = 0.0003703;
                        %dgnuc
f(12,10) = 1;
                        %fdgnuc10
a(13,1) = 0.0000214311; %dnaa
f(13,12) = 1;
                        %fdnan12
a(14,1) = 0.0000145749; %dnag
%fdnan12 = 1; Duplicated, see dnaa reaction 13
a(15,1) = 0.0246572; %gdna
%fdnap9 = 0.42; Duplicated, see adna reaction 3
%fdnap10 = 0.33; Duplicated, see adna reaction 3
a(16,1) = 0.00258804; %gdrnr
f(16,24) = 0.4;
                        %fgdrnr8D
f(16,9) = -1.2;
                        %fgdrnr9
f(16,10) = -0.39;
                        %fgdrnr10
a(17,1) = 0.00879106; %gmpr
f(17,2) = -0.15;
                        %fgmpr2
f(17,20) = -0.01;
                        %fgmpr4M
f(17,21) = -0.02;
                        %fgmpr4D
f(17,22) = -0.04;
                        %fgmpr4T
f(17,7) = -0.76;
                        %fgmpr7
f(17,23) = 0.23;
                        %fgmpr8M
f(17,24) = 0.18;
                        %fgmpr8D
f(17,25) = 0.29;
                        %fgmpr8T
a(18,1) = 0.00424414; %gmps
f(18,22) = 0.12;
                        %fgmps4T
f(18,7) = 0.16;
                        %fgmps7
a(19,1) = 0.0342927; %gnuc
f(19,23) = 0.9;
                        %fgnuc8M
f(19,18) = -0.34;
                        %fgnuc18
```

```
a(20,1) = 0.145077;
                        %gprt
f(20,1) = 1.2;
                        %fgprt1
f(20,23) = -1.2;
                        %fgprt8M
f(20,15) = 0.42;
                        %fgprt15
a(21,1) = 4.76121;
                        %grna
%frnap4T = 0.05; Duplicated, see arna reaction 7
%frnap8T = 0.13; Duplicated, see arna reaction 7
a(22,1) = 0.00567657; %gua
f(22,15) = 0.5;
                        %fgua15
a(23,1) = 0.137843;
                        %hprt
f(23,1) = 1.1;
                        %fhprt1
f(23,2) = -0.89;
                        %fhprt2
f(23,13) = 0.48;
                        %fhprt13
a(24,1) = 0.0000411046; %hxe
f(24,13) = 1.12;
                        %fhxe13
a(25,1) = 0.00293751; %hxd
                        %fhxd13
f(25,13) = 0.65;
a(26,1) = 0.0129618; %impdh
f(26,2) = 0.15;
                        %fimpdh2
f(26,7) = -0.09;
                        %fimpdh7
f(26,23) = -0.03;
                        %fimpdh8M
a(27,1) = 0.00992128; %inuc
f(27,2) = 0.8;
                        %finuc2
f(27,18) = -0.36;
                        %finuc18
a(28,1) = 0.0837889; %mat
f(28,22) = 0.2;
                        %fmat4T
f(28,5) = -0.6;
                        %fmat5
a(29,1) = 0.0031882; \% polyam
f(29,5) = 0.9;
                        %fpolyam5
a(30,1) = 0.00388122; %prpps
f(30,1) = -0.03;
                        %fprpps1
f(30,20) = -0.1;
                        %fprpps4M
f(30,21) = -0.36;
                        %fprpps4D
f(30,22) = 0.007;
                        %fprpps4T
f(30,23) = -0.004;
                        %fprpps8M
f(30,24) = -0.04;
                        %fprpps8D
```

```
%fprpps17
f(30,17) = 0.65;
f(30,18) = 0.7;
                        %fprpps18
a(31,1) = 0.0143271; %pyr
f(31,1) = 1.27;
                        %fpyr1
a(32,1) = 0.000764646; %rnaa
                        %frnan11
f(32,11) = 1;
a(33,1) = 0.000509727; %rnag
%frnan11 = 1; Duplicated, see rnaa reaction 32
a(34,1) = 0.097451;
                        %trans
f(34,5) = 0.33;
                        %ftrans5
a(35,1) = 0.000000969372;%uae
f(35,16) = 2.21;
                        %fuae16
a(36,1) = 0.0000126991; %xe
f(36,14) = 2;
                        %fxe14
                        %xd
a(37,1) = 0.010521;
f(37,14) = 0.55;
                        %fxd14
a(38,1) = 1.90748;
                        %guk
f(38,22) = 0.0909091;
                        %fguk4T
f(38,23) = 0.418605;
                        %fguk8M
a(39,1) = 0.208753;
                        %ndpk
                        %fndpk4T
f(39,22) = 0.411765;
f(39,23) = -0.037037;
                        %fndpk8M
f(39,24) = 0.292453;
                        %fndpk8D
a(40,1) = 218.609;
                        %adok
f(40,19) = 0.444444;
                        %fadok4A
f(40,20) = -0.38835;
                        %fadok4M
f(40,21) = -0.888889;
                        %fadok4D
f(40,22) = 0.0379747;
                        %fadok4T
a(41,1) = 3.48562;
                        %adek
f(41,20) = 0.285714;
                        %fadek4M
                        %fadek4T
f(41,22) = 0.0452261;
                           %anuc
a(42,1) = 0.00000620633;
f(42,20) = 1.37458;
                        %fanuc4M
f(42,18) = -0.2123;
                        %fanuc18
```

```
%phospho
a(43,1) = 7.86588;
                        %fphospho4D
f(43,21) = 0.5;
                        %fphospho4T
f(43,22) = -0.1;
    options = odeset('NonNegative', ones(size(X0)));
    tic
    [t1, Y] = ode15s(@Reactions, tspan, XO, options, a, f);
    toc
    assignin('base', 'Y', Y);
    assignin('base', 'f', f);
    assignin('base', 'a', a);
    assignin('base', 'X0', X0);
    v = Fluxes(Y', a, f);
    assignin('base', 'v', v);
end
function [dxdt] = Reactions(t, X, a, f) %Reaction equations
%PRPP
dxdt(1,1) = a(30,1)*(X(1,1)^f(30,1))*(X(20,1)^f(30,20))*(X(21,1)^f(30,21))*
            (X(22,1)^{f}(30,22))*(X(23,1)^{f}(30,23))*(X(24,1)^{f}(30,24))*
            (X(17,1)^f(30,17))*(X(18,1)^f(30,18))...
    -a(6,1)*(X(1,1)^f(6,1))*(X(20,1)^f(6,20))*(X(6,1)^f(6,6))...
    -a(11,1)*(X(1,1)^f(11,1))*(X(2,1)^f(11,2))*(X(20,1)^f(11,20))*
            (X(21,1)^{f}(11,21))*(X(22,1)^{f}(11,22))*(X(23,1)^{f}(11,23))*
            (X(24,1)^{f}(11,24))*(X(25,1)^{f}(11,25))*(X(18,1)^{f}(11,18))...
    -a(20,1)*(X(1,1)^f(20,1))*(X(23,1)^f(20,23))*(X(15,1)^f(20,15))...
    -a(23,1)*(X(1,1)^f(23,1))*(X(2,1)^f(23,2))*(X(13,1)^f(23,13))...
    -a(31,1)*(X(1,1)^f(31,1));
%IMP
dxdt(2,1) = a(5,1)*(X(20,1)^f(5,20))*(X(25,1)^f(5,25))*(X(18,1)^f(5,18))...
    +a(11,1)*(X(1,1)^f(11,1))*(X(2,1)^f(11,2))*(X(20,1)^f(11,20))*
            (X(21,1)^f(11,21))*(X(22,1)^f(11,22))*(X(23,1)^f(11,23))*
            (X(24,1)^{f}(11,24))*(X(25,1)^{f}(11,25))*(X(18,1)^{f}(11,18))...
    +a(17,1)*(X(2,1)^f(17,2))*(X(20,1)^f(17,20))*(X(21,1)^f(17,21))*
            (X(22,1)^{f}(17,22))*(X(7,1)^{f}(17,7))*(X(23,1)^{f}(17,23))*
            (X(24,1)^f(17,24))*(X(25,1)^f(17,25))...
    +a(23,1)*(X(1,1)^f(23,1))*(X(2,1)^f(23,2))*(X(13,1)^f(23,13))...
    -a(9,1)*(X(2,1)^f(9,2))*(X(20,1)^f(9,20))*(X(25,1)^f(9,25))*
            (X(18,1)^f(9,18))...
    -a(26,1)*(X(2,1)^f(26,2))*(X(7,1)^f(26,7))*(X(23,1)^f(26,23))...
    -a(27,1)*(X(2,1)^f(27,2))*(X(18,1)^f(27,18));
```

```
%S-AMP
dxdt(3,1) = a(9,1)*(X(2,1)^f(9,2))*(X(20,1)^f(9,20))*
            (X(25,1)^f(9,25))*(X(18,1)^f(9,18))...
    -a(8,1)*(X(3,1)^f(8,3))*(X(20,1)^f(8,20));
%SAM
dxdt(5,1) = a(28,1)*(X(22,1)^f(28,22))*(X(5,1)^f(28,5))...
    -a(29,1)*(X(5,1)^f(29,5))...
    -a(34,1)*(X(5,1)^f(34,5));
%Ade
dxdt(6,1) = a(29,1)*(X(5,1)^f(29,5))...
    -a(2,1)*(X(6,1)^f(2,6))...
    -a(6,1)*(X(1,1)^f(6,1))*(X(20,1)^f(6,20))*(X(6,1)^f(6,6));
%XMP
dxdt(7,1) = a(26,1)*(X(2,1)^{f}(26,2))*(X(7,1)^{f}(26,7))*(X(23,1)^{f}(26,23))...
    -a(18,1)*(X(22,1)^f(18,22))*(X(7,1)^f(18,7));
%dAdo dAMP dADP dATP
dxdt(9,1) = a(4,1)*(X(21,1)^f(4,21))*(X(9,1)^f(4,9))*(X(10,1)^f(4,10))...
    +a(13,1)*(X(12,1)^f(13,12))...
    -a(3,1)*(X(9,1)^f(3,9))*(X(10,1)^f(3,10))...
    -a(10,1)*(X(9,1)^f(10,9));
%dGMP dGDP dGTP
dxdt(10,1) = a(14,1)*(X(12,1)^f(13,12))...
    +a(16,1)*(X(24,1)^f(16,24))*(X(9,1)^f(16,9))*(X(10,1)^f(16,10))...
    -a(12,1)*(X(10,1)^f(12,10))...
    -a(15,1)*(X(9,1)^f(3,9))*(X(10,1)^f(3,10));
%RNA
dxdt(11,1) = a(7,1)*(X(22,1)^f(7,22))*(X(25,1)^f(7,25))...
    +a(21,1)*(X(22,1)^f(7,22))*(X(25,1)^f(7,25))...
    -a(32,1)*(X(11,1)^f(32,11))...
    -a(33,1)*(X(11,1)^f(32,11));
%DNA
dxdt(12,1) = a(3,1)*(X(9,1)^f(3,9))*(X(10,1)^f(3,10))...
    +a(15,1)*(X(9,1)^f(3,9))*(X(10,1)^f(3,10))...
    -a(13,1)*(X(12,1)^f(13,12))...
    -a(14,1)*(X(12,1)^f(13,12));
%HX Ino dIno
dxdt(13,1) = a(1,1)*(X(19,1)^f(1,19))...
    +a(10,1)*(X(9,1)^f(10,9))...
```

```
+a(27,1)*(X(2,1)^f(27,2))*(X(18,1)^f(27,18))...
    -a(23,1)*(X(1,1)^f(23,1))*(X(2,1)^f(23,2))*(X(13,1)^f(23,13))...
    -a(24,1)*(X(13,1)^f(24,13))...
    -a(25,1)*(X(13,1)^f(25,13));
%Xa
dxdt(14,1) = a(22,1)*(X(15,1)^f(22,15))...
    +a(25,1)*(X(13,1)^f(25,13))...
    -a(36,1)*(X(14,1)^f(36,14))...
    -a(37,1)*(X(14,1)^f(37,14));
%Gua Guo dGuo
dxdt(15,1) = a(12,1)*(X(10,1)^f(12,10))...
    +a(19,1)*(X(23,1)^f(19,23))*(X(18,1)^f(19,18))...
    -a(20,1)*(X(1,1)^f(20,1))*(X(23,1)^f(20,23))*(X(15,1)^f(20,15))...
    -a(22,1)*(X(15,1)^f(22,15));
%Uric Acid
dxdt(16,1) = a(37,1)*(X(14,1)^f(37,14))...
    -a(35,1)*(X(16,1)^f(35,16));
%Ado
dxdt(19,1) = a(34,1)*(X(5,1)^f(34,5))...
    +a(42,1)*(X(20,1)^f(42,20))*(X(18,1)^f(42,18))...
    -a(1,1)*(X(19,1)^f(1,19))...
    -a(40,1)*(X(19,1)^f(40,19))*(X(20,1)^f(40,20))*
            (X(21,1)^f(40,21))*(X(22,1)^f(40,22));
%AMP
dxdt(20,1) = a(6,1)*(X(1,1)^f(6,1))*(X(20,1)^f(6,20))*(X(6,1)^f(6,6))...
    +a(8,1)*(X(3,1)^f(8,3))*(X(20,1)^f(8,20))...
    +a(18,1)*(X(22,1)^f(18,22))*(X(7,1)^f(18,7))...
    +a(30,1)*(X(1,1)^f(30,1))*(X(20,1)^f(30,20))*(X(21,1)^f(30,21))*
            (X(22,1)^{f}(30,22))*(X(23,1)^{f}(30,23))*(X(24,1)^{f}(30,24))*
            (X(17,1)^f(30,17))*(X(18,1)^f(30,18))...
    +a(32,1)*(X(11,1)^f(32,11))...
    +a(40,1)*(X(19,1)^f(40,19))*(X(20,1)^f(40,20))*(X(21,1)^f(40,21))*
            (X(22,1)^f(40,22))...
    -a(5,1)*(X(20,1)^f(5,20))*(X(25,1)^f(5,25))*(X(18,1)^f(5,18))...
    -a(41,1)*(X(20,1)^f(41,20))*(X(22,1)^f(41,22))...
    -a(42,1)*(X(20,1)^f(42,20))*(X(18,1)^f(42,18));
%ADP
dxdt(21,1) = a(38,1)*(X(22,1)^f(38,22))*(X(23,1)^f(38,23))...
    +a(39,1)*(X(22,1)^f(39,22))*(X(23,1)^f(39,23))*(X(24,1)^f(39,24))...
    +a(40,1)*(X(19,1)^f(40,19))*(X(20,1)^f(40,20))*(X(21,1)^f(40,21))*
```

```
(X(22,1)^f(40,22))...
    +2*a(41,1)*(X(20,1)^f(41,20))*(X(22,1)^f(41,22))...
    -a(4,1)*(X(21,1)^f(4,21))*(X(9,1)^f(4,9))*(X(10,1)^f(4,10))...
    -a(43,1)*(X(21,1)^f(43,21))*(X(22,1)^f(43,22));
%ATP
dxdt(22,1) = a(43,1)*(X(21,1)^f(43,21))*(X(22,1)^f(43,22))...
    -a(7,1)*(X(22,1)^f(7,22))*(X(25,1)^f(7,25))...
    -a(18,1)*(X(22,1)^f(18,22))*(X(7,1)^f(18,7))...
    -a(28,1)*(X(22,1)^f(28,22))*(X(5,1)^f(28,5))...
    -a(30,1)*(X(1,1)^f(30,1))*(X(20,1)^f(30,20))*(X(21,1)^f(30,21))*
            (X(22,1)^f(30,22))*(X(23,1)^f(30,23))*(X(24,1)^f(30,24))*
            (X(17,1)^f(30,17))*(X(18,1)^f(30,18))...
    -a(38,1)*(X(22,1)^f(38,22))*(X(23,1)^f(38,23))...
    -a(39,1)*(X(22,1)^f(39,22))*(X(23,1)^f(39,23))*(X(24,1)^f(39,24))...
    -a(40,1)*(X(19,1)^f(40,19))*(X(20,1)^f(40,20))*(X(21,1)^f(40,21))*
            (X(22,1)^f(40,22))...
    -a(41,1)*(X(20,1)^f(41,20))*(X(22,1)^f(41,22));
%GMP
dxdt(23,1) = a(18,1)*(X(22,1)^f(18,22))*(X(7,1)^f(18,7))...
    +a(20,1)*(X(1,1)^f(20,1))*(X(23,1)^f(20,23))*(X(15,1)^f(20,15))...
    +a(33,1)*(X(11,1)^f(32,11))...
    -a(17,1)*(X(2,1)^f(17,2))*(X(20,1)^f(17,20))*(X(21,1)^f(17,21))*
        (X(22,1)^f(17,22))*(X(7,1)^f(17,7))*(X(23,1)^f(17,23))*
            (X(24,1)^f(17,24))*(X(25,1)^f(17,25))...
    -a(19,1)*(X(23,1)^f(19,23))*(X(18,1)^f(19,18))...
    -a(38,1)*(X(22,1)^f(38,22))*(X(23,1)^f(38,23));
%GDP
dxdt(24,1) = a(9,1)*(X(2,1)^f(9,2))*(X(20,1)^f(9,20))*(X(25,1)^f(9,25))*
            (X(18,1)^f(9,18))...
    +a(38,1)*(X(22,1)^f(38,22))*(X(23,1)^f(38,23))...
    -a(16,1)*(X(24,1)^f(16,24))*(X(9,1)^f(16,9))*(X(10,1)^f(16,10))...
    -a(39,1)*(X(22,1)^f(39,22))*(X(23,1)^f(39,23))*(X(24,1)^f(39,24));
%GTP
dxdt(25,1) = a(39,1)*(X(22,1)^f(39,22))*(X(23,1)^f(39,23))*(X(24,1)^f(39,24))...
    -a(9,1)*(X(2,1)^f(9,2))*(X(20,1)^f(9,20))*(X(25,1)^f(9,25))*
            (X(18,1)^f(9,18))...
    -a(21,1)*(X(22,1)^f(7,22))*(X(25,1)^f(7,25));
```

end

```
v(1,1) = a(1,1)*(Y(19,end)^f(1,19));
v(2,1) = a(2,1)*(Y(6,end)^f(2,6));
v(3,1) = a(3,1)*(Y(9,end)^f(3,9))*(Y(10,end)^f(3,10));
v(4,1) = a(4,1)*(Y(21,end)^f(4,21))*(Y(9,end)^f(4,9))*(Y(10,end)^f(4,10));
v(5,1) = a(5,1)*(Y(20,end)^f(5,20))*(Y(25,end)^f(5,25))*(Y(18,end)^f(5,18));
v(6,1) = a(6,1)*(Y(1,end)^f(6,1))*(Y(20,end)^f(6,20))*(Y(6,end)^f(6,6));
v(7,1) = a(7,1)*(Y(22,end)^f(7,22))*(Y(25,end)^f(7,25));
v(8,1) = a(8,1)*(Y(3,end)^f(8,3))*(Y(20,end)^f(8,20));
v(9,1) = a(9,1)*(Y(2,end)^f(9,2))*(Y(20,end)^f(9,20))*(Y(25,end)^f(9,25))*
          (Y(18,end)^f(9,18));
v(10,1) = a(10,1)*(Y(9,end)^f(10,9));
v(11,1) = a(11,1)*(Y(1,end)^f(11,1))*(Y(2,end)^f(11,2))*(Y(20,end)^f(11,20))*
            (Y(21,end)^f(11,21))*(Y(22,end)^f(11,22))*(Y(23,end)^f(11,23))*
            (Y(24,end)^f(11,24))*(Y(25,end)^f(11,25))*(Y(18,end)^f(11,18));
v(12,1) = a(12,1)*(Y(10,end)^f(12,10));
v(13,1) = a(13,1)*(Y(12,end)^f(13,12));
v(14,1) = a(14,1)*(Y(12,end)^f(13,12));
v(15,1) = a(15,1)*(Y(9,end)^f(3,9))*(Y(10,end)^f(3,10));
v(16,1) = a(16,1)*(Y(24,end)^f(16,24))*(Y(9,end)^f(16,9))*(Y(10,end)^f(16,10));
v(17,1) = a(17,1)*(Y(2,end)^f(17,2))*(Y(20,end)^f(17,20))*(Y(21,end)^f(17,21))*
          (Y(22,end)^f(17,22))*(Y(7,end)^f(17,7))*(Y(23,end)^f(17,23))*
          (Y(24,end)^f(17,24))*(Y(25,end)^f(17,25));
v(18,1) = a(18,1)*(Y(22,end)^f(18,22))*(Y(7,end)^f(18,7));
v(19,1) = a(19,1)*(Y(23,end)^f(19,23))*(Y(18,end)^f(19,18));
v(20,1) = a(20,1)*(Y(1,end)^f(20,1))*(Y(23,end)^f(20,23))*(Y(15,end)^f(20,15));
v(21,1) = a(21,1)*(Y(22,end)^f(7,22))*(Y(25,end)^f(7,25));
v(22,1) = a(22,1)*(Y(15,end)^f(22,15));
v(23,1) = a(23,1)*(Y(1,end)^f(23,1))*(Y(2,end)^f(23,2))*(Y(13,end)^f(23,13));
v(24,1) = a(24,1)*(Y(13,end)^f(24,13));
v(25,1) = a(25,1)*(Y(13,end)^f(25,13));
v(26,1) = a(26,1)*(Y(2,end)^f(26,2))*(Y(7,end)^f(26,7))*(Y(23,end)^f(26,23));
v(27,1) = a(27,1)*(Y(2,end)^f(27,2))*(Y(18,end)^f(27,18));
v(28,1) = a(28,1)*(Y(22,end)^f(28,22))*(Y(5,end)^f(28,5));
v(29,1) = a(29,1)*(Y(5,end)^f(29,5));
v(30,1) = a(30,1)*(Y(1,end)^f(30,1))*(Y(20,end)^f(30,20))*(Y(21,end)^f(30,21))*
            (Y(22,end)^f(30,22))*(Y(23,end)^f(30,23))*(Y(24,end)^f(30,24))*
          (Y(17,end)^f(30,17))*(Y(18,end)^f(30,18));
v(31,1) = a(31,1)*(Y(1,end)^f(31,1));
v(32,1) = a(32,1)*(Y(11,end)^f(32,11));
v(33,1) = a(33,1)*(Y(11,end)^f(32,11));
v(34,1) = a(34,1)*(Y(5,end)^f(34,5));
v(35,1) = a(35,1)*(Y(16,end)^f(35,16));
v(36,1) = a(36,1)*(Y(14,end)^f(36,14));
v(37,1) = a(37,1)*(Y(14,end)^f(37,14));
```

function [v] = Fluxes(Y, a, f) %Flux calculations at end time point

```
 \begin{array}{lll} v(38,1) &=& \  \  \, a(38,1)*(Y(22,end)^f(38,22))*(Y(23,end)^f(38,23)); \\ v(39,1) &=& \  \  \, a(39,1)*(Y(22,end)^f(39,22))*(Y(23,end)^f(39,23))*(Y(24,end)^f(39,24)); \\ v(40,1) &=& \  \  \, a(40,1)*(Y(19,end)^f(40,19))*(Y(20,end)^f(40,20))*(Y(21,end)^f(40,21))* \\ && \quad  \  \, & \quad  \ & \quad  \  \, & \quad  \
```

end